ESCOLA DE DOUTORAMENTO
INTERNACIONAL DA USC

María
Vivero López

Tese de doutoramento

Prophylaxis and topical treatment of infections associated to hearing aids and contact lenses

Santiago de Compostela, 2022

Programa de Doutoramento en Investigación e Desenvolvemento de Medicamentos

DOCTORAL THESIS

PROPHYLAXIS AND TOPICAL TREATMENT OF INFECTIONS ASSOCIATED TO HEARING AIDS AND CONTACT LENSES

María Vivero López

INTERNATIONAL DOCTORAL SCHOOL OF THE UNIVERSITY OF SANTIAGO DE COMPOSTELA

DOCTORAL PROGRAM IN DRUG RESEARCH AND DEVELOPMENT

SANTIAGO DE COMPOSTELA

2022

USC
UNIVERSIDADE
DE SANTIAGO
DE COMPOSTELA

TESE DOUTORAL

PROFILAXE E TRATAMENTO TÓPICO DE INFECCIÓNS ASOCIADAS A AUDIÓFONOS E LENTES DE CONTACTO

María Vivero López

ESCOLA DE DOUTORAMENTO INTERNACIONAL DA UNIVERSIDADE DE SANTIAGO DE COMPOSTELA

PROGRAMA DE DOUTORAMENTO EN INVESTIGACIÓN E DESENVOLVEMENTO DE MEDICAMENTOS

SANTIAGO DE COMPOSTELA

2022

USC
UNIVERSIDADE
DE SANTIAGO
DE COMPOSTELA

AGRADECIMIENTOS

Se habla mucho del éxito, de la suerte y del placer que acompaña a la victoria, pero en pocas ocasiones se habla del fracaso, esfuerzo, disciplina y trabajo duro necesarios para poder alcanzarlo. Y es que yo, sin eso y sin todos a los que aquí doy gracias jamás llegaría a escribir esta Tesis Doctoral.

Me gustaría empezar dando las gracias a mis dos directores de Tesis, los profesores *Carmen Álvarez Lorenzo* y *Ángel Concheiro Nine*. Dos personas que enseñan muchísimo más que lo que consta en los libros. Gracias por haberme abierto las puertas a este maravilloso grupo de investigación, por apoyarme cuando más lo necesito y por permitirme crecer tanto personal como profesionalmente.

A los profesores del Departamento de Farmacología, Farmacia y Tecnología Farmacéutica, en especial a *José Luis Gómez Amoza, Mariana Landín Pérez, Carlos García González, Loli Torres López* y *Francisco Otero Espinar,* por haberme ayudado siempre que lo he necesitado con una sonrisa.

A la profesora *Ana Otero* del Centro de Investigaciones Biológicas de la Universidade de Santiago de Compostela por acogerme como doctoranda adoptiva y brindarme siempre su apoyo y consejos.

A aquellos profesores que han servido de inspiración y que a lo largo de este camino siempre he tenido presentes, porque sin saberlo me habéis ayudado mucho. En especial me gustaría dar las gracias a *Modesto Salgado,* por su apoyo desde el principio de mi carrera y por todo el cariño que muestra hacia toda mi familia.

A los profesores *Ana Paula Serro*, del Instituto Superior Técnico de Lisboa, y *Gonzalo Carracedo,* de la Facultad de Óptica y

USC UNIVERSIDADE DE SANTIAGO DE COMPOSTELA

Optometría de la Universidad Complutense de Madrid, por haberme hecho sentir una más del equipo desde el primer día y enseñarme que hay más de un enfoque para el mismo trabajo.

A todos mis compañeros del *grupo I+D Farma*, técnicos, predoctorales y Doctores que forman parte de él o han venido de estancia, porque me han enseñado que a pesar de lo competitiva que pueda llegar a ser la investigación, un equipo siempre se apoya y se ayuda. Gracias en especial a los que además de compañeros sois amigos y contáis conmigo cada día.

A todos los miembros del *Team Fran* por su infinita ayuda y todos los buenos momentos compartidos.

A mis amigos más cercanos, gracias por entender mi dedicación a la ciencia, escucharme y ser vía de escape en los momentos más difíciles.

A mis abuelos, por todo el empeño puesto en mi educación y el tiempo compartido. En especial a mi abuelo *Quinís* por mostrarse siempre orgulloso de mí y demostrarme que las personas no mueren mientras se las recuerda.

A mis padres, *Susy* y *Manolo*, por apoyarme en cada decisión que tomo y no permitirme caer nunca. Que nunca se os olvide lo orgullosa que estoy yo de vosotros.

A mi familia política, por acogerme con cariño y amor desde el primer día y estar siempre ahí para lo que haga falta pase lo que pase.

Y, por último, pero no menos importante, al amor de mi vida, *Esteban Barcia Galego*. Gracias por ayudarme a ser mejor cada día y por caminar siempre conmigo de la mano.

A todos vosotros gracias de corazón por estar siempre presentes.

USC
UNIVERSIDADE DE SANTIAGO DE COMPOSTELA

AUTHORIZATION OF THE THESIS SUPERVISORS

Prof. Carmen Alvarez Lorenzo and **Prof. Angel Concheiro Nine**

In condition of **Thesis supervisors**

PhD Thesis: **Prophylaxis and topical treatment of infections associated to hearing aids and contact lenses**

REPORT:

That the present Thesis, corresponds to the work carried out by Miss **María Vivero López**, under our supervision, and that we authorize its presentation considering it gathers the necessary requirements of article 34 of the USC Doctoral Studies Regulation, and that as supervisors of this Thesis, it does not incur in the abstention causes established by the law 40/2015

At **Santiago de Compostela**, on **January 17th 2022**

Prof. Carmen Alvarez Lorenzo Prof. Angel Concheiro Nine

USC
UNIVERSIDADE
DE SANTIAGO
DE COMPOSTELA

AUTORIZACIÓN DO DIRECTOR/TITOR DA TESE

Profilaxe e tratamento tópico de infeccións asociadas a audiófonos e lentes de contacto

Dna. **Carmen Alvarez Lorenzo** e D. **Angel Concheiro Nine**

INFORMAN:

Que a presente tese, correspóndese co traballo realizado por Dna. María Vivero López, baixo a nosa dirección/titorización, e autorizamos a súa presentación, considerando que reúne os requisitos esixidos no Regulamento de Estudos de Doutoramento da USC, e que como directores desta non incorre nas causas de abstención establecidas na Lei 40/2015. De acordo co indicado no Regulamento de Estudos de Doutoramento, declaramos tamén que a presente tese de doutoramento é idónea para ser defendida en base á modalidade de Monográfica con reproducción de publicaciones, nos que a participación da doutoranda foi decisiva para a súa elaboración e as publicacións se axustan ao Plan de Investigación.

En **Santiago de Compostela**, **17 de Xaneiro de 2022**

Prof. Carmen Alvarez Lorenzo Prof. Angel Concheiro Nine

USC
UNIVERSIDADE
DE SANTIAGO
DE COMPOSTELA

PhD CANDIDATE STATEMENT

Miss **María Vivero López**

PhD Thesis: **Prophylaxis and topical treatment of infections associated to hearing aids and contact lenses**

I submit my Doctoral Thesis, following the procedure according to the Regulation, stating that:

1) This Thesis gathers the results corresponding to my work.
2) When necessary, explicit mention is given to the collaborations the work may have had.
3) The present document is the final version submitted for its defense and coincides with the document sent in electronic format.
4) I confirm that the Thesis does not incur in any plagiarism of any other authors or documents submitted by me for obtaining other degrees.

At **Santiago de Compostela**, on **January 17th 2022**

Sgd. María Vivero López

USC
UNIVERSIDADE
DE SANTIAGO
DE COMPOSTELA

DECLARACIÓN DO AUTOR/A DA TESE

D./Dna **María Vivero López**

Título da tese: **Prophylaxis and topical treatment of infections associated to hearing aids and contact lenses**

Presento a miña tese, seguindo o procedemento axeitado ao Regulamento, e declaro que:

1) A tese abarca os resultados da elaboración do meu traballo.
2) De ser o caso, na tese faise referencia ás colaboracións que tivo este traballo.
3) Confirmo que a tese non incorre en ningún tipo de plaxio doutros autores nin de traballos presentados por min para a obtención doutros títulos.
4) A tese é a versión definitiva presentada para a súa defensa e coincide a versión impresa coa presentada en formato electrónico.

E comprométome a presentar o Compromiso Documental de Supervisión no caso de que o orixinal non estea na Escola.

En **Santiago de Compostela**, **17 de Xaneiro de 2022**

Asinado. María Vivero López

USC
UNIVERSIDADE
DE SANTIAGO
DE COMPOSTELA

Index

RESUMO **3**

1. INTRODUCTION **19**

1.1 MEDICAL DEVICES 20

1.1.1 Risks associated to the use of medical devices 26

1.2 COMBINATION PRODUCTS 34

1.2.1 Methods to add drugs to medical devices 37

1.3 HEARING AIDS 41

1.3.1 Ear infections and hearing aid-related biofilms 50

1.4 CONTACT LENSES 53

1.4.1 CLs for vision correction 53

1.4.1.1 Eye infections and CL-related biofilms 58

1.4.2 CLs for drug delivery 64

1.5 REFERENCES 71

2. AIMS **91**

3. ANTI-BIOFILM MULTI DRUG-LOADED 3D PRINTED HEARING AIDS **99**

3.1 INTRODUCTION 99

3.2 MATERIALS AND METHODS 103

3.2.1 Materials 103

3.2.2 Preparation of photopolymer solutions 104

3.2.3 3D printing process 105

3.2.4 Determination of hearing aids morphology 105

3.2.5 Scanning electron microscopy (SEM) 106

USC
UNIVERSIDADE DE SANTIAGO DE COMPOSTELA

3.2.6 X-ray powder diffraction (XRPD) 106
3.2.7 Thermal analysis 106
3.2.8 X-ray micro computed tomography (micro-CT) 106
3.2.9 Water contact angle 107
3.2.10 Mechanical evaluation of the slabs 107
3.2.11 Hemolytic activity 108
3.2.12 Anti-biofilm properties 109
3.2.12.1 Bacterial strains and growth conditions 109
3.2.12.2 Culture media preparation 109
3.2.12.3 AAA model preparation 109
3.2.12.4 Pre-inoculum and inoculum preparation 110
3.2.12.5 Plates preparation and incubation 111
3.2.12.6 Biofilm susceptibility 111
3.2.13 Drug release studies 112
3.2.14 Statistical analysis 113
3.3 RESULTS AND DISCUSSION 113
3.3.1 DLP 3D printing 113
3.3.2 Physical characterization of the 3D printed slabs 115
3.3.3 Mechanical evaluation 121
3.3.4 Hemolytic activity 123
3.3.5 Anti-biofilm properties 123
3.3.6 Drug-release studies 128
3.4 CONCLUSIONS 133
3.5 REFERENCES 134
4. RESVERATROL-LOADED HYDROGEL CONTACT LENSES WITH ANTIOXIDANT AND ANTIBIOFILM PERFORMANCE 147
USC
UNIVERSIDADE DE SANTIAGO DE COMPOSTELA

4.1 INTRODUCTION 147
4.2 MATERIALS AND METHODS 151
4.2.1 Materials 151
4.2.2 Hydrogel synthesis 153
4.2.3 Water uptake 154
4.2.4 Transmittance 154
4.2.5 Wettability 155
4.2.6 Mechanical properties 156
4.2.7 Resveratrol loading and release tests 156
4.2.8 Resveratrol stability 158
4.2.9 *Ex vivo* corneal and scleral permeability tests 159
4.2.10 HET-CAM test 161
4.2.11 Protein adsorption 161
4.2.12 Antibiofilm properties 162
4.2.12.1 Bacterial strains and growth conditions 163
4.2.12.2 Pre-inocula and inocula preparion 164
4.2.12.3 AAA model preparation and incubation 164
4.2.12.4 Biofilm susceptibility 165
4.2.13 Antioxidant properties 166
4.2.14 Statistical analysis 167
4.3 RESULTS AND DISCUSSION 167
4.3.1 Hydrogel synthesis 167
4.3.2 Water uptake and wettability 168
4.3.3 Light transmission 173
4.3.4 Mechanical properties 176
4.3.5 Resveratrol loading and release 176

USC
UNIVERSIDADE DE SANTIAGO DE COMPOSTELA

4.3.6 Resveratrol stability 180
4.3.7 Corneal and scleral permeability 182
4.3.8 HET-CAM test 184
4.3.9 Protein adsorption 185
4.3.10 Antibiofilm properties 193
4.3.11 Antioxidant properties 200
4.4 CONCLUSIONS 204
4.5 REFERENCES 205
5. RESVERATROL-LOADED CONTACT LENSES: *IN VITRO* RELEASE AND *IN VIVO* PERFORMANCE 219
5.1 INTRODUCTION 219
5.2 MATERIALS AND METHODS 222
5.2.1 Materials 222
5.2.2 Contact lenses preparation 223
5.2.3 Resveratrol loading and release tests 224
5.2.3.1 Loading of resveratrol in non-sterilized and sterilized CLs 224
5.2.3.3 *In vitro* release of resveratrol from loaded CLs 225
5.2.4 *In vivo* experiments: resveratrol released and accumulated in the ocular tissues 227
5.2.4.1 *In vivo* release 228
5.2.4.2 Quantification of resveratrol in the tear fluid 229
5.2.4.3 Quantification of resveratrol in the ocular tissues 230
5.2.4.4 Quantification of the antioxidant activity of resveratrol remaining in CLs after the *in vivo* wearing 231
5.2.5 Statistical analysis 232
5.3. RESULTS AND DISCUSSION 232
5.3.1. Contact lenses preparation and resveratrol loading 232
USC UNIVERSIDADE DE SANTIAGO DE COMPOSTELA

5.3.2 Release of resveratrol from loaded CLs 234
5.3.3*In vivo* experiments: resveratrol released and accumulated in the ocular tissues 239
5.3.4 Antioxidant activity of resveratrol in worn CL 244
5.3.5 *In vivo – in vitro* correlations (IVIVC) 245
5.4 CONCLUSIONS 248
5.5 REFERENCES 249
6. PLURONIC®/CASEIN MIXED MICELLES FOR OPHTHALMIC DELIVERY OF RESVERATROL 259
6.1 INTRODUCTION 259
6.2 MATERIALS AND METHODS 265
6.2.1 Materials 265
6.2.2 Single and mixed micelles preparation 266
6.2.3 Micelle size, Z-potential and pH 267
6.2.4 Solubility study 268
6.2.5 Stability of loaded and not loaded micelles 269
6.2.6 Rheological behavior 270
6.2.7 HET-CAM test and zebrafish embryo toxicity test 270
6.2.8 Antioxidant properties 271
6.2.9 Ability to inhibit bacterial growth 272
6.2.9.1 Bacterial strains and growth conditions 272
6.2.9.2 Pre-inocula and inocula preparation 273
6.2.9.3 Plates preparation and incubation 273
6.2.10 *Ex vivo* corneal and scleral permeability tests 274
6.2.11 Statistical analysis 276
6.3 RESULTS AND DISCUSSION 276
USC UNIVERSIDADE DE SANTIAGO DE COMPOSTELA

6.3.1. Micelles preparation 276
6.3.2 Micelle size, zeta potential and pH 277
6.3.3 Solubility study 282
6.3.4 Stability of loaded and not loaded micelles 285
6.3.5 Rheological behavior 288
6.3.6 HET-CAM test and zebra fish model 290
6.3.7 Antioxidant properties 294
6.3.8 Ability to inhibit bacterial growth 297
6.3.9 Ex vivo corneal and scleral permeability tests 304
6.4. CONCLUSIONS 308
6.5 REFERENCES 309
7. CONCLUSIONS 325
ANNEXES 331

USC
UNIVERSIDADE DE SANTIAGO DE COMPOSTELA

Resumo

USC
UNIVERSIDADE
DE SANTIAGO
DE COMPOSTELA

USC
UNIVERSIDADE
DE SANTIAGO
DE COMPOSTELA

RESUMO

Os produtos sanitarios téñense convertido nunha parte esencial da atención médica moderna, xogando un papel esencial nos procedementos diagnósticos e terapéuticos comúns e no manexo de pacientes críticos. O seu uso estase a incrementar polas prestacións que ofrecen como substitutos físicos ou funcionais de órganos, e tamén polo envellecemento da poboación que demanda ferramentas que permitan manter a calidade de vida durante máis tempo. Non obstante, os produtos sanitarios de inserción e implantación teñen un risco inherente de provocar reaccións adversas a corpo estraño (resposta inflamatoria que pode producir a encapsulación por fibrose) ou outros efectos secundarios derivados da adhesión das proteínas e células do hóspede ou da proliferación de microorganismos.

O coñecemento dos eventos que ocorren na interface sólido-líquido cando un material se coloca no medio biolóxico é fundamental para o deseño adecuado do produto sanitario en canto á funcionalidade e durabilidade. O sistema inmunitario dos mamíferos está adestrado para detectar e eliminar materiais non propios, principalmente microorganismos. Polo tanto, calquera estrutura estraña que teña unha composición ou patrón non esperado induce unha reacción inmune dirixida a eliminar a estrutura estraña ou as células afectadas se a estrutura xa penetrou nelas. Este mecanismo defensivo funciona

USC
UNIVERSIDADE DE SANTIAGO DE COMPOSTELA

bastante ben contra pequenos microorganismos pero pode fallar contra entidades resistentes a fagolisosomas e grandes corpos estraños. A superficie dos produtos sanitarios constitúe un sustrato idóneo para a adhesión de células e proteínas do portador e tamén de microorganismos. Cando un produto sanitario é implantado no organismo comezan a adherirse na súa superficie proteínas; a natureza e proporción relativas das proteínas determina que se activen as células do hospedador para dar lugar a unha reacción de corpo estraño ou que se poidan adherir microorganismos, que proceden da contaminación coa pel do paciente ou que poden migrar desde outros puntos do organismo. A colonización por microorganismos é un proceso moi rápido e da lugar a secreción de exopolisacáridos que os protexen formando biofilmes. As bacterias cando se atopan formando parte dun biofilme son moito máis resistentes ó sistema inmune e tamén aos diferentes tratamentos antimicrobianos que cando se atopan en forma sésil. No biofilme os mecanismos de comunicación entre as bacterias, coñecidos coma *Quorum Sensing*, fan que éstas sufran cambios xenéticos para actuar como unha comunidade moi coordinada, cun metabolismo máis baixo, sendo menos susceptibles ós antibióticos. Ademais, o biofilme actúa como unha barreira física que dificulta ó acceso dos macrófagos e dos fármacos antimicrobianos ó seu interior. Unha vez instaurado un biofilme é moi difícil de erradicar, polo que é importante a prevención.

Os dispositivos implantables son considerados refuxio para bacterias oportunistas e son responsables de case o 50% de todas as infeccións nosocomiais, que están asociadas a unha considerable morbilidade e mortalidade. Aínda que o risco de infección vai diminuíndo lentamente debido á aplicación de medidas hixiénicas e profilácticas extremas, o aumento do uso de dispositivos médicos debido ao envellecemento da poboación e a crecente incidencia de

USC
UNIVERSIDADE DE SANTIAGO DE COMPOSTELA

enfermidades crónicas dexenerativas fan que as infeccións asociadas aos ser unha preocupación sanitaria moi relevante. Os audiófonos e as lentes de contacto non son unha excepción.

Os audiófonos e as lentes de contacto atópanse entre os produtos sanitarios máis empregados nos países desenvolvidos xa que permiten dar resposta a unha ampla variedade de problemas auditivos ou visuais a calquera idade. De feito estímase que no mundo hai 72 millóns de persoas que precisan audiófonos e máis de 140 millóns de usuarios de lentes de contacto. Para ambos tipos de dispositivos prevese un incremento progresivo no futuro dadas as melloras que se están a facer continuamente no seu deseño e ó abano crecente de posibilidades terapéuticas que ofrecen. Sen embargo, a pesar de todas estas melloras, focalizadas principalmente en aportar unha maior comodidade ao usuario, a incidencia de infeccións asociadas ao seu uso continuado é moi alta. Ademais, as infeccións asociadas ós produtos sanitarios non só obrigan a interromper o seu uso temporalmente senón que, en moitos casos, supoñen o seu abandono permanente. Adicionalmente, os procesos infecciosos poden representar un risco moi importante para a saúde dos usuarios.

As infeccións de oído son unha causa importante de perda de audición temporal. Por outra banda, o uso continuado de audiófonos da lugar a un aumento da temperatura e da humidade na canle auditiva o cal pode alterar a microbiota e incrementar a formación de biofilmes na superficie dos audiófonos, aumentando a súa vez o risco de otite tanto de orixe bacteriano como fúnxico.

No caso das lentes de contacto nos últimos anos, a incidencia de infeccións oculares asociadas non diminuíu. Aproximadamente 4,2 de cada 10.000 usuarios padece queratite microbiana, unha infección ocular severa que pode ocasionar incluso cegueira. As lentes de

USC
UNIVERSIDADE DE SANTIAGO DE COMPOSTELA

contacto continúan sendo o principal factor de risco para o desenvolvemento destas infeccións dada a idoneidade da súa superficie para a formación de biofilmes. Ademais unha vez que se forma o biofilme éste comeza a liberar células sésiles e endotoxinas que poden danar a superficie corneal.

Tanto no caso dos audiófonos coma das lentes de contacto, as dúas bacterias responsables en maior medida da formación de biofilmes son a Gram-positiva *Staphylococcus aureus* e a Gram-negativa *Pseudomonas aeruginosa.*

Por todo isto, cando se leva a cabo o deseño dun novo produto sanitario é moi importante minimizar o risco de efectos adversos orixinados por reacción do organismo a ese corpo estraño e de posibles infeccións. Unha posible estratexia é deseñar produtos sanitarios de combinación cargados con fármacos con capacidade de inhibir o crecemento microbiano ou erradicar infeccións xa existentes. Os fármacos poden incorporarse na superficie do produto sanitario, mediante inmobilización covalente do fármaco, recubrimentos poliméricos, ou enxerto de redes poliméricas, ou poden disporse no entramado do biomaterial, incorporándoos á súa composición durante a fabricación ou por inmersión do produto sanitario nunha disolución co fármaco de interese. A técnica empregada para a preparación do produto de combinación fármaco-produto sanitario depende en gran medida da natureza do fármaco e do produto sanitario así como das funcións que vaia desenrolar o produto sanitario final posto que a incorporación do fármaco non pode ocasionar ningún detrimento na función propia do produto sanitario, e o fármaco debe cumprir coa súa función terapéutica xerando un perfil de cesión adecuado ao contexto clínico particular.

USC
UNIVERSIDADE DE SANTIAGO DE COMPOSTELA

Considerando todo o dito anteriormente, o obxectivo xeral desta Tese de Doutoramento foi explorar a viabilidade de cargar audiófonos e lentes de contacto con substancias capaces de prever a formación de biofilmes ou combater as infeccións xa preestablecidas.

De acordo con este obxectivo, o traballo desenvolveuse en catro etapas cos resultados que se resumen de seguido.

1) Preparación de audiófonos por impresión 3D cargados con fármacos empregados no tratamento tópico convencional das infeccións auditivas. Máis do 99% dos audiófonos que se adaptan á canle auditiva do usuario fabrícanse a medida empregando técnicas de impresión 3D, principalmente a tecnoloxía de fotopolimerización en cuba. A impresión 3D por fotopolimerización é unha das técnicas máis empregadas xa que presenta unha elevada precisión conseguindo obter produtos sanitarios personalizados cun alto grao de detalle que encaixan á perfección coas peculiaridades anatómicas de cada paciente. Demostrouse que este axuste perfecto é fundamental para mellorar os resultados acadados. Sen embargo, o uso continuado dos audiófonos, como se explicou anteriormente, facilita o crecemento de fungos e bacterias tanto na superficie do dispositivo coma no tecido do hóspede desencadeando otite externa. O tratamento convencional desta patoloxía require a interrupción no uso do audiófono coas conseguintes limitacións asociadas para a capacidade auditiva do paciente. As persoas que non empregan audiófonos tamén poden padecer infeccións de oído e, ademais, as propias infeccións auditivas son unha das principais causas de perda auditiva. As persoas con infeccións auditivas poderían beneficiarse do uso dun produto sanitario que liberase de forma sostida a medicación durante os días necesarios de tratamento sen necesidade da instilación frecuente que exixen as gotas óticas, o cal expande a súa utilidade a persoas normoauditivas que ocasionalmente sofren de infeccións de oído

USC UNIVERSIDADE DE SANTIAGO DE COMPOSTELA

empregando dispositivos que só imitan a morfoloxía do audiófono, pero que non incorporan ningunha mellora na capacidade auditiva.

Por iso, co obxectivo de diminuír a taxa de infeccións asociadas ao uso de audiófonos así como garantir o seu uso ininterrompido e tratar as infección auditivas, na primeira etapa da Tese, avaliouse a posibilidade de engadir cantidades terapéuticas de ciprofloxacino e acetónido de fluocinolona, dous dos fármacos máis empregados no tratamento tópico das otites, ás resinas empregadas comunmente na fabricación de audiófonos por fotopolimeración 3D. Os dous fármacos empregados se escolleron atendendo a súa utilidade no manexo das infeccións a nivel clínico e á eficacia mellorada demostrada da combinación dun antibiótico (ciprofloxacino) cun corticosteroide (acetónido de fluocinolona). Ambos fármacos foron engadidos, por primeira vez, xuntos e ao mesmo tempo na mesma resina. Fabricáronse audiófonos empregando resinas comerciais as que se lles incorporou ciprofloxacino e acetónido de fluocinolona nas proporcións 6:0.5 e 12:1 % p/p e se estudou o seu efecto sobre a imprimibilidade e as propiedades mecánicas dos audiófonos xunto coa súa capacidade para prover unha cesión sostida de ambos fármacos. Ademais, avaliouse a capacidade dos audiófonos xerados para impedir a formación de biofilmes de *S. aureus* (Gram-positivo) e *P. aeruginosa* (Gram-negativo).

A incorporación de ambos fármacos nos dispositivos non afectou ás súas propiedades mecánicas sendo estas moi similares ás dos homólogos sen fármaco. Todos os audiófonos cargados presentaron unha superficie hidrofílica, excelente hemocompatibilidade e unha elevada actividade antibiofilm frente ambas bacterias. Ademais, os audiófonos cargados cun 6% de ciprofloxacino e un 0.5% de acetónido de fluocinolona mantiveron unha cesión sostida de ambos fármacos durante máis de sete días e inhibiron non só a formación de

USC UNIVERSIDADE DE SANTIAGO DE COMPOSTELA

biofilm na superficie senón tamén o crecemento bacteriano no medio de cultivo circundante. Esta etapa do traballo levouse a cabo coa colaboración dos grupos do Prof. Abdul W. Basit do University College of London e da Prof. Ana Otero da Universidade de Santiago de Compostela.

2) Deseño de lentes de contacto con capacidade antibiofilm mediante a combinación de monómeros antibiofouling e de axentes antioxidantes naturais con capacidade antimicrobiana. A pesar da evolución dos materiais empregados para preparar lentes de contacto que sexan cada vez máis confortables e ofrezan unha mellor agudeza visual, o risco de que se formen biofilmes na superficie das lentes de contacto non diminuíu. Os hidroxeles empregados na síntese de lentes de contacto son moi propensos á colonización por diversos microorganismos presentes tanto nos dedos durante a inserción como na superficie ocular. Os depósitos de proteínas procedentes do fluído lacrimal promoven a adhesión bacteriana o cal pode levar a formación de biofilmes co uso continuado. De feito, o uso de lentes de contacto continúa a ser o principal factor de risco para o desenvolvemento de queratite microbiana, que a súa vez é unha das principais causas de abandono das lentes de contacto. Non se recomenda o uso profiláctico de antibióticos xa que un uso pouco específico altera a microbiota normal, fomenta a aparición de resistencias bacterianas e causa toxicidade nos tecidos do segmento anterior do ollo. Tense demostrado que os monómeros bioinspirados no grupo fosforilcolina, típico dos fosfolípidos presentes na membrana celular, proporcionan superficies resistentes á adsorción de proteínas. Ata agora, só unha lente de contacto comercial, Proclear®, inclúe 2-metacriloxietil fosforilcolina (MPC) para mellorar a humectabilidade e o confort. Como alternativa ao uso de antibióticos, os compostos naturais que poden actuar como inhibidores da formación de biofilmes están

USC UNIVERSIDADE DE SANTIAGO DE COMPOSTELA

gañando interese. Neste sentido, o resveratrol, un polifenol natural con actividade antioxidante e con boa tolerancia ocular, interfire *in vitro* co proceso de comunicación bacteriana coñecido como *Quorum Sensing* e inhibe a formación de biofilmes por parte de bacterias clinicamente relevantes como *P. aeruginosa* ou *S. aureus.* Ademais, asociado á súa actividade antioxidante, o resveratrol pode axudar na prevención de diversas enfermidades oculares e na curación de células dañadas do epitelio corneal.

Polo tanto, a segunda parte da Tese baseouse na hipótese de que o deseño de hidroxeles con MPC e a incorporación de resveratrol na súa estrutura podía dar lugar a sinerxias en canto á prevención da formación de biofilmes nas lentes de contacto, mentres que o resveratrol tamén podía producir outros efectos beneficiosos relacionados coa súa capacidade antioxidante. Polo tanto, o obxectivo da segunda parte da Tese foi preparar lentes de contacto hidroxel e hidroxel de silicona con MPC e cargalas con resveratrol co fin de diminuír a incidencia de infeccións oculares e mellorar a saúde ocular en patoloxías relacionadas co estrés oxidativo. Para levar a cabo o traballo, se prepararon hidroxeles incorporando o monómero MPC na mestura de monómeros cubrindo un amplio rango de concentracións (0 – 101 mM) e posteriormente se levou a cabo á carga dos mesmos con resveratrol. Avaliáronse os perfiles de carga e cesión de resveratrol, a biocompatibilidade ocular dos hidroxeles mediante o ensaio da membrana coroalantoidea de ovo de galiña (HET-CAM) e levouse a cabo unha ampla caracterización dos materiais que incluíu a avaliación da adsorción de proteínas, da actividade antioxidante e da capacidade para inhibir a formación de biofilmes sobre as lentes de contacto. Os resultados acadados foron comparados cos das lentes Proclear® de uso diario.

USC
UNIVERSIDADE DE SANTIAGO DE COMPOSTELA

Os hidroxeles de HEMA, en comparación cos hidroxeles de silicona, cargaron cantidades menores de resveratrol, pero puideron ceder practicamente a dose total cargada evitando a unión irreversible observada nos hidroxeles de silicona. Ademais demostrouse que o resveratrol mantén as súas propiedades antioxidantes tra-la súa carga e cesión desde os hidroxeles. Os ensaios levados a cabo *ex vivo*, mostraron que o resveratrol pode acumularse tanto en córnea como en esclera. Parte deste traballo levouse a cabo en colaboración co grupo da Prof. Ana Paula Serro do Instituto Superior Técnico, Universidade de Lisboa, no que a doutoranda levou a cabo unha estadía de tres meses.

3) Optimización das lentes de contacto con MPC incorporado e avaliación do proceso de cesión *in vivo*, da penetración nos diferentes tecidos oculares do resveratrol, e posibilidade de obter correlacións *in vivo - in vitro* (IVIVC). A hipótese da terceira etapa da Tese foi que un incremento no contido en MPC das lentes de contacto podería aumentar a cantidade de resveratrol cargada e cedida, incrementando a capacidade antioxidante e inhibitoria da formación de biofilmes. Deste xeito, aumentaría a utilidade das lentes no tratamento e a prevención de infeccións oculares e patoloxías asociadas co estrés oxidativo. As lentes de contacto melloradas poderían prover unha cesión sostida do resveratrol na superficie corneal impedindo a súa eliminación prematura e facilitando o seu acceso aos tecidos posteriores do ollo. Espérase tamén que as lentes preserven a capacidade antioxidante propia do resveratrol durante o tempo no que a lente está exposta á luz do día.

Para levar a cabo o traballo, preparáronse lentes de contacto a base de HEMA con unha proporción en MPC 3.8 veces superior ao acadado na anterior etapa da Tese e ao que presentan as lentes de contacto Proclear®. Avaliáronse os perfiles de carga e cesión de

USC UNIVERSIDADE DE SANTIAGO DE COMPOSTELA

resveratrol antes e despois da esterilización das lentes por autoclave. A esterilización do material non afectou á carga do resveratrol, sen embargo as lentes autoclavadas proporcionaron unha cesión máis sostida do fármaco en relación ás non esterilizadas. En calquera caso, a cantidade de resveratrol liberada foi superior á obtida na anterior etapa da Tese. Os estudios de cesión *in vitro* leváronse a cabo en ausencia e en presencia de lisozima e albúmina, dúas proteínas comunmente presentes no fluído lacrimal. A lisozima non modificou os perfís, pero a albúmina deu lugar a unha marcada ralentización da cesión.

A continuación, unha vez superados con éxito os métodos alternativos e cumprindo cos principios das 3Rs, planificouse un ensaio *in vivo* en coellos branco de New Zeeland para determinar a seguridade e a tolerancia ocular das lentes de contacto deseñadas e a acumulación de resveratrol nos distintos tecidos oculares. Coma control empregouse unha dispersión de Pluronic® cargada con 4 mg/mL de resveratrol. Esta parte do traballo levouse a cabo en colaboración co equipo do Prof. Gonzalo Carracedo de Ocupharm e da Universidade Complutense de Madrid, co correspondente permiso do Comité de Ética e cumprindo as guías de ARVO e ARRIVE.

Tódalas formulación foron ben toleradas *in vivo* e a maior concentración de resveratrol no fluido lacrimal obtívose 5 minutos tras a administración dunha soa gota da dispersión micelar. Despois, a concentración no fluido lacrimal foi caendo ata as 4 h do experimento. As lentes de contacto proporcionaron concentracións iniciais máximas máis baixas de resveratrol, pero os niveis foron significativamente mais altos entre as 2 e 6 horas, en comparación coa dispersión micelar. A avaliación da biodistribución do resveratrol puxo de manifesto que todas as formulacións ensaiadas permiten que alcance a córnea, o humor acuoso, o cristalino, o humor vítreo, a esclera e a retina. Non

USC UNIVERSIDADE DE SANTIAGO DE COMPOSTELA

obstante, os niveis acadados en córnea, humor acuoso e esclera tras oito horas de inserción da lente de contacto foron moi superiores os obtidos coa dispersión micelar. A actividade antioxidante do resveratrol extraído das lentes de contacto ó cabo de 8 horas do ensaio *in vivo* mostrou a capacidade do biomaterial para protexer ao resveratrol da fotodegradación e mantear a súa actividade antioxidante.

Finalmente, a construción do gráfico de Levy coa fin de por de manifesto correlacións *in vivo* - *in vitro* (IVIVC) mostrou que despois dun tempo de retardo inicial, a cesión *in vivo* prodúcese máis rápidamente que *in vitro* nas condicións ensaiadas. Atopouse unha forte correlación entre as porcentaxes de resveratrol cedidas *in vivo* e *in vitro*. En suma, as lentes de contacto preparadas con alta proporción en MPC móstranse como plataformas axeitadas para a liberación sostida de resveratrol destinadas a abordar enfermidades oculares que afectan ao segmento anterior e posterior do ollo e que requiren un manexo antimicrobiano e antioxidante.

4) Deseño de micelas poliméricas cargadas con resveratrol que poidan reforzar os resultados terapéuticos acadados previamente tanto cos audiófonos como coas lentes de contacto. Demostrouse que o resveratrol mellora os efectos citotóxicos dos antibióticos nas células do hóspede. Ademais, o seu poder antioxidante pode aproveitarse para o tratamento de diversas enfermidades oculares relacionas con niveis elevados de estrés oxidativo, como os desencadeados pola exposición prolongada á luz solar e a hiperglicemia. O estrés oxidativo e a inflamación desempeñan un papel fudamental no inicio e na progresión de diversas patoloxías oculares relacionadas coa idade, como os trastornos da superficie (queratocono e ectasia corneal), a dexeneración macular (DMAE), a retinopatía diabética (RD), as cataratas, o glaucoma e a uveíte, as cales poden levar á perda

USC UNIVERSIDADE DE SANTIAGO DE COMPOSTELA

progresiva da visión e á cegueira sen o tratamento adecuado. As micelas poliméricas téñense posicionado como nanotransportadores capaces de protexer e incrementar a solubilidade de axentes lábiles como o resveratrol e de superar as barreiras biolóxicas que se opoñen á penetración dos fármacos nas estruturas máis internas do ollo. Ademais dos copolímeros sintéticos, as micelas naturais de proteínas do leite están atraendo cada vez máis atención como nanotransportadores de fármacos xa que combinan fontes naturais amplamente dispoñibles, capacidades de transportar moléculas pouco solubles (transportadores naturais de fosfato cálcico) e capacidade para eliminar radicais libres. Ata o momento inda non se investigou a encapsulación de resveratrol e outros compostos en micelas de caseina para administración mucosal (ocular, ótica).

En consecuencia, a última parte da Tese centrouse na preparación de micelas simples de Pluronic® e caseína e de micelas mixtas de ambos compostos, co obxectivo de dilucidar se a formación de micelas mixtas podería mellorar o rendemento do sistema de transporte en termos de estabilidade física das micelas, capacidade de carga de resveratrol, características antioxidantes, gelificación *in situ*, permeabilidade *ex vivo* e capacidade para inhibir a formación de biofilmes. A biocompatibilidade ocular avaliuose no HET-CAM e tamén no modelo de embrión de peixe cebra (FET), en colaboración co grupo da Profa. Laura Sánchez Piñón da USC. Por último, a formulación mais adecuada probouse nun modelo de coello ao igual que as lentes deseñas na anterior etapa.

O desenvolvemento de diferentes micelas simples e mixtas compostas por Pluronic® F127 e Pluronic® F127/caseína foi levado a cabo exitosamente. O tamaño das micelas mixtas sen resveratrol aumentou co incremento do contido en Pluronic®, e a carga de resveratrol non afectou ao tamaño das micelas simples. O potencial Z

USC UNIVERSIDADE DE SANTIAGO DE COMPOSTELA

das micelas simples foi cercano a cero, pero negativo para as micelas de caseína. Os valores de pH rexistrados aproximáronse aos valores fisiolóxicos da lágrima o que pode garantir unha boa tolerancia ocular e a estabilidade do resveratrol. A boa tolerancia ocular e a non toxicidade das formulacións máis prometedoras confirmouse por medio das probas HET-CAM e FET. Tamén se demostrou a capacidade de xelificación in situ das formulacións con maior contido en Pluronic® que podería aumentar o tempo de residencia na superficie ocular e a permeabilidade a través dos diferentes tecidos oculares. De feito as micelas facilitaron a penetración do resveratrol a través dos tecidos corneais e esclerais en ensaios *ex vivo* (tecido porcino). Ademais, as formulacións deseñadas aumentaron significativamente a solubilidade do resveratrol e mostraron unha adecuada estabilidade química e física durante un mes de almacenamento a 4 °C protexido da luz. O ensaio antioxidante demostrou a capacidade dos sistemas para cargar e liberar resveratrol sen interferir na súa actividade antioxidante. Tamén se demonstrou a capacidade das micelas simples cun maior contido en resveratrol para inhibir o crecemento de *S. aureus.*

No seu conxunto os resultados acadados nesta Tese Doutoral abren novas portas para o desenvolvemento de produtos de combinación fármaco-produto sanitario que aúnen unha maior comodidade para o paciente e capacidade para previr a formación de filmes bacterianos xunto coa posibilidade de ceder de forma sostida fármacos que reforcen esa capacidade antimicrobiana e que incluso presenten outras propiedades útiles no tratamento de diversas patoloxías óticas e oculares.

USC
UNIVERSIDADE DE SANTIAGO DE COMPOSTELA

USC
UNIVERSIDADE
DE SANTIAGO
DE COMPOSTELA

USC
UNIVERSIDADE
DE SANTIAGO
DE COMPOSTELA

Introduction

The work described in this chapter was published in part in **Bioinspired Hydrogels for Drug-eluting Contact Lenses**, *Acta Biomaterialia* 84, 49-62, 2019, authored by

Carmen Alvarez-Lorenzo[a], Soledad Anguiano-Igea[b], Angela Varela-García[a,b], María Vivero-Lopez[a], and Angel Concheiro[a]

[a] Departamento de Farmacología, Farmacia y Tecnología Farmacéutica, R+D Pharma Group (GI-1645), Facultad de Farmacia and Health Research Institute of Santiago de Compostela (IDIS), Universidade de Santiago de Compostela, 15782 Santiago de Compostela, Spain

[b]HGBeyond Materials Science S.L., Edificio Emprendia, Campus Vida s/n, 15782 Santiago de Compostela, Spain

USC
UNIVERSIDADE DE SANTIAGO DE COMPOSTELA

USC
UNIVERSIDADE
DE SANTIAGO
DE COMPOSTELA

USC
UNIVERSIDADE
DE SANTIAGO
DE COMPOSTELA

1. INTRODUCTION

Medical devices have become an essential part of the modern medical care, playing an important role in common diagnostic and therapeutic procedures and in the management of critically ill patients. Nevertheless, their use has an inherent risk of causing adverse foreign-body reactions (inflammatory response that may result in the encapsulation by fibrosis) or other side-effects derived of the adherence of host proteins and cells or of the proliferation of microorganisms. Hearing aids and contact lenses (CLs) are not an exception. They are used every day by millions of people over the world, successfully counteracting hearing and sight disabilities. The quality of life of people of all range of ages may benefit from wearing hearing aids and CLs. Additionally, as novel functionalities are being added to these devices, in particular to CLs that can be designed to act in diagnosis and pharmacological treatment of ocular diseases, a raised number of wearers can be expected. Nevertheless, the benefits of the wearing are counterbalanced by an increasing risk of suffering infections. In the next sections, a general overview on medical devices and their classification is provided, followed by an overall assessment of the main risks and the feasibilities of being solved by means of a drug-device combination product. Then, hearing aids and CLs are introduced together with their main associated particular risks of infection and proposed solutions.

USC
UNIVERSIDADE DE SANTIAGO DE COMPOSTELA

1.1 MEDICAL DEVICES

Medical devices fit into the general scope of products or equipments intended for medical purposes different from those of a medicine. More specifically, Regulation (EU) 2017/745 of the European Parliament and of The Council of 5 April 2017 on Medical Devices considers medical device as *any instrument, apparatus, appliance, software, implant, reagent, material or other article intended by the manufacturer to be used, alone or in combination, for human beings for one or more of the following specific medical purposes:*

— diagnosis, prevention, monitoring, prediction, prognosis, treatment or alleviation of disease,

— diagnosis, monitoring, treatment, alleviation of, or compensation for, an injury or disability,

— investigation, replacement or modification of the anatomy or of a physiological or pathological process or state,

— providing information by means of in vitro examination of specimens derived from the human body, including organ, blood and tissue donations,

and which does not achieve its principal intended action by pharmacological, immunological or metabolic means, in or on the human body, but which may be assisted in its function by such means.

The following products shall also be deemed to be medical devices: devices for the control or support of conception; products specifically intended for the cleaning, disinfection or sterilisation of devices as referred to in Article 1(4) and of those referred to in the

USC UNIVERSIDADE DE SANTIAGO DE COMPOSTELA

first paragraph of this point [OJEU, 2017]. Similar definitions can be found in regulations that apply for other regions.

Thus, the definition of a medical device is very wide and comprises any tool for healthcare different from the medicines. Namely, medical devices are intended to perform their role through physical, electronic, mechanical or other means.

Classification of medical devices relies on the duration of use and the invasiveness of the device into the host. Duration is quantified in terms of "transient" when the continuous use is for less than 60 min, "short term" when intended to be used in the time range of 60 min to 30 days, and "long term" when the continuous use is for more than 30 days. The invasiveness is evaluated regarding the localization of the device in or on the human body and whether products (components or biodegradation substances) from the device may undergo systemic absorption. An invasive medical device is the one that penetrates (in whole or in part) inside the body through a natural body orifice (this includes the external surface of the eyeball) or through the body surface (in the context of a surgical operation or not).

Active devices and implantable devices deserve particular consideration. Active device means any device that requires a source of energy other than that generated by the human body to operate. Implantable device means any device, including those that are partially or wholly absorbed, which is intended to be either totally introduced into the human body or to replace an epithelial surface or the surface of the eye, by clinical intervention and to remain in place after the procedure, or partially introduced into the human body by clinical intervention and intended to remain in place after the procedure for at least 30 days. Examples of classification of non-invasive devices, invasive devices and active devices are provided in

USC
UNIVERSIDADE DE SANTIAGO DE COMPOSTELA

Tables 1.1 to **1.3**. Depending on the class different safety and performance requirement should be fulfilled.

Table 1.1. Classification of non-invasive devices according to Annex VIII of the Regulation (EU) 2017/745 of the European Parliament and of The Council of 5 April 2017 on Medical Devices [OJEU, 2017]. Information adapted by the author of this PhD Thesis.

Class	Rules
I	Devices intended to be used as a mechanical barrier, for compression or for absorption of exudates into contact with injured skin or mucous membrane. Any other non-invasive device except if it fits in the exceptions indicated below.
IIa	Devices intended to manage the micro-environment of injured skin or mucous membrane. Devices intended for channeling or storing blood, body liquids, cells or tissues, liquids or gases if they may be connected to a class IIa, class IIb or class III active device.
IIb	Devices for injuries to skin which have breached the dermis or mucous membrane and can only heal by secondary intent. Blood bags. Devices intended for modifying the biological or chemical composition of human tissues or cells, blood, other body liquids or other liquids intended for implantation or administration into the body.
III	Devices consisting of a substance or a mixture of substances intended to be used in vitro in direct contact with human cells, tissues or organs taken from the human body or used in vitro with human embryos before their implantation or administration into the body.

USC UNIVERSIDADE DE SANTIAGO DE COMPOSTELA

Table 1.2. Classification of invasive devices according to Annex VIII of the Regulation (EU) 2017/745 of the European Parliament and of The Council of 5 April 2017 on Medical Devices [OJEU, 2017] Information adapted by the author of this PhD Thesis.

Class	Rules
I	Invasive devices with respect to body orifices intended for transient use.
	Invasive devices with respect to body orifices intended for short-term use that are used in the oral cavity as far as the pharynx, in an ear canal up to the ear drum or in the nasal cavity.
	Reusable surgical instruments.
IIa	Invasive devices with respect to body orifices intended for short-term use, except those referred above.
	Invasive devices with respect to body orifices intended for long-term use that are used in the oral cavity as far as the pharynx, in an ear canal up to the ear drum or in the nasal cavity and are not liable to be absorbed by the mucous membrane.
	Invasive devices with respect to body orifices to administer medicinal products by inhalation (unless their mode of action has an essential impact on the efficacy and safety of the administered medicinal product or they are intended to treat life-threatening conditions, which are class IIb).
	All surgically invasive devices intended for transient use with the exceptions considered below.
	All surgically invasive devices intended for short-term with the exceptions considered below.
IIb	Invasive devices with respect to body orifices intended for long-term use, except those referred above.
	Surgically invasive devices intended to supply energy in the form of ionising radiation (for both transient use and short-term use).
	Surgically invasive devices that have a biological effect or are wholly or mainly absorbed (transient use).
	Surgically invasive devices intended to administer medicinal products by means of a delivery system, if such administration is done in a manner that is potentially hazardous (transient use) and for short-term administration.
	Surgically invasive devices intended for short-term use that undergo chemical change in the body (except if placed in the teeth, which are classified as class IIa).
	All implantable devices and long-term surgically invasive devices, with the exceptions detailed below.

USC UNIVERSIDADE DE SANTIAGO DE COMPOSTELA

	Surgically invasive devices intended for transient use or short-term use to control, diagnose, monitor or correct a defect of the heart or of the central circulatory system through direct contact with those parts of the body.
	Surgically invasive devices to be in direct contact with the heart or central circulatory system or the central nervous system (transient, short-term or long-term use).
	Implantable and surgically invasive devices that have a biological effect or are wholly or mainly absorbed (short-term or long-term use).
III	Implantable devices and long-term surgically invasive devices that undergo chemical change in the body (except if placed in the teeth, which are classified as class IIa).
	Implantable devices and long-term surgically invasive devices to administer medicinal products.
	Active implantable devices or their accessories.
	Breast implants or surgical meshes.
	Total or partial joint replacements.
	Spinal disc replacement implants or implantable devices that come into contact with the spinal column.

USC UNIVERSIDADE DE SANTIAGO DE COMPOSTELA

Table 1.3. Classification of active devices according to Annex VIII of the Regulation (EU) 2017/745 of the European Parliament and of The Council of 5 April 2017 on Medical Devices [OJEU, 2017]. Information adapted by the author of this PhD Thesis.

Class	Rules
IIa	All active therapeutic devices intended to administer or exchange energy, except for the cases described below. Active devices intended for diagnosis and monitoring; e.g. image in vivo distribution of radiopharmaceuticals. Exceptions are shown below. Software intended to monitor physiological processes, except for the cases described below. Active devices intended to administer and/or remove medicinal products, body liquids or other substances to or from the body (unless this is done in a manner that is potentially hazardous, which are classified as class IIb).
IIb	Active therapeutic devices that administer energy to or exchange energy with the human body in a potentially hazardous way. All active devices intended to emit ionizing radiation for therapeutic purposes, including devices which control or monitor such devices, or which directly influence their performance. Active devices intended for monitoring of vital physiological parameters and the nature of variations of those parameters is such that it could result in immediate danger to the patient, for instance variations in cardiac performance, respiration, activity of the central nervous system, or they are intended for diagnosis in clinical situations where the patient is in immediate danger. Software intended to provide information which is used to take decisions with diagnosis or therapeutic purposes and such decisions have an impact that may cause a serious deterioration of a person's state of health or a surgical intervention. Software intended for monitoring of vital physiological parameters, where the nature of variations of those parameters is such that it could result in immediate danger to the patient.
III	Active devices that are intended for controlling, monitoring or directly influencing the performance of active implantable devices. Software intended to provide information which is used to take decisions with diagnosis or therapeutic purposes and such decisions have an impact that may cause death or an irreversible deterioration of a person's state of health.

USC UNIVERSIDADE DE SANTIAGO DE COMPOSTELA

1.1.1 Risks associated to the use of medical devices

Medical devices should possess both surface and bulk properties that match the needs of their intended use. Mechanical behavior, optical properties, conductivity, degradability or chemical stability, which are mainly given by the bulk characteristics of the material, must be combined with surfaces capable of dealing with the host body environment, ensuring good performance of the medical device without causing adverse reactions. The knowledge of the events occurring at the solid-liquid interface when a material is placed in the biological environment is critical for the proper design and tailoring of the medical device regarding functionality and durability [Koo et al., 2021].

Mammalian immune system is trained to detect and remove non-self materials, mainly microorganisms. Therefore, any foreign structure bearing a strange composition or pattern induces an immune reaction aimed to remove the foreign structure or the affected cells if the structure already penetrated in them. This defensive mechanism works quite well against small microorganisms but may fail against phagolysosomal-resistant entities and large foreign bodies [Klopfleisch and Jung, 2017]. Medical devices are made with biomaterials that try either to avoid or to direct the reaction of the body. There are a variety of definitions of biomaterial; the most used one defines a biomaterial as *a substance that has been engineered to take a form which, alone or as part of a complex system, is used to direct, by control of interactions with components of living systems, the course of any therapeutic or diagnostic procedure* [Hudecki et al., 2019]. Biomaterials can be designed to be resorbable, i.e., degradable or soluble in the place of implantation, or to be nonresorbable (biostable). Also, biomaterials can be classified as inactive or inert if intended to cause null or minimal tissue response, and as active if

USC UNIVERSIDADE DE SANTIAGO DE COMPOSTELA

designed to interact with or integrate in the surrounding tissue. In any case, all medical devices intended to be in contact with human body should be biocompatible; namely, the response of the host cannot trigger adverse events on the medical device and on the own organism. The biocompatibility is also considered to depend on the health condition of the host and may be specific of the implantation site [Patel and Gohil, 2012].

Foreign body reactions occur in five phases [Klopfleisch and Jung, 2017]:

(i) *Protein adsorption.* It is assumed that as soon as a medical device is inserted or implanted, a race for colonizing its surface starts. The initial protein adsorption onto a biomaterial surface plays a key role in what cells and/or microorganisms colonize the surface and how the body responds to an implanted biomaterial [Pavithra and Doble, 2008]. The cells interact with the provisional protein matrix rather than the surface of the biomaterial. The early step in the protein adsorption is determined by the Vroman effect [Vroman et al., 1980]. This step involves rapid adsorption of high mobility proteins, like albumin, and subsequent replacement by proteins with higher affinity for the specific surface, like fibrinogen, fibronectin or vitronectin. In contact with serum, the adsorption ratio of albumin and fibrinogen is similar to their proportion in the serum. Adsorption of fibronectin and vitronectin facilitates monocyte adhesion and giant cell formation. Additionally, the activation of the complement system causes the release of chemoattractants for phagocytes and the triggering of inflammation and other adverse events. Biomaterials with charged and rough surfaces are more prone to protein adsorption. Also, biomaterials that are stiffer (higher elastic modulus) than the host tissue cause stress to the tissue during movement, which may lead to

USC UNIVERSIDADE DE SANTIAGO DE COMPOSTELA

pro-inflammatory signals and fibrotic capsule [Hilborn and Bjursten 2017].

(ii) *Acute inflammation*. This is a short (few days) phase in which polymorphonuclear leukocytes (PMN) and mast cells arrive to the implantation site. PMN and neutrophiles are activated and degranulate, which attracts more leukocytes, including macrophages. Since the neutrophiles fail in the phagocytosis of the medical device and there is a high concentration in reactive oxygen species (ROS), the medium becomes highly pro-inflammatory and the inflammation may turn into chronic. To minimize acute inflammation the biomaterial should adsorb the less proteins as possible but also its surface should not contain hydrophobic micro- or nano-regions that can perform as Toll-like receptors for PMN and macrophages [Bryers et al., 2012].

(iii) *Chronic inflammation*. This step is characterized by attraction of lymphocytes and monocytes, but foreign body giant cells and fibrous capsule are still not formed. Chemoattractants released in the former step attract monocytes and macrophages, and the binding to the protein layer covering the biomaterial causes the activation of these cells. Depending on the phenotype of the activated macrophages different outcomes can be observed **(Figure 1.1A)** [Rosman et al., 2021]. M1 macrophages are pro-inflammatory and attempt biomaterial degradation by phagocytosis and release of ROS and lysosomal enzymes. Differently, M2 macrophages are anti-inflammatory and induce tissue remodeling [Liu et al., 2014]. Lymphocytes are also attracted to the biomaterial and secrete more cytokines that induce monocyte differentiation into macrophages and foreign body giant cells. Hydrophobic biomaterials and those that are cationically charged at the surface seem to be the most prone to stimulate more intense chronic inflammation [Anderson, 2015].

USC UNIVERSIDADE DE SANTIAGO DE COMPOSTELA

(iv) *Foreign body giant cell formation*. This step is the hallmark of the foreign body reaction **(Figure 1.1A)**. Foreign body giant cells are formed as a consequence of the fusion of macrophages to render multinucleated cells that will persist as long as the biomaterial is in the host. Macrophages fusion occurs when they fail to phagocytose the biomaterial as an attempt of improving their performance and also to avoid apoptosis [Brodbeck et al., 2001]. Foreign body giant cells are a main source of ROS, degrative enzymes and acids that may cause degradation of the medical device and its failure. Biomaterials that adsorb vitronectin and that have cationic surfaces have been shown to promote macrophages fusion [Anderson, 2015].

(v) *Fibrosis or fibrous capsule formation*. Development of chronic inflammation and formation of foreign body giant cells induce the formation of a capsule around the medical device. The capsule consists of collagen and other extracellular matrix proteins that form a granulation tissue, which progressively loses the cells and becomes more fibrous. This capsule may cause a mechanical impairment of the medical device and its failure to interact with the host tissue [DiEgido et al., 2014]. Hydrophobic biomaterials with cationic groups are prone to develop thick fibrotic capsules, while biomaterials endowed with carboxyl groups usually induce thin capsules. The use of anti-inflammatory and anti-adherent groups also attenuates the capsule formation [Barbosa et al., 2006].

Restenosis associated to stents (in-stent restenosis) [Shlofmitz et al., 2021] and posterior capsule opacification after intraocular lens implantation [Wormstone et al., 2020] are two clinically relevant examples of the deleterious effects of host cell growth and proliferation. Moreover, the adhesion to the device of macrophages and foreign body giant cells reduces the bactericidal capacity, favoring

USC UNIVERSIDADE DE SANTIAGO DE COMPOSTELA

the formation of microbial colonies (biofilm) and the persistence of infections.

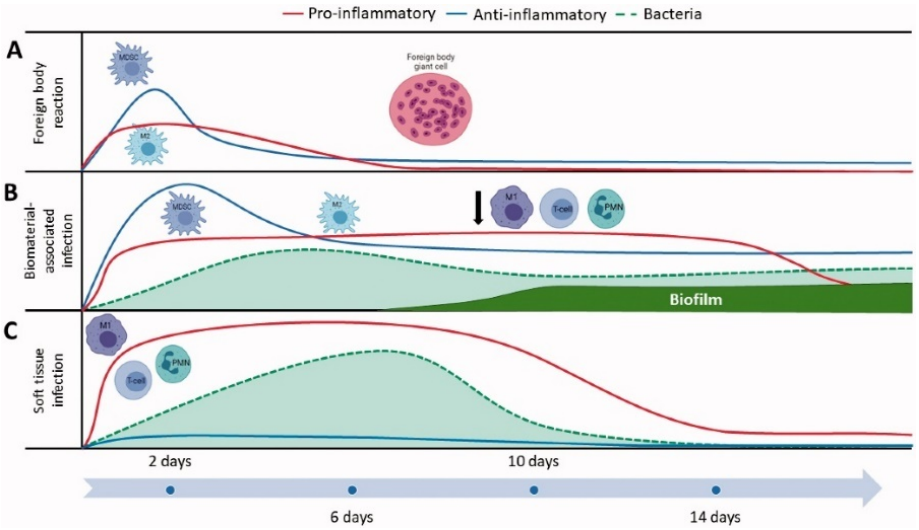


Figure 1.1. Evolution of the immune response (pro- and anti-inflammatory processes) against (A) a foreign body (i.e., medical device), (B) a medical device that becomes contaminated by bacteria (e.g. *Staphylococcus aureus*), and (C) *S. aureus* infecting a tissue. (A) The foreign body reaction against a sterile medical device involves inflammatory phases followed by the formation of foreign body giant cells and the surrounding of the implant with mature monocytes and macrophages. If the medical device is encapsulated, the likelihood of later bacteria colonization is minimal. (B) Insertion of a medical device that becomes contaminated with bacteria causes an increase in both myeloid-derived suppressor cells (MDSCs) and M2 macrophages. *S. aureus* develops the immune-resisting capabilities at day 3 and starts forming biofilm; the bacterial load decreases between day 3 and 5, and the biofilm is evident since day 7. Bacteria in the biofilm may shift the pro-inflammatory phase towards anti-inflammatory response (M2 macrophages) though a variety of mechanisms. (C) If tissue infection occurs in the absence of a medical device, minor anti-inflammatory response (M2 macrophages) is observed. Bacteria can evade the immune system and proliferate, while the host maintains the pro-inflammatory status. In cases B and C the maximum in bacteria content (CFU) occurs 7 days after infection. MDSCs include progenitor cells, immature macrophages, granulocytes, and dendritic cells. Reproduced from Rosman et al. (2021) with permission from Taylor & Francis.

USC UNIVERSIDADE DE SANTIAGO DE COMPOSTELA

The foreign body reaction impairs the capability of the immune system to eradicate the microorganisms attempting to colonize the medical device [Rosman et al., 2021]. In fact, implantable devices are considered a refuge for opportunistic bacteria and are responsible for almost 50% of all nosocomial infections, which are associated with considerable morbidity and mortality [VanEpps and Younger, 2016]. Although the risk of infection is slowly decreasing due to the implementation of extreme hygienic and prophylactic measures, the raising increase in the use of medical devices due to the ageing of the population and the growing incidence of chronic degenerative diseases make medical device-associated infections to be a highly relevant health care concern [Haddad et al., 2017]

Opportunistic bacteria such as *Staphylococcus aureus*, a harmless skin, nasopharynx and gut commensal [Raineri et al., 2021], may transform into a dangerous threat when form biofilms onto medical devices due to the fast acquisition of resistances to antibiotics, evasion of immune defenses, and spreading to surrounding living tissues [O'Gara, 2017]. The infections are often caused by microorganisms present on the medical device after sterilization and/or coming from the contact with the skin or mucosa of the patient at the moment of insertion. If the inoculum exceeds threshold levels or if the host defenses are impaired, the microorganisms can attach to the surface of the medical device and subsequently form a biofilm **(Figure 1.1B)** [Rosman et al., 2021].

Planktonic bacteria (swimmers) that enter into contact with a solid substrate (either a living tissue or an abiotic surface) may adhere or not depending on the chemical composition of the surface, its topology, the presence of conditioning substances (mainly proteins), humidity, nutrient accessibility and external forces. In the case of medical devices, the first layers of proteins adsorbed determine

USC UNIVERSIDADE DE SANTIAGO DE COMPOSTELA

bacteria attachment. The colonization process is quite rapid. For example, since adhesion *S. aureus* requires 3 h to form aggregates that are too large to be phagocytosed and after 6 h the bacteria spreads to cover as much surface as possible (exodus phase) [Moormeier and Bayles, 2017; Ghimire et al., 2019]. Cell-cell interactions and production of extracellular polysaccharides favor the formation of a biofilm matrix.

Microorganisms have developed a communication system, known as *Quorum Sensing*, which relies on the exchange of soluble chemical signals. Depending on the nature and concentration of the signals each microorganism knows whether the surrounding microorganisms are similar (the same species or not). The structure, density and roughness of the biofilm strongly depend on the changes that the *Quorum Sensing* signals trigger on the microorganisms population (phenotype changes). The microbial cells that make up the biofilm (sessile cells) show marked differences with respect to planktonic cells and, in particular, a greatly increased antimicrobial resistance [Mah and O'Toole, 2001; Schierholz and Beuth, 2001]. Microorganisms encapsulated in the biofilm grow more slowly than planktonic cells, probably because the access to nutrients and oxygen is lower, leading to a more lenient metabolic activity and, consequently, to a lower antimicrobial susceptibility [Costerton, 1999; Reid, 1999; Donlan, 2001]. Bacteria in the biofilm promote an anti-inflammatory response of macrophages, which moreover cannot recognize bacteria hidden inside the biofilm. In addition, the biofilm provides a defense barrier against normal surface cleaning procedures and antimicrobial therapy. When the biofilm is overcrowded, some cells detach and move to colonize other surfaces or host tissues and may even cause bacteremia.

When infection and foreign body reaction are concomitant **(Figure 1.1B)**, the exacerbated chronic inflammation finally impairs

USC UNIVERSIDADE DE SANTIAGO DE COMPOSTELA

the phagocytic capability (as explained above). As a consequence, colonization of the medical device and infection occurs at much lower threshold (10^5-fold in case of *S. aureus*) than in tissues without implanted medical devices **(Figure 1.1C)** [Zimmerli and Sendi, 2001; Rosman et al., 2021].

Once a biofilm is established on a medical device, systemic treatment with antibiotics usually fails and thus the medical device should be removed. Replacement of implantable devices is not always feasible or involves complex surgical interventions. Moreover, the microorganisms spread into the surrounding tissues require complete eradication before implantation of the new medical device. Otherwise, they colonize the medical device again starting a vicious cycle that may end compromising the life of the patient [Conlon, 2014]. Since treatment of mature biofilms is quite difficult, preventive measures are required. Prevention demands a deep knowledge on the mode bacteria grow and perform inside biofilms and their interactions with the foreign body reactions, and also effective strategies to adequately modify the surface of the medical devices.

Application of biomimetic approaches for the design of medical devices that can regulate by themselves the interaction with proteins and microorganisms or that can benefit from the release of prophylactic or therapeutic drugs from their surface (combination products) may significantly improve the performance of the medical devices and reduce untoward effects [Alvarez-Lorenzo and Concheiro, 2019]. Since host cells and bacteria participate in “the race to the surface”, the ones that settle first are the ones that will develop. Therefore, a prophylactic strategy may be to favor the adhesion of macrophages, as a defensive barrier against bacteria [da Silva et al., 2015]. Some therapeutic applications of medical devices require simultaneous administration of drugs to regulate pain, inflammation,

USC UNIVERSIDADE DE SANTIAGO DE COMPOSTELA

coagulation, etc. Additionally, as mentioned above, anti-inflammatory, anti-ROS and antimicrobial agents may be needed to minimize the risks of foreign body reactions and infections. Thus, the use of medical devices is commonly associated to the systemic administration of drugs, which are supplied either orally or parentally. The efficacy and safety of the pharmacological treatment could be notably improved if the drug/s could be delivered directly in the site where the medical device is placed. One of the most well-known examples of the advantages of drug-medical device combination is the last generation of drug-containing stents that can successfully minimize the risk of restenosis [Canfield and Totary-Jain, 2018]. In the next section, incorporation of drugs and biologics to medical devices to obtain combination products is addressed.

1.2 COMBINATION PRODUCTS

As already included in its definition, a medical device may be assisted in its function by pharmacological, immunological or metabolic means. From a regulatory point of view, any binary or ternary set of drug, biological product and/or medical device is considered as a combination product. According to the definition of combination product compiled in the US FDA 21 CFR 3.2(e), the term includes:

— A product comprised of two or more regulated components, i.e., drug/device, biologic/device, drug/biologic, or drug/device/biologic, that are physically, chemically, or otherwise combined or mixed and produced as a single entity;

— Two or more separate products packaged together in a single package or as a unit and comprised of drug and device products, device and biological products, or biological and drug products;

USC UNIVERSIDADE DE SANTIAGO DE COMPOSTELA

— *A drug, device, or biological product packaged separately that according to its investigational plan or proposed labeling is intended for use only with an approved individually specified drug, device, or biological product where both are required to achieve the intended use, indication, or effect and where upon approval of the proposed product the labeling of the approved product would need to be changed, e.g., to reflect a change in intended use, dosage form, strength, route of administration, or significant change in dose.*

The fact that combination products incorporate two or more regulated components determines that they act by more than one mechanism. The mode of action (MOA) that contributes most significantly to the overall therapeutic effect is designated as the primary mode of action (PMOA). In the particular case of drug-device combination products two main situations can be distinguished, as follows:

— Medicinal product that include a medical device. In this case the drug is responsible for the PMOA, while the device is used to enable the delivery of the medicine. Transdermal patches and pre-filled inhalers are typical examples of combination products in which the PMOA corresponds to the drug. In them, the medical device is essential for administration, but in the absence of the drug it completely loses its usefulness. The entire product must fulfil the requirements of a medicinal product and, in addition, the safety and performance of the medical device should be ensured in relation to its use with the medicinal product. A guideline on quality documentation for medicinal products when used with a medical device has been published by EMA in July 2021 [EMA, 2021].

— Medical devices with an ancillary medicinal substance. In this case the medical device plays the PMOA and the medicinal substance

USC UNIVERSIDADE DE SANTIAGO DE COMPOSTELA

provides support for the proper functioning of the device. Drug-eluting stents were indeed the first officially recognized combination products. Other examples are bone cements containing an antibiotic or catheters coated with heparin or an antibiotic agent. Medical devices with an ancillary medicinal substance should meet the medical devices legislation and must be CE marked. It should be noted that medicines containing the same medicinal substance have previously been assessed [Antich-Isern et al., 2021].

Drug-medical device combination products offer a wide range of opportunities. With regard to pharmacological treatments, the medical device makes it possible to directly apply a drug to areas of the body that are difficult to access systemically. Furthermore, the implementation of advanced systems that allow regulation of drug release in response to a stimulus opens the possibility of achieving release kinetics adapted to the evolution of the processes to be treated [Alvarez-Lorenzo and Concheiro, 2019]. Even wireless communication systems are being developed to monitor the therapeutic response and make readjustments of the delivery in real time. With regard to the medical device, the incorporation of the drug should prevent adverse responses and prolong the shelf life.

From an economic point of view, the market for combination products is in a phase of expansion. In addition to their therapeutic advantages, candidate drugs to be integrated into medical devices are part of medicines already approved and in many cases with the patent expired, which considerably simplifies and makes the registration process cheaper. All this determines that, compared to a drug based on an innovative molecule, the costs required for development are significantly lower (250 million vs. 500-2000 million euros), the time is shorter (4-8 years vs. 13-15 years) and the success rate is much higher (1/6 vs. 1/10000) [Hupcey and Ekins, 2007; Bayarri, 2015].

USC UNIVERSIDADE DE SANTIAGO DE COMPOSTELA

1.2.1 Methods to add drugs to medical devices

Medical devices can be prepared with a variety of materials, mainly polymers, ceramics, and metals. These materials have been traditionally selected aiming for achieving functionality and biocompatibility. In the attempt to prepare non-adherent surfaces to avoid excessive adsorption of proteins and/or microorganisms, most medical devices also lack affinity for other substances such as drugs. Therefore, direct soaking of the medical device into an aqueous solution of drug generally does not result in efficient loading of therapeutic doses. Also if the drug deposition is limited to the very surface regions of the medical device, burst release may be observed after implantation. Therefore, specific strategies are required to incorporate drugs and other bioactive substances [Zilberman et al., 2010].

Since the distinctive advantage of a combination product is to work together as a functional or structural prosthetic replacement of the host tissue and as a drug delivery system, the implementation of the drug delivery function should not cause any detriment to its function as medical device. On the other hand, to function competently as a delivery system, drug release profiles must match the particular clinical context, taking into account the anatomy and physiology of the implantation site, disease, or pathogen. The local toxicity and clearance mechanisms of the drug must be addressed too. Subtherapeutic levels can lead to failure and, in the case of antimicrobial drugs, may trigger antimicrobial resistances. The large number of formulation parameters that can affect the release pattern and the high doses required to allow long-term release may make the

USC
UNIVERSIDADE DE SANTIAGO DE COMPOSTELA

design of drug-eluting medical devices more complex than that of a conventional medicine [Alvarez-Lorenzo and Concheiro, 2013].

Drugs can be integrated into medical devices either on the surface of the device or in the bulk to form a single entity **(Figure 1.2)**. Confinement of the drug on the surface has the advantage of that the drug is added when the medical device is already formed; therefore, the original processing protocol for the medical device can be kept and the likelihood of that the drug may compromise bulk properties of the medical device (e.g., mechanical behavior) is minor. There are three main approaches to incorporate drugs on a preformed medical device:

(i) *Covalent immobilization of the drug*; this strategy usually involves a pretreatment of the medical device surface to increase its reactivity as well as the modification of the drug to facilitate the binding. Although it is not suitable for all drugs, this strategy may be convenient when long-term permanence of the drug on the device is required for prolonged local activity. Immobilization of antimicrobial drugs has been shown useful to kill microorganisms by contact (contact killing surfaces) [García-Vargas et al., 2014].

(ii) *Coating of the device with a mixture of the drug and a substance (polymer, lipid) that can regulate its release*. This is a priori the simplest strategy although mechanical stability and durability of the coating both during and post-insertion may be challenging. The drug is mixed with coating formatting components to be directly apply to the medical device (e.g., spray coating, electrospinning) or added in a specific step during the coating (e.g., in a layer-by-layer approach). The procedure is very versatile in terms of nature and thus solubility and subsequent biodegradability/biostability of the components. Also, the drug can be encapsulated in nano/microcarriers to improve

USC UNIVERSIDADE DE SANTIAGO DE COMPOSTELA

stability or control of drug release. For example, second generation of drug-eluting stents relies on bioerodible coatings that release the drug and at the same time renovate the surface as the coating erodes, which causes detachment of pre-adsorbed proteins and cells [Huang et al., 2014].

(iii) *Grafting of polymer brushes and networks that can host the drug.* Immobilization of polymer brushes and chemically cross-linked networks by means of wet chemistry, plasma treatment, or gamma-ray activation may open a wide range of possibilities regarding functionalities of the anchored polymers including stimuli-responsive drug loading and release [Alvarez-Lorenzo et al., 2010]. Competitive release of drugs as a function of certain biomarkers or microbial threads has gained notable attention [Alvarez-Lorenzo et al., 2016]. Although preclinical assessment is still limited, successful results *in vitro* and in small animal models regarding medical devices coated with infection-, mechanical-, electric- and near infrared (NIR)-responsive materials may pave the way to a prompt translation to the clinic [Alvarez-Lorenzo and Concheiro, 2019].

USC
UNIVERSIDADE DE SANTIAGO DE COMPOSTELA

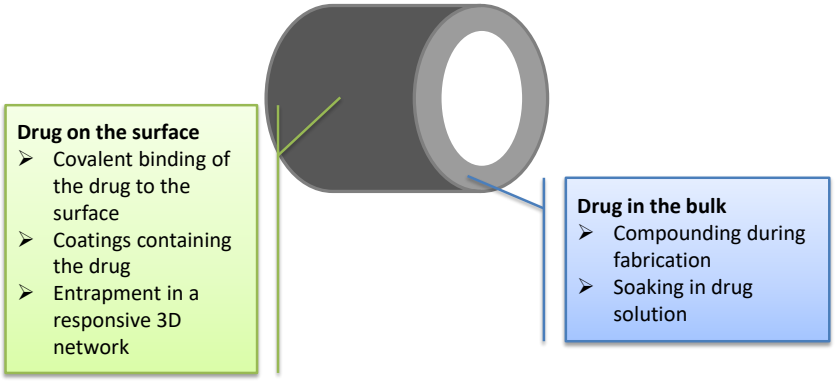


Figure 1.2. Main strategies to integrate drugs on the surface or in the bulk of medical devices. Figure made by the author of this PhD Thesis.

Strategies that involve the incorporation of the drug into the bulk of the device are preferable when either the amount loaded at the surface is not sufficient or the release ends in a short time frame. The two main strategies are compounding and soaking.

(i) *Compounding* implies adding the drug to the components of the medical device during fabrication. Relevant commercially available examples are antibiotic-loaded bone cements, and they also exemplify the challenges to overcome for an adequate design. First combination products using poly(methyl methacrylate) (PMMA) devices had the drawbacks of that few drugs could withstand the high temperature during polymer processing, the release rate was too low to provide inhibition concentration due to the impermeability of the device, and the non-biodegradable device should be removed after antibiotic exhaustion [Ene et al., 2021]. Replacement of PMMA with bioactive glass composites or calcium sulfate composites overcomes some of these limitations. Additionally, PMMA requires 30-40% drug content for efficient percolation, i.e., that the drug can be released, which notably compromises the mechanical properties. Recently designed ultrahigh molecular weight polyethylene (UHMWPE)

USC UNIVERSIDADE DE SANTIAGO DE COMPOSTELA

prosthesis in which the drug forms small clusters requires only 6-8% drug to reach the percolation threshold, and thus no detrimental effect on the mechanical strength are observed [Suhardi et al., 2017].

(ii) *Soaking*. Medical devices made of swellable polymers or porous materials with a mesh size design that allows for free diffusion of small molecules from one side to other (e.g. prosthetic meshes, contact lenses) can be loaded with the drug by soaking in a drug solution. This strategy relies in the immersion of the device in a solvent that causes the swelling of the polymer structure to allow drug diffusion inside the device. Once the required loading is achieved, removal of the solvent should lead to the same dimensions as those of the pristine device. In most cases the medical device swelling is greater in organic solvents, which may compromise the safety, and the contraction after solvent removal may lead to devices with lower or higher dimensions, which may compromise the fitting to the host tissue [Pérez-Köhler et al., 2016]. This soaking strategy is also being evaluated for the drug loading of 3D printed scaffolds by swelling either the filament before printing or the final scaffold [Farto-Vaamonde et al., 2019].

1.3 HEARING AIDS

Hearing impairment affects 0.3% newborns and up to 70% of people over 70 years. Currently, 5% of world´s population, 432 million adults and 34 million children, suffer disabling hearing loss (hearing loss greater than 35 decibels) and require hearing aids [WHO, 2021]. Hearing loss is usually accompanied by social isolation, increased rates of depression and magnification of other pathologies. The impact on the quality of life (mainly independence) of patients and their families is very relevant [Hampson, 2012].

USC UNIVERSIDADE DE SANTIAGO DE COMPOSTELA

Hearing loss is classified as mild, moderate, severe (hard of hearing), or profound (deafness), and a variety of causes may be behind **(Figure 1.3)**. Early detection and treatment are critical for children affected of hearing loss. Otherwise, their communication and speech and, in turn education and future employment, become notably compromised. Early cochlear implantation (for severe to profound cases) and the use of hearing aids, established in some countries since 1990s, can notably shift the daily life and children´s own perception of their disability [Anmyr et al., 2011]. As shown in **Figure 1.3**, multiple causal agents are behind sensorineural and conductive hearing loss in children and adults, but ear infection is a relevant cause of temporary and permanent hearing loss. In the case of elderly people, presbycusis due to age-related changes in the auditory system notably contributes to hearing loss.

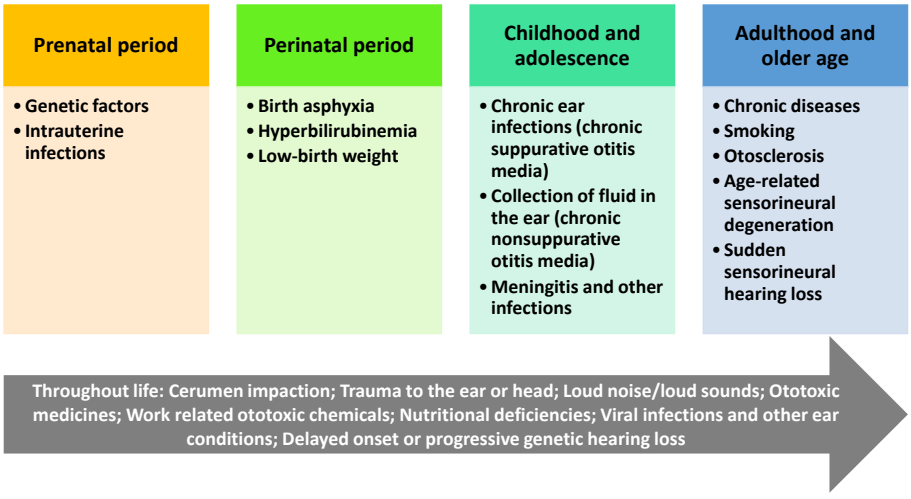


Figure 1.3. Main causes of hearing impairment. Some factors are predominant in specific periods across life span, while others represent threats throughout life. Data taken from WHO Deafness and hearing loss. 2021 https://www.who.int/news-room/fact-sheets/detail/deafness-and-hearing-loss; Accessed January 2022. Figure made by the author of this PhD Thesis.

USC UNIVERSIDADE DE SANTIAGO DE COMPOSTELA

Hearing aids are intended to amplify sound by means of a microphone that detects the sound, which is transformed into acoustic signals by a receiver (loudspeaker). The sound is digitally processed to amplify the frequency at levels that favor speech recognition, while attenuating the background (environmental) noise and also the externally audible signal that could be amplified via the microphone. Hearing aids are medical devices class II according to FDA [FDA, 2021] and active medical devices class IIa according to EMA [EHIMA, 2020].

A variety of hearing aids are commercially available **(Figure 1.4)**. Selection criteria rely on the specific needs of the patient in terms of degree and type of amplification needed, the size and shape of the ear canal, the ability to manage and understand the functioning of the aids, and personal preferences [Hampson, 2012]. There are four main types of hearing aids:

— behind-the-ear (BTE), which is adequate for mild to profound hearing loss. Most components are integrated in a small case behind the ear, which connects with receiver placed in the canal by means of more or less clear tubing. In the Mini-BTE the tube is very thin and the ear canal remains open which attenuates the booming sound of the wearer own voice. BTEs are the easiest aids to handle, but still poor aesthetically attractive and the most susceptible to damage.

— in-the-ear (ITE). The whole device is inside a shell that fills in the outer part of the ear.

— in-the-canal (ITC). The device shell is smaller and fits partially into the ear canal.

— completely-in-the-canal (CIC). The device shell is also small size and fits completely into the ear canal.

USC UNIVERSIDADE DE SANTIAGO DE COMPOSTELA

The two last hearing aids are less visible and show a growing market, but hold smaller batteries (shorter time in use) and their capability for amplification of signals is smaller due to the short distance between microphone and receiver. The small size may be a drawback for handling by some patients.



Figure 1.4. Main types of hearing aids. Reproduced from https://advancedhearingcarecenter.com/what-to-expect/; Accessed in January 2022.

USC
UNIVERSIDADE DE SANTIAGO DE COMPOSTELA

The market of hearing aids is expanding, both as hearing devices and hearing implants. Hearing aids are one of the best examples of personalized medical devices that have benefited from the development of 3D printing technology [Gregoret, 2019]. The first reported ear impression was made in 1890 for an ear trumpet, which lacked any kind of electronic amplification. Wax was used to make that first known impression. Since the mid-1940s other materials such as acrylic resins and silicone appeared, but the process evidenced notably limitations to provide good replicates of the quite tortuous cavity of the ear. Additionally, the removal of the mold from the ear channel was very difficult. Desktop impression scanning came about in the late 1990s, and digital shell modeling and 3D printing revolutionized how custom hearing aids are being produced since the 2010´s **(Figure 1.5)**. Nowadays more than 90% of the manufactured hearing aids are fitted to the patient's ear anatomy by 3D scanning and subsequent 3D printing.

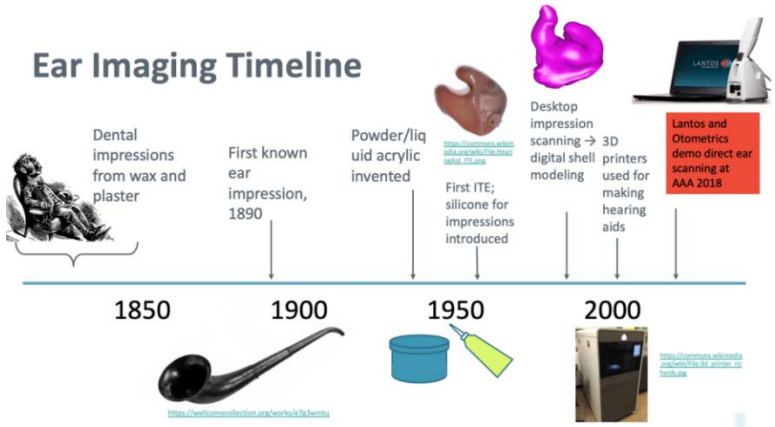


Figure 1.5. Evolution of the devices used to improve hearing, from the first trumpets based in the materials used to take dental impressions to the synthetic molds in the 1950´s and the most advanced scanners and 3D impression machines since the 2000´s. Reproduced from Gregoret (2019). Retrieved from Audiology Online Continuing Education http://www.audiologyonline.com; Accessed in January 2022

USC UNIVERSIDADE DE SANTIAGO DE COMPOSTELA

3D printing is an additive manufacture technology, which means that the object is constructed by layer by layer deposition of the material instead of subtraction from a bulk piece of material. 3D printing enables a fine control of the shape of the final object and the spatial distribution of the components according to a previously prepared 3D image. In the case of the hearing aids, scan images of the patient ear can be easily transformed into printable 3D images.

3D printing was adopted in the period of 2008-2009 by main producers of hearing aids to prepare personalized shells [Sandström, 2016]. The shells for ITE, ITC and CIC should contain the microphone, the electronic signal processor, the battery and the loudspeaker inside a small shell that should fit to the patient anatomy. Production starting from molds of the patient´s ear canal involves many tedious steps that imply costly manual processing, not exempt of errors. 3D printing offers more precise construction of the piece that perfectly fits to the patient demands (improving comfort and acoustic performance), and the piece production can be accurately reiterated as many times as needed in case the patient requires replacement of the hearing aids. Simplification and automatization of the process with an increase in speed, efficiency and quality control assessment directly impact in the final quality of the hearing aid and in the cost, which is becoming more affordable. Among the different 3D printing technologies, stereolithography (SLA) is the most widely used to prepare hearing aids. SLA allows preparing shells similar to those manually created in terms of appearance and functionality, which favored a smooth introduction in the market of the 3D printed hearing aids.

SLA is a type of VAT polymerization 3D printing technology; namely, it involves computer spatially-controlled photopolymerization. Compared to other more widespread 3D printing

USC UNIVERSIDADE DE SANTIAGO DE COMPOSTELA

technologies such as fused deposition modeling, VAT polymerization has the advantages of higher accuracy and resolution and faster production speed. Thus, VAT polymerization is preferable for fast production of complex objects with intricate design [Xu et al., 2020]. VAT photopolymerization techniques are categorized as a function of the source of light used to cure reactive resins, into SLA which uses a laser, Digital Light Processing (DLP) which uses a projector, and Continuous Liquid Interface Production (CLIP) which involves light-emitting diodes (LEDs) and oxygen [Pagac et al., 2021].

Briefly, in SLA a platform is immersed in a transparent container that contains the photopolymerizable material, usually a resin that is cross-linked under the UV light **(Figure 1.6)**. A laser beam is moved to be projected into specific regions of the resin to solidify the material in the required areas of one layer according to the 3D model. Once a layer is made, the platform moves down or up (depending on the setup) to create the next layer either top-down or bottom-up. The resolution of the SLA object is given by the diameter of the laser beam at the curing point (in the hundreds of microns scale).

USC
UNIVERSIDADE DE SANTIAGO DE COMPOSTELA

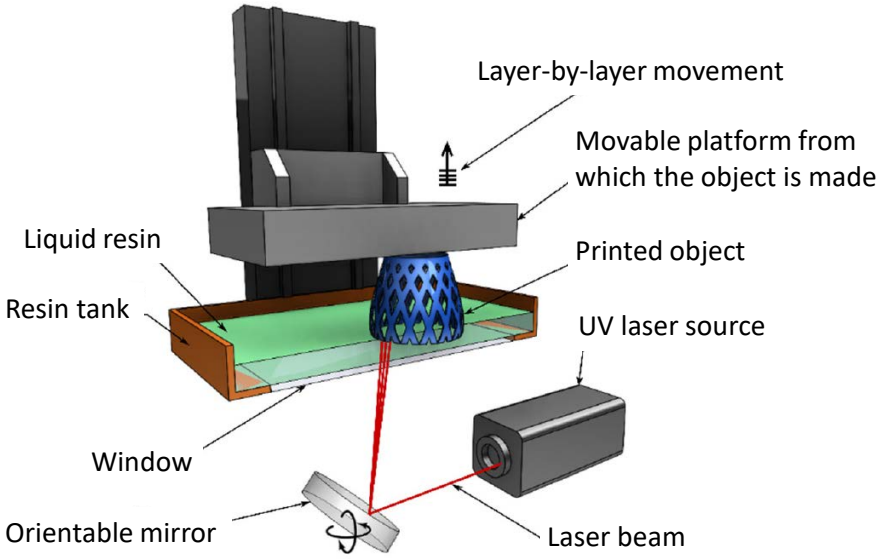


Figure 1.6. Scheme of the set-up of a SLA 3D printer. Reproduced with permission from Pgac et al., (2021). This article is an open access article distributed under the terms and conditions of the Creative Commons Attribution (CC BY) license.

DLP 3D printing is similar to SLA but uses a digital light projector instead of a mirror to reflect the light. DLP has the advantage of faster layer formation since each layer is entirely exposed at once **(Figure 1.7)**. It should be noted that the printed object can be made with layers of different composition by exchanging the resin of the tank or by replacing the entire tank with other tank containing a different resin [Sampson et al., 2021].

USC
UNIVERSIDADE DE SANTIAGO DE COMPOSTELA

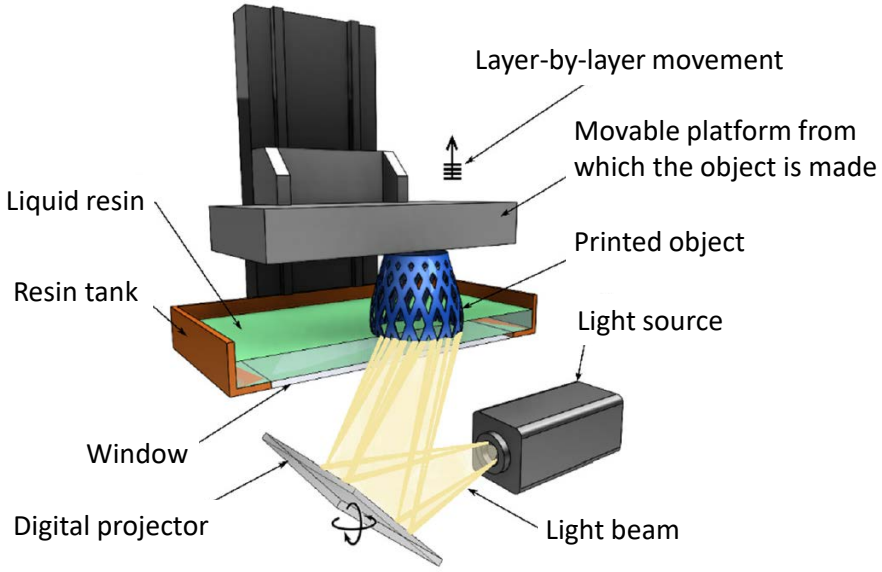


Figure 1.7. Scheme of the set-up of a DLP 3D printer. Reproduced with permission from Pgac et al. (2021). This article is an open access article distributed under the terms and conditions of the Creative Commons Attribution (CC BY) license.

CLIP technology is similar to DLP but uses LEDs and a window that is permeable to oxygen **(Figure 1.8)**. The oxygen that gets access to the bottom of the resin tank inhibits the polymerization of a very thin layer of resin. Such liquid resin layer (dead zone) increases the resolution and minimizes peeling forces, and in turn the risk of rupture of the object that is being formed. Instead of forming the object layer-by-layer, the platform of CLIP 3D printers is designed to move continuously minimizing the staircase appearance [Pgac et al., 2021].

USC UNIVERSIDADE DE SANTIAGO DE COMPOSTELA

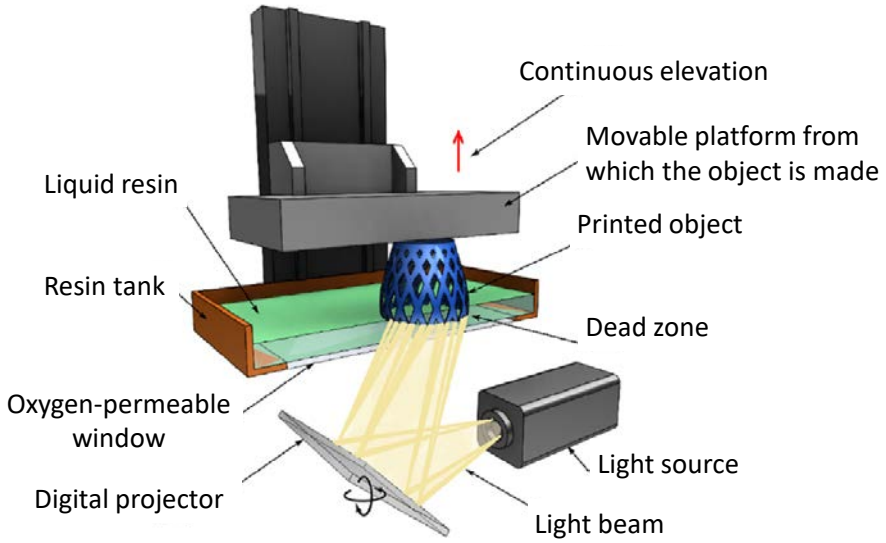


Figure 1.8. Scheme of the set-up of a CLIP 3D printer. Reproduced with permission from Pgac et al. (2021). This article is an open access article distributed under the terms and conditions of the Creative Commons Attribution (CC BY) license.

1.3.1 Ear infections and hearing aid-related biofilms

Discontinuation of the use of hearing aids during childhood is mostly related to esthetic features, as children find hearing aids "boring" or "ugly". Also, young hearing aids wearers complain about pain in neck and shoulders as well as hearing limitations during outdoor activities and practice of team sports [Anmyr et al., 2011]. In the case of elder people, discontinuation is mostly associated to lack of physical ability to use the hearing aids and to misunderstanding of the proper functioning of the devices by both the user and the caregiver [Hampson, 2012]. Nevertheless, for people of all ages ear infections are both main causal agents of hearing loss and of discontinuation of hearing aid use. The growth of microorganisms on

USC UNIVERSIDADE DE SANTIAGO DE COMPOSTELA

ear tissue and on the device shell is prone to lead to biofilms that are hard to eradicate [Fusconi et al., 2011].

Otitis externa is a highly recurrent pathology, with a 10% worldwide prevalence. Normal ear canal microbiota comprises *Staphylococcus*, Corynebacterium species and Streptococci [Stroman et al., 2001]. The pH in the ear canal is in the 5.0 to 5.7 range which, together with the hydrophobic features of cerumen, prevents from microorganisms growth [Martinez Devesa et al., 2003]. The incidence of otitis externa is associated to water exposure and increased humidity in the ear canal, which favors the development of polymicrobial infections particularly when predisposing factors also concur [Wiegand et al., 2019]. A variety of Gram-positive and Gram-negative bacteria as well as fungi, mainly *Aspergillus* sp. and *Candida* sp. have been isolated in patients with otitis externa. The bacteria species more frequently isolated in acute otitis externa are *Pseudomonas aeruginosa* (38%), *Staphylococcus epidermidis* (9.1%), *Staphylococcus aureus* (7.8%), and *Microbacterium otitidis* (6.6%) [Roland and Stroman, 2002]. First line treatment involves cleaning of the ear canal and local administration of mixtures of antibiotics and corticosteroids. The corticosteroids improve the antimicrobial outcomes and solve the inflammatory edema. The efficacy of the topical treatment has been suggested to be increased if the drug solution is impregnated in a gauze strip to remain in the ear canal for 24-48 h [Kaushik et al., 2010] or if the drugs are delivered from in situ gelling hydrogels [Serban et al., 2017]. To the best of our knowledge, in-the-canal controlled release systems that can avoid frequent administration and facilitate patient self-administration and treatment adherence are still to be developed.

Prolonged wearing of hearing aids may alter the ear canal microbiota, due to an occlusal effect, and increases the risk of

USC UNIVERSIDADE DE SANTIAGO DE COMPOSTELA

infections by providing local increase in temperature and humidity that favor the growth of bacteria and fungi. Additionally, it has been demonstrated that the external surface of the hearing aids can act as reservoir of microorganisms, mainly staphylococci, *Pseudomonas* sp., and *Candida* sp., that can lead to recurrent otitis externa. Indeed, handling of the hearing aid devices by patients and audiologists, and in some cases the caregivers, increases the likelihood of microbial contamination and even cross infection by microorganisms typical of cerumen but also by non-typical ones [Ahmad et al., 2007]. Before development of infection, ear irritation and itching in hearing aid wearers can be considered as a first sign of changes in the microbiota. Canal debris and microorganisms are more abundant in ears with hearing aids and may evolve into fungal or bacteria otitis externa that results in non-tolerance of the hearing aid [Orji et al., 2014].

Otitis media is highly recurrent during childhood associated to anatomical reasons [Grevers, 2010]. Main etiologic agents of otitis media are *Haemophilus influenzae*, *P. aeruginosa*, and *S. aureus*, which are known to readily form biofilms. It should also be mentioned that implantable hearing aids (e.g., bone conduction hearing aids, middle ear implants, and cochlear implants) have even increased risk of infection, compared to in-the-canal hearing aids, due to the natural open conduct between the middle ear cavity and the nose/nasopharynx, which is prone to be colonized by a variety of pathological microorganisms [Georgescu et al., 2017]. Bacteria can migrate from contaminated regions and colonize middle ear cavity and Eustachian tube, forming biofilms. Biofilm development causes chronic otitis media, which is hardly addressed by innate antibodies and conventional antibiotics. Additionally, the growth of biofilm onto the implantable devices has detrimental effects on their performance and may even cause their failure. Failure obligates to an unexpected

USC
UNIVERSIDADE DE SANTIAGO DE COMPOSTELA

additional surgery since implantable hearing aid devices are intended for the entire life of the wearer.

Several strategies are being considered to prevent biofilm formation onto hearing aids. Implantable devices require sterile surgical maneuvers and also the prophylactic use of antibiotics [Georgescu et al., 2017]. These two steps do not apply when non-implantable devices (BTE, ITE, ITC and CIC) are used. Also, wiping the shell with 70% ethanol solution has been shown to be inefficient to remove polymicrobial deposits and even increases the risk of shell cracking [Ahmad et al., 2007]. Regarding the devices, adhesion of components from blood and transudates (mainly proteins) facilitates subsequent adhesion of microorganisms. It has been shown that smooth surface and no dead-spaces may prevent bacteria adhesion [Zimmerli, 1993]. Anti-microbial coating may confer contact-killing performance, but the information is still limited [Gheorghe et al., 2021].

1.4 CONTACT LENSES

1.4.1 CLs for vision correction

The casual finding of that pieces of PMMA (Plexiglas®) windows did not trigger rejection response in the pilots of first airplanes opened the path towards the first polymer-based CL [McMahon and Zadnik, 2000]. Industrial production of PMMA began in 1936, and 10 years later the first hard CLs were tried in humans. However, shortly after they were replaced by the introduction of poly(2-hydroxyethyl methacrylate) (pHEMA), first synthesized in 1954. Otto Wichterle and his Czech colleagues developed in 1961 a semi-industrial method of preparing hydrogel CLs based on pHEMA, which opened the path for

USC UNIVERSIDADE DE SANTIAGO DE COMPOSTELA

the popularization of CLs for vision correction [Wichterle and Lim, 1960]. These acrylic-based polymers combined the high optical clarity of glass with lower density and better mechanical properties, and served as a starting point to design new copolymers capable of improving lens quality [Nicolson and Vogt, 2001]. Soft (hydrogel) CLs with high content in water were developed in the 1970s to allow oxygen to be dissolved in the aqueous phase and to minimize eye hypoxia. The search for more oxygen permeable materials rendered in the 1980s silicone-based hard gas-permeable CLs, but their high hydrophobicity compromised the ocular comfort. Advances in monomers and polymerization techniques allowed preparing in 1998 the first silicone hydrogel CLs, which were aimed to combine the high permeability of silicone components with the ocular biocompatibility and comfort of hydrophilic hydrogels. Since then, a variety of demulcents and strategies to increase the wettability and softness of the CLs have been developed [González-Chomón et al., 2013]. Today there are more than 140 million CL wearers, and the number is steadily increasing as new functionalities are being added to CLs [Barr and Mack, 2011].

CLs are named according to ISO 18369-1:2017 standard [ISO, 2017] and subsequent modification UNE-EN ISO 18369-1 [UNE, 2018] with seven elements code:

1- Prefix, which informs about the monomers and cross-linkers.

2- Radical, which may be –filcon (for CLs with water content ≥ 10% by weight) and –focon (for CLs with water content <10%).

3- Series suffix. The first member of a serie has not suffix. The suffix indicates a change in the original proportion of the monomers although the qualitative composition is the same. The letter A is used

USC UNIVERSIDADE DE SANTIAGO DE COMPOSTELA

for the first change in proportions; letters B, C,… are used for subsequent changes.

4- Group suffix. It consists of arabic numbers. In the case of –filcon materials, the group suffix indicates the range of water content and the percentage range of ionic monomers. In the case of –focon materials, the group suffix refers to presence/absence of silicone and fluorine. The group suffices are collected in **Table 1.4**.

5- Dk, which is the oxygen permeability referred to mmHg.

6- Water content, as amount of water (expressed as a percentage by mass fraction) present in the hydrated material.

7- Modification code. The letter “m” is used for CLs of groups 1 to 4 that have been modified at the surface by means of, for example, plasma treatment, acid-base hydrolysis, or a material that migrates to the surface. For CLs of group 5, the letter “c” indicates chemical modification of the surface (with chemical groups or plasma treatment), while the letter “w” refers to materials that contain in the bulk or that release wetting agents that form part of interpenetrating networks.

USC
UNIVERSIDADE DE SANTIAGO DE COMPOSTELA

Table 1.4. Classification of CLs according to the group suffix. Information adapted from UNE-EN ISO 18369-1 [UNE, 2018] by the author of this PhD Thesis.

Classification	Group	Description
Non-hydrogel materials (-focon)	1	Without silicon and fluorine
	2	With silicon but not fluorine
	3	With silicon and fluorine
	4	With fluorine but not silicon
Hydrogel materials (-filcon)	1	Low water content (<50%) and non-ionic (≤ 0.5% monomers that are ionized at pH 6-8).
	2	Medium-to-high water content (≥ 50%) and non-ionic (≤ 0.5% monomers that are ionized at pH 6-8).
	3	Low water content (<50%) and ionic (>0.5% monomers that are ionized at pH 6-8).
	4	High water content (≥ 50%) and ionic (>0.5% monomers that are ionized at pH 6-8).
	5 [a]	Materials with increased oxygen permeability (e.g. silicone hydrogels or silicone elastomer) Dk > 40 mmHg
	5A	Ionic subgroup, with monomers or oligomers that are ionized at pH 6-8.
	5B	High water content subgroup (water content ≥ 50%; without monomers or oligomers that are ionized at pH 6-8)
	5C	Low water content subgroup (water content < 50%; without monomers or oligomers that are ionized at pH 6-8)

a: These materials are biphasic, showing hydrophilic and hydrophobic regions.

Currently, FDA classifies daily wear CLs as class II and extended wear CLs as class III [CFR, 2021], while according to EU Directive corrective CLs for short-term use are class IIa and corrective CLs for long-term use are class IIb [Zaki et al., 2019].

USC UNIVERSIDADE DE SANTIAGO DE COMPOSTELA

CLs are also classified according to the intended use as: (1) non-therapeutic CLs (e.g., for correction of refractive ametropia, aphakia, and presbyopia); (2) CLs for specialized use (e.g., for the treatment of keratoconus) and (3) therapeutic CLs that serve as a tool in the treatment of a wide variety of ophthalmic disorders refractory to other treatment modalities [Shah et al., 2003]. Main applications of therapeutic CLs in corneal and ocular surface diseases are pain relief, enhancing corneal healing, corneal sealing, corneal protection, and drug delivery **(Figure 1.9)** [Lim and Lim, 2020]. Several bandage CLs have been evaluated to attenuate pain in the handling of bullous keratopathy and epithelial abrasions and in the post-operation of refractive surgery [Sánchez-González et al., 2019]. Silicone hydrogel CLs have been shown particularly suitable to favor corneal healing by acting as a scaffold that facilitates the spread of tear fluid, particularly after keratoplasty procedures. CLs also serve as a shield that protects cornea from eyelids and eyelashes, especially in patients with trichiasis, post-ptosis surgery, tarsal scarring and recurrent corneal erosions [Miller et al., 2019]. Small perforations (< 2 mm in diameter), lacerations and burns can be healed using silicone hydrogel CLs [Bendoriene and Vogt, 2006].

CLs could act also as platforms for the ocular delivery of drugs that may aid in the healing of the tissues and also to manage other ocular diseases (e.g. glaucoma) and ameliorate risks of the use of CLs (e.g. dry eye syndrome, infections). This later application of CLs as drug delivery systems is tackled in more detail in section 1.4.2. A decision tree of the use of CLs for therapeutic reasons, as an alternative to other strategies such as eye drops and keratoplasty, is depicted in **Figure 1.9**. It should be noted that a suspect of eye infection is a reason to discard CLs for therapeutic uses, and also that

USC
UNIVERSIDADE DE SANTIAGO DE COMPOSTELA

the use of CLs by itself increases the risk of suffering eye infections. Infections associated to CLs are overviewed in next section.

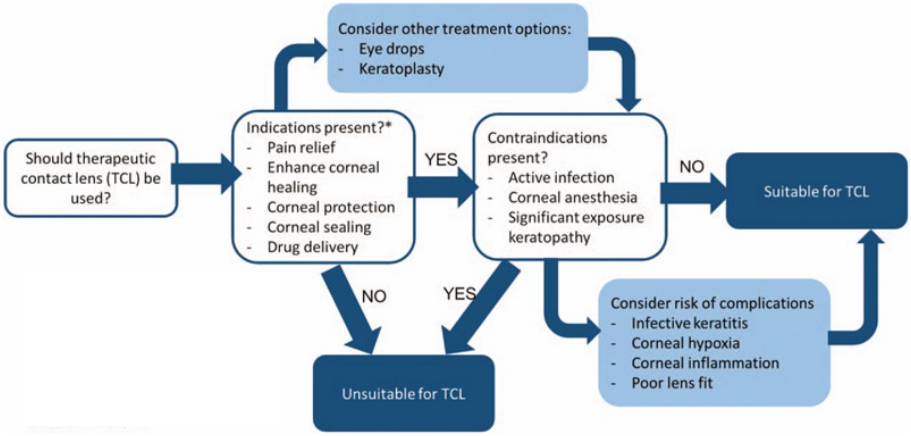


Figure 1.9. Decision tree for the use of CLs for the therapeutic purposes. Reproduced from Lim and Lim (2020) with permission of Wolters Kluwer Health, Inc.

1.4.1.1 Eye infections and CL-related biofilms

There are a wide variety of microorganisms present in or on the eyes. All together constitute the ocular microbiota [Willcox, 2013]. Commensal microbiota has been shown to regulate host physiology and host defense against pathogen invasion. Similarly, dysregulation of the microbiota (dysbiosis) may lead to overgrowth of pathogenic microorganisms, triggering a variety of inflammatory reactions [Li et al., 2020]. The eye is an immunologically privileged organ, which means that multiple mechanisms inhibit overt immune response, but it still allows, upon need, the selective entrance of immune cells for repair and healing. The eye as other parts of the

USC UNIVERSIDADE DE SANTIAGO DE COMPOSTELA

mammalian central nervous system (brain and spinal cord) is quite sealed from the blood stream, and thus the counting of immune cells is typically low to avoid excessive inflammation that can damage the eye tissues. As a drawback, this restricted immune response has been associated to the poor regenerative ability of optic nerve. Nevertheless, differently from the classical idea of that the immunologically privilege blocks immune cell entry, recent findings indicate that under certain pathological conditions selected immune cells can get access to contribute to solve the damage [London and Schwartz, 2012].

Changes in microbiota have been identified as a cause of access of immune cells into the eye, and may be also behind the inflammatory processes attributed to degenerative diseases, such as age-related macular degeneration (AMD). Indeed, commensal bacteria have been pointed out as an environmental factor that plays a role in AMD development because bacteria participate in lipids metabolism and the drusen in AMD has been demonstrated to contain a variety of anti-microbial substances [Wen et al., 2018]. Relationships between microbial pathogen and host factors in intraocular inflammation are receiving increasing attention [Li et al., 2020]. Recently gathered information suggests that, instead of the widely instituted treatments with anti-inflammatory drugs for acute and chronic degenerative diseases, modulation of the immune response may be more beneficial. Indeed, targeting ocular microbiota may become a novel therapy for diseases that present with inflammation, as observed for bowel diseases that target gut microbiota [Gunardi et al., 2021].

The eye surface counts with the synergic antimicrobial tools of eye blinking and lysozyme in tear fluid, which may kill bacteria and remove them from the surface **(Figure 1.10)** [McDermott, 2013; Fleiszig et al., 2020]. Nevertheless, a wide variety of microorganisms

USC UNIVERSIDADE DE SANTIAGO DE COMPOSTELA

persist on ocular surface, conjunctiva and eye lid, mainly Gram-positive bacteria like coagulase-negative *Staphylococcus, Streptococcus, Propionibacterium, Corynebacterium, Diphtheroid bacteria* and *Micrococcus* [Miller and Iovieno, 2009; Doan et al., 2016]. Gram-negative bacteria typical of the gut are less frequent as well as fungi. Overall, the most abundant microorganism in the ocular surface is *S. aureus* although its ratio may change with age, sex and eye pathologies [Lu and Liu, 2016; Wen et al., 2017].

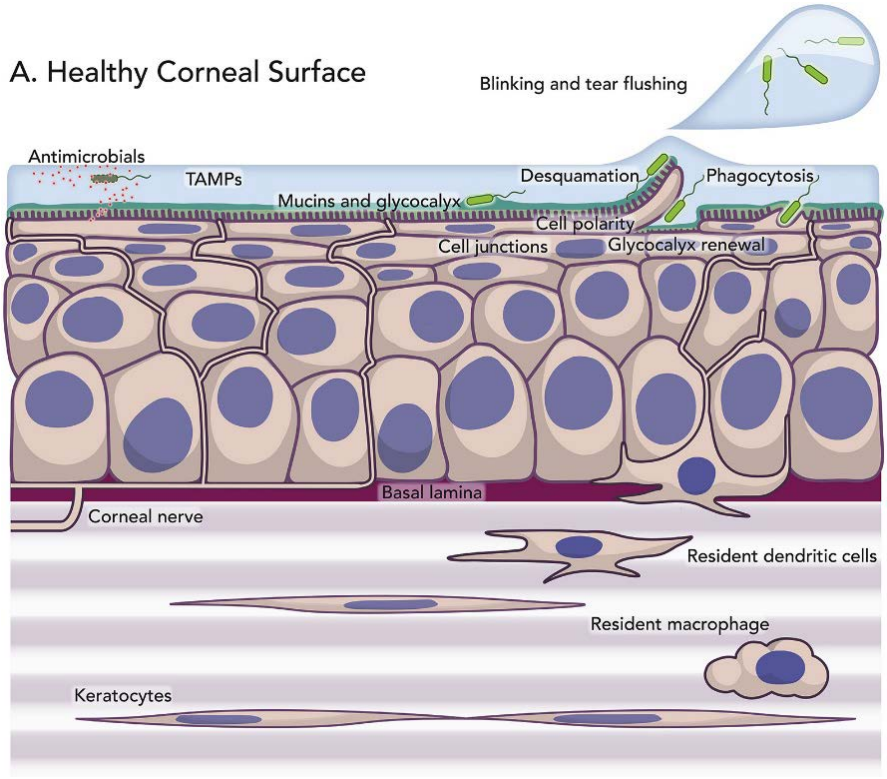


Figure 1.10. Antimicrobial defenses of healthy cornea are constituted by tear fluid, epithelium, basal lamina and resident immune cells. These defenses can be upregulated in response to Tear-Associated Molecular Patterns (TAMPs), which include microbial and non-microbial ligands. Reproduced from Fleiszig et al. (2020) with permission of Elsevier.

USC UNIVERSIDADE DE SANTIAGO DE COMPOSTELA

The intraocular compartments are considered to be sterile (at least the intraocular microbiome has not been deciphered yet), but microorganisms can easily enter after eye surface damage and ocular surgery (e.g. cataract extraction) [Rahmani and Eliott, 2018]. Also microorganisms can get access from the blood stream (main source of microorganisms is a permeable gut wall) in the case of chronic diseases affecting retinal vasculature, such as in the case of diabetic retinopathy, or may enter from the nerves if an infection (mainly by virus) of the central nervous system occurs [Camelo et al., 2001; Beli et al., 2018]. Both aqueous humor and vitreous humor are excellent culture media and, therefore, contaminating microorganisms can easily develop inside the eye [Egger et al., 1997].

Wearing of CLs is one of the most relevant risk factors for developing microbial keratitis (up to 20 cases per 10,000 wearers), with an incidence 80-fold higher than in non-wearers [Cheung et al., 2016; Lim et al., 2018]. As any other biomaterial, CLs are prone to be colonized by microorganisms, but the wearing itself may induce changes in the eyes that favor infections **(Figure 1.11)** [Fleiszig et al., 2020]. Since cornea is avascular, it relies on the precorneal tear film for the supply of oxygen, nutrients and the clearance of metabolic products. CLs disrupt the tear film and the prolonged wearing causes hypoxia, which triggers erythema and tissue swelling and impairs the removal of microorganisms [Weissman and Mondino, 2002]. CL-induced acute red eye response is exacerbated by endotoxins from Gram-negative bacteria, such as *P. aeruginosa* and *H. influenzae*, and Gram-positive species such as *S. pneumoniae* [Sankaridurg et al., 1996]. Additionally, biofilms can develop on both CLs and CL cases.

USC
UNIVERSIDADE DE SANTIAGO DE COMPOSTELA

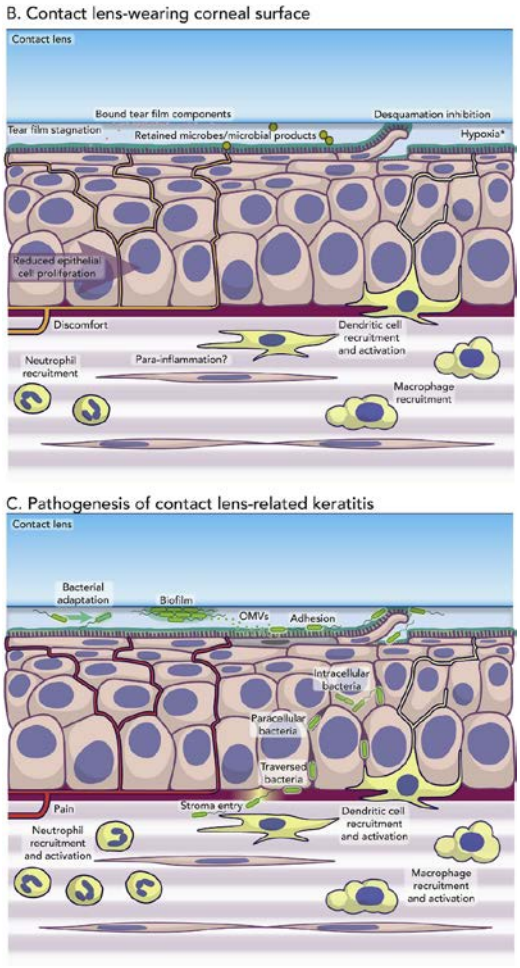


Figure 1.11. CLs may alter eye defenses by binding tear components and reducing basal epithelial cell proliferation and surface cell desquamation. CLs also cause tear film stagnation, may bind commensal microbiota and activate pro-inflammatory mechanisms (e.g. dendritic cell activation) (plot B). *P. aeruginosa* readily forms biofilms on CLs undergoing phenotypic and genotypic changes that make bacteria to become resistant to natural defenses and antimicrobial agents (plot C). Bacteria in the biofilm release membrane vesicles (OMVs) containing virulence factors that alter host cell functions and facilitate bacterial adhesion and subsequent intracellular or paracellular penetration through epithelium. Reproduced from Fleiszig et al. (2020) with permission of Elsevier.

USC UNIVERSIDADE DE SANTIAGO DE COMPOSTELA

Nonadherence with the recommended strict hygienic practices notably contributes to contamination and proliferation of microorganisms; thus, daily disposable CLs are less prone to cause microbial keratitis [Stapleton and Carnt, 2012]. No relevant differences in morbidity have been found among hydrogel and silicone hydrogel CLs; *P. aeruginosa* being the main causal agent [Fleiszig et al., 2020].

Wearing at night increases even more the risk of infection. In particular, the use of orthokeratology CLs for myopia control is associated to an increased likelihood of *Acanthamoeba* infection [Wu and Xie,2021]. Keratitis caused by *Acanthamoeba*, although quite infrequent, have a poor prognosis and may lead to vision loss. The infection with this free-living protozoan usually occurs after washing the CLs or the CL cases with tap water. The risk of developing the infection is higher for soft CL wearers compared to regular rigid permeable CLs, but the overnight use for orthokeratology increases the risk. The shape of orthokeratology CLs is different from that of regular CLs because they are intended to flatten the central cornea curvature and reduce the axial elongation. Thus, orthokeratology CLs exert a force against cornea that causes the thinning of central corneal epithelium and probably surface cell damage, which is increased under the oxygen deprivation conditions of overnight wearing [Zhang et al., 2020]. These changes weaken the host tissue barrier and favor microorganism adhesion, as also observed for *P. aeruginosa* [Wei et al., 2014]. If there is a suspicion of infection, CLs should be withdrawn and the wearing discontinued until complete eye health recovery.

USC
UNIVERSIDADE DE SANTIAGO DE COMPOSTELA

1.4.2 CLs for drug delivery

CLs were proposed as ocular drug delivery systems since the first prototypes of soft CLs were synthesized nearly 50 years ago, but only in the first 2000´s the implementation of specific methodologies for drug loading and controlled release become feasible [White et al., 2011; González-Chomón et al., 2013; Hui and Willcox, 2016].

Once applied onto the eye, the CL compartmentalizes the tear film into two layers; the outer pre-lens tear film and the inner post-lens tear film **(Figure 1.12)** [Willcox et al., 2017]. Such a compartmentalization triggers relevant biophysical and biochemical changes, which may be exploited for the sustained release of a drug towards the cornea. The post-lens tear film is very thin (1-2 μm) and causes the stagnation of the liquid beneath the CL. The slower turnover has been associated to certain complications during prolonged CL wear, as the flushing of debris and metabolic byproducts from the cornea surface is slowed down [Muntz et al., 2015]. As mentioned above, complications are mainly shown as increased risk of infections and dry eye symptoms. Nevertheless, nearly 50 years of history of CL wearing avail their biocompatibility, and the development of advanced materials makes prolonged wearing feasible. Additionally, innovative performances such as drug delivery, visual augmentation and biosensing could be coupled to the vision correction performance of the CLs [Papas, 2017; Alvarez-Lorenzo et al., 2019].

USC
UNIVERSIDADE DE SANTIAGO DE COMPOSTELA

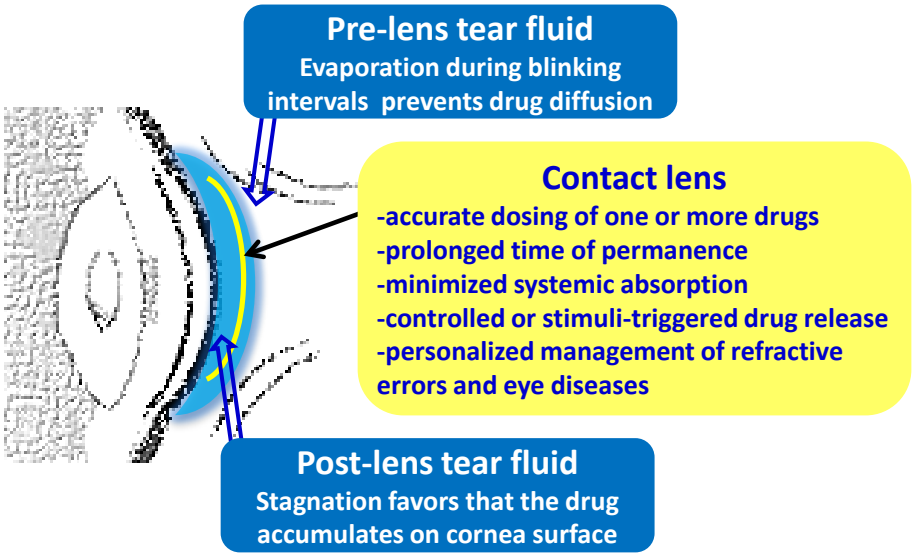


Figure 1.12. Scheme of anterior eye segment and compartmentalization of tear film once a CL is inserted. Potential performances of CLs as drug delivery systems are listed. Reproduced from Alvarez-Lorenzo et al. (2019) with permission of Elsevier.

A drug-loaded CL mainly releases the drug to the post-lens tear film. Since the turnover of this film occurs slowly, greater drug levels can be attained, which promotes cornea penetration. The amount released towards the outer pre-lens tear film layer is approx. 5 times smaller because of the dry periods of the anterior face of the CL during the blinking interval [Li and Chauhan, 2006]. Drug corneal permeability is usually in the 10^{-5} to 10^{-7} cm/s range [Prausnitz and Noonan, 1998]. If drug diffusion from a CL happens at a slower rate than penetration through the cornea, drug levels in the ocular structures may be regulated by the release rate [Liu et al., 2016]. The released drug is rapidly transferred through the post-lens tear fluid (in a timeframe of few seconds) showing perfectly sink conditions [Gause

USC UNIVERSIDADE DE SANTIAGO DE COMPOSTELA

et al., 2016]. Prolonged permanence of the drug on the cornea favors intraocular accumulation, which in turn remarkably improves the pharmacological response compared to eye drops administration [Vandorselaer et al., 2001; Hiratani et al., 2005; Jaishankar et al., 2016]. Adequately designed CLs may enhance ocular bioavailability up to 50%. In some cases, better exploitation of the drug administered can even allow decreasing the dose required to attain the desired therapeutic effect [Hiratani et al., 2005; Hui and Willcox, 2016; Dominguez-Godinez et al., 2018]. Sustained release of lower dose should also contribute to attenuate the systemic absorption through conjunctiva or nasolachrymal system observed for eye drops, and thus the collateral untoward effects.

Compared to eye drops and other ocular drug delivery systems, CLs may offer unique features [Alvarez-Lorenzo et al., 2019]:

— accurate dosing,

— feasibility of incorporating two or more active substances in relatively high quantity,

— preservation of epithelium integrity and visual accuracy,

— prolonged time of permanence on the ocular surface, which allows convenient once-a-day application,

— delayed tear turnover, which facilitates drug accumulation on the cornea surface,

— minimized systemic absorption, since the drug is mainly delivered towards the cornea,

— controlled drug release, avoiding strong fluctuation in drug levels,

USC UNIVERSIDADE DE SANTIAGO DE COMPOSTELA

— personalized drug dose, release rate, and dimensions of the CLs covering specific surface areas of cornea and/or sclera for modulating drug penetration,

— possibility of triggering drug release as a function of inner or externally applied stimuli,

— possibility of simultaneous correction of refractive errors and supply of pharmaceutical treatment.

Regarding patient acceptance, several surveys have evidenced that most patients with ocular chronic diseases would accept CLs better than other drug delivery systems such as plugs or subconjunctival injections if CLs demonstrate greater efficacy than eye drops [Ghazal et al., 2019]. Moreover, it has been recorded that the wearing of therapeutic bandage CLs after cataract surgery significantly improves the comfort feeling and the tear film stability without delaying corneal incision healing [Shi et al., 2018].

In spite of all these *a priori* advantages, materialization of CLs as drug delivery platforms has to face up to the problem of that simple soaking of commercially available CLs into a drug solution usually does not lead to therapeutic loadings. Additionally, most CLs rapidly release the small amount loaded immediately once applied onto the eye or even in the storage solution. These facts pose relevant scientific and technological challenges. Additionally, there are translational and regulatory issues to be solved too. The absence of standardized *in vitro* drug release tests and the difficulties in mimicking the dynamics of the post-lens tear fluid make the comparison of the results obtained in different laboratories difficult and the prediction of the *in vivo* performance poorly realistic [Tieppo et al., 2014; Hui and Willcox, 2016]. Attempts in this regard to identify critical variables are very valuable, as well as the development of animal models that can

USC UNIVERSIDADE DE SANTIAGO DE COMPOSTELA

provide information not only on the formulation safety but also on the efficacy [Awwad et al., 2015; Mann et al., 2018]. There have been also many advances in mathematical modeling of drug diffusion through CLs, tear film and cornea [Gause et al., 2016; Pimenta et al., 2016], and also in *ex vivo* set-ups for cornea/sclera permeability [Agarwal and Rupenthal, 2016] and even in "eye-on-a-chip" for pharmacokinetic and pharmacological screening [Estlack et al., 2017]. Also some studies have pointed out the delay that bacteria biofilm formation on CLs may cause on drug release rate [Brothers et al., 2014].

These modeling and experimental data may provide useful feed-back for the optimization of the CL design. From a regulatory point of view, drug-eluting CLs are considered as a subclass of combination products and thus depending on whether the drug or the medical device plays the primary mode of action different regulatory guidelines and policies should be followed [Novack, 2009; Luk and Juannarkar, 2013]. The investment risks associated to the approval process and subsequent commercialization are also significant barriers for the industrial development of drug-eluting CLs [Laniert et al., 2020].

Main strategies tested so far to improve drug loading in CLs as well as to prolong drug release are summarized in **Table 1.5**.

USC
UNIVERSIDADE DE SANTIAGO DE COMPOSTELA

Table 1.5. Main technologies implemented to endow CLs with ability to incorporate therapeutic doses of drugs and to sustain their release. Data compiled by the author of this PhD Thesis.

Tech.	Main features	Pros	Cons	Ref.
Coating with a drug-loaded film	Conventional CLs are coated with a drug and a hydrophobic polymer or vitamin E, covering the whole surface or leaving a central window.	-Suitable for any CL. -Precise regulation of drug release through adequate choice of the coating. -Release profile can be extended for weeks.	-Organic solvents may be needed, or sandwich approaches -Some coatings cause the opacity of the CLs and may compromise patient acceptability.	Sekar and Chauhan, 2019; Bengani et al., 2020
Layer-by-layer coatings	Conventional CLs are coated layer-by-layer exploiting ionic interactions between oppositely charged hydrophilic polymers. The drug is entrapped inside the coating.	-Suitable for any CL. -Precise regulation of drug release through adequate choice of the coating. -Release profile can be extended for weeks.	-Time consuming due to the several steps for preparing the coatings. -Hydrophilic drugs may be prematurely released. -Chemical cross-linking of the coated may be required.	Silva et al., 2021; Wang et al., 2021
Drug immobilized via labile bond	The drug is bonded to the CL by means of labile covalent bond intended to be broken by enzymes on the ocular surface.	-Precise control of amount loaded.	-Chemical modification of the drug is required. -Possible high inter- and intra-individual variability.	Vairon et al., 1992
Incorporation of drug-loaded nanocarriers during CL	Nanocarriers are preloaded with the drug and then dispersed in the monomers solution with the aim of remaining entrapped in the CL and regulating drug release.	-A variety of drugs can be encapsulated and the total loading can be higher than by soaking. -Release can be sustained or even stimuli-responsive.	-Particle size and total content in nanocarriers determine the light transparency. -Most nanocarriers do not withstand conventional steam-heat sterilization method. -Risk of premature release in the packaging solution.	Maulvi et al., 2017; Xu et al., 2019

USC UNIVERSIDADE DE SANTIAGO DE COMPOSTELA

Incorporation of drug-loaded nanocarriers after CL synthesis	Drug-loaded nanocarriers can be surface immobilized or diffuse into the CL network.	-No interference in CL synthesis. -Encapsulation protect the drug and provides sustained release patterns.	-Poor control of the chemical reactions for surface immobilization. -Poor loading of the nanocarriers by soaking in water. Organic solvents may be needed.	Danion et al., 2007
CL containing cyclodextrins	Cyclodextrin monomers are used as comonomers during CL synthesis or grafted in a subsequent step-	-Capability of cyclodextrins to form inclusion complexes may enhance drug loading by soaking in aqueous solutions and also to regulate drug release.	-Synthesis of cyclodextrin monomers may be needed. -Multireactive cyclodextrins may increase the cross-linking degree of the network leading to stiffer CL.	dos Santos et al., 2009; Xu et al., 2010
CL prepared with monomers that have affinity for the drug	Monomers bearing ionizable groups may interact with oppositely charged drugs. Alternatively, monomers that exploit other kind of interactions (hydrophobic, hydrogen bonding) can be used.	-Easy synthesis in the absence of the drug. -Drug loading and release can be finely tuned by regulating the nature and content of the functional monomer.	-Limited list of monomers suitable for CL. -Changes in swelling degree during use if the CL contains strongly ionisable monomers. -Risk of sorption of proteins.	Kakisu et al., 2013; Varela-Garcia et al., 2020
Molecularly imprinted CLs	Drug molecules are used as template during CL synthesis to aid in the spatial arrangement of the functional monomers according to their affinity. The arrangement is fixed during polymerization and then the template drug molecules are removed to create artificial receptors.	-High drug (re)loading, particularly when the affinity of conventional CLs is low. -Controlled release. -Strategies bioinspired in the natural receptor of the drug in the human body may improve the outcomes.	-Specific design for each drug. -Risk of drug degradation during polymerization. -Time consuming removal step.	Ribeiro et al., 2011; Alvarez-Rivera et al., 2019; DiPasquale et al., 2021

USC UNIVERSIDADE DE SANTIAGO DE COMPOSTELA

Analysis of literature on drug-eluting CLs reveals that there is not a universal process that may be suitable for any drug or disease condition. Differently, the strategy should be adapted to the therapeutic aim, the nature (hydrophobicity) and stability of the drug, the required tear levels and the time that they should be prolonged. Moreover, the properties that are critical for the CL to act as an ophthalmic medical device (mechanical properties, light transparency, oxygen permeability) should be fulfilled. In the case of antimicrobial performances, in addition to the controlled release of antibiotics once an eye infection is settled, the search for strategies bioinspired on how the nature tackles biofouling may provide tools useful for prophylaxis [Alvarez-Lorenzo et al., 2019]. Although the information is still limited, recent reports pointed out zwitterionic monomers, which resemble the phospholipids of cell membranes, as potentially suitable antibioufouling components of CLs able to reduce protein adsorption and microorganisms adherence and, in some cases, even increase the affinity for the drug [Huang et al., 2007; Xu et al., 2014; Ogawa et al., 2020].

1.5 REFERENCES

Agarwal, P., & Rupenthal, I. D. (2016). In vitro and ex vivo corneal penetration and absorption models. *Drug Delivery and Translational Research*, *6*(6), 634-647.

Ahmad, N., Etheridge, C., Farrington, M., & Baguley, D. M. (2007). Prospective study of the microbiological flora of hearing aid moulds and the efficacy of current cleaning techniques. *Journal of Laryngology & Otology*, *121*(2), 110-113.

USC UNIVERSIDADE DE SANTIAGO DE COMPOSTELA

Alvarez-Lorenzo, C., Anguiano-Igea, S., Varela-García, A., Vivero-Lopez, M., & Concheiro, A. (2019). Bioinspired hydrogels for drug-eluting contact lenses. *Acta Biomaterialia*, *84*, 49-62.

Alvarez-Lorenzo, C., Bucio, E., Burillo, G., & Concheiro, A. (2010). Medical devices modified at the surface by γ-ray grafting for drug loading and delivery. *Expert Opinion on Drug Delivery*, *7*(2), 173-185.

Alvarez-Lorenzo, C., & Concheiro, A. (2013). Drug/medical device combination products with stimuli-responsive eluting surface. *Smart Materials for Drug Delivery*, *2*, 313-348.

Alvarez-Lorenzo, C., & Concheiro, A. (2019). Smart drug release from medical devices. *Journal of Pharmacology and Experimental Therapeutics*, *370*(3), 544-554.

Alvarez-Lorenzo, C., Garcia-Gonzalez, C. A., Bucio, E., & Concheiro, A. (2016). Stimuli-responsive polymers for antimicrobial therapy: drug targeting, contact-killing surfaces and competitive release. *Expert Opinion on Drug Delivery*, *13*(8), 1109-1119.

Alvarez-Rivera, F., Serro, A. P., Silva, D., Concheiro, A., & Alvarez-Lorenzo, C. (2019). Hydrogels for diabetic eyes: Naltrexone loading, release profiles and cornea penetration. *Materials Science and Engineering: C*, *105*, 110092.

Anderson, J. M. (2015). Exploiting the inflammatory response on biomaterials research and development. *Journal of Materials Science: Materials in Medicine*, *26*(3), 121.

Anmyr, L., Olsson, M., Larson, K., & Freijd, A. (2011). Children with hearing impairment–living with cochlear implants or hearing aids. *International Journal of Pediatric Otorhinolaryngology*, *75*(6), 844-849.

Antich-Isern, P., Caro-Barri, J., & Aparicio-Blanco, J. (2021). The combination of medical devices and medicinal products revisited from the

USC UNIVERSIDADE DE SANTIAGO DE COMPOSTELA

new European Legal framework. *International Journal of Pharmaceutics*, *607*, 120992.

Awwad, S., Lockwood, A., Brocchini, S., & Khaw, P. T. (2015). The PK-Eye: a novel in vitro ocular flow model for use in preclinical drug development. *Journal of Pharmaceutical Sciences*, *104*(10), 3330-3342.

Barbosa, J. N., Madureira, P., Barbosa, M. A., & Aguas, A. P. (2006). The influence of functional groups of self-assembled monolayers on fibrous capsule formation and cell recruitment. *Journal of Biomedical Materials Research Part A*, *76*(4), 737-743.

Barr, J., & Mack, C. (2011). Contact lenses yesterday, today, and the best yet to come. *Contact Lens Spectrum*, *26*(1), 14-15.

Bayarri, L. (2015). Drug-device combination products: regulatory landscape and market growth. *Drugs of Today*, *51*(8), 505-513.

Beli, E., Yan, Y., Moldovan, L., Vieira, C. P., Gao, R., Duan, Y., ... & Grant, M. B. (2018). Restructuring of the gut microbiome by intermittent fasting prevents retinopathy and prolongs survival in db/db mice. *Diabetes*, *67*(9), 1867-1879.

Bendoriene, J., & Vogt, U. (2006). Therapeutic use of silicone hydrogel contact lenses in children. *Eye & Contact Lens*, *32*(2), 104-108.

Bengani, L. C., Kobashi, H., Ross, A. E., Zhai, H., Salvador-Culla, B., Tulsan, R., ... & Ciolino, J. B. (2020). Steroid-eluting contact lenses for corneal and intraocular inflammation. *Acta Biomaterialia*, *116*, 149-161.

Brodbeck, W. G., Shive, M. S., Colton, E., Nakayama, Y., Matsuda, T., & Anderson, J. M. (2001). Influence of biomaterial surface chemistry on the apoptosis of adherent cells. *Journal of Biomedical Materials Research*, *55*(4), 661-668.

Brothers, K. M., Nau, A. C., Romanowski, E. G., & Shanks, R. M. (2014). Dexamethasone diffusion across contact lenses is inhibited by *Staphylococcus epidermidis* biofilms in vitro. *Cornea*, *33*(10), 1083.

USC UNIVERSIDADE DE SANTIAGO DE COMPOSTELA

Bryers, J. D., Giachelli, C. M., & Ratner, B. D. (2012). Engineering biomaterials to integrate and heal: the biocompatibility paradigm shifts. *Biotechnology and Bioengineering*, *109*(8), 1898-1911.

Camelo, S., Castellanos, J., Lafage, M., & Lafon, M. (2001). Rabies virus ocular disease: T-cell-dependent protection is under the control of signaling by the p55 tumor necrosis factor alpha receptor, p55TNFR. *Journal of Virology*, *75*(7), 3427-3434.

Canfield, J., & Totary-Jain, H. (2018). 40 years of percutaneous coronary intervention: history and future directions. *Journal of Personalized Medicine*, *8*(4), 33.

CFR - Code of Federal Regulations Title 21. PART 886 -- OPHTHALMIC DEVICES. https://www.accessdata.fda.gov/scripts/cdrh/cfdocs/cfcfr/cfrsearch.cfm?fr=886.5925; Accessed January 2022

Cheung, N., Nagra, P., & Hammersmith, K. (2016). Emerging trends in contact lens-related infections. *Current Opinion in Ophthalmology*, *27*(4), 327-332.

Conlon, B. P. (2014). *Staphylococcus aureus* chronic and relapsing infections: evidence of a role for persister cells: an investigation of persister cells, their formation and their role in *S. aureus* disease. *Bioessays*, *36*(10), 991-996.

Costerton, J. W. (1999). Introduction to biofilm. *International Journal of Antimicrobial Agents*, *11*(3-4), 217-221.

Danion, A., Arsenault, I., & Vermette, P. (2007). Antibacterial activity of contact lenses bearing surface-immobilized layers of intact liposomes loaded with levofloxacin. *Journal of Pharmaceutical Sciences*, *96*(9), 2350-2363.

da Silva Domingues, J. F., Roest, S., Wang, Y., van der Mei, H. C., Libera, M., van Kooten, T. G., & Busscher, H. J. (2015). Macrophage phagocytic

USC UNIVERSIDADE DE SANTIAGO DE COMPOSTELA

activity toward adhering staphylococci on cationic and patterned hydrogel coatings versus common biomaterials. *Acta Biomaterialia*, *18*, 1-8.

DiEgidio, P., Friedman, H. I., Gourdie, R. G., Riley, A. E., Yost, M. J., & Goodwin, R. L. (2014). Biomedical implant capsule formation: lessons learned and the road ahead. *Annals of Plastic Surgery*, *73*(4), 451-460.

DiPasquale, S. A., Wuchte, L. D., Mosley, R. J., Demarest, R. M., Voyles, M. L., & Byrne, M. E. (2021). One week sustained in vivo therapeutic release and safety of novel extended-wear silicone hydrogel contact lenses. *Advanced Healthcare Materials*, 2101263.

Doan, T., Akileswaran, L., Andersen, D., Johnson, B., Ko, N., Shrestha, A., ... & Van Gelder, R. N. (2016). Paucibacterial microbiome and resident DNA virome of the healthy conjunctiva. *Investigative Ophthalmology & Visual Science*, *57*(13), 5116-5126.

Dominguez-Godinez, C., Carracedo, G., & Pintor, J. (2018). Diquafosol delivery from silicone hydrogel contact lenses: improved effect on tear secretion. *Journal of Ocular Pharmacology and Therapeutics*, *34*(1-2), 170-176.

Donlan, R. M. (2001). Biofilm formation: a clinically relevant microbiological process. *Clinical Infectious Diseases*, *33*(8), 1387-1392.

dos Santos, J. F. R., Alvarez-Lorenzo, C., Silva, M., Balsa, L., Couceiro, J., Torres-Labandeira, J. J., & Concheiro, A. (2009). Soft contact lenses functionalized with pendant cyclodextrins for controlled drug delivery. *Biomaterials*, *30*(7), 1348-1355.

Egger, S. F., Buxbaum, A., Georgopoulos, M., Scholda, C., Vecsei, V. P., Huber-Spitzy, V., & Georgopoulos, A. (1997). Bacterial growth in human vitreous humor. *Experimental Eye Research*, *65*(6), 791-795.

EHIMA - European Hearing Instrument Manufacturers Association. Classification of Hearing Aids and Accessories. February 1, 2020.

USC
UNIVERSIDADE DE SANTIAGO DE COMPOSTELA

https://www.ehima.com/wp-content/uploads/2020/02/Classification-Document-v15.1.pdf, Accessed January 2022

EMA (2021). Guideline on quality documentation for medicinal products when used with a medical device. https://www.ema.europa.eu/en/documents/scientific-guideline/guideline-quality-documentation-medicinal-products-when-used-medical-device-first-version_en.pdf; Accessed January 2022.

Ene, R., Nica, M., Ene, D., Cursaru, A., & Cirstoiu, C. (2021). Review of calcium-sulphate-based ceramics and synthetic bone substitutes used for antibiotic delivery in PJI and osteomyelitis treatment. *EFORT Open Reviews*, *6*(5), 297-304.

Estlack, Z., Bennet, D., Reid, T., & Kim, J. (2017). Microengineered biomimetic ocular models for ophthalmological drug development. *Lab on a Chip*, *17*(9), 1539-1551.

FDA (2021). Medical Devices; Ear, Nose, and Throat Devices; Establishing Over-the Counter Hearing Aids. Federal Register 86, 58150. https://www.federalregister.gov/documents/2021/10/20/2021-22473/medical-devices-ear-nose-and-throat-devices-establishing-over-the-counter-hearing-aids; Accessed January 2022

Farto-Vaamonde, X., Auriemma, G., Aquino, R. P., Concheiro, A., & Alvarez-Lorenzo, C. (2019). Post-manufacture loading of filaments and 3D printed PLA scaffolds with prednisolone and dexamethasone for tissue regeneration applications. *European Journal of Pharmaceutics and Biopharmaceutics*, *141*, 100-110.

Fleiszig, S. M., Kroken, A. R., Nieto, V., Grosser, M. R., Wan, S. J., Metruccio, M. M., & Evans, D. J. (2020). Contact lens-related corneal infection: Intrinsic resistance and its compromise. *Progress in Retinal and Eye Research*, *76*, 100804.

Fusconi, M., Petrozza, V., Taddei, A. R., Vinciguerra, V., De Virgilio, A., Chiarini, F., ... & de Vincentiis, M. (2011). Is biofilm the cause of chronic otitis externa?. *The Laryngoscope*, *121*(12), 2626-2633.

García-Vargas, M., González-Chomón, C., Magariños, B., Concheiro, A., Alvarez-Lorenzo, C., & Bucio, E. (2014). Acrylic polymer-grafted polypropylene sutures for covalent immobilization or reversible adsorption of vancomycin. *International Journal of Pharmaceutics*, *461*(1-2), 286-295.

Gause, S., Hsu, K. H., Shafor, C., Dixon, P., Powell, K. C., & Chauhan, A. (2016). Mechanistic modeling of ophthalmic drug delivery to the anterior chamber by eye drops and contact lenses. *Advances in Colloid and Interface Science*, *233*, 139-154.

Georgescu, M., Vrinceanu, D., Radulescu, L., Tusaliu, M., Martu, C., Curutiu, C., ... & Budu, V. (2017). Microbial biofilms and implantable hearing aids. *Romanian Biotechnological Letters*, *22*(4), 12681-12686.

Ghazal, H., Ahmadouk, J., Dhanji, S., El-Bushra, A., Kayyali, R., & ElShaer, A. (2019). Patients' and prescribers' perception of contact lenses as a potential ocular drug delivery system. *Contact Lens and Anterior Eye*, *42*(2), 190-195.

Gheorghe, D. C., Ilie, A., Niculescu, A. G., & Grumezescu, A. M. (2021). Preventing biofilm formation and development on ear, nose and throat medical devices. *Biomedicines*, *9*(8), 1025.

Ghimire, N., Pettygrove, B. A., Pallister, K. B., Stangeland, J., Stanhope, S., Klapper, I., ... & Stewart, P. S. (2019). Direct microscopic observation of human neutrophil-*Staphylococcus aureus* interaction in vitro suggests a potential mechanism for initiation of biofilm infection on an implanted medical device. *Infection and Immunity*, *87*(12), e00745-19.

González-Chomón, C., Concheiro, A., & Alvarez-Lorenzo, C. (2013). Soft contact lenses for controlled ocular delivery: 50 years in the making. *Therapeutic Delivery*, *4*(9), 1141-1161.

USC
UNIVERSIDADE DE SANTIAGO DE COMPOSTELA

Gregoret, L. (2019). The Movin' Groovin' outer ear. Audiology Online, Article 25805. Retrieved from Audiology Online Continuing Education. https://www.audiologyonline.com/articles/the-moovin-groovin-outer-ear-25805; Accessed January 2022

Grevers, G. (2010). Challenges in reducing the burden of otitis media disease: an ENT perspective on improving management and prospects for prevention. *International Journal of Pediatric Otorhinolaryngology*, *74*(6), 572-577.

Gunardi, T. H., Susantono, D. P., Victor, A. A., & Sitompul, R. (2021). Atopobiosis and dysbiosis in ocular diseases: is fecal microbiota transplant and probiotics a promising solution?. *Journal of Ophthalmic & Vision Research*, *16*(4), 631.

Haddad, F. S., Ngu, A., & Negus, J. J. (2017). Prosthetic joint infections and cost analysis?. *A Modern Approach to Biofilm-Related Orthopaedic Implant Infections*, 93-100.

Hampson, R. (2012). Hearing aids. *European Geriatric Medicine*, *3*(3), 198-200.

Hilborn, J., & Bjursten, L. M. (2007). A new and evolving paradigm for biocompatibility. *Journal of Tissue Engineering and Regenerative Medicine*, *1*(2), 110-119.

Hiratani, H., Fujiwara, A., Tamiya, Y., Mizutani, Y., & Alvarez-Lorenzo, C. (2005). Ocular release of timolol from molecularly imprinted soft contact lenses. *Biomaterials*, *26*(11), 1293-1298.

Huang, Y., Ng, H. C. A., Ng, X. W., & Subbu, V. (2014). Drug-eluting biostable and erodible stents. *Journal of Controlled Release*, *193*, 188-201.

Huang, X. D., Yao, K., Zhang, H., Huang, X. J., & Xu, Z. K. (2007). Surface modification of silicone intraocular lens by 2-methacryloyloxyethyl phosphoryl-choline binding to reduce *Staphylococcus epidermidis* adherence. *Clinical & Experimental Ophthalmology*, *35*(5), 462-467.

USC UNIVERSIDADE DE SANTIAGO DE COMPOSTELA

Hudecki, A., Kiryczyński, G., & Łos, M. J. (2019). Biomaterials, definition, overview. In *Stem Cells and Biomaterials for Regenerative Medicine* (Los, M.J., Hudecki, A., Wiecheć, E., Eds.), Academic Press, pp. 85-98.

Hui, A., & Willcox, M. (2016). In vivo studies evaluating the use of contact lenses for drug delivery. *Optometry and Vision Science*, *93*(4), 367-376.

Hupcey, M. A., & Ekins, S. (2007). Improving the drug selection and development process for combination devices. *Drug Discovery Today*, *12*(19-20), 844-852.

ISO 18369-1:2017(en). Ophthalmic optics — Contact lenses — Part 1: Vocabulary, classification system and recommendations for labelling specifications, 2017. https://www.iso.org/standard/66338.html; Accessed January 2022.

Jaishankar, D., Buhrman, J. S., Valyi-Nagy, T., Gemeinhart, R. A., & Shukla, D. (2016). Extended release of an anti–heparan sulfate peptide from a contact lens suppresses corneal herpes simplex virus-1 infection. *Investigative Ophthalmology & Visual Science*, *57*(1), 169-180.

Kakisu, K., Matsunaga, T., Kobayakawa, S., Sato, T., & Tochikubo, T. (2013). Development and efficacy of a drug-releasing soft contact lens. *Investigative Ophthalmology & Visual Science*, *54*(4), 2551-2561.

Kaushik, V., Malik, T., & Saeed, S. R. (2010). Interventions for acute otitis externa. *Cochrane Database of Systematic Reviews*, *1*, CD004740.

Klopfleisch, R., & Jung, F. (2017). The pathology of the foreign body reaction against biomaterials. *Journal of Biomedical Materials Research Part A*, *105*(3), 927-940.

Koo, J. H., Song, J. K., Kim, D. H., & Son, D. (2021). Soft implantable bioelectronics. *ACS Materials Letters*, *3*(11), 1528-1540.

Lanier, O. L., Christopher, K. G., Macoon, R. M., Yu, Y., Sekar, P., & Chauhan, A. (2020). Commercialization challenges for drug eluting contact lenses. *Expert Opinion on Drug Delivery*, *17*(8), 1133-1149.

USC UNIVERSIDADE DE SANTIAGO DE COMPOSTELA

Li, C. C., & Chauhan, A. (2006). Modeling ophthalmic drug delivery by soaked contact lenses. *Industrial & Engineering Chemistry Research*, *45*(10), 3718-3734.

Li, J. J., Yi, S., & Wei, L. (2020). Ocular microbiota and intraocular inflammation. *Frontiers in Immunology*, *11*, 3388.

Lim, L., & Lim, E. W. L. (2020). Therapeutic contact lenses in the treatment of corneal and ocular surface diseases—A review. *The Asia-Pacific Journal of Ophthalmology*, *9*(6), 524-532.

Lim, C. H., Stapleton, F., & Mehta, J. S. (2018). Review of contact lens–related complications. *Eye & Contact Lens*, *44*, S1-S10.

Liu, D. E., Dursch, T. J., Taylor, N. O., Chan, S. Y., Bregante, D. T., & Radke, C. J. (2016). Diffusion of water-soluble sorptive drugs in HEMA/MAA hydrogels. *Journal of Controlled Release*, *239*, 242-248.

Liu, Y. C., Zou, X. B., Chai, Y. F., & Yao, Y. M. (2014). Macrophage polarization in inflammatory diseases. *International Journal of Biological Sciences*, *10*(5), 520.

London, A., & Schwartz, M. (2012). The privileged immunity of immune privileged organs: the case of the eye. *Frontiers in Immunology*, *3*, 296.

Lu, L. J., & Liu, J. (2016). Focus: microbiome: human microbiota and ophthalmic disease. *Yale Journal of Biology and Medicine*, *89*(3), 325.

Luk, A., & Junnarkar, G. (2013). Critical challenges to the design of drug-eluting medical devices. *Therapeutic Delivery*, *4*(4), 471-477.

Mah, T. F. C., & O'Toole, G. A. (2001). Mechanisms of biofilm resistance to antimicrobial agents. *Trends in Microbiology*, *9*(1), 34-39.

Mann, B. K., Stirland, D. L., Lee, H. K., & Wirostko, B. M. (2018). Ocular translational science: A review of development steps and paths. *Advanced Drug Delivery Reviews*, *126*, 195-203.

USC
UNIVERSIDADE DE SANTIAGO DE COMPOSTELA

Martinez Devesa, P., Willis, C. M., & Capper, J. W. R. (2003). External auditory canal pH in chronic otitis externa. *Clinical Otolaryngology & Allied Sciences*, *28*(4), 320-324.

Maulvi, F. A., Desai, A. R., Choksi, H. H., Patil, R. J., Ranch, K. M., Vyas, B. A., & Shah, D. O. (2017). Effect of surfactant chain length on drug release kinetics from microemulsion-laden contact lenses. *International Journal of Pharmaceutics*, *524*(1-2), 193-204.

McDermott, A. M. (2013). Antimicrobial compounds in tears. *Experimental Eye Research*, *117*, 53-61.

McMahon, T. T., & Zadnik, K. (2000). Twenty-five years of contact lenses: the impact on the cornea and ophthalmic practice. *Cornea*, *19*(5), 730-740.

Miller, D. D., Hasan, S. A., Simmons, N. L., & Stewart, M. W. (2019). Recurrent corneal erosion: a comprehensive review. *Clinical Ophthalmology (Auckland, NZ)*, *13*, 325.

Miller, D., & Iovieno, A. (2009). The role of microbial flora on the ocular surface. *Current Opinion in Allergy and Clinical Immunology*, *9*(5), 466-470.

Moormeier, D. E., & Bayles, K. W. (2017). *Staphylococcus aureus* biofilm: a complex developmental organism. *Molecular Microbiology*, *104*(3), 365-376.

Muntz, A., Subbaraman, L. N., Sorbara, L., & Jones, L. (2015). Tear exchange and contact lenses: A review. *Journal of Optometry*, *8*(1), 2-11.

Nicolson, P. C., & Vogt, J. (2001). Soft contact lens polymers: an evolution. *Biomaterials*, *22*(24), 3273-3283.

Novack, G. D. (2009). Ophthalmic drug delivery: development and regulatory considerations. *Clinical Pharmacology & Therapeutics*, *85*(5), 539-543.

USC UNIVERSIDADE DE SANTIAGO DE COMPOSTELA

OJEU, Official Journal of the European Union (2017). Regulation (EU) 2017/745 of the European Parliament and of the Council of 5 April 2017 on medical medical devices, amending Directive 2001/83/EC, Regulation (EC) No 178/2002 and Regulation (EC) No 1223/2009 and repealing Council Directives 90/385/EEC and 93/42/EEC; https://eur-lex.europa.eu/legal-content/EN/TXT/HTML/?uri=CELEX:32017R0745&from=EN; Accessed January 2022.

O'Gara, J. P. (2017). Into the storm: Chasing the opportunistic pathogen *Staphylococcus aureus* from skin colonisation to life-threatening infections. *Environmental Microbiology*, *19*(10), 3823-3833.

Ogawa, H., Nakaji-Hirabayashi, T., Matsumura, K., Yoshikawa, C., Kitano, H., & Saruwatari, Y. (2020). Novel anti-biofouling and drug releasing materials for contact lenses. *Colloids and Surfaces B: Biointerfaces*, *189*, 110859.

Orji, F. T., Onyero, E. O., & Agbo, C. E. (2014). The clinical implications of ear canal debris in hearing aid users. *Pakistan Journal of Medical Sciences*, *30*(3), 483.

Pagac, M., Hajnys, J., Ma, Q. P., Jancar, L., Jansa, J., Stefek, P., & Mesicek, J. (2021). A review of vat photopolymerization technology: Materials, applications, challenges, and future trends of 3D printing. *Polymers*, *13*(4), 598.

Papas, E. B. (2017). Contact lens technology to 2020 and beyond: a review of recent patent literature. *Clinical and Experimental Optometry*, *100*(5), 529-536.

Patel, N. R., & Gohil, P. P. (2012). A review on biomaterials: scope, applications & human anatomy significance. *International Journal of Emerging Technology and Advanced Engineering*, *2*(4), 91-101.

Pavithra, D., & Doble, M. (2008). Biofilm formation, bacterial adhesion and host response on polymeric implants—issues and prevention. *Biomedical Materials*, *3*(3), 034003.

USC UNIVERSIDADE DE SANTIAGO DE COMPOSTELA

Pérez-Köhler, B., Bayon, Y., & Bellón, J. M. (2016). Mesh infection and hernia repair: a review. *Surgical Infections*, *17*(2), 124-137.

Pimenta, A. F. R., Valente, A., Pereira, J. C., Pereira, J. F., Filipe, H. P., Mata, J. L. G., ... & Serro, A. P. (2016). Simulation of the hydrodynamic conditions of the eye to better reproduce the drug release from hydrogel contact lenses: experiments and modeling. *Drug Delivery and Translational Research*, *6*(6), 755-762.

Prausnitz, M. R., & Noonan, J. S. (1998). Permeability of cornea, sclera, and conjunctiva: a literature analysis for drug delivery to the eye. *Journal of Pharmaceutical Sciences*, *87*(12), 1479-1488.

Rahmani, S., & Eliott, D. (2018). Postoperative endophthalmitis: a review of risk factors, prophylaxis, incidence, microbiology, treatment, and outcomes. *Seminars in Ophthalmology* , *33*, 95-101.

Raineri, E. J., Altulea, D., & van Dijl, J. M. (2021). Staphylococcal trafficking and infection—from 'nose to gut'and back. *FEMS Microbiology Reviews*, Online ahead of print.

Reid, G. (1999). Biofilms in infectious disease and on medical devices. *International Journal of Antimicrobial Agents*, *11*(3-4), 223-226.

Ribeiro, A., Veiga, F., Santos, D., Torres-Labandeira, J. J., Concheiro, A., & Alvarez-Lorenzo, C. (2011). Receptor-based biomimetic NVP/DMA contact lenses for loading/eluting carbonic anhydrase inhibitors. *Journal of Membrane Science*, *383*(1-2), 60-69.

Roland, P. S., & Stroman, D. W. (2002). Microbiology of acute otitis externa. *Laryngoscope*, *112*(7), 1166-1177.

Rosman, C. W., van Dijl, J. M., & Sjollema, J. (2021). Interactions between the foreign body reaction and Staphylococcus aureus biomaterial-associated infection. Winning strategies in the derby on biomaterial implant surfaces. *Critical Reviews in Microbiology*, Online ahead of print.

USC UNIVERSIDADE DE SANTIAGO DE COMPOSTELA

Sampson, K. L., Deore, B., Go, A., Nayak, M. A., Orth, A., Gallerneault, M., ... & Paquet, C. (2021). Multimaterial vat polymerization additive manufacturing. *ACS Applied Polymer Materials*, *3*(9), 4304-4324.

Sánchez-González, J. M., López-Izquierdo, I., Gargallo-Martínez, B., De-Hita-Cantalejo, C., & Bautista-Llamas, M. J. (2019). Bandage contact lens use after photorefractive keratectomy. *Journal of Cataract & Refractive Surgery*, *45*(8), 1183-1190.

Sandström, C. G. (2016). The non-disruptive emergence of an ecosystem for 3D Printing—Insights from the hearing aid industry's transition 1989–2008. *Technological Forecasting and Social Change*, *102*, 160-168.

Sankaridurg, P. R., Willcox, M. D., Sharma, S., Gopinathan, U., Janakiraman, D., Hickson, S., ... & Holden, B. A. (1996). *Haemophilus influenzae* adherent to contact lenses associated with production of acute ocular inflammation. *Journal of Clinical Microbiology*, *34*(10), 2426-2431.

Schierholz, J. M., & Beuth, J. (2001). Implant infections: a haven for opportunistic bacteria. *Journal of Hospital Infection*, *49*(2), 87-93.

Sekar, P., & Chauhan, A. (2019). Effect of vitamin-E integration on delivery of prostaglandin analogs from therapeutic lenses. *Journal of Colloid and Interface Science*, *539*, 457-467.

Serban, B. A., Stipe, K. T., Alverson, J. B., Johnston, E. R., Priestley, N. D., & Serban, M. A. (2017). A controlled antibiotic release system for the development of single-application otitis externa therapeutics. *Gels*, *3*(2), 19.

Shah, C., Raj, C. V., & Foulks, G. N. (2003). The evolution in therapeutic contact lenses. *Ophthalmology Clinics of North America*, *16*(1), 95-101.

Shi, D. N., Song, H., Ding, T., Qiu, W. Q., & Wang, W. (2018). Evaluation of the safety and efficacy of therapeutic bandage contact lenses on post-cataract surgery patients. *International Journal of Ophthalmology*, *11*(2), 230.

USC
UNIVERSIDADE DE SANTIAGO DE COMPOSTELA

Shlofmitz, E., Case, B. C., Chen, Y., Chezar-Azerrad, C., Hashim, H., Garcia-Garcia, H. M., ... & Waksman, R. (2021). Waksman in-stent restenosis classification: A mechanism-based approach to the treatment of restenosis. *Cardiovascular Revascularization Medicine*, *33*, 62-67.

Silva, D., de Sousa, H. C., Gil, M. H., Santos, L. F., Amaral, R. A., Saraiva, J. A., ... & Saramago, B. (2021). Imprinted hydrogels with LbL coating for dual drug release from soft contact lenses materials. *Materials Science and Engineering: C*, *120*, 111687.

Stapleton, F., & Carnt, N. (2012). Contact lens-related microbial keratitis: how have epidemiology and genetics helped us with pathogenesis and prophylaxis. *Eye*, *26*(2), 185-193.

Stroman, D. W., Roland, P. S., Dohar, J., & Burt, W. (2001). Microbiology of normal external auditory canal. *Laryngoscope*, *111*(11), 2054-2059.

Suhardi, V. J., Bichara, D. A., Kwok, S. J. J., Freiberg, A. A., Rubash, H., Malchau, H., ... & Oral, E. (2017). A fully functional drug-eluting joint implant. *Nature Biomedical Engineering*, *1*(6), 1-11.

Tieppo, A., Boggs, A. C., Pourjavad, P., & Byrne, M. E. (2014). Analysis of release kinetics of ocular therapeutics from drug releasing contact lenses: best methods and practices to advance the field. *Contact Lens and Anterior Eye*, *37*(4), 305-313.

UNE. Óptica oftálmica. Lentes de contacto. Parte 1: vocabulario, sistema de clasificación y recomendaciones para el etiquetado de las especificaciones. ISO 18369-1: 2017, Versión corregida 2017-10-01. Madrid, 2018.

Vairon, J. P., Yean, L., Meslard, J. C., Subira, F., & Bunel, C. (1992). Immobilisation reversible sur polymers et liberation controlee. Application aux lentilles corneennes reservoirs de medicaments. *L'actualité Chimique*, 330-335.

Vandorselaer, T., Youssfi, H., Caspers-Valu, L. E., Dumont, P., & Vauthier, L. (2001). Treatment of traumatic corneal abrasion with contact lens

USC UNIVERSIDADE DE SANTIAGO DE COMPOSTELA

associated with topical nonsteroid anti-inflammatory agent (NSAID) and antibiotic: a safe, effective and comfortable solution. *Journal Francais D'ophtalmologie*, *24*(10), 1025-1033.

VanEpps, J. S., & Younger, J. G. (2016). Implantable device related infection. *Shock*, *46*(6), 597.

Varela-Garcia, A., Concheiro, A., & Alvarez-Lorenzo, C. (2020). Cytosine-functionalized bioinspired hydrogels for ocular delivery of antioxidant transferulic acid. *Biomaterials Science*, *8*(4), 1171-1180.

Vroman, L., Adams, A.L., Fischer, G.C., & Munoz, P.C. (1980). Interaction of high molecular-weight kininogen, factor-XII, and fibrinogen in plasma at interfaces. *Blood*, *55*, 156–159.

Wang, R., Lu, D., Wang, H., Zou, H., Bai, T., Feng, C., & Lin, Q. (2021). "Kill-release" antibacterial polysaccharides multilayer coating based therapeutic contact lens for effective bacterial keratitis treatment. *RSC Advances*, *11*(42), 26160-26167.

Wei, C., Zhu, M., Petroll, W. M., & Robertson, D. M. (2014). *Pseudomonas aeruginosa* infectious keratitis in a high oxygen transmissible rigid contact lens rabbit model. *Investigative Ophthalmology & Visual Science*, *55*(9), 5890-5899.

Weissman, B. A., & Mondino, B. J. (2002). Risk factors for contact lens associated microbial keratitis. *Contact Lens and Anterior Eye*, *25*(1), 3-9.

Wen, X., Hu, X., Miao, L., Ge, X., Deng, Y., Bible, P. W., & Wei, L. (2018). Epigenetics, microbiota, and intraocular inflammation: New paradigms of immune regulation in the eye. *Progress in Retinal and Eye Research*, *64*, 84-95.

Wen, X., Miao, L., Deng, Y., Bible, P. W., Hu, X., Zou, Y., ... & Wei, L. (2017). The influence of age and sex on ocular surface microbiota in healthy adults. *Investigative Ophthalmology & Visual Science*, *58*(14), 6030-6037.

USC
UNIVERSIDADE DE SANTIAGO DE COMPOSTELA

White, C. J., Tieppo, A., & Byrne, M. E. (2011). Controlled drug release from contact lenses: a comprehensive review from 1965-present. *Journal of Drug Delivery Science and Technology*, *21*(5), 369-384.

WHO. Deafness and hearing loss. 2021. https://www.who.int/news-room/fact-sheets/detail/deafness-and-hearing-loss; Accessed January 2022

Wichterle, O., & Lim, D. (1960). Hydrophilic gels for biological use. *Nature*, *185*(4706), 117-118.

Wiegand, S., Berner, R., Schneider, A., Lundershausen, E., & Dietz, A. (2019). Otitis externa: investigation and evidence-based treatment. *Deutsches Ärzteblatt International*, *116*(13), 224.

Willcox, M. D. (2013). Characterization of the normal microbiota of the ocular surface. *Experimental Eye Research*, *117*, 99-105.

Willcox, M. D., Argüeso, P., Georgiev, G. A., Holopainen, J. M., Laurie, G. W., Millar, T. J., ... & Jones, L. (2017). TFOS DEWS II tear film report. *Ocular Surface*, *15*(3), 366-403.

Wormstone, I. M., Wormstone, Y. M., Smith, A. J. O., & Eldred, J. A. (2020). Posterior capsule opacification: What's in the bag?. *Progress in Retinal and Eye Research*, *82*, 100905.

Wu, J., & Xie, H. (2021). Orthokeratology lens-related Acanthamoeba keratitis: case report and analytical review. *Journal of International Medical Research*, *49*(3), doi:10.1177/03000605211000985.

Xu, X., Awad, A., Martinez, P. R., Gaisford, S., Goyanes, A., & Basit, A. W. (2020). Vat photopolymerization 3D printing for advanced drug delivery and medical device applications. *Journal of Controlled Release*, 329, 743-757

Xu, L., Ma, P., Yuan, B., Chen, Q., Lin, S., Chen, X., ... & Shen, J. (2014). Anti-biofouling contact lenses bearing surface-immobilized layers of zwitterionic polymer by one-step modification. *RSC Advances*, *4*(29), 15030-15035.

USC UNIVERSIDADE DE SANTIAGO DE COMPOSTELA

Xu, J., Li, X., & Sun, F. (2010). Cyclodextrin-containing hydrogels for contact lenses as a platform for drug incorporation and release. *Acta Biomaterialia*, *6*(2), 486-493.

Xu, J., Ge, Y., Bu, R., Zhang, A., Feng, S., Wang, J., ... & Tang, X. (2019). Co-delivery of latanoprost and timolol from micelles-laden contact lenses for the treatment of glaucoma. *Journal of Controlled Release*, *305*, 18-28.

Zaki, M., Pardo, J., & Carracedo, G. (2019). A review of international medical device regulations: Contact lenses and lens care solutions. *Contact Lens and Anterior Eye*, *42*(2), 136-146.

Zhang, J., Li, J., Li, X., Li, F., & Wang, T. (2020). Redistribution of the corneal epithelium after overnight wear of orthokeratology contact lenses for myopia reduction. *Contact Lens and Anterior Eye*, *43*(3), 232-237.

Zilberman, M., Kraitzer, A., Grinberg, O., & Elsner, J. J. (2010). Drug-eluting medical implants. *Drug Delivery*, 299-341.

Zimmerli, W. (1993). Experimental models in the investigation of device-related infections. *Journal of Antimicrobial Chemotherapy*, *31*(suppl_D), 97-102.

Zimmerli, W., & Sendi, P. (2011). Pathogenesis of implant-associated infection: the role of the host. *Seminars in Immunopathology*, *33* (3), 295-306.

USC
UNIVERSIDADE DE SANTIAGO DE COMPOSTELA

Aims

USC
UNIVERSIDADE
DE SANTIAGO
DE COMPOSTELA

USC
UNIVERSIDADE
DE SANTIAGO
DE COMPOSTELA

2. AIMS

Medical devices have become indispensable tools in healthcare enabling from the diagnosis of diseases to the physical replacement of loss organs or their functions. Medical devices intended to help compensate for impairment of the senses, primarily sight and hearing, are particularly valuable for the quality of life of an increasing number of people around the world. Nevertheless, the prolonged use of a medical device also involves risks, mainly the development of infections associated to biofilm formation on the surface of the medical device, as highlighted in the introduction. The general aim of this PhD Thesis was to explore the feasibility of loading hearing aids and contact lenses with substances that can prevent biofilm formation or address already established infections.

According to this general aim, three specific aims were identified and developed as follows.

1. To prepare 3D printing hearing aids loaded with drugs used in the conventional topical treatments of ear infections. More than 99% of the hearing aids that fit in user's ear canal are custom-manufactured by 3D printing, mainly by VAT photopolymerization technologies. This approach allows obtaining personalized devices that perfectly fit to the anatomic peculiarities of each patient. Such perfect fit has been shown to be critical for improving the outcomes of the hearing aid.

USC
UNIVERSIDADE DE SANTIAGO DE COMPOSTELA

However, the continuous wearing of the hearing aid has the drawback of causing a local increase in temperature and humidity, which may alter the microbiota in the ear canal. Fungi and bacteria may grow on the device surface as well as on the host tissue triggering otitis externa. Conventional ear infection treatment requires discontinuation of the hearing aid, with the associated constrains for the hearing ability of the patient. Also non-wearers can develop ear infections and it should be noted that ear infections themselves are one main cause of hearing loss. Patients with ear infections might also benefit from using a device that would sustainedly release the medication for the required days without the need of the frequent instillation that otic drops demand. Thus, in-the-canal hearing aids-like devices loaded with drugs used for addressing ear infections may be beneficial both for people that require improvements in the hearing ability and for normal hearing people that occasionally suffer from ear infections (devices that only resemble the morphology of the hearing aid).

In this first part of the Thesis, the feasibility of adding therapeutic amounts of ciprofloxacin and fluocinolone acetonide to the resins commonly used for VAT photopolymerization was investigated. To the best of our knowledge simultaneous addition of two drugs has not been tested before during VAT 3D printing. Clinical outcomes of otitis externa have been demonstrated to be better when the antibiotic is combined with the corticosteroid. It should be noted that the drugs have notable different structural and physicochemical properties, which may compromise their dispersion in the resin and also subsequent release from the device. Thus, in the mixtures ciprofloxacin:fluocinolone acetonide were tested at two different levels 6%:0.5% and 12%:1% w/w, and their effects on the printability and mechanical properties of the hearing aids and their capabilities to provide controlled drug release were evaluated. Moreover, the

USC
UNIVERSIDADE DE SANTIAGO DE COMPOSTELA

efficacy of the 3D printed devices to avoid biofilm formation was evaluated against *Pseudomonas aeruginosa* (Gram-negative) and *Staphylococcus aureus* (Gram-positive), two avid biofilm formers involved in chronic ear infections. This work was carried out from a multidisciplinary perspective with the collaboration of team of Prof. Abdul W. Basit at University College of London, in the part of 3D printing, and of Prof. Ana Otero at Universidade de Santiago de Compostela in the part of biofilm assessment.

2. To design contact lenses (CLs) endowed with antibiofilm features through the combination of anti-biofouling monomers and natural antioxidants with antimicrobial capability. In spite of the evolution of materials used to prepare CLs that are more and more comfortable and offer better visual acuity, the risk of undergoing biofilm formation on CLs surface has not decreased. Hydrogels used to prepare the CLs are very prone to be colonized by microorganisms present on the fingers during insertion and on the ocular surface. Deposits of proteins from tear fluid promote bacteria adhesion, which may proliferate in the form of biofilm during extended use. CLs wearing continues to be the most relevant risk factor for the development of microbial keratitis, which in turn is one of the main causes of CLs discontinuation. Prophylactic use of antibiotics is not recommended since their untargeted use alters normal microbiota, fosters resistances and causes toxicity to the anterior segment tissues. Monomers bioinspired in the phosphorylcholine group typical of phospholipid headgroups present in the cell membrane have been shown to provide protein-resistant surfaces. So far only one commercially available CL, Proclear®, includes 2-methacryloyloxyethyl phosphorylcholine (MPC) to improve wettability and comfort. As an alternative to antibiotic drugs, natural

USC UNIVERSIDADE DE SANTIAGO DE COMPOSTELA

compounds that can act as biofilm inhibitors are gaining attention. In this regard, resveratrol, which is a natural polyphenol antioxidant with good ocular tolerance, has been reported to interfere in vitro with the bacterial communication process known as *Quorum Sensing* (QS) and to inhibit biofilm formation by clinically relevant bacteria. Interestingly, associated to its antioxidant activity, resveratrol may help in the prevention of a variety of eye diseases and in the healing of corneal epithelial cells.

The second part of the Thesis relied on the hypothesis of that the design of hydrogels containing MPC moieties and incorporating resveratrol may exhibit a synergism in terms of the prevention of biofilm formation on CLs, while resveratrol may also lead to other beneficial effects related to its antioxidant capability. To the best of our knowledge, loading of resveratrol in CLs has not been tested before. Thus, the work was aimed to prepare hydrogel CLs and silicone hydrogel CLs containing MPC and loaded with resveratrol to decrease the incidence of ocular infections and manage some eye diseases caused by oxidative stress mechanisms. To carry out the work, hydrogels were prepared covering a wide range of MPC ratios and then the loading and release profiles of resveratrol were evaluated. Ocular biocompatibility was screened using the hen's egg-chorioallantoic membrane (HET-CAM) test, as preliminary assay alternative to the in vivo testing. An extensive characterization of the materials, comprising the evaluation of their protein adsorption and antibiofilm and antioxidant capabilities, was performed. Commercially available Proclear® 1 day CLs were used as a control for comparison purposes. Part of this work was carried out in collaboration with the group of Prof. Ana Paula Serro at Instituto Superior Técnico, Universidade de Lisboa, in which the candidate acquired training in protein adsorption studies during a research stay.

USC
UNIVERSIDADE DE SANTIAGO DE COMPOSTELA

3. To optimize CLs bearing MPC and to evaluate the *in vivo* release and ocular tissue penetration of resveratrol. The aim of this part of the Thesis was to critically analyse the information gathered in the former section and to improve the performance of the CL in terms of antibiofilm information by increasing MPC content. A second relevant aim was to investigate whether the CLs could deliver therapeutically relevant amounts of resveratrol to the ocular surface to provide antibiofilm and antioxidant outcomes. Successful design of CLs for resveratrol release on the ocular surface should ensure controlled release capability to avoid premature clearance from the cornea and to facilitate the access to aqueous humor and vitreous humor, and should also preserve the antioxidant features of resveratrol along time which may be compromised by the prolonged exposure to the day light. After successful pass of alternative methods and fulfilling 3R´s principles, an *in vivo* test in rabbit animal model may provide relevant information on the safety and ocular tolerance of the medicated contact lenses and is a mandatory first step for clinical translation. Thus, in collaboration with the team Prof. Gonzalo Carracedo at Ocupharm and University Complutense of Madrid, an *in vivo* study was planned with the corresponding permission of the Ethics Committee. Correlations between the release profile of resveratrol in vitro and during the in vivo tests were investigated, and levels of resveratrol in different eye tissues were analysed from the perspective of potential antioxidant and antimicrobial outcomes.

4. To design polymeric micelles loaded with resveratrol that may reinforce the therapeutic outcomes of both hearing aids and CLs. Resveratrol has been shown to ameliorate the host cell cytotoxic effects of antibiotics. Additionally, the antioxidant performance may be exploited for the treatment of eye disease related to high oxidative

USC UNIVERSIDADE DE SANTIAGO DE COMPOSTELA

stress levels, as triggered by prolonged sun light exposure and hyperglycemia. Oxidative stress and inflammation play a key role in the initiation and progression of a variety of age-related ocular diseases like surface disorders (keratoconus and corneal ectasia), macular degeneration (AMD), diabetic retinopathy (DR), cataract, glaucoma and uveitis, which can lead to progressive loss of vision and blindness without proper treatment. Polymeric micelles have been positioned as relevant drug nanocarriers able to protect and increase the solubility of labile agents (as resveratrol) and to overcome biological barriers that oppose to mucosal drug penetration. In addition to synthetic block copolymers, natural milk protein micelles are attracting increasing attention as drug nanocarriers since they combine widely available natural sources, capability to transport poorly-soluble molecules (natural transporters of calcium phosphate) and activity as radical scavengers. To the best of our knowledge, encapsulation of resveratrol or other compounds in casein micelles for mucosal (ocular, otic) delivery has not been investigated yet.

Accordingly, the last part of the Thesis was devoted to the preparation of single micelles of Pluronic® and casein and mixed micelles of both compounds with the aim of elucidating whether the formation of mixed micelles could enhance the performance of the nanocarrier system in terms of physical stability of the micelles, resveratrol loading capability, antioxidant features, in situ gelling, ex vivo permeability and antibiofilm properties. Ocular biocompatibility was assessed first in HET-CAM as well in zebra fish model. Finally, the most suitable formulation was tested in a rabbit model in collaboration with the team Prof. Gonzalo Carracedo at Ocupharm and University Complutense of Madrid.

USC
UNIVERSIDADE DE SANTIAGO DE COMPOSTELA

Chapter 3

The work described in this chapter was published in **Anti-biofilm multi drug-loaded 3D printed hearing aids**, *Materials Science & Engineering C* 119, 111606, 2021, authored by

María Vivero-Lopez[a], Xiaoyan Xu[b], Andrea Muras[c], Ana Otero[c], Angel Concheiro[a], Simon Gaisford[b,d], Abdul W. Basit[b,d], Carmen Alvarez-Lorenzo[a], Alvaro Goyanes[a,d]

[a] Departamento de Farmacología, Farmacia y Tecnología Farmacéutica, I+D Farma (GI-1645), Facultad de Farmacia, and Health Research Institute of Santiago de Compostela (IDIS), Universidade de Santiago de Compostela, 15782 Santiago de Compostela, Spain

[b] Department of Pharmaceutics, UCL School of Pharmacy, University College London, 29-39 Brunswick Square, London, WC1N 1AX, UK

[c] Departamento de Microbiología, Facultad de Biología, Edificio CIBUS, Universidade de Santiago de Compostela, 15782 Santiago de Compostela, Spain

[d] FabRx Ltd., 3 Romney Road, Ashford, Kent TN24 0RW, UK

USC
UNIVERSIDADE DE SANTIAGO DE COMPOSTELA

USC
UNIVERSIDADE
DE SANTIAGO
DE COMPOSTELA

3. ANTI-BIOFILM MULTI DRUG-LOADED 3D PRINTED HEARING AIDS

3.1 INTRODUCTION

Three-dimensional (3D) printing is an innovative and fast additive manufacturing technology based on the production of a physical object in a layer-by-layer manner from a computerized 3D model. The 3D models can be created by computer-aided design (CAD) software or obtained from imaging techniques (e.g. 3D scanner, computed tomography scan, magnetic resonance imaging) that capture images of the real object [Goyanes et al., 2016]. Due to its cost-efficiency, reproducibility and flexibility, 3D printing is forecast to be a disruptive technology in healthcare and drug delivery, changing manufacturing paradigms by allowing the fabrication of bespoke and individualized objects [Trenfield et al., 2019; Banks, 2013; Elbadawi et al., 2020].

A wide variety of 3D printing technologies coexist today, and they can be classified depending on the nature of the material used (e.g. resins, plastics, ceramics), the deposition technology, and the mechanism used to form the layers or the characteristics of the final products [Alhnan et al., 2016]. Depending on the additive process

USC UNIVERSIDADE DE SANTIAGO DE COMPOSTELA

involved, the American Society for Testing and Materials (ASTM) classifies these technologies into seven main categories: VAT photopolymerization, material extrusion, directed energy deposition, powder bed fusion, binder jetting, material jetting and sheet lamination [Liang et al., 2019].

In the pharmaceutical industry, various 3D printing technologies included in the previously cited categories have been evaluated to prepare personalized medicines including fused deposition modelling (FDM) [Genina et al., 2017; Gioumouxouzis et al., 2020; Maroni et al., 2017], semi-solid extrusion (SSE) [Conceição et al., 2019; Goyanes et al., 2019] and selective laser sintering (SLS) [Awad et al., 2019; Fina et al., 2018]. Formulations with tailored drug release profiles [Isreb et al., 2019; Sadia et al., 2018] and unique functions [Awad et al., 2020; Goyanes et al., 2018; Khaled et al., 2015; Smith et al., 2018] have been previously introduced. However, the application of 3D printing has not stopped at the production of oral dosage forms. Multiple customized medical devices have been prepared by incorporating different drugs into the 3D printed structures for intrauterine [Genina et al., 2016], subcutaneous [Holländer et al., 2016], vaginal [Fu et al., 2018], topical [Goyanes et al., 2016], intravesical [Melocchi et al., 2019a], and oral [Liang et al., 2018; Melocchi et al., 2019b] drug delivery, and tissue scaffolds [Farto-Vaamonde et al., 2019].

VAT photopolymerization 3D printing techniques, such as stereolithography (SLA), continuous liquid interface production (CLIP) and digital light projection (DLP) are processes where a liquid photopolymerizable resin is selectively solidified using light irradiation (e.g. a laser, UV and visible light). Such 3D printing techniques provide high accuracy and superior resolution [Melchels et al., 2010], and have been tested for biomedical and pharmaceutical

USC UNIVERSIDADE DE SANTIAGO DE COMPOSTELA

applications [Xu et al., 2020], including fabrications of polypills [Robles-Martinez et al., 2019; Xu et al., 2020], patient-specific implants [Bloomquist et al., 2018], personalized devices [Goyanes et al., 2016], microneedles [Economidou et al., 2019; Yao et al., 2020; Lim et al., 2017], dental devices [Dentca, 2016], and hearing aids [EnvisionTEC, 2020]. Hearing aids manufacturing is the paramount example of personalized medical devices that have been benefiting from the development of 3D printing. In fact, more than 99% of the hearing aids that fit in user's ear canal are custom-manufactured by 3D printing [Banks, 2013; Materialise, 2020], mainly by VAT photopolymerization technologies. Manufacturers such as Envision TEC [EnvisionTEC, 2020], Formlabs [Formlabs, 2020], and Sonova [Sonova, 2020] have been employing 3D printing technology for production of shells for in-the-ear hearing aids to custom-made earpieces for behind-the-ear and receive-in-canal hearing aids as well ear products such as ear moulds and earbuds.

Around 5% of the population worldwide has disabling hearing loss, which affects approximately one third of people over 65 years [WHO, 2020]. Multiple causal agents are behind sensorineural and conductive hearing loss, but ear infection is a relevant cause of temporary hearing loss. Also, the prolonged use of hearing aids may alter the ear canal microbiota and increase the risk of fungal and bacterial otitis externa [Orji et al., 2014]. There is the need to prevent infections in hearing aids, however hearing aids with anti-biofilm properties have not yet been developed. In the case of ear infections, topical antibiotics are better than aural toilet (ear cleaning using dry mopping or irrigation) alone, and systemic or topical fluoroquinolones (e.g. ciprofloxacin, ofloxacin) are more effective than other types of antibiotics [Brennan-Jones et al., 2020; Onali et al., 2018]. It has also been reported that the use of ciprofloxacin in combination with

USC UNIVERSIDADE DE SANTIAGO DE COMPOSTELA

fluocinolone acetonide is more effective than treatment with each drug individually for acute otitis media with tympanostomy tubes (AOMT) in children and is safe and well tolerated [Spektor et al., 2017; Lorente et al., 2014].

Reports about manufacture of 3D printed devices with antibiofilm properties are limited [Ballard et al., 2019]. To date, only a 3D printed device with nitrofurantoin to prevent the biofilm formation of *S. aureus* [Sandler et al., 2014], an Ag-decorated 3D printed implant with antibiofilm activity against *E. coli* and *S. aureus* [Deng et al., 2017], and a 3D-printed PLA-collagen-minocycline-nanohydroxyapatite scaffold against *S. aureus* [Martin et al., 2019] were prepared. All of the above-mentioned examples were fabricated using FMD 3D printing technology, but the low resolution and mechanical properties of the produced objects may limit its applications in the production of complex devices such as hearing aids.

To the best of our knowledge, there are no previous studies on 3D printed hearing devices that may act as drug release platforms in the outer-middle ear canal. As such, here we seek to explore the possibility of employing DLP 3D printing in fabrication of drug-loaded hearing aids for patients with ear infections. This novel drug-device combination product would avoid discontinuation of hearing aids use due to infections and may be even useful for normal hearing people suffering ear infections. A combination of ciprofloxacin and fluocinolone acetonide was chosen since it is commonly used in ear drops to address ear infections. The effect of the incorporation of two drugs on the printability and mechanical properties of the hearing aids and their capabilities to provide controlled drug release were evaluated. Moreover, the efficacy of a 3D printed device to avoid biofilm formation was evaluated against *Pseudomonas aeruginosa*

USC UNIVERSIDADE DE SANTIAGO DE COMPOSTELA

(Gram-negative) and *Staphylococcus aureus* (Gram-positive), two avid biofilm formers involved in chronic ear infections [Kostakioti et al., 2013; Parrish et al., 2019].

3.2 MATERIALS AND METHODS

3.2.1 Materials

Ciprofloxacin hydrochloride USP was purchased from Fagron (Spain) and fluocinolone acetonide (Ref. Mg93950) was from Guinama (Spain). Kudo 3DSR flexible resin (30-60% acrylate monomer; 35-69% acrylate oligomer; 1-5% photoinitiator) and Kudo 3DSR ENG hard resin (30-60% acrylate monomer; 30-68% acrylate oligomer; 1-10% photoinitiator; 1-10% pigment) were purchased from Kudo3D Inc. (USA). 3-(4,5-Dimethylthiazol-2-yl)-2,5-diphenyltetrazolium bromide (MTT) and orthophosphoric acid (H_3PO_4, 85%) were from Merck KGaA (Darmstadt, Germany); isopropyl alcohol and ethanol absolute 99.9% from VWR Chemicals (Fontenary-Sous-Bois, France); sodium chloride (NaCl, analytical grade) and tryptic soy broth (TSB) from Oxoid (UK); sodium hydroxide (NaOH, 98.5-100.5%) from VWR Chemicals (Leuven, Belgium); bacto™ tryptone and bacto™ yeast extract from Becton, Dickinson and Company (Le Pont de Claix, France); acetonitrile (≥. 99.9% purity, HPLC grade) from Scharlab S.L. (Barcelona, Spain). Water was purified using reverse osmosis (resistivity > 18 MΩ·cm, MilliQ Millipore® Spain).

USC UNIVERSIDADE DE SANTIAGO DE COMPOSTELA

3.2.2 Preparation of photopolymer solutions

Flexible resin and ENG hard resin were used to prepare the photoreactive solutions. Flexible or ENG hard resins were mixed with 12% ciprofloxacin – 1% fluocinolone acetonide or 6% ciprofloxacin – 0.5% fluocinolone acetonide (w/w) to a total mass of 20 g **(Table 3.1)**. The ciprofloxacin:fluocinolone acetonide mass ratio was fixed at 12:1, resembling the ratio in the marketed ear drops formulations [Lorente et al., 2014]. The drugs were added to the resin solutions and the system was kept under magnetic stirring for at least 2 hours until the drugs were apparently dissolved. The resulting photopolymer solutions were immediately loaded into the printer. Flexible resin-based devices and ENG hard resin-based devices were coded starting with the letter F or H, respectively, followed by the content (in percentage) of each drug. Control formulations (without drug) were also printed and coded as FND or HND.

Table 3.1. Compositions of the 3D printed hearing aids. FND and HND are the codes for the blank hearing aids without drug

Hearing aid code	Resin	Drugs
FND	Flexible	-
F6-0.5	Flexible	6% ciprofloxacin - 0.5%fluocinolone acetonide
F12-1	Flexible	12% ciprofloxacin - 1%fluocinolone acetonide
HND	ENG hard	-
H6-0.5	ENG hard	6% ciprofloxacin - 0.5%fluocinolone acetonide
H12-1	ENG hard	12% ciprofloxacin - 1%fluocinolone acetonide

USC UNIVERSIDADE DE SANTIAGO DE COMPOSTELA

3.2.3 3D printing process

A commercial Kudo3D Titan 2 HR 3D printer (Kudo3D Inc., USA) equipped with a digital projector (DLP) was utilized for printing the hearing aids. The printer allows fabrication of objects with high resolution and a layer thickness of 23 µm. The templates used to print the hearing aids were obtained from the moulds of the right ears of two volunteers and exported as a stereolithography file (.stl) into the 3D printer software (Kudo3D Print Job Software, Kudo3D Inc., USA). Additionally, circular discs (10mm diameter x 1mm height) and rectangular-shape slabs (10mm x 20mm x 1mm) were printed for microbiology studies and material testing. The printing time was 6 s per layer (60 s for the 1st layer) with a layer thickness of 25 µm. The post printing process consisted of a wash of 1 min in isopropyl alcohol and a cure process of 60 min at 60 °C with UV-visible light (254-366 nm).

3.2.4 Determination of hearing aids morphology

Pictures of the devices were taken with a Nikon CoolpixS6150 camera with the macro option of the menu. The dimensions of the hearing aids were determined by measuring the device in the X, Y, and Z axes. The images of the devices obtained from X-ray micro computed tomography were reconstructed, processed (as indicated in **Section 3.2.8**), and saved in stl. format. The stl. files were then imported in the 3D printer software (Kudo3D Print Job Software, Kudo3D Inc., USA) to obtain the size of the device in the X, Y and Z axes. The obtained values were then compared to the dimensions of the original 3D models.

USC UNIVERSIDADE DE SANTIAGO DE COMPOSTELA

3.2.5 Scanning electron microscopy (SEM)

3D printed slabs were sputter coated with iridium, and SEM images of the surface and cross-section were recorded in a Zeiss FESEM Ultra Plus microscope (Oberkochen, Germany).

3.2.6 X-ray powder diffraction (XRPD)

X-ray powder diffraction (XRPD) pattern of the drugs and the 3D printed slabs were recorded on a Philips type powder diffractometer fitted with a PW1710 control unit, a PW1820/00 goniometer and an Enraf Nonius FR590 generator. Spectra were made by measuring the scintillation response to Cu Kα radiation in the 2-50° 2θ range, with a step size of 0.04° and counting time of 6 s per step.

3.2.7 Thermal analysis

Differential scanning calorimetry (DSC) measurements of the drugs and the 3D printed slabs were performed using a differential scanning calorimeter Q200 DSC (TA Instruments, USA) previously calibrated with indium. The samples were accurately weighed in a 40 µL aluminum pan, and then heated from 25 to 50 °C, cooled to 0 °C and then heated to 300 °C at a scanning rate of 10 °C/min in nitrogen atmosphere (50 mL/min).

3.2.8 X-ray micro computed tomography (micro-CT)

A high-resolution X-ray micro computed tomography (Micro-CT) scanner (SkyScan1172, Bruker-microCT, Kontich, Belgium) was used to visualize the internal structure of the hearing aids as in a previous

USC UNIVERSIDADE DE SANTIAGO DE COMPOSTELA

study [Awad et al., 2019]. Each image was acquired by rotating the object through 180° with a frame averaging of 4 and a 0.5° rotation step using medium camera resolution (2000 x 1048 pixels). NRecon software (Version 1.7.0.4, Bruker-microCT, Kontich, Belgium) was used to reconstruct the images and the reconstructed images were processed using the software CTVox (version 2.3.2.0) to create the images. The software CT Analyzer (CTan version 1.16.4.1) was used to analyze the collected data and calculate porosity and dimensions of the devices.

3.2.9 Water contact angle

Water contact angles on 3D printed slabs were recorded for 10 s after the deposition of a water drop (5 µL) taking one image per second. The measurements were carried out in triplicate using a Phoenix-300 plus video-based optical goniometer (SEO, Korea).

3.2.10 Mechanical evaluation of the slabs

3D printed slabs (10mm x 20mm x 1mm) were tested in triplicate at room temperature in a TA.XT Plus Texture Analyzer (Stable Micro Systems, Ltd., UK) fitted with a 30 Kgf load cell. In each test, the slab was fixed to the upper and lower clamps with a gap of 6 mm. The tensile test was carried out at a crosshead speed of 0.1 mm/s until rupture. The stress-strain data were converted to engineering strength (force per cross-sectional area) versus the engineering strain (the change in active length divided by the original length), and the Young's modulus was calculated from the slope of the straight-line portion, as follows:

USC UNIVERSIDADE DE SANTIAGO DE COMPOSTELA

$$E = \frac{\frac{F}{A_0}}{\frac{\Delta L}{L_0}} \qquad \text{Eq. (3.1)}$$

Where E is the Young's modulus, F is the force applied on the sample under tension, A_0 is the cross-sectional area, ΔL is the change in length of the sample and L_0 is the original length of the sample.

3.2.11 Hemolytic activity

The hemolysis assay was carried out in accordance with the direct test described in ISO10993-4 [Weber et al., 2018]. Fresh blood from anonymized healthy donors (Galician Transfusion Center, Spain) was diluted 1:30 (v/v) in NaCl 0.9% aq. medium. Aliquots (1 mL) were poured in Eppendorf® tubes to which pieces of the slabs were added (40-80 mm^2 side; 50-90 mg). Diluted blood without samples was used as negative control. The positive control was prepared adding 100 µL of Triton X-100 4% to tubes containing diluted blood. All tubes were incubated for 60 min in a Mini-Shaker (100 osc/min) at 37 °C and then they were centrifuged (Sigma 2-16P; Sigma Laboratory Centrifuges, Germany) at 10,000*g* for 10 min. The supernatants (150 µL) were transferred to 96-well plate and the absorbance was recorded at 540 nm (FLUOstar Optima; BMG Labtech, Germany). Hemolysis percentage was calculated as follows:

$$Hemolysis\ (\%) = \frac{Abs_{sample} - Abs_{negative\ control}}{Abs_{positive\ control} - Abs_{negative\ control}} \qquad \text{Eq. (3.2)}$$

USC UNIVERSIDADE DE SANTIAGO DE COMPOSTELA

3.2.12 Anti-biofilm properties

3.2.12.1 Bacterial strains and growth conditions

The Gram-negative *Pseudomonas aeruginosa* PAO1 (Lausanne sub-line, donated by M. Cámara, Univ. of Nottingham) and the Gram-positive bacteria *Staphylococcus aureus* ATCC25923 (ATCC, Manassas, VA, USA) were routinely cultured at 37 °C in Luria-Bertani Broth (LB) and 1% Tryptic Soy Broth (TSB-1), respectively.

3.2.12.2 Culture media preparation

LB (10 g/L of tryptone, 5 g/L yeast extract, 10 g/L NaCl) and TSB-1 (30 g/L TSB Scharlau, 5 g/L NaCl) were prepared in distilled water. Culture media were magnetically stirred at 200 rpm until complete dissolution and autoclaved (121 °C, 15 min).

3.2.12.3 AAA model preparation

Bacterial biofilms were grown on dried materials submerged in culture medium using a modified AAA-model [Exterkate et al., 2010; Mayer et al., 2018] assembled with the tested materials and microscope glass coverslips (18 x 18 mm, submerged surface 3.80 cm^2) as controls. The coverslips were carefully placed in the silicone supports (borosilicate glass Menzel-Glaser, Thermo Scientific) of special metallic covers for 12-wells cell culture plates **(Figure 3.1)** with the help of a scalpel and tongs before being autoclaved (121 °C, 1 atm, 15 min). The sterilized covers were dried in an oven at 60 °C for 12-24 h. The tested slabs were disinfected by immersion in ethanol 70º for 5 s and then placed in the autoclaved AAA-model covers **(Figure 3.1)**. The covers with the mounted materials were left to dry for 1 h at room temperature in a biological safety cabinet before being

USC UNIVERSIDADE DE SANTIAGO DE COMPOSTELA

submerged in 12-wells cell-culture plates containing 4 mL of culture media inoculated with the corresponding bacterial species.

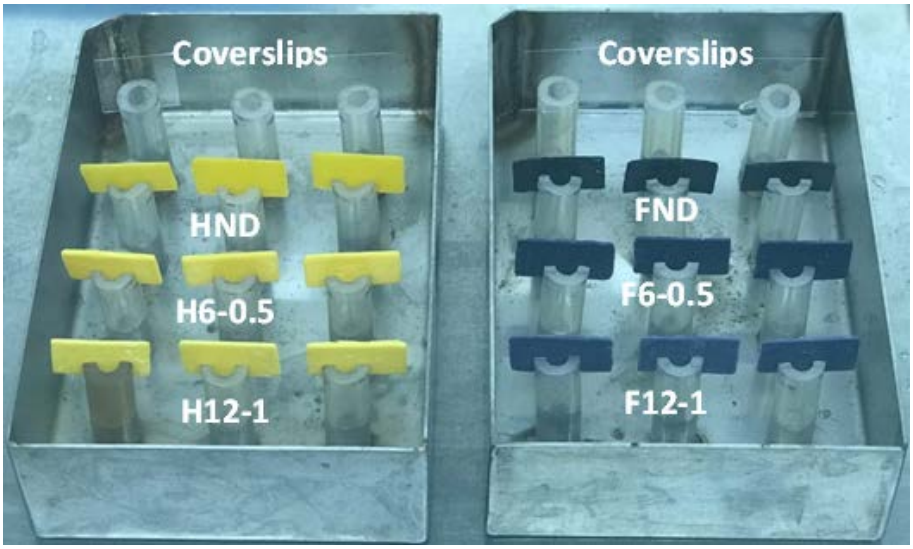


Figure 3.1. Covers for the AAA-model biofilm cultivation system assembled with the tested materials and coverslips. Covers were placed onto 12-wells cell culture plates containing the culture medium inoculated with the biofilm-forming bacteria.

3.2.12.4 Pre-inoculum and inoculum preparation

Pre-inocula were prepared by inoculating sterile Erlenmeyer flasks containing 10-mL of culture medium with a colony of the corresponding bacterial pathogen. Flasks were incubated at 37 °C for 12 h *(P. aeruginosa)* or 24 h *(S. aureus)* at 100 rpm. After incubation, optical density was measured at 600 nm (UV-Vis spectrophotometer Thermo Scientific Helios Omega) and adjusted to 0.05 *(S. aureus)* or 0.01 *(P. aeruginosa)* by dilution with the corresponding culture medium in sterile 50 mL Falcon® tubes. The required dilutions were 1/326 for *P. aeruginosa* and 1/125 for *S. aureus*. The inocula were

USC UNIVERSIDADE DE SANTIAGO DE COMPOSTELA

gently homogenized and distributed in the 12-wells cell culture plates (4 mL per well). All procedures were performed in a biological safety cabinet.

3.2.12.5 Plates preparation and incubation

All materials were tested in triplicate and incubated at 37 ºC for 12 and 48 h for *P. aeruginosa* and *S. aureus* respectively. The *S. aureus* medium was changed every 12 h by moving the models to new cell-culture plates previously filled with 4 mL/well of fresh TSB-1. In all cases, after each media exchange period, the absorbance of the culture medium was measured at 600 nm (UV-Vis spectrophotometer Thermo Scientific Helios Omega) after homogenization in order to assess planktonic bacterial growth.

3.2.12.6 Biofilm susceptibility

After the incubation period at 37 °C, the viability of the bacterial biofilms was analyzed using MTT assay modified as previously reported [Cady et al., 2012; Nuryastuti et al., 2009]. For this purpose, slabs and coverslips were individually placed in sterile tubes containing 3.6 mL of PBS (6.4 g of NaCl, 0.16 g of KCl, 1.152 g of $NaHPO_4$ and 0.192 g of KH_2PO_4 for 500 mL) and then sonicated for 15 min in order to detach and homogenize the biofilms. After that, MTT solution (5 mg/mL, 400 µL) was added to each tube, and the tubes were incubated at 37 °C for 30 min. The half of the MTT-containing PBS medium was removed and replaced with acid isopropanol (5% (v/v) 1M HCl in isopropanol). After 5-min vortexing, aliquots (1 mL) of the medium were taken and their absorbance measured at 570 nm (UV-Vis spectrophotometer Thermo Scientific Helios Omega). PBS medium without samples was treated in the same way and used as a blank.

USC UNIVERSIDADE DE SANTIAGO DE COMPOSTELA

3.2.13 Drug release studies

Drug release studies were carried out from the 3D printed F6-0.5 and H6-0.5 **(Table 3.1)** discs (10 mm diameter x 1mm height and 0.1 g average weight) in 4 mL of 50% (v/v) ethanol and 50% (v/v) water for 67 days at 37 °C and 400 rpm (n = 4). The tubes were protected from light to avoid drug degradation. Blank (without drug) 3D printed discs were used as control. At predetermined time intervals, 500 µL aliquots were withdrawn from each tube and replaced with the same volume of the release medium. The samples were filtered through a 0.22 µm Nylon filter and the concentration of each drug was then determined using a JASCO (Tokyo, Japan) HPLC (AS-4140 Autosampler, PU-4180 Pump, LC-NetII/ADC Interface Box, CO-4060 Column Oven, MD-4010 Photodiode Array Detector), fitted with a C18 column (Waters Symmetry C18, 5 µm, 4.6 × 250 mm) and operated with ChromNAV software (ver. 2, JASCO, Tokyo, Japan). The mobile phase consisted of 45% (v/v) 0.1% ortophosphoric acid (pH 2.2) and 55% (v/v) acetonitrile at 30 °C, and the flow rate was kept at 0.9 mL/min. The injection volume was 20 µL and the eluent was detected at a wavelength of 246 nm with a total run time of 10 min (retention time of ciprofloxacin and fluocinolone acetonide was 1.82 min and 7.21 min, respectively). Ciprofloxacin and fluocinolone acetonide contents in the samples were calculated from a validated calibration curve. The standard solutions were 2.5-200 µg/mL of ciprofloxacin and 0.5-60 µg/mL of fluocinolone acetonide in 50% (v/v) ethanol and 50% (v/v) water. At the end of the release test, all discs were dried in an oven (37 °C, 72 h) and weighed to determine the mass loss over the release time and SEM images were obtained.

Drug release data was fit to the square root kinetics (Higuchi equation):

USC
UNIVERSIDADE DE SANTIAGO DE COMPOSTELA

$$Q = k_H \cdot t^{\frac{1}{2}} \qquad \text{Eq. (3.3)}$$

where Q is the amount of drug released over time t and k_H is the Higuchi rate constant.

3.2.14 Statistical analysis

The effects of formulation composition on hemolysis and biofilm activity were analyzed using ANOVA and multiple range test (Statgraphics Centurion 18, StatPoint Technologies Inc., Warrenton, VA).

3.3 RESULTS AND DISCUSSION

3.3.1 DLP 3D printing

As everyone's ear anatomy is unique and different, hearing aids remain are one of the customized medical devices that are extensively manufactured via VAT photopolymerization-based technology as a result of its high resolution and great efficiency. Compared with other manufacturing methods such as moulding, 3D printing was found to be cost effective when the production volume is low and avoids the need of making moulds, which requires extra costs on machinery, material and labour [Awad et al., 2018]. We successfully demonstrated the possibility of manufacture hearing aids loaded with two drugs, ciprofloxacin and fluocinolone acetonide, via DLP 3D printing. Previously, SLA has been utilized to produce polyprintlets (3D printed polypills) where multiple drugs were incorporated within a single pill but physically separated in different compartments [Robles-Martinez et al., 2019; Xu et al., 2020]. So far, there have not

USC UNIVERSIDADE DE SANTIAGO DE COMPOSTELA

been examples of using photopolymerisation-based 3D printing techniques to produce drug delivery systems that combine more than one drug incorporated at the same time in the same resin. Herein, we demonstrated the possibility of preparing multi drug-loaded medical devices for personalized therapy.

Prior to the printing process, pure ciprofloxacin and fluocinolone acetonide were readily dispersed (apparently dissolved) in the Flexible or ENG hard resins under magnetic stirring. All the devices were successfully fabricated similar to the 3D scan model with smooth surface finish and good consistency in dimension regardless of drug loadings **(Figure 3.2)**. The fabricated hearing devices appeared the same colors as the used resins, yellow for ENG hard **(Figure 3.2B)** and black for Flexible **(Figure 3.2C)**. With the drug loading of ciprofloxacin-fluocinolone acetonide increasing, from 6%-0.5% to 12%-1%, the density of color slightly decreased.

USC
UNIVERSIDADE DE SANTIAGO DE COMPOSTELA

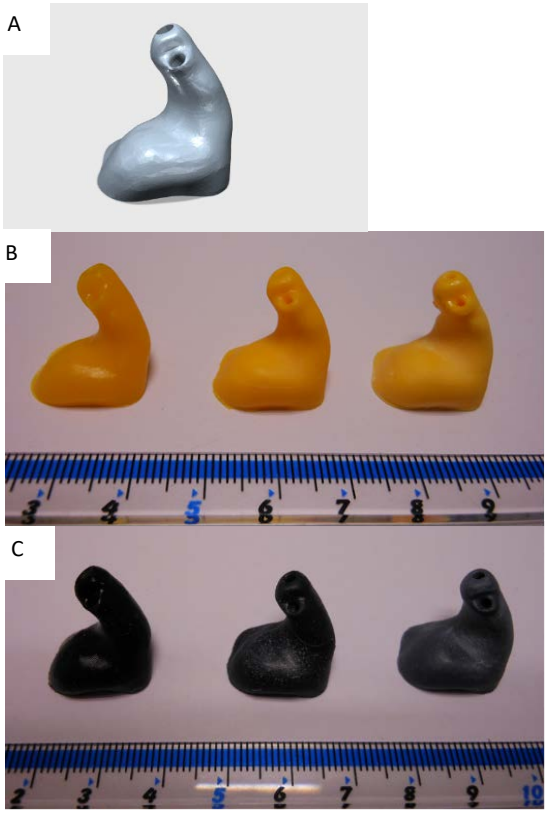


Figure 3.2. 3D scan model of the hearing aid (A) and DLP 3D printed hearing aids using (B) ENG hard resin and (C) Flexible resin. In (B) and (C), from left to right, hearing aids fabricated without drug, with ciprofloxacin-fluocinolone acetonide 6%-0.5% and 12%-1%, respectively. Scale in cm.

3.3.2 Physical characterization of the 3D printed slabs

SEM images of the control 3D printed slabs (without drugs) revealed homogeneous matrices lacking pores **(Figures 3.3 and 3.4)**. Similar appearance was observed for F6-0.5 and H6-0.5 although with a minor increase in roughness. Conversely, F12-1 and H12-1 showed small particles dispersed inside the slab (cross-section views) and

USC UNIVERSIDADE DE SANTIAGO DE COMPOSTELA

acicular marks on the surface. These empty marks may correspond to drug particles located in the outer surface of the slab that were removed during the washing process with isopropanol.

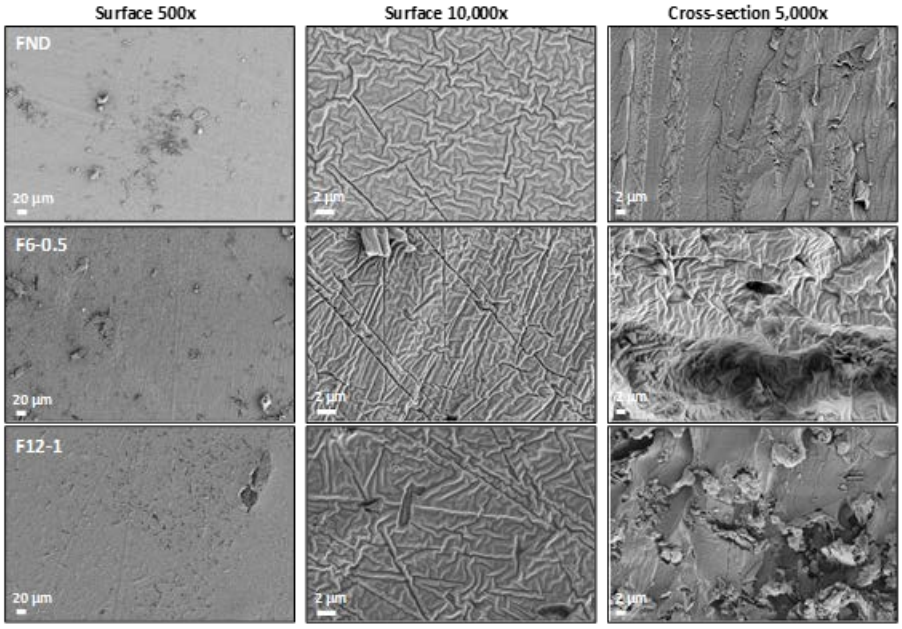


Figure 3.3. SEM images of freshly prepared 3D printed slabs FND, F6-0.5 and F12-1.

USC
UNIVERSIDADE DE SANTIAGO DE COMPOSTELA

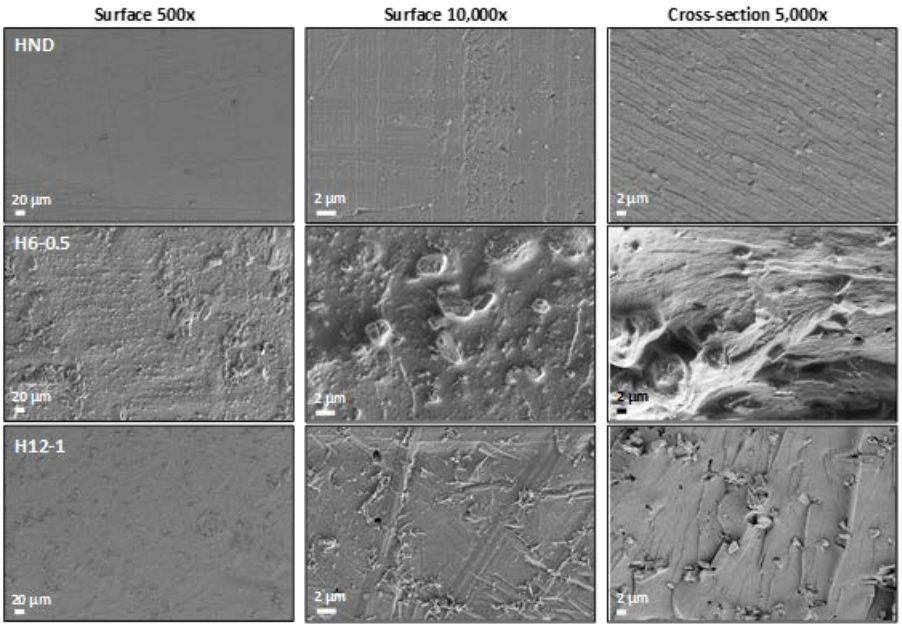


Figure 3.4. SEM images of freshly prepared 3D printed slabs HND, H6-0.5 and H12-1.

To gain an insight into the crystalline structure of the drugs after DLP 3D printing, DSC and XRPD spectra were obtained **(Figure 3.5)**. FND and HND were amorphous and DSC scans only revealed small decomposition peaks at 177 °C and 174 °C, respectively. Differently, F12-1 and H12-1 showed a thermal event at 151 °C, which is the typical dehydration temperature of ciprofloxacin salt **(Figure 3.5A)**. In good agreement, XRPD spectra of F12-1 and H12-1 also evidenced crystalline peaks of ciprofloxacin at 8.33°, 9.17°, 19.44° and 26.64° 2θ **(Figure 3.5B)**. Fluocinolone acetonide (less polar and in less amount) seemed to have been dissolved completely in the resins, and no crystalline peaks corresponding to this drug were observed in the slabs. In the case of the polar ciprofloxacin hydrochloride, the resins only allowed the molecular dispersion of a certain proportion of drug

USC UNIVERSIDADE DE SANTIAGO DE COMPOSTELA

(up to ca. 6% ciprofloxacin in the blend) while the rest of the drug remained as small crystalline particles. Endothermic events typical of ciprofloxacin have also been previously recorded for 3D printed filaments used for FDM for a variety of polymers both when the drug was blended with the components and adsorbed onto preformed filaments [Qamar et al., 2019; Saviano et al., 2019]. Reports evidenced that ciprofloxacin is indeed immiscible with the matrix of urinary catheters made of poly(D,L-lactide-co-ε-caprolactone) [Fernández et al., 2018].

USC
UNIVERSIDADE DE SANTIAGO DE COMPOSTELA

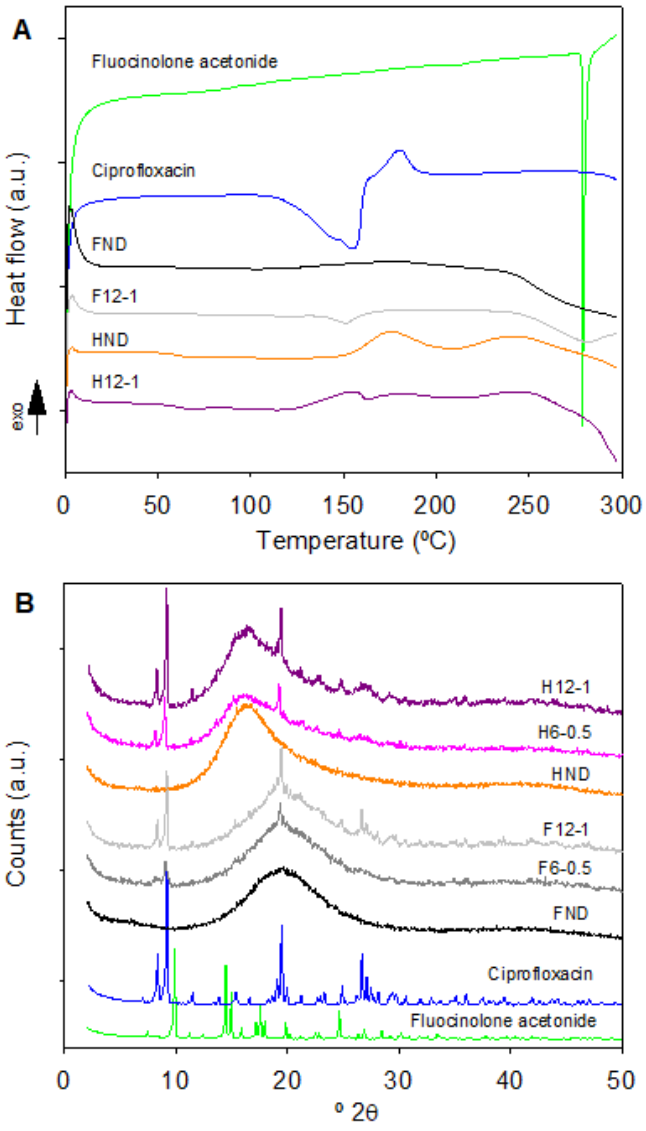


Figure 3.5. DSC thermograms (A) and XRPD spectra (B) of the drugs, 3D printed control slabs FND and HND (without drug) and 3D printed drug-loaded slabs. Codes as in Table 3.1.

USC
UNIVERSIDADE DE SANTIAGO DE COMPOSTELA

X-ray micro-CT imaging was used to three-dimensionally visualize the internal structure of the fabricated hearing aids. As can be seen from **Figure 3.6,** the images indicated that hearing aids loaded with drugs had more dense regions (in blue color) compared with the ones printed without drug. By increasing the drug loading of the devices from 6% ciprofloxacin – 0.5% fluocinolone acetonide (w/w) to 12% - 1%, an increased amount of blue color can be observed. In order to estimate the dimensional accuracy of the 3D printed devices, their dimensions were compared with the dimensions of the 3D model **(Table 3.2)**. The results demonstrated that the measured dimensions were similar to the dimensions in the 3D design except for the slightly higher variability in the x-axis values, indicating the suitable precision and reproducibility of the 3D printing process. The porosity results showed that all the 3D printed devices had a total porosity percentage in the range of 0.3%-2%, indicating that the devices are not porous.

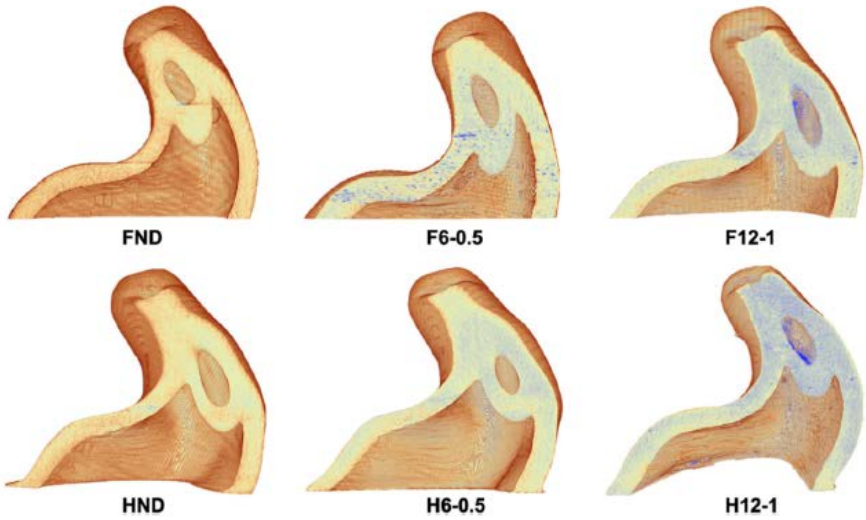


Figure 3.6. X-ray micro-CT images of the hearing devices. Codes as in Table 3.1.

USC
UNIVERSIDADE DE SANTIAGO DE COMPOSTELA

Table 3.2. Dimensions of the 3D model and the 3D printed hearing aids.

Hearing aid code	X (mm)	Y (mm)	Z (mm)
3D model	15.82	18.66	17.68
FND	17.05	18.82	17.92
F6-0.5	18.70	17.83	17.59
F12-1	16.36	18.30	17.81
HND	16.70	18.37	16.95
H6-0.5	17.03	18.11	17.73
H12-1	18.08	18.18	17.66

3.3.3 Mechanical evaluation

Since drug-loaded devices obtained by VAT photopolymerization 3D printing have been barely investigated [Ballard t al., 2019], a first step was to elucidate whether the addition of antimicrobial and anti-inflammatory agents at clinically relevant proportions may have an impact on the mechanical properties of the hearing aids. 3D printed FND and HND slabs showed quite different mechanical properties **(Figure 3.7)**. As expected, FND slabs made of Flexible resin were able to deform more than 60% in length before breaking. The Young's modulus of FND was 2.5 (s.d. 0.2) MPa **(Table 3.3)**. The addition of ciprofloxacin and fluocinolone acetonide caused a slight increase in the modulus up to 3.7 and 4.1 MPa for F6-0.5 and F12-1, respectively. The reinforcement of the mechanical properties, although with minor practical impact, can be attributed to the presence of drug crystalline particles.

On the other hand, HND slabs made of ENG Hard resin were more brittle and started to develop cracks at lower strain values. The Young's modulus was remarkably high, 152.7 (s.d. 1.8) MPa. The addition of the drugs made the slabs more brittle, but the Young's

USC UNIVERSIDADE DE SANTIAGO DE COMPOSTELA

modulus remained in the range of 154-156 MPa. Overall, the 3D printed slabs were able to accommodate quite high proportions of drugs while still maintaining their typical mechanical properties.

Table 3.3. Characteristics of the 3D printed slabs. Mean values and, in parenthesis standard deviations (n = 3).

Hearing aid code	Young's modulus (MPa)	Haemolysis (%)
FND	2.5 (0.2)	2.3 (1.3)
F6-0.5	3.7 (0.4)	1.6 (0.3)
F12-1	4.1 (0.4)	1.9 (1.0)
HND	152.7 (1.8)	1.0 (0.3)
H6-0.5	154.0 (2.5)	1.7 (1.3)
H12-1	155.6 (1.9)	1.1 (0.9)

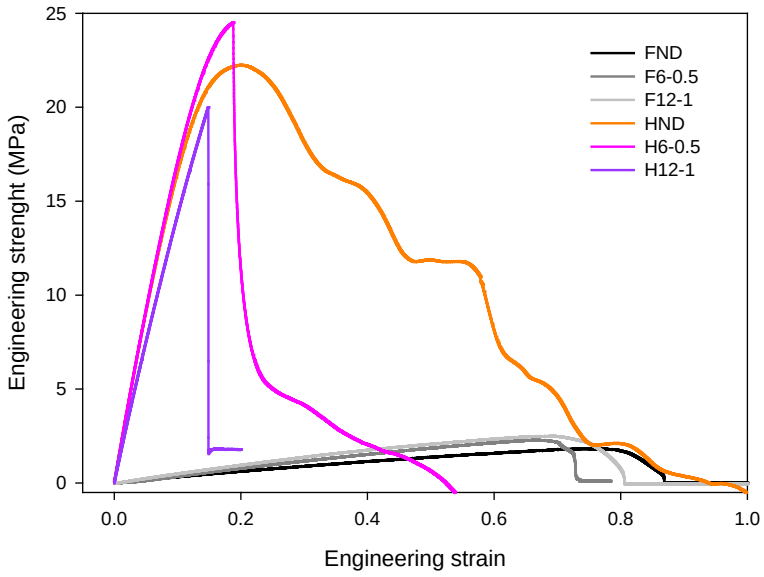


Figure 3.7. Stress-strain curves of the DLP 3D printed slabs as a function of different drug loadings (n = 3).

USC UNIVERSIDADE DE SANTIAGO DE COMPOSTELA

3.3.4 Hemolytic activity

Although hearing aids are not expected to enter into contact with the human blood, ear wounds and infections as well as incorrect handling may expose the device to blood [Zivic and Zivic, 2011]. 3D printed slabs of each resin with and without drug combinations were evaluated using an agitated blood incubation model [Weber et al., 2018]. Triton X-100 was used to cause 100% hemolysis and referred as the positive control. All slabs showed an excellent blood compatibility with hemolysis percentages well below 5% **(Table 3.3)** and no significant differences were found among the formulations (ANOVA, $p = 0.5650$). This finding also indicated that traces of residual monomers, if any, and the amounts of drugs eluted to the medium do not compromise the safety of the device.

3.3.5 Anti-biofilm properties

All 3D printed slabs showed hydrophilic surface, with water contact angles in the 61-64° range for slabs prepared with the ENG hard resin and in the 63-68° range for those made with the Flexible resin **(Figure 3.8)**. These values were not altered by the incorporation of drugs (ANOVA, $p > 0.05$).

USC
UNIVERSIDADE DE SANTIAGO DE COMPOSTELA

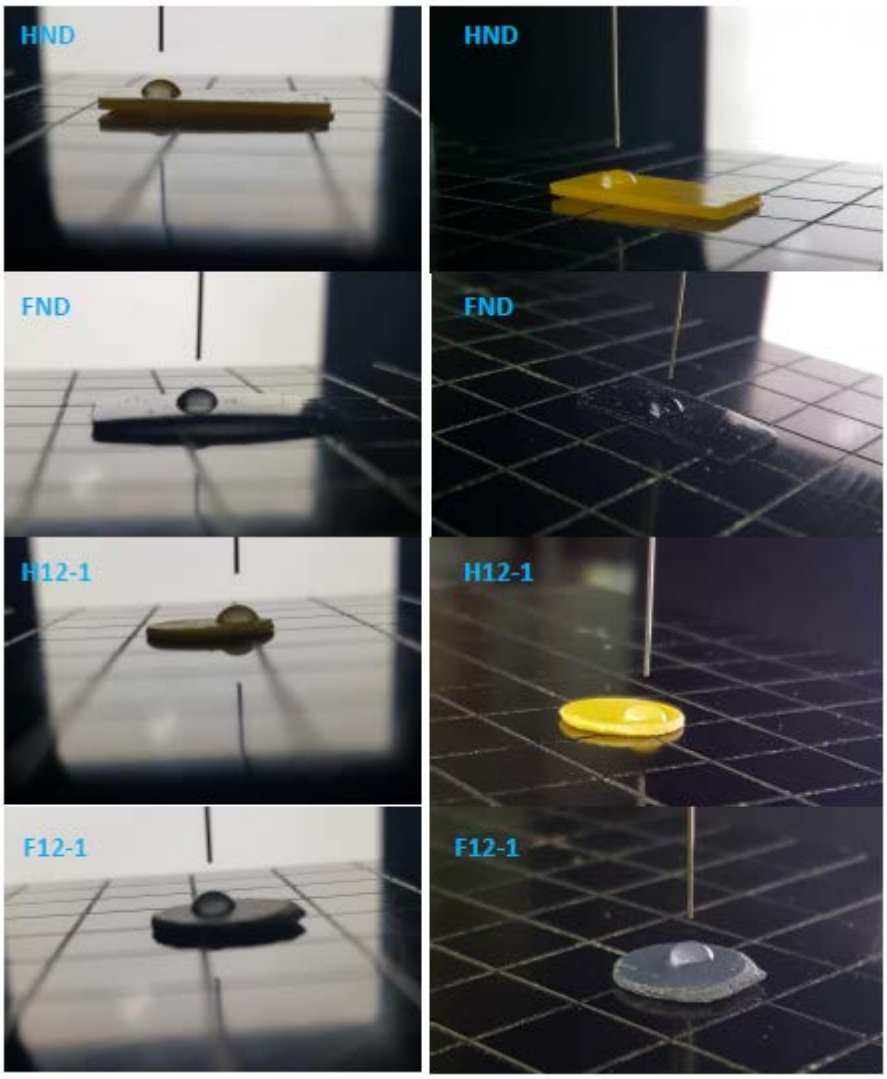


Figure 3.8. View of water drops on slabs prepared with and without drugs. Codes as in Table 3.1.

USC
UNIVERSIDADE DE SANTIAGO DE COMPOSTELA

The anti-biofilm properties of the DLP 3D printed slabs were evaluated against biofilm formation by two bacteria commonly responsible for chronic suppurative otitis media, *P. aeruginosa* and *S. aureus* [Bankaitis, 2002; Ikeda et al., 2015; Mansoor et al., 2009; Nia et al., 2011]. Drug loaded and blank devices were tested, and glass coverslips were used as positive controls of bacteria growth. The AAA biofilm growth model was used for testing biofilm formation on different substrate materials with a high reproducibility [Exterkate et al., 2010; Mayer et al., 2018]. This setup allowed elucidating whether the drugs (mainly ciprofloxacin) or any other substance is leached from the hearing aids may alter biofilm growth on the surface of the devices. Moreover, bacterial planktonic growth was also monitored in the medium surrounding the 3D printed slabs in order to assess the degree of leaching of the drugs to the culture medium

In the case of *P. aeruginosa* **(Figure 3.9)**, after 12 h of incubation, biofilm was successfully developed on the control glass coverslips and also on the blank hearing aids FND and HND (ANOVA, $p = 0.3962$). Also, no relevant changes in the absorbance of the surrounding growth medium were observed, which means that the planktonic growth of this Gram-negative bacterium was similar. Therefore, blank hearing aids themselves did not possess biocide surface and did not release bactericide substances to the growth medium. Differently, the drug loaded devices exhibited an efficient anti-biofilm activity. The growth on the surface of the devices was completely inhibited in all cases, and the bacteria remaining in the medium was remarkably decreased. The growth of *P. aeruginosa* in the medium was statistically lower for the drug-loaded hearing aids than for FND, HND and the coverslips (ANOVA, $p < 0.0001$). No significant differences were observed among F6-0.5, F12-1, H6-0.5 and H12-1, which means that the amount of ciprofloxacin released

USC UNIVERSIDADE DE SANTIAGO DE COMPOSTELA

was much higher than the level required for the antibiofilm effect, reported to be 40 µg/mL for *P. aeruginosa* [Masadeh et al., 2019].

In the case of *S. aureus* **(Figure 3.9)**, biofilm formation took more time and therefore it was evaluated after 48 h of incubation. As observed for *P. aeruginosa*, blank hearing aids performed as the control glass coverslips allowed the development of the Gram-positive bacteria biofilm. Drug-loaded devices completely avoided biofilm formation on their surfaces and also hindered the bacteria growth in the surrounding medium. The statistical analysis confirmed that the bacteria growth on FND and HND was similar and slightly lower that that recorded for the coverslips (ANOVA, $p = 0.0392$) while the growth of *S. aureus* in the medium was the same for FND, HND and the coverslips (ANOVA, $p = 0.4514$). Minimum bactericidal and biofilm eradication concentrations of ciprofloxacin against methicillin-resistant *S. aureus* have been estimated to be 0.625 and 438 µg/mL, respectively [Masadeh et al., 2019]. Assuming a weight of 0.15 g per slab, the amount of ciprofloxacin in the F6-0.5 and H6-0.5 slab would be 9 mg. The total volume of culture medium was 4 mL. Therefore, the minimum bactericidal concentration can be reached with the release of only 0.023% drug content, while the biofilm eradication may require the release of 19.5% ciprofloxacin content.

The efficacy of ciprofloxacin preventing the biofilm formation of *P. aeruginosa* has been shown before [Ahire et al., 2015; Aslam et al., 2004; Gupta et al., 2016; Ikeda et al., 2015; Mansoor et al., 2009; Nia et al., 2011] and was attributed to the inhibition of the *Quorum Sensing* mechanism [Gupta et al., 2016]. The efficacy against *S. aureus* agreed with previous reports [Ahire et al., 2015; Nia et al., 2011] and ciprofloxacin-loaded electrospun nanofibers have demonstrated ability to inhibit the biofilm formation by a methicillin-resistant *S. aureus* [Ahire et al., 2015]. In addition, the fabricated

USC UNIVERSIDADE DE SANTIAGO DE COMPOSTELA

devices showed great stability under the storage condition of room temperature for 3 months without losing the efficacy.

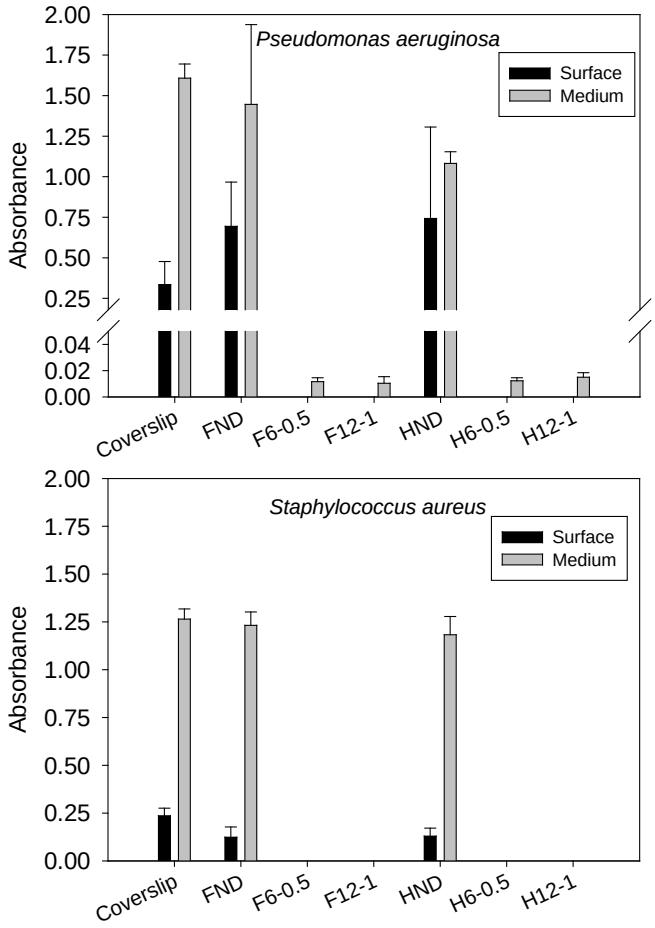


Figure 3.9. Growth of *P. aeruginosa* and *S. aureus* on the surface (biofilm) and in the medium surrounding the slabs after 12 and 48 h incubation, respectively. As controls, glass coverslips were used. Mean values and standard deviations (n = 3). The absorbance values were recorded at 570 nm for the MTT assay (growth on the surface) and at 600 nm for planktonic bacteria growth in the medium.

USC
UNIVERSIDADE DE SANTIAGO DE COMPOSTELA

3.3.6 Drug-release studies

Since drug-loaded slabs F6-0.5 and H6-0.5 demonstrated to be highly efficient against both Gram-negative and Gram-positive bacteria, only F6-0.5 and H6-0.5 were chosen for a detailed monitoring of the drug release profiles to avoid waste of drug and concerns on toxicity. This information should allow the prediction for how long the hearing aids could continue delivering the drugs keeping in mind that otitis requires one or two weeks of pharmacological treatment [Brennan-Jones et al., 2020]. Ciprofloxacin hydrochloride is a hydrophilic antimicrobial agent (solubility 170 µg/mL in PBS; log P -0.94) [Olivera et al., 2011], while fluocinolone acetonide is a relatively hydrophobic corticosteroid (solubility 17 µg/mL in PBS; log P 2.24) [Thakur et al., 2011]. Therefore, the release medium, 50% (v/v) ethanol and 50% (v/v) water, was chosen to attend a two-fold criterion: i) to generate a less polar environment than water and thus to resemble better the environment in the ear canal (a mixture of sweat and cerumen); and ii) to provide sink conditions for both drugs [Sheshala et al., 2019]. Hydroalcoholic medium is commonly used as receptor medium to provide sink conditions in diffusion and release studies of corticosteroid drugs intended for skin application [Christensen et al., 2011].

DLP 3D printed drug-loaded discs F6-0.5 and H6-0.5 sustained the releases of both drugs for 20 days and then the releases continued with much slower rates **(Figure 3.10)**. The slowdown of the releases may be attributed to less accessible drug molecules entrapped in the inner regions of the discs. F6-0.5 provided faster release profiles than H6-0.5. Particularly, the amount of ciprofloxacin released after 23 days from F6-0.5 was 16.5 (s.d. 1.3) mg/g, equivalent to 27.6 (s.d. 2.2) % loading. In the case of H6-0.5 the cumulative amount of ciprofloxacin released was 1.8 (s.d. 0.2) mg/g, equivalent to 3.0 (s.d. 0.3) % loading.

USC UNIVERSIDADE DE SANTIAGO DE COMPOSTELA

Similarly, fluocinolone acetonide release occurred faster from F6-0.5 and reached 4.6 (s.d. 0.1) mg/g at day 23, which represent more than 90% loading (93.1, s.d. 2.3, %). In the case of H6-0.5, the amount of fluocinolone acetonide released was 0.52 (s.d. 0.04) mg/g, equivalent to 10.3 (s.d. 0.9) % loading. Thus, overall, release of fluocinolone acetonide occurred faster and more efficiently than for ciprofloxacin.

Release profiles recorded in the first week of release fitted quite well to the square-root kinetics **(Table 3.4, Eq. 3.3)**. In the case of ciprofloxacin released from H6-0.5 data recorded for the first two weeks was used for the fitting to obtain reliable values.

Drug release rate constants (K_H) evidenced that the release of any of the drugs was one order of magnitude faster from the Flexible resins than for the ENG hard resins. Therefore, it is possible to cover a wide range of therapeutic demands by modifying the compositions of the photocurable resin, as observed also for different polymers employed in the fabrication of other 3D printed drug-loaded implants and oral dosage forms [Kempin et al., 2017; Kotta et al., 2018; Martinez et al., 2017].

USC
UNIVERSIDADE DE SANTIAGO DE COMPOSTELA

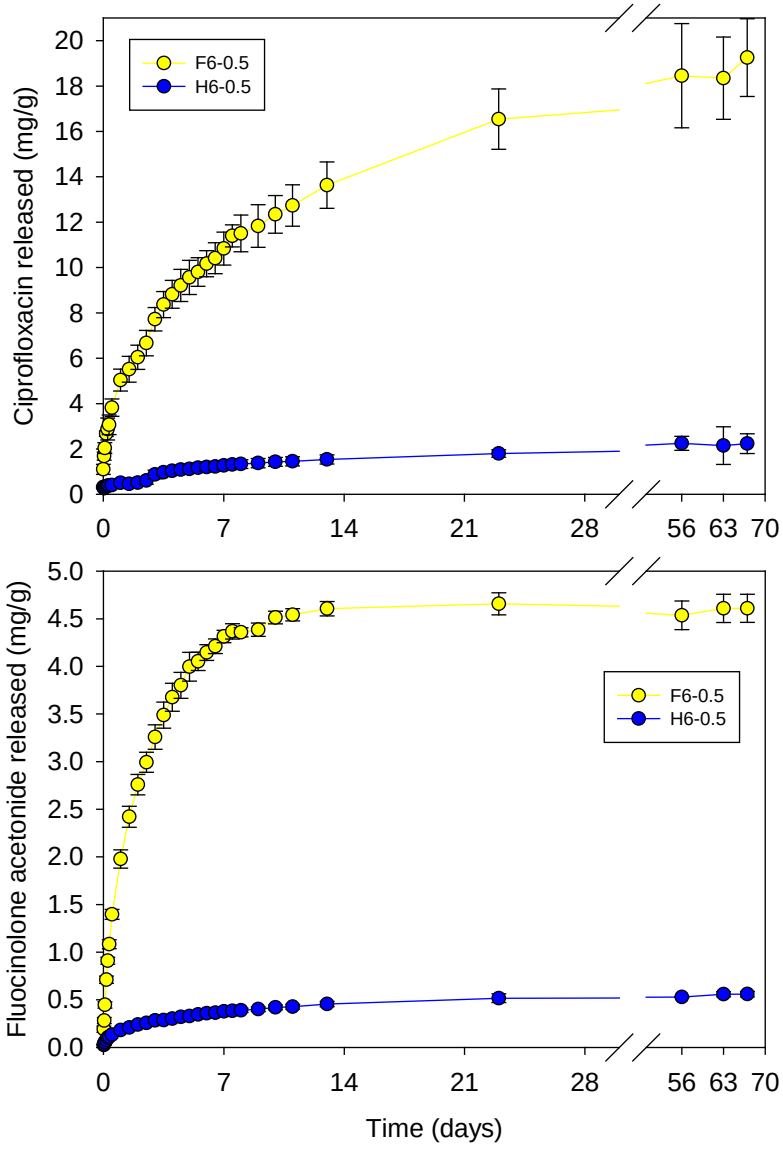


Figure 3.10. Drug release profiles of ciprofloxacin hydrochloride (top) and fluocinolone acetonide (bottom) for 3D printed discs F6-0.5 and H6-0.5.

USC
UNIVERSIDADE DE SANTIAGO DE COMPOSTELA

Table 3.4. Results of fitting of Higuchi equation (square root kinetics) to the drug release profiles

Hearing aid code	Ciprofloxacin		Fluocinolone acetonide	
	K_H ($mg \cdot g^{-1} \cdot h^{-0.5}$)	R^2	K_H ($mg \cdot g^{-1} \cdot h^{-0.5}$)	R^2
F6-0.5	0.78 (s.d. 0.06)	> 0.99	0.35 (s.d. 0.01)	> 0.99
H6-0.5	0.083 (s.d. 0.0011)	> 0.95	0.028 (s.d. 0.002)	> 0.99

After the drug release test, the discs were washed, dried and weighed again. The mean weight loss recorded was 11% for F6-0.5 and 1.1% for H6-0.5. These values were two-fold larger than those predicted from the leakage of the drugs, which suggested that there is dissolution of materials from the slabs after 2 months in the dissolution medium. FND and HND discs stored in the dissolution medium exhibited an appearance like the freshly prepared ones **(Figure 3.11)**. After the dissolution study, the F6-0.5 disc had rougher surface while the H6-0.5 disc showed a variety of pores ranging in size from few nanometers to few microns compared to the freshly prepared ones. This finding suggested that the drug dissolution created channels in the structure that may facilitate partial loss of polymer components.

Although there are none other 3D printed drug-loaded hearing aids for comparison, the release of more than 7 days for both drugs may satisfy the therapeutic guidelines for the treatment of AOMT using the ciprofloxacin and fluocinolone acetonide combinations [Lorente et al., 2014], which could ensure greater therapeutic compliance and effectiveness compared with ear drops. In addition to the antimicrobial efficacy of ciprofloxacin, the clinical management of otitis has been shown to benefit from the combination with fluocinolone acetonide; the combination being more efficient than

USC UNIVERSIDADE DE SANTIAGO DE COMPOSTELA

ciprofloxacin alone to address the associated oedema, otalgia, and otorrhoea, and therefore a faster and more complete recovery of the patient [Lorente et al., 2014].

The work highlights the potential of using DLP 3D printing to manufacture drug-loaded hearing aids that required personalization to fit the ear anatomy of the patient. The manufacture approach was easy, less expensive and in just one step. In this scenario, drug could be eluted out from the device via diffusion, providing sustained drug release at local site and hence increasing the residence time. Apart from antibiotics, other agents are possibly to be incorporated for drug delivery to the ear depending on patient's need. Moreover, in order to extend the applicability of our work, cochlear implants may be a potential application to be coupled with DLP 3D printing to the inner ear [Plontke et al., 2017].

USC
UNIVERSIDADE DE SANTIAGO DE COMPOSTELA

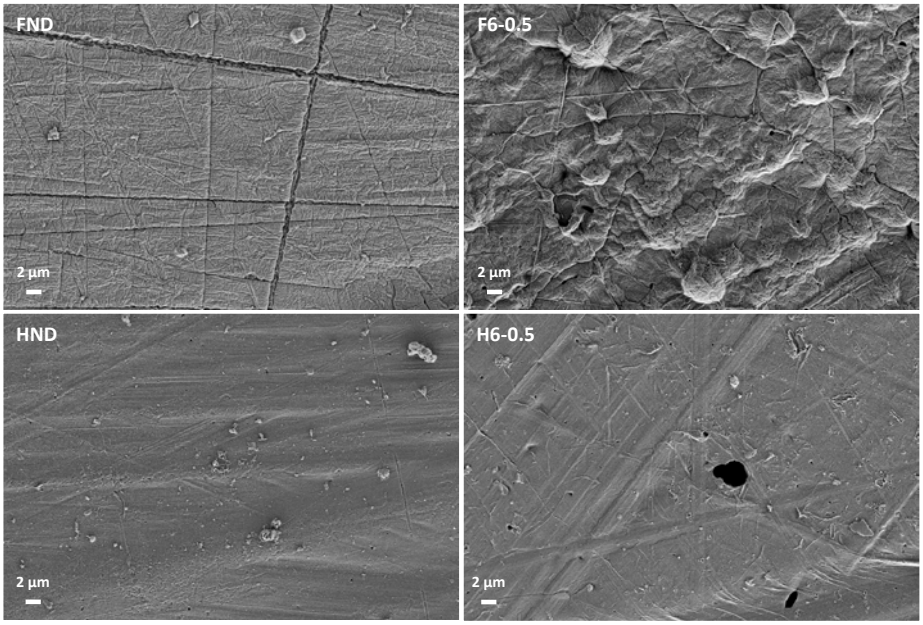


Figure 3.11. SEM images of 3D printed slabs after being 70 days in the release medium (5000x). Scale bar 2 µm.

3.4 CONCLUSIONS

This work demonstrates for first time the possibility of incorporating a combination of ciprofloxacin and fluocinolone acetonide, typically used as drops to address ear infections, into DLP 3D printed hearing aids to prevent or treat biofilm-related infections. Drug-loaded hearing aids were successfully prepared using two types of commercial resins, Flexible and ENG hard with different drug loadings. DLP 3D printed drug-loaded slabs exhibited similar mechanical properties and demonstrated excellent blood compatibility. *In vitro* drug release studies showed that the devices

USC UNIVERSIDADE DE SANTIAGO DE COMPOSTELA

could be sterilized and were able to provide sustained drug release for more than 7 days for both drugs, satisfying the therapeutic efficacy for the treatment of AOMT. Anti-biofilm properties were evaluated against *P. aeruginosa* and *S. aureus*, showing no bacteria growth on the surface of the devices and decreased growth in the surrounding medium. This proof-of-concept study shows that VAT photopolymerization 3D printing technologies can be a viable technology for the manufacture of drug-loaded medical devices with anti-biofilm properties. The outcome of this work could be translated and extended for the treatment of other diseases with other devices, allowing personalized therapy.

3.5 REFERENCES

Ahire, J. J., Neveling, D. P., Hattingh, M., & Dicks, L. M. (2015). Ciprofloxacin-eluting nanofibers inhibits biofilm formation by Pseudomonas aeruginosa and a methicillin-resistant *Staphylococcus aureus*. *PLoS One*, *10*(4), e0123648.

Alhnan, M. A., Okwuosa, T. C., Sadia, M., Wan, K. W., Ahmed, W., & Arafat, B. (2016). Emergence of 3D printed dosage forms: opportunities and challenges. *Pharmaceutical Research*, *33*(8), 1817-1832.

Aslam, M. A., Ahmed, Z., & Azim, R. (2004). Microbiology and drug sensitivity patterns of chronic suppurative otitis media. *Journal of the College of Physicians and Surgeons-Pakistan: JCPSP*, *14*(8), 459-461.

Awad, A., Fina, F., Trenfield, S. J., Patel, P., Goyanes, A., Gaisford, S., & Basit, A. W. (2019). 3D printed pellets (miniprintlets): A novel, multi-drug, controlled release platform technology. *Pharmaceutics*, *11*(4), 148.

USC
UNIVERSIDADE DE SANTIAGO DE COMPOSTELA

Awad, A., Trenfield, S. J., Goyanes, A., Gaisford, S., & Basit, A. W. (2018). Reshaping drug development using 3D printing. *Drug Discovery Today*, *23*(8), 1547-1555.

Awad, A., Yao, A., Trenfield, S. J., Goyanes, A., Gaisford, S., & Basit, A. W. (2020). 3D printed tablets (printlets) with braille and moon patterns for visually impaired patients. *Pharmaceutics*, *12*(2), 172.

Ballard, D. H., Tappa, K., Boyer, C. J., Jammalamadaka, U., Hemmanur, K., Weisman, J. A., ... & Woodard, P. K. (2019). Antibiotics in 3D-printed implants, instruments and materials: Benefits, challenges and future directions. *Journal of 3D Printing in Medicine*, *3*(2), 83-93.

Bankaitis, A. U. (2002). What's growing on your patients' hearing aids? A study gives you an idea. *The Hearing Journal*, *55*(6), 48-54.

Banks, J. (2013). Adding value in additive manufacturing: researchers in the United Kingdom and Europe look to 3D printing for customization. *IEEE Pulse*, *4*(6), 22-26.

Bloomquist, C. J., Mecham, M. B., Paradzinsky, M. D., Janusziewicz, R., Warner, S. B., Luft, J. C., ... & DeSimone, J. M. (2018). Controlling release from 3D printed medical devices using CLIP and drug-loaded liquid resins. *Journal of Controlled Release*, *278*, 9-23.

Brennan-Jones, C. G., Head, K., Chong, L. Y., Burton, M. J., Schilder, A. G., & Bhutta, M. F. (2020). Topical antibiotics for chronic suppurative otitis media. *Cochrane Database of Systematic Reviews*, (1), CD013051

Cady, N. C., McKean, K. A., Behnke, J., Kubec, R., Mosier, A. P., Kasper, S. H., ... & Musah, R. A. (2012). Inhibition of biofilm formation, quorum sensing and infection in *Pseudomonas aeruginosa* by natural products-inspired organosulfur compounds. *PLoS One*, *7*(6), e38492.

Christensen, J. M., Chuong, M. C., Le, H., Pham, L., & Bendas, E. (2011). Hydrocortisone diffusion through synthetic membrane, mouse skin, and epiderm™ cultured skin. *Archives of Drug Information*, *4*(1), 10-21.

USC UNIVERSIDADE DE SANTIAGO DE COMPOSTELA

Conceição, J., Farto-Vaamonde, X., Goyanes, A., Adeoye, O., Concheiro, A., Cabral-Marques, H., ... & Alvarez-Lorenzo, C. (2019). Hydroxypropyl-β-cyclodextrin-based fast dissolving carbamazepine printlets prepared by semisolid extrusion 3D printing. *Carbohydrate Polymers*, *221*, 55-62.

Deng, L., Deng, Y., & Xie, K. (2017). AgNPs-decorated 3D printed PEEK implant for infection control and bone repair. *Colloids and Surfaces B: Biointerfaces*, *160*, 483-492.

Dentca, 2016. DENTCA 3D Printed Dentures. https://www.dentca.com/products/dentca-3d ; Accessed April 2020

Economidou, S. N., Pere, C. P. P., Reid, A., Uddin, M. J., Windmill, J. F., Lamprou, D. A., & Douroumis, D. (2019). 3D printed microneedle patches using stereolithography (SLA) for intradermal insulin delivery. *Materials Science and Engineering: C*, *102*, 743-755.

Elbadawi, M., Castro, B. M., Gavins, F. K., Ong, J. J., Gaisford, S., Pérez, G., ... & Goyanes, A. (2020). M3DISEEN: A novel machine learning approach for predicting the 3D printability of medicines. *International Journal of Pharmaceutics*, *590*, 119837.

EnvisionTEC, The Top Choice for 3D Printed Hearing Aids, Inner-Ear Devices. https://envisiontec.com/3d-printing-industries/medical/hearing-aid/; Accessed April 2020

Exterkate, R. A. M., Crielaard, W., & Ten Cate, J. M. (2010). Different response to amine fluoride by *Streptococcus mutans* and polymicrobial biofilms in a novel high-throughput active attachment model. *Caries Research*, *44*(4), 372-379.

Farto-Vaamonde, X., Auriemma, G., Aquino, R. P., Concheiro, A., & Alvarez-Lorenzo, C. (2019). Post-manufacture loading of filaments and 3D printed PLA scaffolds with prednisolone and dexamethasone for tissue regeneration applications. *European Journal of Pharmaceutics and Biopharmaceutics*, *141*, 100-110.

USC
UNIVERSIDADE DE SANTIAGO DE COMPOSTELA

Fernández, J., Ribeiro, I. A., Martin, V., Martija, O. L., Zuza, E., Bettencourt, A. F., & Sarasua, J. R. (2018). Release mechanisms of urinary tract antibiotics when mixed with bioabsorbable polyesters. *Materials Science and Engineering: C*, *93*, 529-538.

Fina, F., Goyanes, A., Madla, C. M., Awad, A., Trenfield, S. J., Kuek, J. M., ... & Basit, A. W. (2018). 3D printing of drug-loaded gyroid lattices using selective laser sintering. *International journal of Pharmaceutics*, *547*(1-2), 44-52.

Formlabs, 3D Printing for Audiology, 2020. https://formlabs.com/uk/industries/audiology/; Accessed September 2020

Fu, J., Yu, X., & Jin, Y. (2018). 3D printing of vaginal rings with personalized shapes for controlled release of progesterone. *International Journal of Pharmaceutics*, *539*(1-2), 75-82.

Genina, N., Boetker, J. P., Colombo, S., Harmankaya, N., Rantanen, J., & Bohr, A. (2017). Anti-tuberculosis drug combination for controlled oral delivery using 3D printed compartmental dosage forms: From drug product design to in vivo testing. *Journal of Controlled Release*, *268*, 40-48.

Genina, N., Holländer, J., Jukarainen, H., Mäkilä, E., Salonen, J., & Sandler, N. (2016). Ethylene vinyl acetate (EVA) as a new drug carrier for 3D printed medical drug delivery devices. *European Journal of Pharmaceutical Sciences*, *90*, 53-63.

Gioumouxouzis, C. I., Tzimtzimis, E., Katsamenis, O. L., Dourou, A., Markopoulou, C., Bouropoulos, N., ... & Fatouros, D. G. (2020). Fabrication of an osmotic 3D printed solid dosage form for controlled release of active pharmaceutical ingredients. *European Journal of Pharmaceutical Sciences*, *143*, 105176.

Goyanes, A., Det-Amornrat, U., Wang, J., Basit, A. W., & Gaisford, S. (2016). 3D scanning and 3D printing as innovative technologies for fabricating personalized topical drug delivery systems. *Journal of Controlled Release*, *234*, 41-48.

USC UNIVERSIDADE DE SANTIAGO DE COMPOSTELA

Goyanes, A., Fernández-Ferreiro, A., Majeed, A., Gomez-Lado, N., Awad, A., Luaces-Rodríguez, A., ... & Basit, A. W. (2018). PET/CT imaging of 3D printed devices in the gastrointestinal tract of rodents. *International Journal of Pharmaceutics*, *536*(1), 158-164.

Goyanes, A., Madla, C. M., Umerji, A., Piñeiro, G. D., Montero, J. M. G., Diaz, M. J. L., ... & Basit, A. W. (2019). Automated therapy preparation of isoleucine formulations using 3D printing for the treatment of MSUD: First single-centre, prospective, crossover study in patients. *International Journal of Pharmaceutics*, *567*, 118497.

Gupta, P., Chhibber, S., & Harjai, K. (2016). Subinhibitory concentration of ciprofloxacin targets quorum sensing system of *Pseudomonas aeruginosa* causing inhibition of biofilm formation & reduction of virulence. *The Indian Journal of Medical Research*, *143*(5), 643.

Holländer, J., Genina, N., Jukarainen, H., Khajeheian, M., Rosling, A., Mäkilä, E., & Sandler, N. (2016). Three-dimensional printed PCL-based implantable prototypes of medical devices for controlled drug delivery. *Journal of Pharmaceutical Sciences*, *105*(9), 2665-2676.

Ikeda, K., Misawa, S., & Kusunoki, T. (2015). Comparative bactericidal activity of four fluoroquinolones against *Pseudomonas aeruginosa* isolated from chronic suppurative otitis media. *BMC Ear, Nose and Throat Disorders*, *15*(1), 1-3.

Isreb, A., Baj, K., Wojsz, M., Isreb, M., Peak, M., & Alhnan, M. A. (2019). 3D printed oral theophylline doses with innovative 'radiator-like'design: Impact of polyethylene oxide (PEO) molecular weight. *International Journal of Pharmaceutics*, *564*, 98-105.

Kempin, W., Franz, C., Koster, L. C., Schneider, F., Bogdahn, M., Weitschies, W., & Seidlitz, A. (2017). Assessment of different polymers and drug loads for fused deposition modeling of drug loaded implants. *European Journal of Pharmaceutics and Biopharmaceutics*, *115*, 84-93.

USC
UNIVERSIDADE DE SANTIAGO DE COMPOSTELA

Khaled, S. A., Burley, J. C., Alexander, M. R., Yang, J., & Roberts, C. J. (2015). 3D printing of five-in-one dose combination polypill with defined immediate and sustained release profiles. *Journal of Controlled Release*, *217*, 308-314.

Kostakioti, M., Hadjifrangiskou, M., & Hultgren, S. J. (2013). Bacterial biofilms: development, dispersal, and therapeutic strategies in the dawn of the postantibiotic era. *Cold Spring Harbor Perspectives in Medicine*, *3*(4), a010306.

Kotta, S., Nair, A., & Alsabeelah, N. (2018). 3D printing technology in drug delivery: recent progress and application. *Current Pharmaceutical Design*, *24*(42), 5039-5048.

Liang, K., Brambilla, D., & Leroux, J. C. (2019). Is 3D printing of pharmaceuticals a disruptor or enabler?. *Advanced Materials*, *31*(5), 1805680.

Liang, K., Carmone, S., Brambilla, D., & Leroux, J. C. (2018). 3D printing of a wearable personalized oral delivery device: A first-in-human study. *Science Advances*, *4*(5), eaat2544.

Lim, S. H., Ng, J. Y., & Kang, L. (2017). Three-dimensional printing of a microneedle array on personalized curved surfaces for dual-pronged treatment of trigger finger. *Biofabrication*, *9*(1), 015010.

Lorente, J., Sabater, F., Rivas, M. P., Fuste, J., Risco, J., & Gómez, M. (2014). Ciprofloxacin plus fluocinolone acetonide versus ciprofloxacin alone in the treatment of diffuse otitis externa. *The Journal of Laryngology & Otology*, *128*(7), 591-598.

Mansoor, T., Musani, M. A., Khalid, G., & Kamal, M. (2009). *Pseudomonas aeruginosa* in chronic suppurative otitis media: sensitivity spectrum against various antibiotics in Karachi. *Journal of Ayub Medical College Abbottabad*, *21*(2), 120-3.

USC
UNIVERSIDADE DE SANTIAGO DE COMPOSTELA

Maroni, A., Melocchi, A., Parietti, F., Foppoli, A., Zema, L., & Gazzaniga, A. (2017). 3D printed multi-compartment capsular devices for two-pulse oral drug delivery. *Journal of Controlled Release*, *268*, 10-18.

Martin, V., Ribeiro, I. A., Alves, M. M., Gonçalves, L., Claudio, R. A., Grenho, L., ... & Bettencourt, A. F. (2019). Engineering a multifunctional 3D-printed PLA-collagen-minocycline-nano Hydroxyapatite scaffold with combined antimicrobial and osteogenic effects for bone regeneration. *Materials Science and Engineering: C*, *101*, 15-26.

Martinez, P. R., Goyanes, A., Basit, A. W., & Gaisford, S. (2017). Fabrication of drug-loaded hydrogels with stereolithographic 3D printing. *International Journal of Pharmaceutics*, *532*(1), 313-317.

Masadeh, M. M., Alzoubi, K. H., Ahmed, W. S., & Magaji, A. S. (2019). In vitro comparison of antibacterial and antibiofilm activities of selected fluoroquinolones against *Pseudomonas aeruginosa* and methicillin-resistant *Staphylococcus aureus*. *Pathogens*, *8*(1), 12.

Materialise, the hearing-aid industry will never be the same again, 2020 https://www.materialise.com/en/cases/phonak-3d-printed-hearing-aid; Acccessed September 2020

Mayer, C., Muras, A., Romero, M., López, M., Tomás, M., & Otero, A. (2018). Multiple quorum quenching enzymes are active in the nosocomial pathogen *Acinetobacter baumannii* ATCC17978. *Frontiers in Cellular and Infection Microbiology*, *8*, 310.

Melchels, F. P., Feijen, J., & Grijpma, D. W. (2010). A review on stereolithography and its applications in biomedical engineering. *Biomaterials*, *31*(24), 6121-6130.

Melocchi, A., Inverardi, N., Uboldi, M., Baldi, F., Maroni, A., Pandini, S., ... & Gazzaniga, A. (2019). Retentive device for intravesical drug delivery based on water-induced shape memory response of poly (vinyl alcohol): design concept and 4D printing feasibility. *International Journal of Pharmaceutics*, *559*, 299-311.

USC UNIVERSIDADE DE SANTIAGO DE COMPOSTELA

Melocchi, A., Uboldi, M., Inverardi, N., Briatico-Vangosa, F., Baldi, F., Pandini, S., ... & Gazzaniga, A. (2019). Expandable drug delivery system for gastric retention based on shape memory polymers: Development via 4D printing and extrusion. *International Journal of Pharmaceutics*, *571*, 118700.

Nia, K. M., Sepehri, G. Sepehri., Khatmi, H., & Shakibaie, M. R. (2011). Isolation and antimicrobial susceptibility of bacteria from chronic suppurative otitis media patients in Kerman, Iran. *Iranian Red Crescent Medical Journal*, *13*(12), 891.

Nuryastuti, T., van der Mei, H. C., Busscher, H. J., Iravati, S., Aman, A. T., & Krom, B. P. (2009). Effect of cinnamon oil on icaA expression and biofilm formation by *Staphylococcus epidermidis*. *Applied and Environmental Microbiology*, *75*(21), 6850-6855.

Olivera, M. E., Manzo, R. H., Junginger, H. E., Midha, K. K., Shah, V. P., Stavchansky, S., ... & Barends, D. M. (2011). Biowaiver monographs for immediate release solid oral dosage forms: Ciprofloxacin hydrochloride. *Journal of Pharmaceutical Sciences*, *100*(1), 22-33.

Onali, M. A., Bareeqa, S. B., Zia, S., Ahmed, S. I., Owais, A., & Ahmad, A. N. (2018). Efficacy of empirical therapy with combined ciprofloxacin versus topical drops alone in patients with tubotympanic chronic suppurative otitis media: A randomized double-blind controlled trial. *Clinical Medicine Insights: Ear, Nose and Throat*, *11*, 1179550617751907.

Orji, F. T., Onyero, E. O., & Agbo, C. E. (2014). The clinical implications of ear canal debris in hearing aid users. *Pakistan Journal of Medical Sciences*, *30*(3), 483.

Parrish, J. M., Soni, M., & Mittal, R. (2019). Subversion of host immune responses by otopathogens during otitis media. *Journal of Leukocyte Biology*, *106*(4), 943-956.

Plontke, S. K., Götze, G., Rahne, T., & Liebau, A. (2017). Intracochlear drug delivery in combination with cochlear implants. *Hno*, *65*(1), 19-28.

USC UNIVERSIDADE DE SANTIAGO DE COMPOSTELA

Qamar, N., Abbas, N., Irfan, M., Hussain, A., Arshad, M. S., Latif, S., ... & Ghori, M. U. (2019). Personalized 3D printed ciprofloxacin impregnated meshes for the management of hernia. *Journal of Drug Delivery Science and Technology*, *53*, 101164.

Robles-Martinez, P., Xu, X., Trenfield, S. J., Awad, A., Goyanes, A., Telford, R., ... & Gaisford, S. (2019). 3D printing of a multi-layered polypill containing six drugs using a novel stereolithographic method. *Pharmaceutics*, *11*(6), 274.

Sadia, M., Arafat, B., Ahmed, W., Forbes, R. T., & Alhnan, M. A. (2018). Channelled tablets: An innovative approach to accelerating drug release from 3D printed tablets. *Journal of Controlled Release*, *269*, 355-363.

Sandler, N., Salmela, I., Fallarero, A., Rosling, A., Khajeheian, M., Kolakovic, R., ... & Vuorela, P. (2014). Towards fabrication of 3D printed medical devices to prevent biofilm formation. *International Journal of Pharmaceutics*, *459*(1-2), 62-64.

Saviano, M., Aquino, R. P., Del Gaudio, P., Sansone, F., & Russo, P. (2019). Poly (vinyl alcohol) 3D printed tablets: The effect of polymer particle size on drug loading and process efficiency. *International Journal of Pharmaceutics*, *561*, 1-8.

Sheshala, R., Anuar, N. K., Samah, N. H. A., & Wong, T. W. (2019). In vitro drug dissolution/permeation testing of nanocarriers for skin application: A comprehensive review. *AAPS PharmSciTech*, *20*(5), 1-28.

Smith, D. M., Kapoor, Y., Klinzing, G. R., & Procopio, A. T. (2018). Pharmaceutical 3D printing: Design and qualification of a single step print and fill capsule. *International Journal of Pharmaceutics*, *544*(1), 21-30.

Spektor, Z., Pumarola, F., Ismail, K., Lanier, B., Hussain, I., Ansley, J., ... & Hernández, F. J. (2017). Efficacy and safety of ciprofloxacin plus fluocinolone in otitis media with tympanostomy tubes in pediatric patients: a randomized clinical trial. *JAMA Otolaryngology–Head & Neck Surgery*, *143*(4), 341-349.

USC UNIVERSIDADE DE SANTIAGO DE COMPOSTELA

Sonova, 3D Printing Technology for Improved Hearing, 2020. https://www.sonova.com/en/story/innovation/3d-printing-technology-improved-hearing; Accessed September 2020.

Thakur, A., Kadam, R. S., & Kompella, U. B. (2011). Influence of drug solubility and lipophilicity on transscleral retinal delivery of six corticosteroids. *Drug Metabolism and Disposition*, *39*(5), 771-781.

Trenfield, S. J., Awad, A., Madla, C. M., Hatton, G. B., Firth, J., Goyanes, A., ... & Basit, A. W. (2019). Shaping the future: recent advances of 3D printing in drug delivery and healthcare. *Expert Opinion on Drug Delivery*, *16*(10), 1081-1094.

Weber, M., Steinle, H., Golombek, S., Hann, L., Schlensak, C., Wendel, H. P., & Avci-Adali, M. (2018). Blood-contacting biomaterials: in vitro evaluation of the hemocompatibility. *Frontiers in Bioengineering and Biotechnology*, *6*, 99.

WHO, Deafness and Hearing loss (2020). https://www.who.int/en/news-room/fact-sheets/detail/deafness-and-hearing-loss; Accessed March 2020

Xu, X., Awad, A., Martinez, P. R., Gaisford, S., Goyanes, A., & Basit, A. W. (2020). Vat photopolymerization 3D printing for advanced drug delivery and medical device applications. *Journal of Controlled Release*.

Xu, X., Robles-Martinez, P., Madla, C. M., Joubert, F., Goyanes, A., Basit, A. W., & Gaisford, S. (2020). Stereolithography (SLA) 3D printing of an antihypertensive polyprintlet: Case study of an unexpected photopolymer-drug reaction. *Additive Manufacturing*, *33*, 101071.

Yao, W., Li, D., Zhao, Y., Zhan, Z., Jin, G., Liang, H., & Yang, R. (2020). 3D printed multi-functional hydrogel microneedles based on high-precision digital light processing. *Micromachines*, *11*(1), 17.

Živic, L., & Živic, D. (2011). Ear injuries caused by parts of hearing aid. *Medicinski Glasnik*, *8*(2).

USC UNIVERSIDADE DE SANTIAGO DE COMPOSTELA

USC
UNIVERSIDADE
DE SANTIAGO
DE COMPOSTELA

USC
UNIVERSIDADE
DE SANTIAGO
DE COMPOSTELA

USC
UNIVERSIDADE
DE SANTIAGO
DE COMPOSTELA

Chapter 4

The work described in this chapter was published in **Resveratrol-loaded hydrogel contact lenses with antioxidant and antibiofilm performances**, *Pharmaceutics* 13, 532, 2021, authored by

María Vivero-Lopez[a], Andrea Muras[b], Diana Silva[c], Ana Paula Serro[c,d], Ana Otero[b], Angel Concheiro[a] and Carmen Alvarez-Lorenzo[a]

[a]Departamento de Farmacología, Farmacia y Tecnología Farmacéutica, I+D Farma (GI-1645), Facultad de Farmacia and Health Research Institute of Santiago de Compostela (IDIS), Universidade de Santiago de Compostela, 15782 Santiago de Compostela, Spain.

[b]Departamento de Microbiología, Facultad de Biología, Edificio CIBUS, Universidade de Santiago de Compostela, 15782 Santiago de Compostela, Spain.

[c]Centro de Química Estrutural, Instituto Superior Técnico, Universidade de Lisboa, Av. Rovisco Pais, 1049-001 Lisboa, Portugal.

[d]CIIEM, Instituto Superior de Ciências da Saúde Egas Moniz, Campus Universitário, Quinta da Granja, Monte de Caparica, 2829-511 Caparica, Portugal.

USC
UNIVERSIDADE DE SANTIAGO DE COMPOSTELA

USC
UNIVERSIDADE
DE SANTIAGO
DE COMPOSTELA

4. RESVERATROL-LOADED HYDROGEL CONTACT LENSES WITH ANTIOXIDANT AND ANTIBIOFILM PERFORMANCE

4.1 INTRODUCTION

The surfaces of contact lenses (CLs) and intraocular lenses (IOLs) are quite prone to the formation of bacterial biofilms, which may cause severe infections in the ocular structures [Fleiszig et al., 2020; Wiley et al., 2012]. Although CL materials have undergone a profound evolution over the last few years, the incidence of microbial-related ocular diseases has not decreased [Dutta and Willcox, 2014]. Approximately 4.2 out of 10,000 CL wearers suffer from microbial keratitis, mainly caused by bacteria (>90%) [Arshad et al., 2019]. CL wearing continues to be the most relevant risk factor for the development of microbial keratitis, although not all CLs are the same in terms of being prone to bacterial growth [Fleiszig et al., 2020; Wiley et al., 2012; Bispo et al., 2015; El-Ganiny et al., 2017]. The risk increases in the following order: daily wear rigid gas permeable CLs < daily wear soft CLs < extended (overnight) wear CLs [Fleiszig et al., 2020, Bispo et al., 2015; Robertson, 2013]. Bacteria can come into contact with the eye through the fingers when inserting and removing the lens or through the CL itself if the care solutions or storage cases are contaminated [Fleiszig et al., 2020]. Once the CL is inserted into

USC UNIVERSIDADE DE SANTIAGO DE COMPOSTELA

the eye, proteins and other tear components adsorb onto its surface, which facilitates the adhesion of bacteria. Bacterial biofilms grown on CLs play a crucial role in keratitis disease, being generally associated with the Gram-negative *Pseudomonas aeruginosa* and the Gram-positive *Staphylococcus aureus* [Fleiszig et al., 2020; Wiley et al., 2012; Dutta and Willcox, 2014; El-Ganiny et al., 2017]. Ocular biofilms can remain on the CL surface for long periods of time, regularly releasing planktonic cells and bacterial products such as endotoxins that can damage the corneal epithelium and induce other ophthalmic diseases, such as dry eye [Wiley et al., 2012; Zegans et al., 2005]. CLs do not only support biofilm formation but also interfere with the normal host defense mechanisms, such as tearing and blinking, and modify the corneal epithelium, facilitating the adhesion and colonization by opportunistic bacteria [Wiley et al., 2012; Bispo et al., 2015; Robertson, 2013]. Once bacteria adhere to the injured corneal epithelium, microbial keratitis can progress [Fleiszig et al., 2020].

Biofilm formation is also a problem for the safety of IOLs. After placement of an IOL in cataract surgery, patients may develop endophthalmitis, a serious form of intraocular inflammation caused by the introduction of a microbial pathogen in the posterior segment of the eye [Bispo et al., 2015; Filipe et al., 2019]. The process starts with the contamination of IOLs with bacteria that can be present in the conjunctiva (e.g., *S. epidermidis*, *S. aureus* or *P. aeruginosa*) during insertion and their subsequent transport from the ocular surface to the posterior chamber. The relatively static environment of vitreous humor favors the development of the biofilm and the associated infection [Bispo et al., 2015]. Overall, although CLs and IOLs have shown great success in improving vision problems, the incidence of eye infections associated with these devices represents a significant

USC UNIVERSIDADE DE SANTIAGO DE COMPOSTELA

concern regarding their use. Hence, the development of new lenses with antibiofilm substances in their composition is receiving increasing attention [Dutta and Willcox, 2014; Khan an Lee, 2020].

Consequently, 2-Methacryloyloxyethyl phosphorylcholine (MPC) **(Figure 4.1)** has been explored to endow polymeric networks with improved biocompatibility and protein-resistant surfaces [Wang and Li, 2011; Wang et al., 2017; Tan et al., 2017; Li and Xin, 2011; Shimizu eet al., 2010; Zhang et al., 2016]. MPC is highly hydrophilic and its bioinspired phosphorylcholine group resembles the phospholipid headgroups present in the cell membrane. In this regard, CLs made of copolymers of 2-hydroxyethyl methacrylate (HEMA) and MPC, commercially available as Proclear®, claim to remain wet for prolonged periods of time and thus to provide improved comfort to the wearers [Goda and Ishihara, 2006]. Surface grafting of MPC has been shown to enhance the ocular tolerance of hydrophobic acrylic IOLs [Tan et al., 2017] and silicone IOLs [Huang et al., 2010]. Furthermore, antifouling coatings based on MPC may provide biomaterials with higher wettability and lower protein adsorption [Xu et al., 2014] and have been shown to be useful to prevent the adhesion of bacteria due to the formation of highly hydrated, flexible interfaces that avoid the deposition of conditioning substances [Huang et al., 2007].

In parallel to the design of surfaces that may prevent the adhesion of bacteria, the incorporation into the lenses of natural compounds that can act as biofilm inhibitors is gaining attention. In this regard, resveratrol (trans-3,5,4′-trihydroxystilbene) **(Figure 4.1)**, which is a natural antioxidant polyphenol [Bsotanghadiri et al., 2017] with good ocular tolerance [Natesan et al., 2017; Dinte et al., 2020], has been reported to interfere in vitro with the bacterial communication process known as *Quorum Sensing* (QS) and to inhibit biofilm formation by

USC UNIVERSIDADE DE SANTIAGO DE COMPOSTELA

clinically relevant bacteria such as *S. aureus*, *P. aeruginosa* and *Vibrio cholerae* [Augustine et al., 2014; Qin et al., 2014; Vasavi et al., 2017; Zhou et al., 2018]. The interference in QS processes may increase the susceptibility to antibiotics and downregulate natural, industrial and clinical biofilms [Richter et al., 2017; Muras et al., 2020]. Resveratrol is also believed to cause bacterial growth inhibition due to a combination of mechanisms involving membrane damage and inhibition of ATP synthase and efflux pumps, which facilitates the intracellular accumulation of other antimicrobial substances [Subramanian et al., 2014; Nohr-Meldgaard et al., 2018]. The minimum inhibitory concentration (MIC) of resveratrol for the Gram-positive *S. aureus*, *Streptococcus pyogenes* and *Enterococcus faecalis* was reported to be between 100 and 200 µg/mL; meanwhile, Gram-negative bacteria such as *P. aeruginosa*, *E. coli* or *Klebsiella pneumoniae* showed lower susceptibility to resveratrol [Paulo et al., 2010].

This work relies on the hypothesis that the design of hydrogels containing MPC moieties and incorporating resveratrol may exhibit a synergism in terms of the prevention of biofilm formation on CLs, while resveratrol may also lead to other beneficial effects related to its antioxidant capability. Some eye diseases caused by oxidative stress mechanisms, such as age-related macular degeneration, cataracts and glaucoma, may be treated or prevented with antioxidants [Dinte et al., 2020; Bhatt et al., 2020]. To the best of our knowledge, loading of resveratrol in CLs has not been tested before. Thus, the aim of this work was to prepare hydrogel CLs and silicone hydrogel CLs containing MPC and loaded with resveratrol to decrease the incidence of ocular infections and manage some eye diseases caused by oxidative stress mechanisms. To carry out the work, hydrogels were prepared covering a wide range of MPC ratios and then the loading

USC UNIVERSIDADE DE SANTIAGO DE COMPOSTELA

and release profiles of resveratrol were evaluated. An extensive characterization of the materials, comprising the evaluation of their protein adsorption and antibiofilm and antioxidant capabilities, was performed. Commercially available Proclear® 1 day CLs were used as a control for comparison purposes.

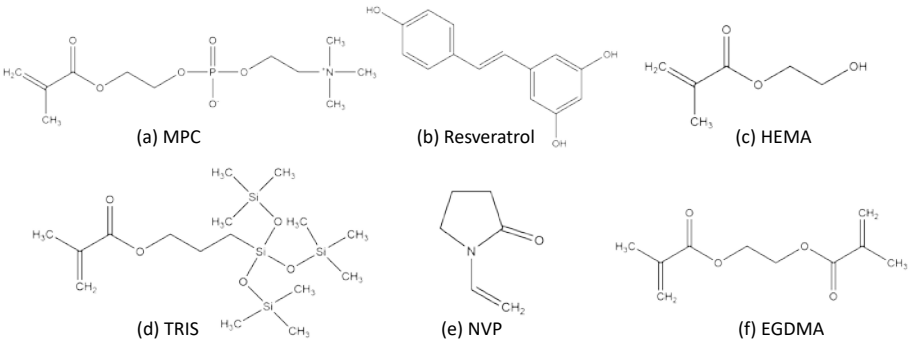


Figure 4.1. Chemical structure of (a) 2-methacryloyloxyethyl phosphorylcholine (MPC), (b) *trans*-resveratrol, (c) 2-hydroxyethyl methacrylate (HEMA), (d) 3-(methacryloyloxy)propyltris(trimethylsiloxy)silane (TRIS), (e) *N*-vinylpyrrolidone (NVP) and (f) ethylene glycol dimethacrylate (EGDMA).

4.2 MATERIALS AND METHODS

4.2.1 Materials

Firstly, 3-(Methacryloyloxy)propyltris(trimethylsiloxy)silane (TRIS) was from Alfa Aesar by Thermo Fisher (Kandel, Germany); 2-Hydroxyethyl methacrylate (HEMA), (3-(4,5-dimethylthiazol-2-yl)-2,5-diphenyltetrazolium bromide) (MTT), calcium chloride dihydrate ($CaCl_2 \cdot 2H_2O$) and sodium dihydrogen phosphate monohydrate ($NaH_2PO_4 \cdot H_2O$) were from Merck KGaA (Darmstadt, Germany); 2-Methacryloyloxyethyl phosphorylcholine (MPC), 1-vinyl-2-

USC UNIVERSIDADE DE SANTIAGO DE COMPOSTELA

pyrrolidinone, ethylene glycol dimethacrylate (EGDMA), dichlorodimethylsilane, 2,2′-azobis(2-methylpropionitrile) (AIBN), 2,2-diphenyl-1-picrylhydrazyl and lysozyme from chicken egg white were from Sigma-Aldrich (St. Louis, MO, USA). Resveratrol was from ChemCruz, Santa Cruz Biotechnology Inc. (Dallas, Texas). Albumin bovine fraction V standard grade (pH 7) was from SERVA Electrophoresis GmbH (Heidelberg, Germany). Di-sodium hydrogen phosphate anhydrous (Na_2HPO_4), magnesium chloride 6-hydrate ($MgCl_2 \cdot 6H_2O$) and potassium di-hydrogen phosphate (KH_2PO_4) were from PanReac Química S.L.U. (Barcelona, Spain). Sodium bicarbonate ($NaHCO_3$) was from Probus S.A. (Barcelona, Spain). Potassium chloride (KCl), sodium chloride (NaCl) and calcium chloride anhydrous ($CaCl_2$) were from Scharlab S.L. (Barcelona, Spain). Ethanol absolute 99.9% and sodium hydroxide (NaOH) were from VWR Chemicals (Fontenary-Sous-Bois, France). Bacto™ tryptone and bacto™ yeast extract were from Becton, Dickinson and Company (Le Pont de Claix, France) and tryptic soy broth (TSB) was from Oxoid S.A. (Madrid, Spain). Ultrapure water (resistivity >18.2 MΩ·cm) was obtained by reverse osmosis (MilliQ®, Millipore Ibérica, Madrid, Spain). Phosphate-buffered saline (PBS) medium was prepared with 8 g of NaCl, 0.3 g of KCl, 0.73 g of Na_2HPO_4 and 0.2 g of KH_2PO_4 for 1 L with pH 6.5. Carbonate buffer was prepared with 1.24 g of NaCl, 0.071 g of KCl, 0.02 g of $NaH_2PO_4 \cdot H_2O$, 0.49 g of $NaHCO_3$, 0.023 g of $CaCl_2$ and 0.031 g of $MgCl_2 \cdot 6H_2O$ for 200 mL with pH 7.2. Simulated lachrymal fluid (SLF) was prepared with the following composition: 6.78 g/L NaCl, 2.18 g/L $NaHCO_3$, 1.38 g/L KCl and 0.084 g/L $CaCl_2 \cdot 2H_2O$ with pH 7.5 [Alvarez-Rivera et al., 2019]. Proclear® 1 day CLs (Omafilcon A, CooperVision®, USA), diopter -3.00, water content 60%, Dk/t 28, were acquired from a local optical store.

USC
UNIVERSIDADE DE SANTIAGO DE COMPOSTELA

4.2.2 Hydrogel synthesis

Different monomer solutions **(Table 4.1)** were prepared at room temperature under magnetic stirring (400 rpm). EGDMA was used as crosslinker and AIBN as initiator. The monomer solutions were injected (25 G needle) into molds made of presilanized glass plates (12 × 14 cm) fixed with 0.30 mm Teflon frame (silicone-hydrogels) or 0.45 mm silicone frame (HEMA-hydrogels). The polymerization was carried out at 50 °C for 12 h and at 70 °C for other 24 h.

Table 4.1. Hydrogels composition.

Hydrogel	Code	MPC (mg)	TRIS (mL)	NVP (mL)	HEMA (mL)	EGDMA (µL)	AIBN (mg)
Silicone	S1	0	1.58	2.50	0.92	32	12.50
	S2	14.76	1.58	2.50	0.92	32	12.50
	S3	29.52	1.58	2.50	0.92	32	12.50
	S4	44.29	1.58	2.50	0.92	32	12.50
	S5	118.1	1.58	2.50	0.92	32	12.50
	S6	150.0	1.58	2.50	0.92	32	12.50
HEMA	H1	0	-	-	4	6.04	6.57
	H2	11.81	-	-	4	6.04	6.57
	H3	23.62	-	-	4	6.04	6.57
	H4	35.43	-	-	4	6.04	6.57
	H5	70.90	-	-	4	6.04	6.57
	H6	120.0	-	-	4	6.04	6.57

After polymerization, hydrogel sheets were demolded by injecting a small amount of water into the molds with a syringe, washed in 1 L of boiling distilled water for 15 min to remove unreacted monomers and cut with punches into different sizes according to the needs of each test. Hydrogel pieces were washed in MilliQ® water (1 L) at room temperature, replacing the medium two or three times per day

USC UNIVERSIDADE DE SANTIAGO DE COMPOSTELA

until the complete removal of unreacted monomers, which was confirmed by measuring the absorbance of aliquots of the washing medium (UV-Vis spectrophotometer Agilent 8453, Germany), and dried at 70 °C for 24 h. Proclear® 1 day CLs were washed using the same procedure and dried at 40 °C for 2 h and 70 °C for a further 2 h. Some hydrogel pieces were directly freeze-dried and scanning electron microscopy (SEM) images of their surfaces were recorded (FESEM Zeiss Ultra Plus, Germany).

4.2.3 Water uptake

Dry Proclear® 1 day CLs and discs of each hydrogel (10 mm diameter) were weighed and placed into Falcon® tubes with 5 mL of water, SLF or resveratrol solution (100 µg/mL in ethanol:water 10:90 *v/v*) at room temperature. Three replicates were tested. At preset times (each hour during the first 8 h and then every 24 h for 5 days), the discs were weighed after carefully wiping their surfaces with absorbent paper to remove excess water. The increase in weight was recorded to calculate the water uptake as a percentage using the following equation (4.1).

$$Water\ uptake\ (\%) = \frac{W_t - W_0}{W_0} \times 100 \qquad \text{Eq. (4.1)}$$

In this equation, W_0 and W_t represent the weight of dry hydrogel and swollen hydrogel at time t, respectively.

4.2.4 Transmittance

The light transmittance (%) of swollen hydrogel discs and Proclear® 1 day CLs was recorded using a UV-Vis spectrophotometer

USC UNIVERSIDADE DE SANTIAGO DE COMPOSTELA

(Agilent Cary 60 UV-Vis, Waldbronn, Germany) from 200 to 700 nm with 1 nm intervals. All the measurements were carried out at least in triplicate after swelling in water, SLF and resveratrol solution (100 µg/mL in ethanol:water 10:90 *v/v*).

4.2.5 Wettability

The wettability of the hydrogels was determined by the captive bubble method, following a methodology described previously [Sanchez et al., 2020]. Hydrogel discs (10 mm in diameter) were hydrated in 5 mL of water for at least 24 h. Then, the discs were placed horizontally in a measuring cell filled with water. Air bubbles (3–4 µL) were formed and released underneath the inferior surface of the discs, using a micrometer syringe with an end-curved needle. The bubbles adhered to the hydrogel surface and the water contact angle was measured as the angle formed between the hydrogel surface and the tangent to the bubble at the triple point where water/air/hydrogel coexists **(Figure 4.2)**. Images were taken at set time intervals for 1 min using a video camera (JAI CV-A50, Copenhagen, Denmark) mounted on an optical microscope (Wild M3Z, Leica Microsystems, Jena, Germany) and connected to a frame grabber (Data Translation DT3155, Measuring Computing Corp., Norton, MA, USA). The acquisition and analysis of the images were performed using the ADSA-P software (Axisymmetric Drop Shape Analysis Profile; Applied Surface Thermodynamics Research Associates, Toronto, Canada). Three discs were used for each formulation, and eight to ten bubbles were created for each disc; in total, there were 30 bubbles per formulation.

USC UNIVERSIDADE DE SANTIAGO DE COMPOSTELA

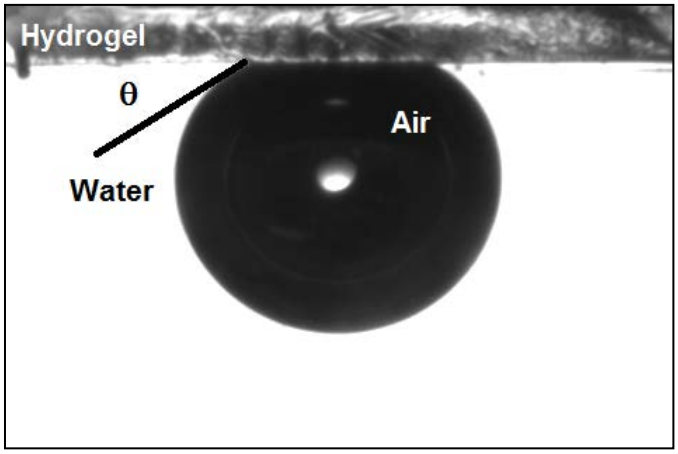


Figure 4.2. Image of a bubble adhered to a hydrogel contact lens when the captive bubble method was used for the measurement of the water contact angle (θ).

4.2.6 Mechanical properties

HEMA- and silicone-hydrogel-hydrated (in water) strips (16 × 9 mm) were fixed at room temperature to the upper and lower clamps (gap 7 mm) of a TA.XT Plus Texture Analyzer (Stable Micro Systems, Ltd., UK) fitted with a 5 Kg load cell. Stress–strain plots were recorded at a crosshead speed of 0.1 mm·s^{-1} at least in triplicate. Young's modulus was calculated from the slope of the linear portion of the stress versus strain curves. The Young's modulus of Proclear® 1 day CLs was also evaluated.

4.2.7 Resveratrol loading and release tests

HEMA-hydrogel-dried discs (37 °C, 24 h) with 10 mm diameter (average weight 39 mg), silicone-hydrogel-dried discs (37 °C, 24 h) with 10 mm diameter (average weight 13 mg) and Proclear® 1 day

USC UNIVERSIDADE DE SANTIAGO DE COMPOSTELA

dried CLs (37 °C, 24 h) with 14.2 mm diameter (average weight 13 mg) were placed, in separate Falcon® tubes with 7 mL of resveratrol in ethanol:water 10:90 *v/v* solution (100 µg/mL). Then, they were placed in an Incubating Mini Shaker (VWR) at 36 °C and 180 rpm protected from light. The test was carried out in quadruplicate.

The absorbance of the loading solution was monitored at 305 nm (UV–Vis spectrophotometer Agilent 8534, Germany) by taking aliquots of 250 µL for the first 8 h and aliquots of 500 µL for subsequent measurements (the liquid removed was not replaced with fresh solution). The aliquots were leveled to 5 mL with ethanol:water 10:90 *v/v* before absorbance measurement. The amount of resveratrol loaded was calculated from the difference between the initial and the final amount of drug in the solution using a validated calibration curve obtained in ethanol:water 10:90 *v/v* and considering the amount of resveratrol lost in the monitoring. A loading test was also carried out for 72 h without intermediate measurements. The network/water partition coefficient ($K_{N/W}$) was calculated as the difference between the total amount loaded and the amount that could be hosted in the aqueous phase (using the water uptake values) and divided by the concentration of resveratrol in the loading solution [Alvarez-Rivera et al., 2019].

Release experiments were carried out by placing resveratrol-loaded discs (previously rinsed with NaCl 0.9%) in Falcon® tubes with 6 mL of NaCl 0.9%. The tubes were kept in an Incubating Mini Shaker (VWR) at 36 °C and 180 rpm protected from light. The test was carried out in quadruplicate. Samples of the medium were taken every hour in the first 8 h of the experiment, and the absorbance was measured at 305 nm using a UV–Vis spectrophotometer (Agilent 8534, Germany). The samples were immediately returned to the corresponding vial, except for HEMA hydrogels and Proclear® 1 day

USC UNIVERSIDADE DE SANTIAGO DE COMPOSTELA

CLs. For these hydrogels, aliquots (1 mL) of the release medium sampled in the 3 to 8 h interval were replaced with the same volume of NaCl 0.9% fresh solution. Once the 8 h time point samples were measured, the release medium in all tubes was increased to 12 mL with the addition of 6 mL of NaCl 0.9% fresh solution. Therefore, from this time point (8 h) until 25 h was reached, the volume of the release medium was 12 mL. At 25 h, HEMA hydrogels and Proclear® 1 day CLs were transferred to new Falcon® tubes containing 12 mL of NaCl 0.9% fresh solution, and the test proceeded for one month. Contrastingly, silicone hydrogels remained in the initial Falcon® tubes since the concentration of resveratrol achieved was quite low. Resveratrol concentration values were calculated from the absorbance at 305 nm using a calibration curve of resveratrol dissolved in NaCl 0.9% solution. The amounts removed and the corresponding dilution of the sample, if needed, were considered to calculate the total amount released.

4.2.8 Resveratrol stability

Since *trans*-resveratrol is highly sensitive to certain light conditions [Zupancic et al., 2015], stability during storage under dark and once exposed to various light conditions was investigated. First, solutions of resveratrol in ethanol:water 10:90 *v/v* (5 µg/mL) and NaCl 0.9% (6 µg/mL) were placed into Falcon® tubes (36 °C, 180 rpm) for 24 h and 20 days, respectively, protected from light, and the UV–Vis spectra recorded at preset times (UV–Vis spectrophotometer Agilent 8534, Germany). The stability of resveratrol in ethanol:water 10:90 *v/v* (5 µg/mL) against white light (HITACHI 8 W F8T5 daylight, Japan) (14 cm gap from the lamp) and the light in the working area of the laboratory was also evaluated for 24 h by monitoring the UV–Vis

USC UNIVERSIDADE DE SANTIAGO DE COMPOSTELA

spectrum. To evaluate the capacity of the hydrogels to protect resveratrol from light degradation, resveratrol-loaded HEMA- and silicone-based hydrogels (soaked in a 100 µg/mL resveratrol in ethanol:water 10:90 *v/v* solution for 72 h) were placed into empty quartz cells and exposed to white light (HITACHI 8 W F8T5 daylight, Japan) for 3 h (14 cm gap from the lamp) at room temperature. The amount of resveratrol loaded and released was monitored, following the same procedure as described above.

4.2.9 *Ex vivo* corneal and scleral permeability tests

Resveratrol corneal and scleral permeability tests were carried out, in triplicate, according to a previously described protocol [Varela-Garcia et al., 2020] for selected silicone- and HEMA-based hydrogels. The assay was also carried out for resveratrol-loaded Proclear® 1 day CLs and a resveratrol solution (1 mL, 70 µg/mL in ethanol:water 10:90 *v/v*) prepared considering the maximum amount that the hydrogels could release in 6 h (estimated from release tests described in **Section 4.2.7**). Fresh porcine eyes from a local slaughterhouse were transported immersed in PBS in an iced bath. Then, intact scleras and corneas with 2–3 mm of surrounding sclera were isolated with the help of a scalpel and tongs, washed with PBS and fitted into vertical diffusion Franz cells. Donor and receptor chambers were filled with carbonate buffer with a pH of 7.2. The receptor medium (6 mL) was kept at 37 °C under gentle magnetic stirring (400 rpm). After 30 min equilibration, the buffer of the donor chambers was removed and replaced with resveratrol-loaded discs (soaked in 100 µg/mL resveratrol in ethanol:water 10:90 *v/v* solution for 72 h at 36 °C and 180 rpm) immersed in 2 mL of NaCl 0.9%. The area available for permeation was 0.785 cm^2. The donor chambers were covered with

USC UNIVERSIDADE DE SANTIAGO DE COMPOSTELA

parafilm to prevent evaporation and protected from light to avoid resveratrol degradation. At 30 min and then each hour for 6 h, 1 mL of sample was taken from the receptor chamber and replaced with the same volume of carbonate buffer with a pH of 7.2, taking care to remove any bubbles from the diffusion cells.

The amount of resveratrol permeated was quantified using a JASCO (Tokyo, Japan) HPLC (AS-4140 Autosampler, PU-4180 Pump, LC-NetII/ADC Interface Box, CO-4060 Column Oven, MD-4010 Photodiode Array Detector), fitted with a C18 column (Waters Symmetry C18, 5 µm, 4.6 × 250 mm) and operated with ChromNAV software (ver. 2.2.8.5, JASCO, Tokyo, Japan). The analysis was done by isocratic elution with a mobile phase of water:methanol (50:50) at 1 mL/min, at 35 °C and with a run time of 8 min. The injection volume was 50 µL and the UV detector was set at 305 nm. Retention time was 4.6 min. The method was validated using two different calibration curves of resveratrol in methanol:water 50:50 *v/v*, one in the 0.05–2 µg/mL range and other in the 1–6 µg/mL range. The detection and quantification limits were calculated from the first calibration curve to be 0.007 and 0.016 µg/mL, respectively. This low-range calibration curve included many points for the precise and accurate quantification of resveratrol in the diluted samples.

After 6 h of assay, aliquots of the donor chambers were collected to quantify the amount of resveratrol remnant. The corneas and scleras were visually inspected to verify that none of them had cracks or modifications and then placed in Falcon® tubes with 3 mL of ethanol:water (50:50 *v/v*) medium at 37 °C under agitation. After 24 h, they were sonicated for 99 min at 37 °C, centrifuged (1000 rpm, 5 min, 25 °C), and the supernatant was filtered (Scharlau® Syringe Filter, 0.22 µm 13 mm PTFE hydrophilic), centrifuged again (14,000

USC UNIVERSIDADE DE SANTIAGO DE COMPOSTELA

rpm, 20 min, 25 °C) and filtered again to be analyzed by HPLC, as described above.

4.2.10 HET-CAM test

The Hen's Egg Test on the Chorioallantoic Membrane (HET-CAM) assay was carried out using fertilized hens' eggs (50–60 g, Coren, Spain) after incubation in a climatic chamber (Ineltec CC SR 0150, Barcelona, Spain), as previously described [Alvarez-Rivera et al., 2016]. On the ninth day, a circular cut of 1 cm in diameter was made on the wider extreme to remove the eggshell. The inner membrane was wetted and removed, and resveratrol-loaded hydrogel discs (as explained above) were placed on the CAM. Solutions of 0.1 N NaOH and 0.9% NaCl (300 µL) were used as positive and negative control, respectively. The vessels of CAM were observed for 5 min and the time at which hemorrhage (vessels bleeding), vascular lysis (vessels disintegration) or coagulation (denaturalization of intra and extravascular proteins) appeared was recorded. The irritation score (IS) was calculated as previously reported [ICCVAM, 2010].

4.2.11 Protein adsorption

A quartz crystal microbalance with dissipation (QCM-D, E4 from Q-Sense, Sweden) was used to study the adsorption of albumin and lysozyme onto selected silicone- and HEMA-based hydrogels **(Table 4.1)**. As previously described [Silva et al., 2016], gold-coated quartz crystals (5 MHz) were treated with UV–ozone for 15 min, rinsed with water and dried with nitrogen. The crystals were coated with a layer of polystyrene (20 µL, 2% wt in toluene) by spin coating (2000 rpm, 30 s) and 20 µL of the correspondent silicone–monomer mixture was

USC UNIVERSIDADE DE SANTIAGO DE COMPOSTELA

deposited over this layer by spin coating (5000 rpm, 30 s). The polystyrene film was only applied for silicone-based mixtures since the direct adhesion of these onto the gold surface was poor. For HEMA-based mixtures, the deposition could be done directly on the gold-coated quartz crystals. In both cases, the polymerization was then carried out at 50 °C for 30 min and 70 °C for 1 h [Teichroeb et al., 2008].

The crystals were mounted on the QCM-D cells and the experimental baselines were obtained with the hydrogel films pre-hydrated in SLF. Normalized frequency (Δf/n, where *n* corresponds to the number of the harmonic) and dissipation (ΔD) changes for the 1st, 3rd, 5th, 7th, 9th and 11th harmonics were registered throughout the experiments. Protein solutions (albumin 0.05 mg/mL in SLF and lysozyme 1.9 mg/mL in SLF) were added and remained for approximately 2.5 h in contact with the crystals. A final rinsing was done with SLF and the monitored signals were left to stabilize for 20 min. The experiments were carried out in quadruplicate at 36 °C. After each assay, the crystals were retrieved by dipping for 5 s in piranha solution (H_2SO_4:H_2O_2, 7:3 *v/v*), followed by washing in a 2% (*v/v*) Hellmanex solution and washing two times in DD water under ultrasound for 15 min each. Finally, the crystals were dried using nitrogen flux and stored.

4.2.12 Antibiofilm properties

Silicone and HEMA hydrogels (1, 4, 5 and 6) and Proclear® 1 day CLs were tested in triplicate for 6 h of growth against *P. aeruginosa* and 48 h of growth against *S. aureus*. Bacterial biofilms were grown on hydrated hydrogel pieces immersed in culture medium using a modified Amsterdam Active Attachment (AAA) model [Mayer et al.,

USC UNIVERSIDADE DE SANTIAGO DE COMPOSTELA

2018] assembled with the tested materials **(Figure 4.3)**. Both non-loaded and resveratrol-loaded hydrogels were tested. As controls, bacteria growth on glass coverslips was monitored both in the absence and in the presence of resveratrol in the culture medium. For this, resveratrol solutions in ethanol:water 10:90 *v/v* previously filtered (Biofil® Syringe Filter, 0.22 µm PES membrane) were added to Luria–Bertani Broth (LB) for *P. aeruginosa* (4, 12 and 250 µg/mL resveratrol final concentration) and Tryptic Soy Broth (TSB-1) for *S. aureus* (5, 17 and 250 µg/mL resveratrol final concentration). In any case, the growth medium was diluted less than 5% with the resveratrol solution.

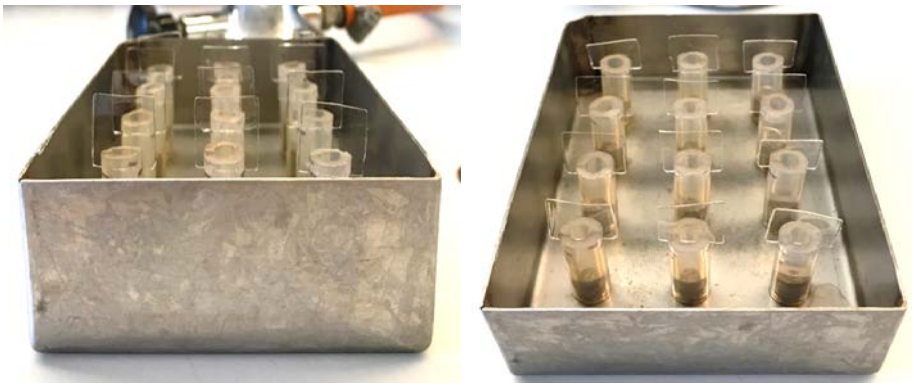


Figure 4.3. Amsterdam Active Attachment (AAA) model assembled with the tested hydrogels pieces.

4.2.12.1 Bacterial strains and growth conditions

S. aureus ATCC25923 (ATCC, Manassas, VA, USA) and *P. aeruginosa* PAO1 (Lausanne sub-line, donated by M. Cámara, Univ. of Nottingham, Nottingham, UK) biofilm-forming bacteria were routinely cultured at 37 °C in TSB-1 and LB, respectively. TSB-1 (15

USC UNIVERSIDADE DE SANTIAGO DE COMPOSTELA

g of TSB and 2.5 g of NaCl for 500 mL) and LB (5 g of tryptone, 2.5 g of yeast extract and 5 g of NaCl for 500 mL) media were prepared in distilled water. Both culture media were magnetically stirred at 200 rpm until complete dissolution and then autoclaved (121 °C, 1 atm, 15 min) to avoid contamination.

4.2.12.2 Pre-inocula and inocula preparion

Pre-inocula were prepared by inoculating sterile Erlenmeyer flasks containing culture medium (10 mL) with a colony of a 24 h plate of the corresponding biofilm-forming bacterial pathogen. The flasks were incubated at 37 °C for 12 h (*P. aeruginosa*) or 24 h (*S. aureus*) at 100 rpm. For inocula preparation, the optical density of the pre-inocula was measured after incubation at 600 nm (UV–Vis spectrophotometer Thermo Scientific Helios Omega) and adjusted to 0.05 (*S. aureus*) or 0.01 (*P. aeruginosa*) by dilution with the corresponding culture medium in sterile Falcon® tubes of 50 mL. The pre-inocula were diluted around 400 and 100-fold for *P. aeruginosa* and *S. aureus*, respectively. Finally, the inocula were gently homogenized and divided among 12-well cell culture plates (4 mL per well). All procedures were performed in a biological safety cabinet.

4.2.12.3 AAA model preparation and incubation

The hydrogels were loaded with resveratrol (as explained above), with the only difference being that they were autoclaved (121 °C, 1 atm, 15 min) and dried for 72 h at 37 °C before soaking in the resveratrol solution (7 mL, 37 °C, 100 rpm). The amount loaded was estimated from the difference between the initial and final amount of resveratrol in the solution, calculated from absorbance measurements performed at 305 nm (as above).

USC
UNIVERSIDADE DE SANTIAGO DE COMPOSTELA

All loaded hydrogel pieces were carefully placed in the silicone supports of special metallic covers previously autoclaved (121 °C, 1 atm, 15 min), using a scalpel and tongs, in a biological safety cabinet. Then, the setup was immersed in the 12-well cell culture plates containing 4 mL of the corresponding culture media and bacteria.

All hydrogels were tested in triplicate and incubated at 37 °C under static conditions for 6 h and 48 h for *P. aeruginosa* and *S. aureus*, respectively. The *S. aureus* medium was changed every 12 h by moving the models to new cell culture plates previously filled with 4 mL of fresh TSB-1 per well. In all cases, after each media exchange period, the absorbance of the culture medium was measured at 600 nm (UV–Vis spectrophotometer Thermo Scientific Helios Omega), to evaluate planktonic bacterial growth. A similar protocol was used to monitor bacteria growth onto glass coverslips when the medium was supplemented with different concentrations of resveratrol.

4.2.12.4 Biofilm susceptibility

After the incubation period at 37 °C, the viability of the bacterial biofilms was evaluated using a modified MTT assay [Vivero-Lopez et al., 2021]. Hydrogel pieces were individually placed in sterile tubes containing 3.6 mL of PBS and then sonicated for 15 min to separate and homogenize the biofilms. Then, MTT solution (5 mg/mL, 400 µL) was added to each tube and the tubes were incubated at 37 °C for 30 min. Half of the MTT-containing PBS medium was removed and replaced with acid isopropanol (5% (*v/v*) 1M HCl in isopropanol). After 5 s vortexing, aliquots of the medium (1 mL) were taken and their absorbance measured at 570 nm (UV–Vis spectrophotometer Thermo Scientific Helios omega). PBS medium treated in the same way was used as blank.

USC UNIVERSIDADE DE SANTIAGO DE COMPOSTELA

4.2.13 Antioxidant properties

The antioxidant activity of resveratrol released from Proclear® 1 day CLs, HEMA and silicone hydrogels was determined using a modified DPPH assay [Gülçin, 2010]. The antioxidant activity was proportional to the disappearance of radical 2,2-diphenyl-1-picrylhydrazyl (DPPH•) in the samples by accepting hydrogen from resveratrol, with the corresponding change in color from purple to yellow and decrease in absorption at 517 nm [Moon et al., 2009]. HEMA- and silicone-hydrogel-dried discs were loaded with resveratrol (as above) and, then, the release was carried out, as described previously, for 12 and 24 h. The antioxidant activities of the loading solution (100 µg/mL in ethanol:water 10:90 *v/v* medium) and the freshly prepared release medium (NaCl 0.9%) were also quantified. Non-loaded hydrogels in NaCl 0.9% were used as controls to confirm that there were no leaching substances that could cause false antioxidant activity during the test. To carry out the test, a 0.1 mM solution of DPPH• in ethanol was freshly prepared and stored in a flask protected from light. Then, an aliquot of each release medium (1 mL) was mixed with 1 mL of DPPH• solution and vortexed for 5 s. After 30 min of incubation in the dark, the absorbance was measured at 517 nm (UV–Vis spectrophotometer Agilent 8534, Germany). The test was carried out at least in triplicate. The DPPH• scavenging capacity was expressed as µg/mL of DPPH in the reaction medium and calculated from a validated calibration curve of DPPH• in ethanol (4–25 µg/mL). The DPPH• scavenging effect (%) was obtained using the following equation (4.2), where A_C is the absorbance at 517 nm of the control and A_S is the absorbance of the test compound.

$$DPPH\ scavenging\ effect\ (\%) = \left(1 - \frac{A_S}{A_C}\right) \times 100 \qquad \text{Eq. (4.2)}$$

USC UNIVERSIDADE DE SANTIAGO DE COMPOSTELA

The results were expressed also as Trolox equivalent antioxidant capacity (TEAC) calculated from a validated calibration curve of Trolox in NaCl 0.9% (5–35 µM), processed in the same way as the samples for comparative purposes.

The antioxidant capacity of a resveratrol solution in ethanol:water 10:90 *v/v* medium after being exposed to white light (HITACHI 8 W F8T5 daylight, Japan) for 3 h (14 cm gap from the lamp) was also tested.

4.2.14 Statistical analysis

The effects of hydrogel composition on swelling, drug loading, permeability through porcine eye tissues and biofilm formation were analyzed using ANOVA and multiple range test (Statgraphics Centurion XVII, StatPoint Technologies Inc., Warrenton VA, USA).

4.3 RESULTS AND DISCUSSION

4.3.1 Hydrogel synthesis

HEMA and silicone hydrogels were designed to combine the features demanded by CLs (water uptake, light transmittance, mechanical properties) while adding antibiofilm capacity, with the aim of attenuating the risk of ocular infections associated with CL wearing [Shimizu et al., 2010; Xu et al., 2014]. Two strategies were followed to endow CLs with antibiofilm features: copolymerization with MPC and loading of resveratrol. To the best of our knowledge, resveratrol-eluting CLs have not been previously investigated, although resveratrol may find applications in the ocular field as an antioxidant, anti-inflammatory, antiangiogenic and anticarcinogenic

USC UNIVERSIDADE DE SANTIAGO DE COMPOSTELA

agent [Bhat et al., 2020; Chen et al., 2019; Lançon et al., 2016]. MPC is a component of one commercially available soft (HEMA-based) CL brand (Proclear®) that claims to retain more water on its surface. MPC is also being tested as a surface component of post-synthesis-modified CLs [Li and Xin, 2011; Shimizu et al., 2010]. In the present study, MPC was added as comonomer during the synthesis of the hydrogels. The highest content in MPC was limited by the compatibility of this hydrophilic monomer with the silicone-based mixture. MPC can make the silicone hydrogels whitish due to the microphase separation of silicone and hydrophilic monomers [Nicolson and Vogt, 2001], which was indeed evident for S5 and S6 hydrogels (as discussed below). Proclear® 1 day CLs are reported to have 3% MPC [Liu, 2011], which is equivalent to 101 mM; therefore, this proportion was chosen as the highest one to be investigated. Hydrogel codes H1, H2, H3, H4, H5 and H6 in **Table 4.1** correspond to 0, 10, 20, 30, 60 and 101 mM MPC; similarly, S1, S2, S3, S4, S5 and S6 correspond to 0, 10, 20, 30, 80 and 101 mM MPC.

4.3.2 Water uptake and wettability

The water uptake **(Table 4.2 and Figure 4.4)** was higher for silicone hydrogels than for HEMA hydrogels despite the hydrophobic character of TRIS. The addition of hydrophilic monomers, mainly NVP [Tran and Yang, 2019; Chien and Kuo, 2019] and, to a lesser extent, MPC [Goda and Ishihara, 2006], explains the greater water uptake of silicone hydrogels. In fact, the designed silicone hydrogels showed a higher water content than that previously recorded for other silicone hydrogels [Nicolson and Vogt, 2001; Tran and Yang, 2019], even with a very similar composition [Paradiso et al., 2014]. The water uptake of HEMA hydrogels was in good agreement with

USC UNIVERSIDADE DE SANTIAGO DE COMPOSTELA

previously reported values [Alvarez-Rivera et al., 2019; dos Santos et al., 2009] and was similar to that obtained for other HEMA hydrogels copolymerized with acrylic acid and 4-vinyl pyridine [Alvarez-Lorenzo et al., 2006]. The amount of water absorbed for both types of hydrogels slightly increased with the addition of MPC. For a given composition, no significant changes in swelling were observed between water and SLF. Contrastingly, the percentage of swelling was statistically higher ($p < 0.05$) for hydrogels immersed in the resveratrol solution in ethanol:water 10:90 medium due to the presence of ethanol [Sekar et al., 2019]. The highest value of water uptake was observed for Proclear® 1 day CLs.

USC UNIVERSIDADE DE SANTIAGO DE COMPOSTELA

Table 4.2. Water uptake at equilibrium and Young's modulus (mean values ± S.D.) for all non-loaded silicone hydrogels (S1–S6) and HEMA hydrogels (H1-H6) immersed in water at room temperature and amounts of resveratrol loaded when the hydrogels were soaked in a resveratrol solution (100 μg/mL) in ethanol:water 10:90 *v/v* medium at 36 °C and 180 rpm for 72 h without intermediate measurements.

Hydrogel code	Water uptake (%)	Young's modulus (MPa)	Resveratrol loaded (μg/mg)
S1	91.9 ± 0.6	2.00 ± 0.07	37.37 ± 0.68
S2	92.2 ± 0.5	2.29 ± 0.17	49.22 ± 1.74
S3	93.2 ± 1.1	2.01 ± 0.37	41.66 ± 0.96
S4	92.4 ± 1.5	2.46 ± 0.09	47.87 ± 0.72
S5	105.8 ± 0.9	2.47 ± 0.09	50.11 ± 2.06
S6	107.3 ± 0.9	2.32 ± 0.21	58.58 ± 4.05
H1	56.4 ± 0.5	0.61 ± 0.03	8.57 ± 0.56
H2	57.4 ± 0.3	0.67 ± 0.01	8.80 ± 0.35
H3	58.4 ± 0.6	0.68 ± 0.04	8.32 ± 0.22
H4	59.2 ± 0.1	0.67 ± 0.05	8.66 ± 0.53
H5	62.6 ± 0.8	0.66 ± 0.01	9.27 ± 0.75
H6	67.6 ± 0.1	0.60 ± 0.01	8.40 ± 0.09
Proclear® 1 day	139.9 ± 2.3	0.44 ± 0.08	13.59 ± 0.36

USC UNIVERSIDADE DE SANTIAGO DE COMPOSTELA

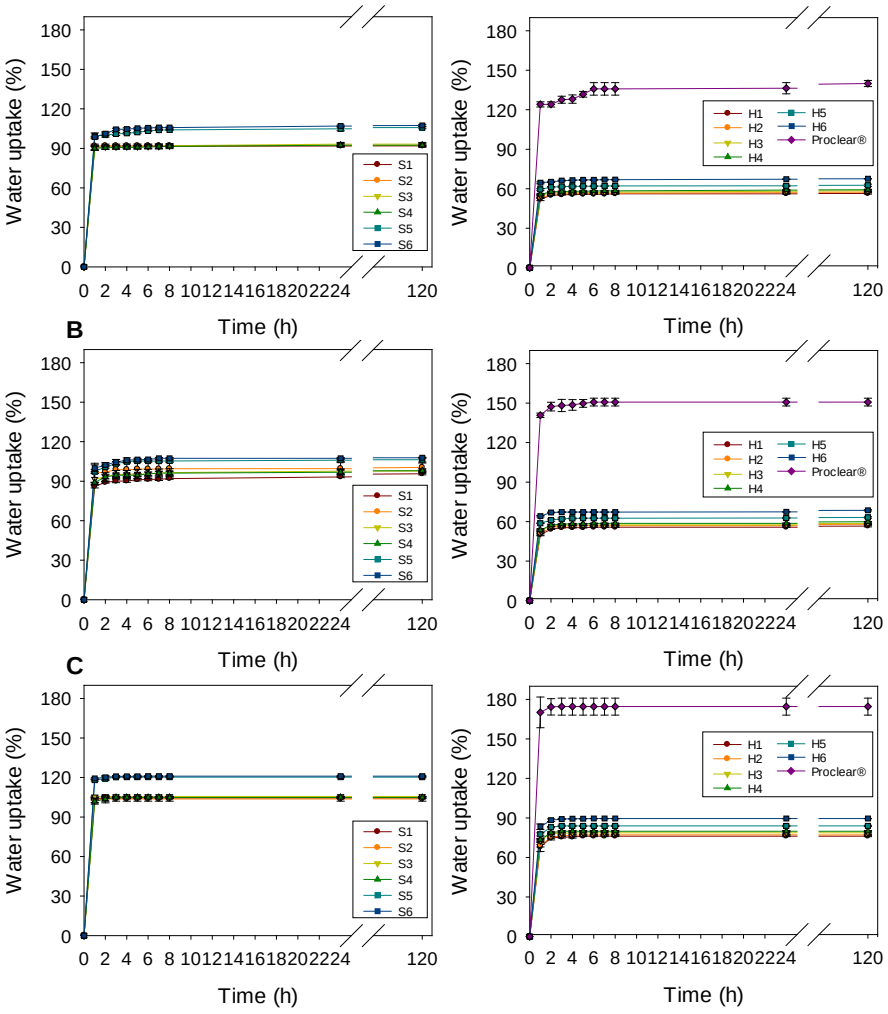


Figure 4.4. Water uptake (%) of silicone (left) and HEMA (right) hydrogels in water (A), SLF (B) and resveratrol loading solution (C)

The hydrogels' surface wettability was determined by measuring the contact angle using the captive bubble method [Sanchez et al., 2020]. Compared to the sessile drop method commonly used to

USC UNIVERSIDADE DE SANTIAGO DE COMPOSTELA

characterize rigid gas permeable CLs, the captive bubble method is particularly advantageous for hydrogel materials that may lose water when exposed to air and may deform (swell) when the drop enters into contact with the surface. The captive bubble method is carried out with hydrogel pieces immersed in water (which prevents changes in swelling degree) and, although the recording of the bubble shape can be time-consuming, the measurements are more reliable [Sanchez et al., 2020]. The contact angle values were very similar for all compositions, in the range of 37° to 41° for HEMA hydrogels and 32° to 46° range for silicone ones **(Figure 4.5).** It is known that in the dry state, silicone-based hydrogels are more hydrophobic than HEMA-based ones, due to the presence of siloxane groups in the former [Paradiso et al., 2014]. However, upon hydration, the silicone-based hydrogel acquired a similar hydrophilicity to HEMA, since, in the presence of water (polar solvent), reorientation of the hydrophilic and hydrophobic groups of the chains may occur: the hydrophobic siloxane groups are mainly hidden, and the hydrophilic functionalities of HEMA and NVP become exposed to the surface. Although the addition of MPC led to higher water uptake values in both types of hydrogel, the measurements of water contact angle did not show a significant effect on surface hydrophilicity. This may be due to the small amount of MPC, whose effect is minor when compared to that induced by the other hydrophilic monomers present in the hydrogel matrix. Other authors found a reduction in the water contact angle with an increase in MPC amount, but for hydrogels with MPC grafted to the surface [Wang and Liu, 2011; Vales et al., 2020] or with much higher amounts of MPC [Chang et al., 2020]. It should be noted that the contact angles obtained for all compositions fell in the range of the values typical of commercial CLs and were similar to the contact

USC
UNIVERSIDADE DE SANTIAGO DE COMPOSTELA

angle reported for Proclear® (47.4 ± 7.5°) [Lin and Svitova, 2010] using the same technique.

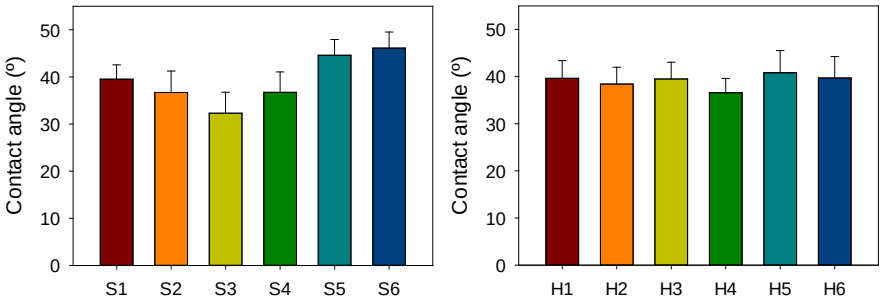


Figure 4.5. Water contact angles on the silicone-based hydrogels (left) and HEMA-based hydrogels (right). The error bars are ± the standard deviations.

4.3.3 Light transmission

Light transmittance of all hydrogel compositions in water, SLF and resveratrol solution (in ethanol:water 10:90 *v/v* medium) showed values above 90% in the visible range (600 nm), except for the S5 and S6 hydrogels, which were slightly opalescent **(Figures 4.6 and 4.7)**. Although all hydrogels had an apparently smooth surface, SEM images of freeze-dried hydrogels recorded at high magnification evidenced the roughness of S5 and S6 hydrogels, showing islet-like patterns typical of microphase separation **(Figure 4.8)** [Shimizu et al., 2010]. S4 images were quite similar to those of S1, which suggests that the low MPC content did not trigger phase separation. No significant differences in light transmittance were observed between hydrogels swollen in water, SLF or resveratrol solution, besides the fact that the loading of resveratrol provided very efficient protection against UV radiation **(Figure 4.6 C1 and C2)**. The beneficious UV

USC UNIVERSIDADE DE SANTIAGO DE COMPOSTELA

filter effect had a nondetrimental impact on the light transmission above 400 nm.

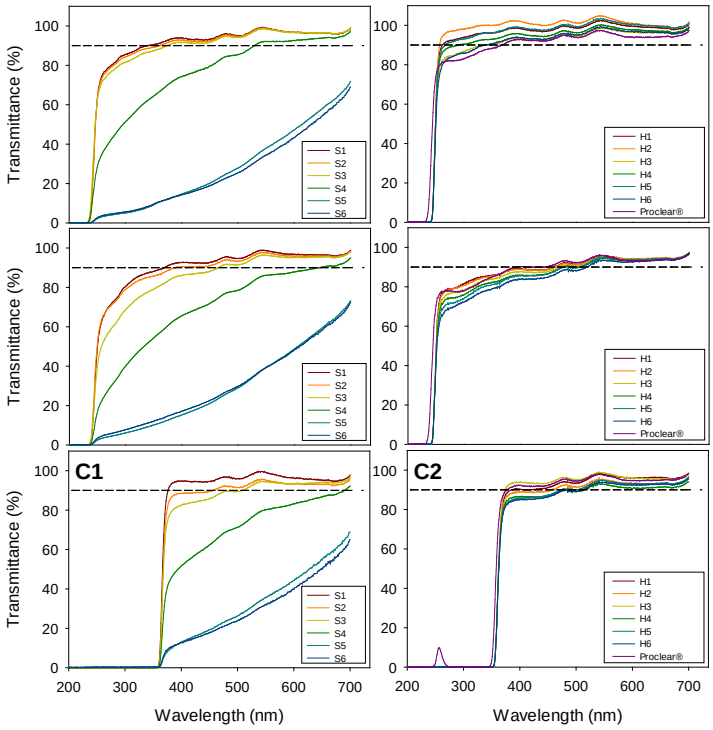


Figure 4.6. Light transmission of silicone (left) and HEMA (right) hydrogels swollen in water (A), SLF (B) and resveratrol loading solution (C). Dashed lines indicate the acceptance value of 90% transmittance.

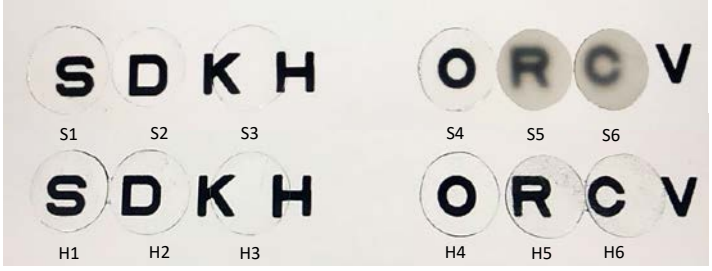


Figure 4.7. Reading test for silicone (up) and HEMA (down) hydrogels.

USC UNIVERSIDADE DE SANTIAGO DE COMPOSTELA

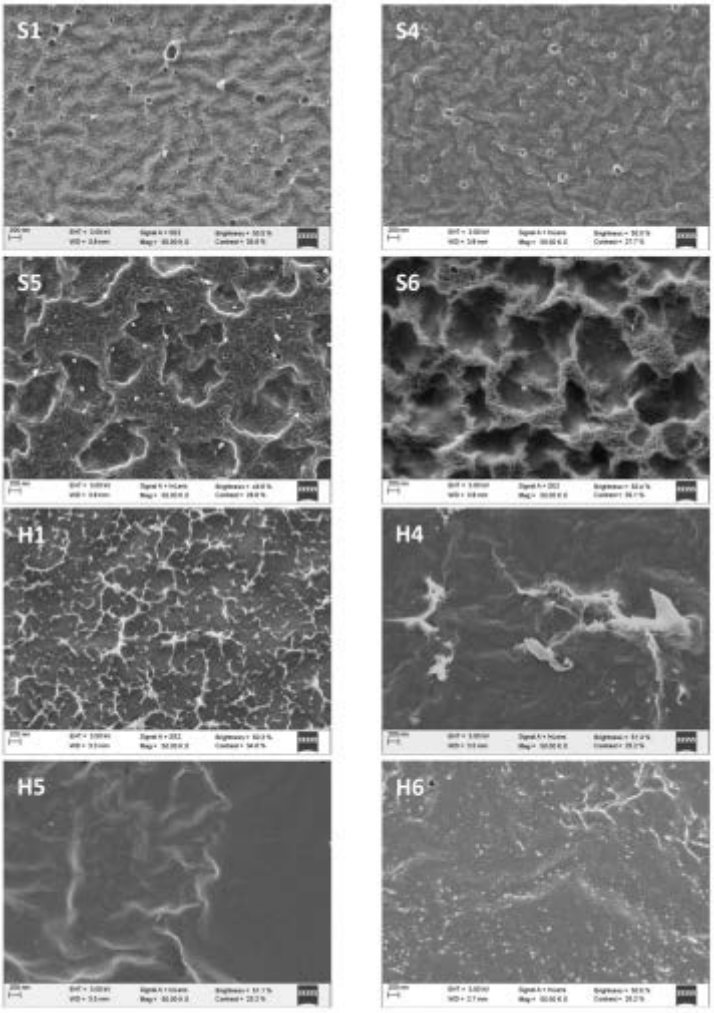


Figure 4.8. SEM images of freeze-dried hydrogels recorded at high magnification (50,000×). The scale bar corresponds to 200 nm.

USC
UNIVERSIDADE DE SANTIAGO DE COMPOSTELA

4.3.4 Mechanical properties

The Young's modulus values of the swollen strips are shown in **Table 4.2** for all hydrogel compositions. Silicone hydrogels had a Young's modulus larger than HEMA hydrogels, in agreement with the behavior reported in the literature [Horst et al., 2012]. The Young's modulus of the HEMA hydrogels was in the range of those typical of soft contact lenses [Chan et al., 2020]. The Young's modulus registered for Proclear® 1 day CLs matched the value of the data sheet (0.4 MPa). The values recorded for the silicone hydrogels were close to the first-generation silicone hydrogels, although it should be noted that, at the eye temperature, the values may be slightly lower [Horst et al., 2012]. Interestingly, MPC at the highest proportion investigated only caused a minor decrease (not statistically significant) in the mechanical properties of the CLs, in contrast to the previously reported decrease in Young's moduli observed for HEMA–MPC networks prepared with larger proportions of MPC [Chang et al., 2020].

4.3.5 Resveratrol loading and release

Resveratrol loading was carried out by soaking the hydrogel discs in a resveratrol solution (100 µg/mL) in ethanol:water 10:90 *v/v* medium until no changes in the absorbance of the loading medium were observed. Loading of the hydrogels during polymerization by the addition of resveratrol to the monomer solution was discarded since the antioxidant power of resveratrol may have hindered the polymerization [Varela-Garcia et al., 2020]. All hydrogels were soaked for at least 3 days, but equilibrium was attained in less than 48 h **(Figure 4.9 A1 and B1)**. Silicone hydrogels captured more than 75% resveratrol initially present in the loading solution (estimated

USC UNIVERSIDADE DE SANTIAGO DE COMPOSTELA

from the difference between resveratrol amount in the loading medium at time 0 and at the end of the test). HEMA hydrogels rapidly sorbed resveratrol, and the final loading corresponded to ~44% resveratrol available. To monitor the loading, aliquots of the medium were taken for subsequent dilution before absorbance measurements. This caused some loss of resveratrol available for loading. Thus, a second loading study was carried out without intermediate measurements for 72 h; the amount loaded by silicone hydrogels corresponded to more than 80% resveratrol initially present in the loading solution and to ~50% for HEMA hydrogels (data shown in **Table 4.2**). Compared to the designed HEMA hydrogels, Proclear® 1 day CLs showed higher loading, as expressed per unit of weight. The greater surface contact area with the Proclear® 1 day CLs (14.2 mm diameter), and the lower thickness (center thickness of 0.09 mm) compared to the HEMA hydrogels (10 mm diameter, 0.45 mm thickness), may have contributed to faster and more efficient loading. Nevertheless, the total amount loaded per CL was lower for Proclear® 1 day CLs than for the other HEMA hydrogel discs due to the lower weight of the CLs.

USC UNIVERSIDADE DE SANTIAGO DE COMPOSTELA

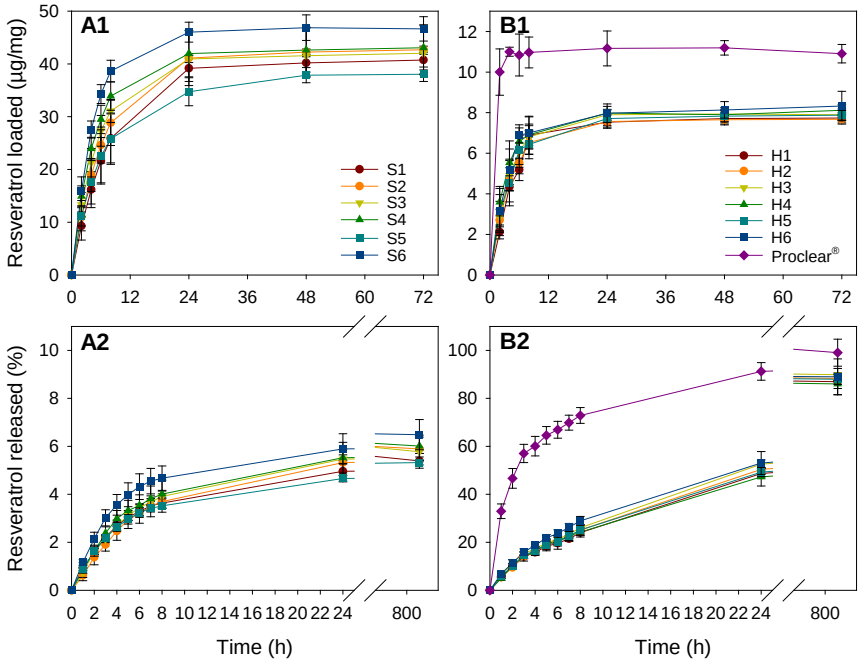


Figure 4.9. Resveratrol loading profiles for silicone (A1) and HEMA (B1)-based hydrogels at 36 °C and 180 rpm for 72 h, and release profiles from silicone (A2) and HEMA (B2)-based hydrogels in NaCl 0.9% medium at 36 °C.

Overall, both types of hydrogel had high affinity for resveratrol, but the network/water partition coefficient for silicone hydrogels ($K_{N/W}$ in the 373 to 492 range) was four/six-fold higher than that recorded for HEMA hydrogels ($K_{N/W}$ in the 77–81 range). Proclear® 1 day CLs had $K_{N/W}$ values (~100) slightly higher than those recorded for HEMA hydrogels. These values are in the range of or even greater than those previously reported for related silicone hydrogels [Pimenta et al., 2016] and HEMA hydrogels [Alvarez-Rivera et al., 2018] in the presence of other active ingredients. In any case, the large $K_{N/W}$ values obtained indicated that resveratrol was loaded not only in the aqueous phase of the hydrogel but also interacting with the network [Varela-

USC UNIVERSIDADE DE SANTIAGO DE COMPOSTELA

Garcia et al., 2020]. No evident effect of MPC addition on resveratrol loading was found.

Resveratrol release profiles from both types of hydrogel were remarkably different **(Figure 4.9 A2 and B2).** The test was carried out in Falcon® tubes with a sufficient volume of liquid in order to avoid saturation (resveratrol solubility in NaCl 0.9% was quantified as 27.4 (s.d. 1.4) μg/mL) and under gentle stirring (180 rpm) in order to avoid pseudo-equilibrium and artifact plateaus. Reliable in vitro release methods for drug-loaded CLs that can serve to predict drug release in vivo are still needed [Tieppo et al., 2014]. Nevertheless, a requirement that any in vitro method must meet is to avoid the occurrence of false balances between the drug remaining in the contact lens and the drug already delivered, leading to delivery rates much slower than would be expected in vivo.

Silicone hydrogels strongly retained resveratrol and released less than 8% of the amount loaded in five weeks. Contrastingly, HEMA hydrogels provided sustained release of 33% load in the first 8 h. The amount of resveratrol released from Proclear® was above 80% in the first 8 h. In comparison with other similar silicone-based hydrogels that were loaded with chlorhexidine, moxifloxacin and diclofenac [Silva et al., 2018], the release was slower, and no burst was recorded. This finding suggests more intense hydrophobic interactions between the silicone network and resveratrol.

The amount of resveratrol released was above the minimum required (2.28 μg/mL) in cell cultures to protect retinal pigment epithelial cells from UVA-induced oxidative damage [Chan et al., 2015] and also to protect retinal pigment epithelial cells against hyperglycemia-induced inflammation and gap junction intercellular communication degradation [Losso et al., 2010]. Thus far, no

USC UNIVERSIDADE DE SANTIAGO DE COMPOSTELA

resveratrol-loaded CLs have been described in the literature for the ophthalmic administration of resveratrol, and most information relies on its topical ocular [Abengózar-Vela et al., 2019] and oral administration through food or dietary supplements [Abu-Amero et al., 2016; Goutham et al., 2017; Wang et al., 2017]. Although the minimum effective concentration of resveratrol needed in the tear fluid for therapeutic effects is unknown, assuming that the concentration reported above (2.28 µg/mL) is sufficient and considering that the volume of tear produced per day is 4.32 mL (i.e., ~3 µL/min), the minimum amount that the CL should supply is 9.84 µg. Assuming that the weight of a common CL is 13 mg, all designed hydrogels can easily provide more resveratrol than the minimum required (9.84/13 = 0.75 µg/mg) after the first 2 h of wearing, according to the release profiles shown in **Figure 4.9**.

Regarding the minor effect of MPC on the resveratrol loading and release results, only formulations prepared without (S1, H1) and with the highest proportions of MPC (S4, S5, S6 and H4, H5 and H6) were considered for subsequent studies.

4.3.6 Resveratrol stability

Since *trans*-resveratrol is quite prone to isomerization and degradation [Zupancic et al., 2015], stability studies were carried out to gain an insight into the feasibility of using resveratrol for topical ophthalmic administration. No changes in the UV–Vis spectra of resveratrol in ethanol:water 10:90 *v/v* medium and in NaCl 0.9% solution were recorded for 24 h and 10 days, respectively, under the loading and release conditions (dark, 36 °C and 180 rpm) **(Figure 4.10 A and B)**. When resveratrol loading solution was exposed to white light for 24 h **(Figure 4.10 C and D)**, the absorbance at 305 nm

USC UNIVERSIDADE DE SANTIAGO DE COMPOSTELA

(maximum for *trans*-resveratrol) decreased, and thus the ratio of absorbance at 286 nm (maximum of *cis*-resveratrol) to absorbance at 305 nm increased, which indicated its transformation into the less active isomer [Silva et al., 2013]. This phenomenon occurred more slowly when the resveratrol solution was exposed to the usual light conditions of the laboratory **(Figure 4.10D).**

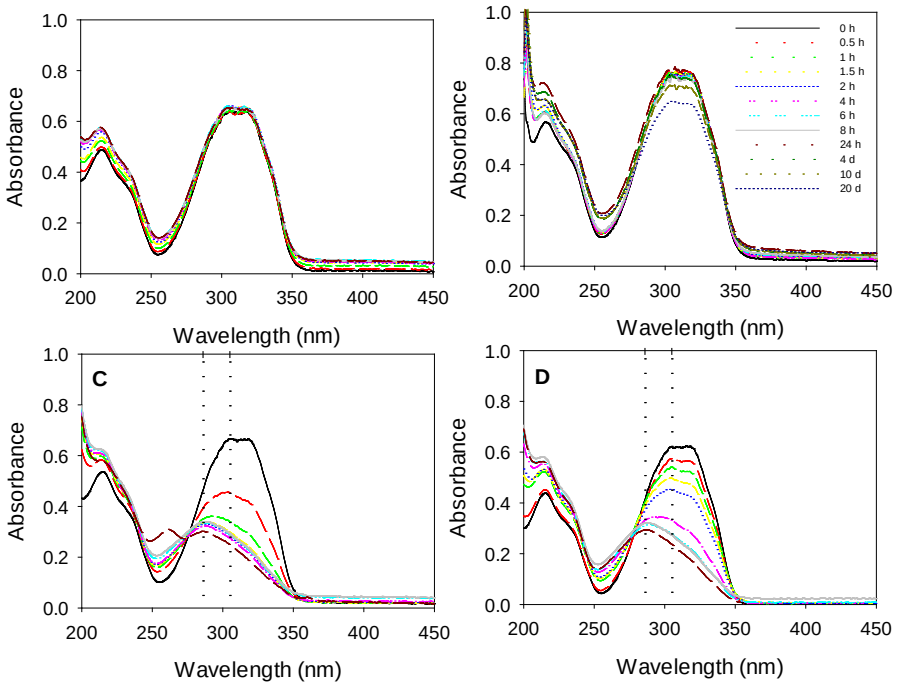


Figure 4.10. UV–Vis spectra recorded for resveratrol in ethanol:water 10:90 *v/v* medium (A) and resveratrol in NaCl 0.9% (B) without light at 36 °C and 180 rpm for 24 h, and resveratrol in ethanol:water 10:90 *v/v* medium exposed to white light (C) and working area light (D) for 24 h. Dashed lines indicate the maximum wavelength of *cis*-resveratrol (286 nm) and *trans*-resveratrol (305 nm).

To investigate whether the hydrogels could protect resveratrol from light degradation, resveratrol-loaded HEMA- and silicone-based hydrogels (by soaking in ethanol:water solution for 72 h as in **Section**

USC UNIVERSIDADE DE SANTIAGO DE COMPOSTELA

4.3.5) were removed from the loading medium and directly placed into empty quartz cells and exposed to a white light lamp (HITACHI 8 W F8T5 daylight, Japan) for 3 h at room temperature. Then, the release profiles were recorded **(Figure 4.11)**; the UV–Vis patterns were very similar, as well as the amounts released, to those recorded for hydrogels that were not exposed to the white light **(Figure 4.9)**. This suggested that the hydrogels could protect resveratrol against photodegradation, as later confirmed by the antioxidant tests **(Section 4.3.10)**.

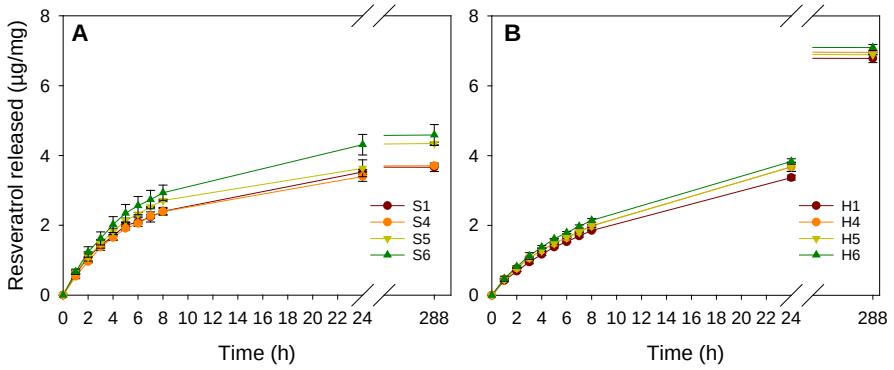


Figure 4.11. Release profiles of resveratrol in NaCl 0.9% from silicone- (A) and HEMA (B)-based hydrogels. After being loaded with resveratrol, the hydrogels were exposed for 3 h to white light. The release profiles were constructed considering the absorbance maximum of *trans*-resveratrol.

4.3.7 Corneal and scleral permeability

The permeability and retention capacity of resveratrol released from the most promising hydrogels and Proclear® 1 day CLs were investigated using porcine eyes, which are the most similar to human eyes considering the globe size, corneal thickness, ratio of globe diameter to corneal length, presence of Bowman's layer, sclera histology and collagen bundle organization [Alambiaga-Caravaca et

USC UNIVERSIDADE DE SANTIAGO DE COMPOSTELA

al., 2020]. As a control, a resveratrol concentrated solution (70 µg/mL in ethanol:water 10:90 *v/v* medium) was used.

Resveratrol crossed neither the cornea nor the sclera, regardless of whether it was released from the hydrogels or directly applied as a concentrated solution. Resveratrol solubility in NaCl 0.9% was measured to be 27.4 (s.d. 1.6) µg/mL and the experimental setup ensured that the receptor chamber was not saturated. Therefore, a sufficient concentration gradient could exist between the donor and the receptor chamber. For example, when the concentrated resveratrol solution was tested, the donor chamber contained 1 mL of 70 µg/mL (in ethanol:water 10:90 *v/v*). Since the volume of receptor medium was 6 mL, if all resveratrol could pass to the receptor (assuming no adsorption to the cornea or sclera), the maximum concentration that could be reached in the receptor would be 10 µg/mL. Therefore, the absence of resveratrol in the receptor chamber cannot be attributed to low solubility in the receptor medium. In the 6 h time frame of the study, measurable amounts of resveratrol in the receptor chamber were not recorded in any case. Contrastingly, resveratrol accumulated in the cornea and sclera tissue **(Figure 4.12)**. Accumulation was higher in the sclera than in the cornea for all formulations. The highest amount accumulated was recorded for the resveratrol solution (24.5 ± 1.2 and 21.6 ± 0.8 µg/cm^2 for sclera and cornea, respectively). This finding clearly correlated with the lower resveratrol levels that the hydrogel formulations can provide to the donor chamber, as shown in **Figure 4.12**. In good agreement with the release profiles shown in **Figure 4.9**, HEMA hydrogels provided more resveratrol to the donor chamber than silicone hydrogels.

Differences in silicone hydrogel composition did not cause any change in the amount of resveratrol accumulated in the cornea or

USC UNIVERSIDADE DE SANTIAGO DE COMPOSTELA

sclera (no statistically significant differences for a given tissue). For H1 and H4 hydrogels, the amount of resveratrol accumulated in the sclera (13.6 ± 1.4 and 13.6 ± 1.1 μg/cm^2) was statistically higher than for H6 and Proclear® (10.1 ± 1.1 and 9.9 ± 1.2 μg/ cm^2). Regarding cornea tests, the amount of resveratrol accumulated was, surprisingly, higher for Proclear® CLs, which may be related to the faster release provided by these CLs. Interestingly, the amounts of resveratrol accumulated in the cornea and sclera once released from HEMA hydrogels were remarkably higher than those previously reported for the antioxidant transferulic acid [Varela-Garcia et al., 2020].

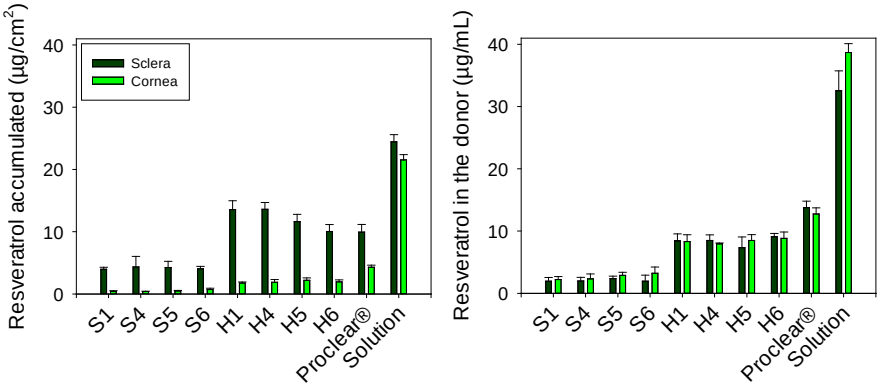


Figure 4.12 Amounts of resveratrol accumulated in cornea and sclera (left) and remaining in the donor chamber (right) when delivered as resveratrol-loaded silicone and HEMA hydrogels, and Proclear® CLs, or as resveratrol solution (70 μg/mL).

4.3.8 HET-CAM test

The Hen's Egg Test on the Chorioallantoic Membrane (HET-CAM) assay was used to gain an insight into the compatibility of the developed hydrogels with the ocular surface. The vasculature of the

USC UNIVERSIDADE DE SANTIAGO DE COMPOSTELA

CAM of fertilized eggs is comparable to the conjunctiva structure [ICCVAM, 2010]. All hydrogel compositions could be considered non-irritating because none of them caused hemorrhage, vascular lysis or coagulation of CAM vessels during the 5 min of the test **(Figure 4.13)** [Alvarez-Rivera et al., 2018]. The IS registered for the positive control was 19.4.

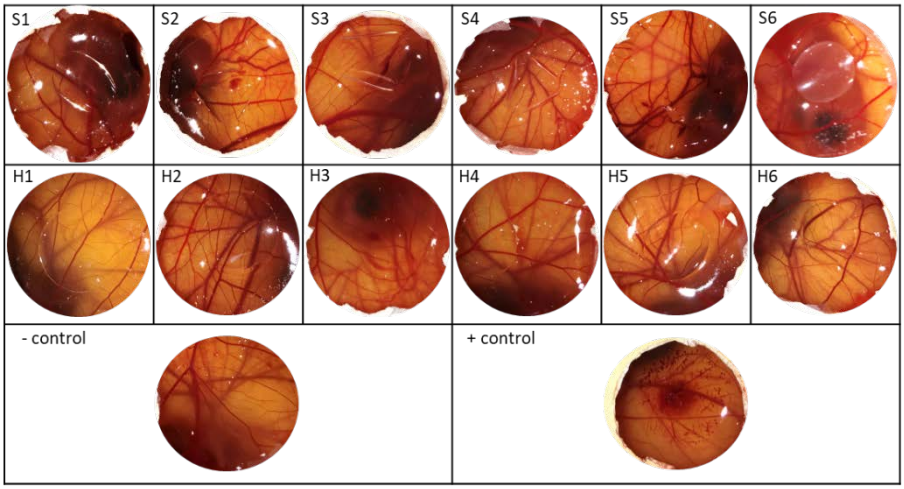


Figure 4.13. Images of the HET-CAM test. Codes as in Table 4.1.

4.3.9 Protein adsorption

The adsorption of albumin and lysozyme, as two of the major proteins present in the tear fluid, was evaluated using a QCM-D. Changes in the values of frequency (Δf/n) and dissipation (ΔD) are shown in **Figures 4.14–4.17** and summarized in **Table 4.3** for the third harmonic.

USC UNIVERSIDADE DE SANTIAGO DE COMPOSTELA

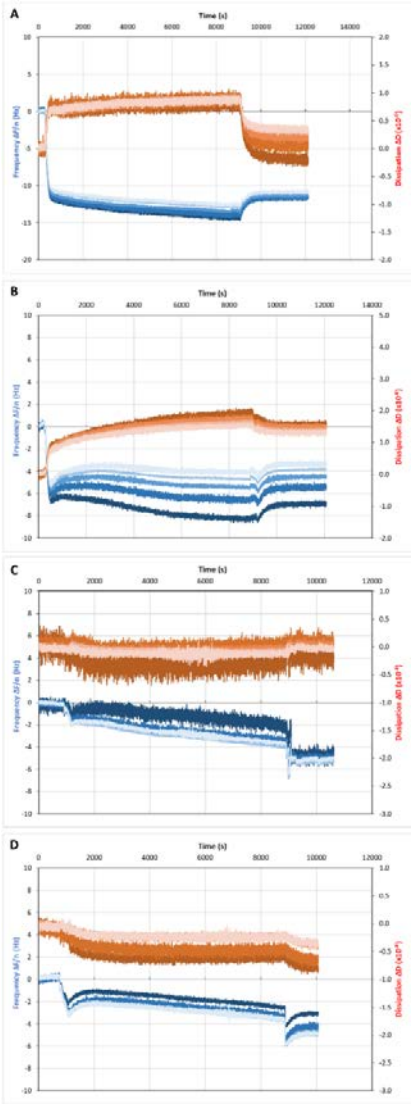


Figure 4.14. Normalized shift in the frequency, Δf/n, (blue line, left y-axis) and shift in the dissipation, ΔD, (red line, right y-axis) for the 3rd, 5th, 7th, 9th, and 11th harmonics of the resonant frequency of quartz crystal sensors coated with S1 (**A**), S4 (**B**), S5 (**C**) and S6 (**D**) hydrogel film. After few minutes equilibration in SLF, albumin solution was added (for ~150 min), and finally SLF rising solution was passed.

USC
UNIVERSIDADE DE SANTIAGO DE COMPOSTELA

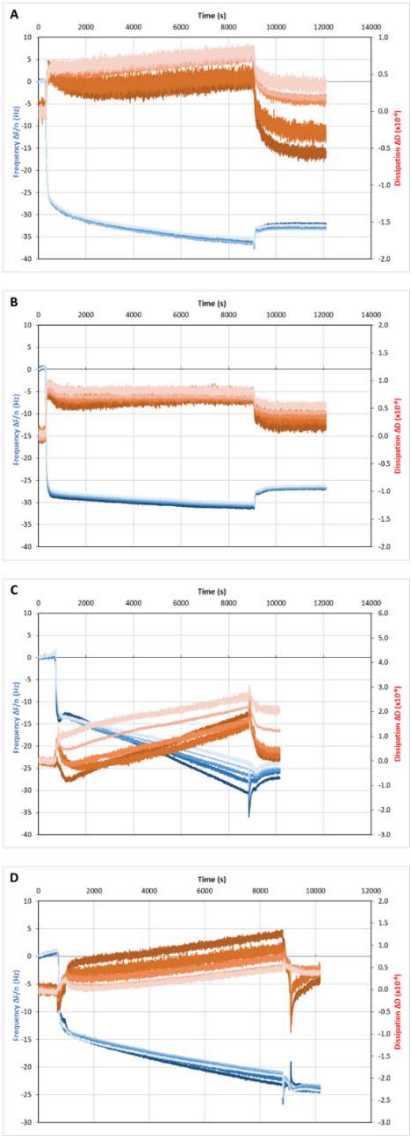


Figure 4.15. Normalized shift in the frequency, Δf/n, (blue line, left y-axis) and shift in the dissipation, ΔD, (red line, right y-axis) for 3rd, 5th, 7th, 9th, and 11th harmonics of the resonant frequency of quartz crystal sensors coated with S1 (**A**), S4 (**B**), S5 (**C**) and S6 (**D**) hydrogel film. After few minutes equilibration in SLF, lysozyme solution was added (for ~150 min), and finally SLF rising solution was passed.

USC UNIVERSIDADE DE SANTIAGO DE COMPOSTELA

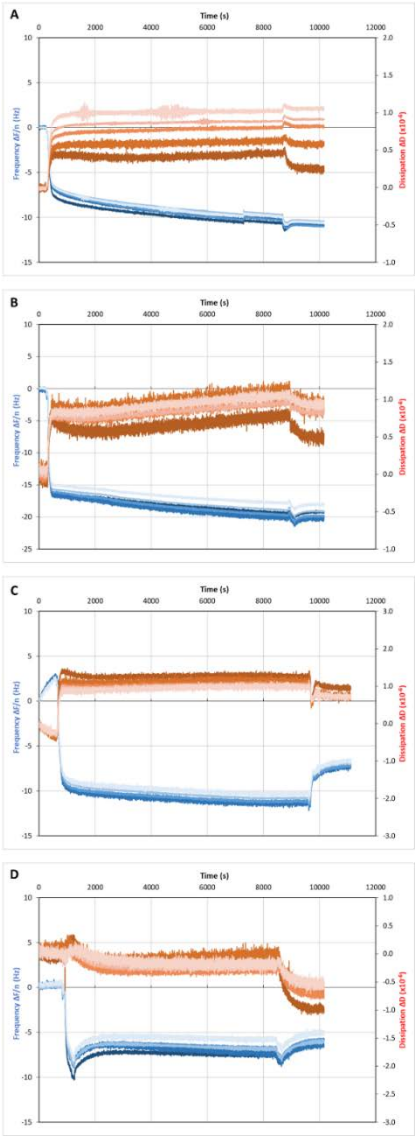


Figure 4.16. Normalized shift in the frequency, Δf/n, (blue line, left y-axis) and shift in the dissipation, ΔD, (red line, right y-axis) for the 3rd, 5th, 7th, 9th, and 11th harmonics of the resonant frequency of quartz crystal sensors coated with H1 (**A**), H4 (**B**), H5 (**C**) and H6 (**D**) hydrogel film. After few minutes equilibration in SLF, albumin solution was added (for ~150 min), and finally SLF rising solution was passed.

USC UNIVERSIDADE DE SANTIAGO DE COMPOSTELA

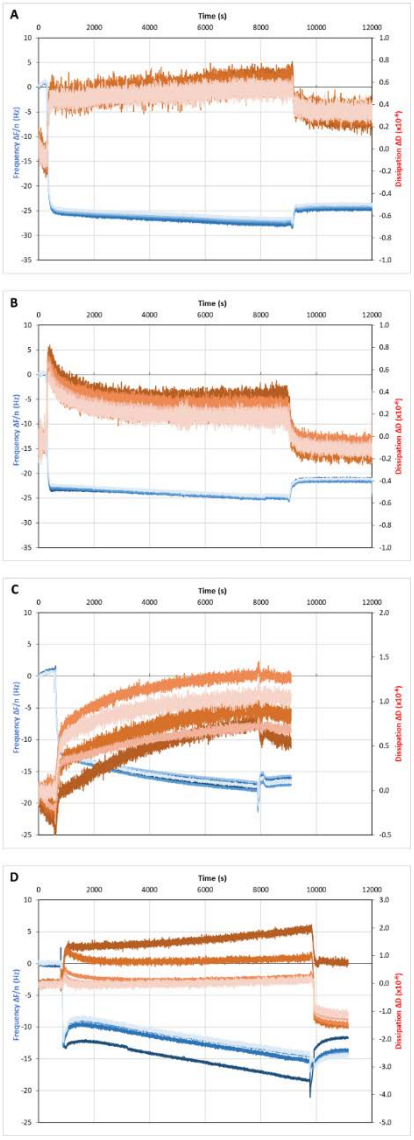


Figure 4.17. Normalized shift in the frequency, Δf/n, (blue line, left y-axis) and shift in the dissipation, ΔD, (red line, right y-axis) for the 3rd, 5th, 7th, 9th, and 11th harmonics of the resonant frequency of quartz crystal sensors coated with H1 (**A**), H4 (**B**), H5 (**C**) and H6 (**D**) hydrogel film. After few minutes equilibration in SLF, lysozyme solution was added (for ~150 min), and finally SLF rising solution was passed.

USC UNIVERSIDADE DE SANTIAGO DE COMPOSTELA

Table 4.3. Frequency (Δf/n) and dissipation (ΔD) variations for the 3rd harmonic for albumin and lysozyme adsorption onto silicone and HEMA hydrogels, obtained by QCM-D. Estimated values for mass variation (*Δ*m) and layer thickness (d_{eff}) are also presented (average ± standard deviation, *n* = 4).

Hydrogel	Protein	*Δ*f/n (Hz)	*Δ*D (x10^{-6})	*Δ*m (ng/cm^2)	D_{eff} (nm)
S1	Albumin	-15.5 ± 4.1	0.9 ± 0.6	275 ± 72	2.4 ± 0.6
S4		-7.0 ± 1.5	0.9 ± 1.1	124 ± 27	1.1 ± 0.2
S5		-4.3 ± 0.5	-0.2 ± 0.6	77 ± 9	0.6 ± 0.1
S6		-3.8 ± 0.8	-0.9 ± 0.4	68 ± 15	0.5 ± 0.1
S1	Lysozyme	-31.8 ± 6.3	0.4 ± 0.6	562 ± 110	4.1 ± 0.8
S4		-31.0 ± 3.4	0.6 ± 0.2	548 ± 60	4.0 ± 0.4
S5		-24.1 ± 7.8	0.1 ± 0.1	427 ± 140	3.1 ± 1.0
S6		-21.3 ± 0.6	0.9 ± 0.5	377 ± 11	2.7 ± 0.1
H1	Albumin	-15.6 ± 6.4	0.6 ± 0.3	275 ± 114	2.4 ± 1.0
H4		-14.1 ± 5.4	0.1 ± 1.1	250 ± 96	2.2 ± 0.8
H5		-8.1 ± 1.7	0.9 ± 0.1	150 ± 30	1.5 ± 0.4
H6		-6.4 ± 0.8	0.1 ± 0.9	114 ± 15	1.0 ± 0.1
H1	Lysozyme	-29.0 ± 4.7	1 ± 0.3	513 ± 83	3.7 ± 0.6
H4		-24.0 ± 7.3	0.1 ± 0.5	424 ± 129	3.1 ± 0.9
H5		-19.5 ± 2.2	1.4 ± 0.6	345 ± 39	2.5 ± 0.3
H6		-8.5 ± 2.4	1.8 ± 1.5	151 ± 43	1.1 ± 0.3

The addition of lysozyme and albumin led to a decrease in frequency in all cases, demonstrating that both proteins adsorbed onto the surfaces. The decrease in frequency was more accentuated in the case of lysozyme, independently of the nature of the hydrogel (silicon-based or HEMA-based), indicating that a higher amount of protein adsorbed onto the hydrogel's surface. In all cases, the adsorption was

USC UNIVERSIDADE DE SANTIAGO DE COMPOSTELA

attenuated with the increase in the MPC amount in the hydrogels, which confirmed the capacity of MPC to avoid protein adsorption [Luensmann and Jones, 2012]. This effect was more pronounced for lysozyme on HEMA-based hydrogels.

The degree of overlapping of the curves Δf/n versus time obtained for the different harmonics was analyzed to predict the viscoelastic character of the adsorbed film. The obtained graphics presented a high degree of overlapping, indicating that the protein adsorbed layers showed high stiffness. The rigid nature of the formed films was confirmed by the low values of ΔD, which indicates that a low amount of energy was dissipated.

For rigid films, the variation in frequency (Δf/n) is proportional to the mass of the adsorbed film (Δm) according to the Sauerbrey equation (4.3):

$$\Delta m = -C \times \frac{\Delta_f}{n} \qquad \text{Eq. (4.3)}$$

where C is the sensitivity constant based on the physical properties of the quartz crystal (C = 17.7 ng cm^{-2} Hz^{-1} for a 5 MHz crystal) [Carapeto et al., 2010; Gispert et al., 2008]. Additionally, the thickness (d_{eff}) of the adhering films can be estimated through equation (4.4), considering 1.15 g/cm^3 [Gispert et al., 2008] and 1.38 g/cm^3 [Jin et al., 2015] as the density of albumin and lysozyme films [Fulga et al., 2006]:

$$deff = \frac{\Delta_m}{\rho eff} \qquad \text{Eq. (4.4)}$$

Overall, MPC demonstrated a significant antifouling effect for both proteins: for the hydrogels with the highest value of MPC, lower thickness and Δm values were obtained. This is in agreement with

USC UNIVERSIDADE DE SANTIAGO DE COMPOSTELA

previous studies that found that the existence of zwitterionic MPC moieties on the surfaces of the HEMA- and silicone-based hydrogels decreased the adsorption of proteins, such as lysozyme, fibrinogen and albumin [Wang et al., 2011; Vales et al., 2020; Chang et al., 2020]. This protein repulsion capacity was attributed to the high hydration of the phosphorylcholine groups present on MPC [Wang et al., 2011; Chang et al., 2020]. It is known that the increase in the ratio of MPC increases the amount of free water but decreases that of bound water [Al-Sohani et al., 2017]. Therefore, when a protein comes into contact with the hydrogel surface, it may remain in this native state, not altering its structure. This facilitates the release of loosely bound protein molecules, leading to a decrease in protein adsorption.

The differences between the adsorbed amounts of albumin and lysozyme may be related to the size, shape, charge, conformational stability of the proteins and their concentration in the adsorbing solution. Protein adsorption is a complex phenomenon, and it is difficult to identify the weight of the different contributions. Albumin is a large, anionic, soft protein (MW 66.4 kDa) with a heart shape (8 mm side × 3 nm thickness) while lysozyme is a small, ellipsoid, cationic, hard protein (MW 14.7 kDa) with axes of 2.6 nm and 4.5 nm [Yang and Mattison, 2003]. In this work, different concentrations of each protein were used to perform the adsorption experiments (0.05 mg/mL for albumin and 1.9 mg/mL for lysozyme). This may explain the lower amount of adsorbed albumin on the hydrogels.

The inhibitory effect of MPC on protein adsorption was less evident for lysozyme on silicon-based hydrogels, which may be due to the stronger interactions between the protein and the surface. In fact, the hydrogel surface should be negatively charged (high affinity to positive polyelectrolytes was previously found [Silva et al., 2021]), enhancing the binding to the positively charged protein. Such a

USC UNIVERSIDADE DE SANTIAGO DE COMPOSTELA

preferential binding of lysozyme on MPC-containing hydrogels may readily occur after placement on the eye's surface [Garrett et al., 1999], which may contribute to the antimicrobial performance [Diaz-Gomez et al., 2018].

4.3.10 Antibiofilm properties

First, the susceptibility to soluble resveratrol of the two main causal agents of ocular infections, *S. aureus* and *P. aeruginosa* [Bispo et al., 2015], was evaluated by quantifying the effect of different concentrations of resveratrol on bacteria growth and biofilm formation on inert glass surfaces. *P. aeruginosa* biofilm formation on the surface of the coverslips immersed in growth medium supplemented with resveratrol was lower than without resveratrol **(Figure 4.18A1)**, although the differences were not statistically significant for the two lower concentrations tested (4 and 12 µg/mL). The biofilm formation significantly decreased for a 250 µg/mL resveratrol solution, showing the capacity of resveratrol to inhibit biofilm formation against *P. aeruginosa* and also to prevent the growth of planktonic bacteria **(Figure 4.18A2)**. These findings agree well with previous reports on Resveramax^{TM} (oily alimentary supplement) that evidenced that resveratrol was active against *P. aeruginosa* PAO1 biofilm [Vasavi et al., 2017; Shimamura et al., 2017]. In contrast, the biofilm formation after 48 h of growth of *S. aureus* **(Figure 4.18B1)** was higher for 5 µg/mL of resveratrol than for the controls, but the biofilm was completely inhibited when the resveratrol concentration was raised to 250 µg/mL. The bacterial growth in the medium surrounding the coverslips was in good agreement with the absorbances recorded for the surfaces **(Figure 4.18B2)**. The increase in biofilm formation observed at low resveratrol concentrations for *S. aureus* may be the

USC UNIVERSIDADE DE SANTIAGO DE COMPOSTELA

result of a stress response of the cells in the presence of sub-inhibitory concentrations of this compound, since the slower growth of bacteria in the biofilm may have had a protective effect against resveratrol. An increase in biofilm formation as a response to the cell stress caused by antimicrobial agents has been described before [Mah and O'Toole, 2001].

In all cases, it should be noted that the MTT assay used to evaluate the biofilm formation determines mitochondrial activity since it is based on the conversion of MTT into formazan crystals by living cells and not only biofilm biomass or cell number, being therefore a highly sensitive method [Van Meerloo et al., 2011]. Resveratrol has been suggested to alter the MTT reduction rate in mammalian cell cultures, not because of a direct effect on MTT reduction but through an indirect effect on cell metabolism [Stepanenko et al., 2015]. Such an effect is of small magnitude and has not been reported for bacteria.

USC
UNIVERSIDADE DE SANTIAGO DE COMPOSTELA

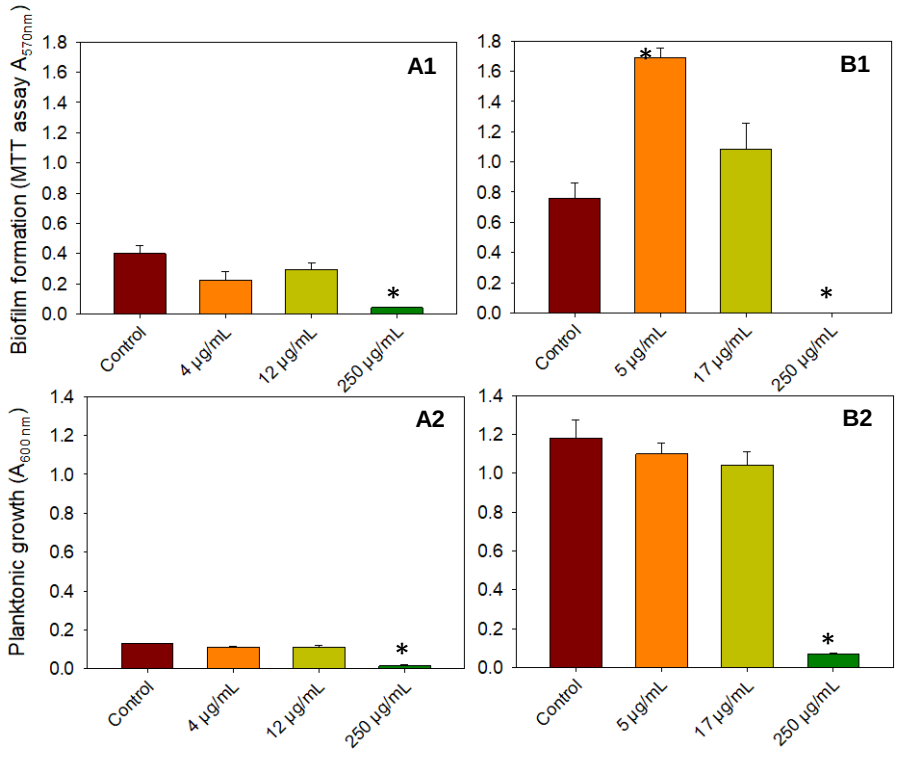


Figure 4.18. Growth of *Pseudomonas aeruginosa* (A1, A2) and *Staphylococcus aureus* (B1, B2) biofilm on the surface of glass coverslips measured with the MTT assay (A1, B1) and in the culture medium surrounding the coverslips (A2, B2), to which resveratrol at different concentrations was added. * indicates a statistically significant difference with respect to the control without resveratrol ($p < 0.05$).

Next, the antibiofilm performance of silicone and HEMA hydrogels with and without MPC in their composition and loaded or not with resveratrol was investigated. In the case of *P. aeruginosa*, more biofilm was formed on the hydrogels without resveratrol **(Figure 4.19A1 and B1)** compared to those loaded with resveratrol. No differences were recorded for Proclear® 1 day CLs with and without resveratrol, which may be related to the fact that the amount

USC UNIVERSIDADE DE SANTIAGO DE COMPOSTELA

loaded per lens was the lowest (see **Table 4.2**). In HEMA hydrogels, the inhibitory effect of the resveratrol loading was more evident, probably due to the greater amounts released. The absorbance of the supernatants was also measured **(Figure 4.19A2 and B2)** and the planktonic bacterial growth was very similar in the culture media around the hydrogels loaded and not with resveratrol. Notably, although the biofilm formation was clearly lower in the resveratrol-loaded HEMA hydrogels than in their respective unloaded controls **(Figure 4.19B1**), planktonic growth was generally higher in the presence of resveratrol-loaded lenses **(Figure 4.19B2)**, indicating the specific antibiofilm activity of the compound for *P. aeruginosa*.

USC
UNIVERSIDADE DE SANTIAGO DE COMPOSTELA

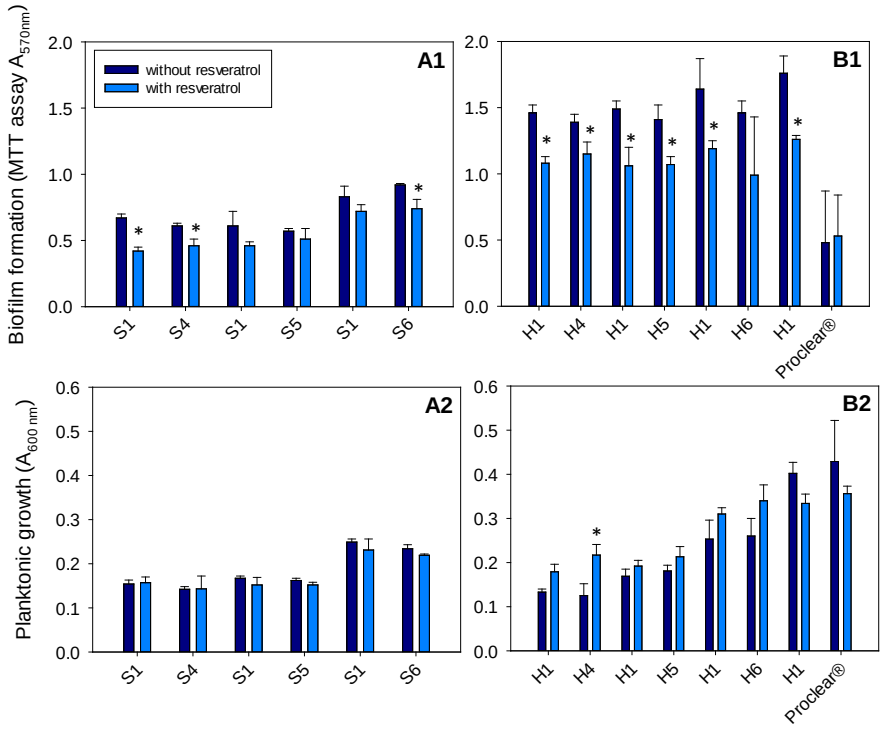


Figure 4.19. Growth of *Pseudomonas aeruginosa* PAO1 biofilm on the surfaces of silicone (A1) and HEMA (B1) hydrogels (without and with resveratrol) measured with the MTT assay, and in the culture medium surrounding the silicone (A2) and HEMA (B2) hydrogels (without and with resveratrol) after 6 h of incubation. * indicates a statistically significant difference between hydrogels with and without resveratrol ($p < 0.05$). In each experiment, a silicone hydrogel prepared with MPC (S4, S5 and S6) was evaluated in parallel to the silicone hydrogel without MPC (S1). Similarly, the HEMA hydrogels prepared with MPC (H4, H5 and H6) were evaluated in parallel to the HEMA hydrogel without MPC (H1).

In the case of *S. aureus*, the biofilm formation after 48 h of incubation **(Figure 4.20A1 and B1)** for all hydrogels was lower than for *P. aeruginosa* despite the much higher bacterial growth in the medium surrounding the hydrogels **(Figure 4.20A2 and B2)**. For all

USC UNIVERSIDADE DE SANTIAGO DE COMPOSTELA

HEMA-and silicone-based hydrogels, the biofilm formation was almost the same and no statistically significant differences were observed with the addition of MPC and/or resveratrol. This finding agreed with two other studies where resveratrol did not reduce biofilm formation and confirms that strain variation and assay conditions may influence the efficacy [Lee et al., 2014; Cho et al., 2015]. Unexpectedly, no remarkable antibiofilm effect could be assigned to MPC, which could be related to the fact that, in the designed hydrogels, the MPC monomer was copolymerized during the synthesis process and not added later as a surface modification process, as commonly reported in the literature [Fujii et al., 2008]. Therefore, MPC is expected to be evenly distributed in the bulk of the hydrogel and not confined to the surface. This may have caused the density of MPC chains on the surface to be insufficient to prevent bacteria adhesion.

The adhesion of bacteria is usually higher on hydrophobic hydrogels than on hydrophilic ones [Dutta and Willcox, 2014; Willcox et al., 2001; Bruinsma et al., 2001; Henriques et al., 2005]. Here, the biofilm formation for both bacteria was lower for silicone hydrogels. Although the wettability of the silicone- and HEMA-based hydrogels was not significantly different, the lower biofilm formation could be related to the higher water uptake observed for silicone hydrogels due to the presence of hydrophilic monomers (mainly NVP), as explained above.

USC
UNIVERSIDADE DE SANTIAGO DE COMPOSTELA

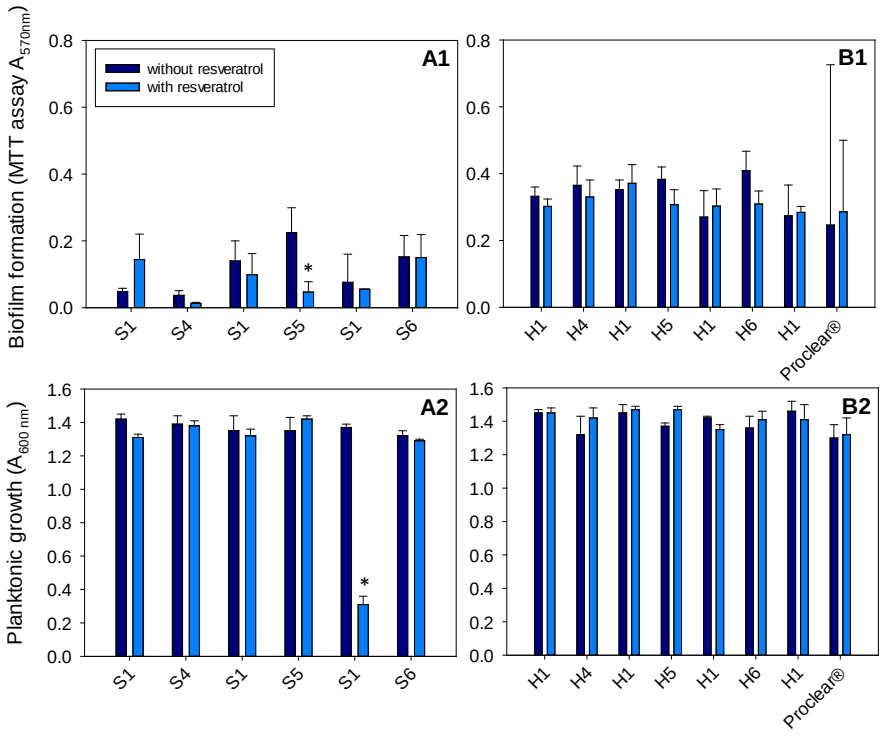


Figure 4.20. Growth of *Staphylococcus aureus* biofilm on the surface of silicone (A1) and HEMA (B1) hydrogels (without and with resveratrol) and in the medium surrounding the silicone (A2) and HEMA (B2) hydrogels (without and with resveratrol) after 48 h of incubation. In each experiment, a silicone hydrogel prepared with MPC (S4, S5 and S6) was evaluated in parallel to the silicone hydrogel without MPC (S1). Similarly, the HEMA hydrogels prepared with MPC (H4, H5 and H6) were evaluated in parallel to the HEMA hydrogel without MPC (H1). * indicates a statistically significant difference between hydrogels with and without resveratrol ($p < 0.05$).

USC UNIVERSIDADE DE SANTIAGO DE COMPOSTELA

4.3.11 Antioxidant properties

The DPPH assay was used to check whether resveratrol maintained its antioxidant activity after being loaded and released from HEMA and silicone hydrogels. Freshly prepared NaCl 0.9% release medium, as well as NaCl 0.9% solutions in which non-loaded hydrogels were soaked, were also tested to verify that there were no leaching substances that could cause false antioxidant activity during the assay. The DPPH• scavenging capacity was expressed as µg/mL in the reaction medium, as a percentage, as explained previously [Gülçin, 2010], and as Trolox equivalent antioxidant capacity (TEAC) for comparative purposes. Analysis of freshly prepared resveratrol loading solution led to 3.5 ± 1.2 µg/mL DPPH levels and 40.5 ± 2.8 µM TEAC. Samples from the release tests are expected to cover a wide range of resveratrol concentrations (according to **Figure 4.9** and **4.11**) but well below the concentration of the loading solution.

According to the results **(Table 4.4-4.5, Figures 4.21–4.23)**, the levels of DPPH• radicals registered for NaCl 0.9% medium without resveratrol (20.1 µg/mL) were higher than for the release medium of the resveratrol-loaded hydrogels. This finding indicates that the released resveratrol maintained its capacity to reduce the free radicals and thus retained its antioxidant activity after being loaded and released from the HEMA and silicone hydrogels. At the same time, the effect registered was very similar within the same type of hydrogel, but antioxidant capability was higher for HEMA than for silicone hydrogels, as expected, since HEMA hydrogels released higher amounts of resveratrol into the medium. Non-loaded hydrogels showed values of TEAC that were close to zero or even negative, meaning that they did not release any substance that may have interfered with the test.

USC
UNIVERSIDADE DE SANTIAGO DE COMPOSTELA

The antioxidant capacity of resveratrol solutions after being exposed to white light (HITACHI 8 W F8T5 daylight, Japan) for 3 h was confirmed despite isomerization from *trans* to *cis* (13.2 ± 0.03 µg/mL DPPH levels, and 16.37 ± 0.07 µM TEAC). Overall, both HEMA and silicone hydrogels helped resveratrol to maintain its antioxidant activity, which may be useful in managing ocular diseases that benefit from a decrease in reactive oxygen species (ROS) levels.

Table 4.4. DPPH• levels (µg/mL) and DPPH scavenging effect (%). All data are mean ± SDs (n = 3).

Hydrogel	DPPH (µg/mL)		DPPH scavenging effect (%)	
	12 h	24 h	12 h	24 h
S1	15.6 ± 0.2	14.8 ± 0.9	26.1 ± 1.1	29.0 ± 4.3
S2	16.3 ± 2.3	13.4 ± 0.6	27.8 ± 2.4	41.8 ± 2.6
S3	15.6 ± 0.6	14.2 ± 0.3	38.7 ± 2.6	27.6 ± 1.5
S4	15.7 ± 2.1	13.2 ± 0.3	30.3 ± 9.6	33.4 ± 1.7
S5	15.1 ± 1.3	13.2 ± 0.7	35.5 ± 5.7	45.3 ± 3.1
S6	14.6 ± 0.9	13.6 ± 1.7	26.0 ± 4.9	36.8 ± 7.9
H1	11.5 ± 0.1	10.0 ± 1.0	44.0 ± 0.7	51.6 ± 4.9
H2	12.1 ± 0.8	11.9 ± 2.1	39.1 ± 4.3	40.2 ± 11.0
H3	13.0 ± 0.9	11.6 ± 1.7	36.4 ± 4.4	42.0 ± 8.8
H4	12.2 ± 0.4	10.8 ± 0.7	41.7 ± 2.0	47.7 ± 3.3
H5	11.3 ± 0.5	12.1 ± 3.6	48.1 ± 2.4	38.4 ± 18.9
H6	11.3 ± 0.8	9.8 ± 0.5	44.0 ± 4.1	58.9 ± 2.1
Proclear®	11.0 ± 0.4	11.1 ± 1.4	47.5 ± 2.0	46.5 ± 7.0

USC UNIVERSIDADE DE SANTIAGO DE COMPOSTELA

Table 4.5. Trolox equivalent antioxidant capacity (TEAC). All data are mean ± SDs (*n* = 3).

Hydrogel	TEAC (μM)	
	12 h	24 h
S1	10.6 ± 0.5	12.6 ± 2.2
S2	8.9 ± 5.6	15.9 ± 1.4
S3	10.5 ± 1.6	14.0 ± 0.7
S4	10.3 ± 5.2	16.5 ± 0.8
S5	11.8 ± 3.2	16.5 ± 1.8
S6	13.1 ± 2.3	15.6 ± 4.1
H1	20.5 ± 0.3	24.4 ± 2.4
H2	19.2 ± 2.0	19.6 ± 5.3
H3	17.0 ± 2.2	20.5 ± 4.2
H4	19.1 ± 1.0	22.3 ± 1.6
H5	21.3 ± 1.2	19.2 ± 8.9
H6	21.1 ± 2.0	24.9 ± 1.2
Proclear®	22.0 ± 1.0	21.6 ± 3.5

USC UNIVERSIDADE DE SANTIAGO DE COMPOSTELA

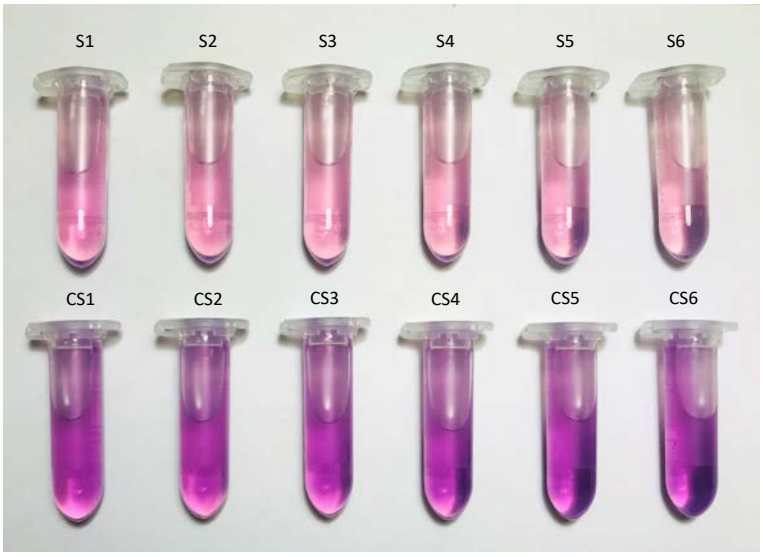


Figure 4.21. Antioxidant activity of resveratrol released from silicone-hydrogels (up) and their respective controls (down).

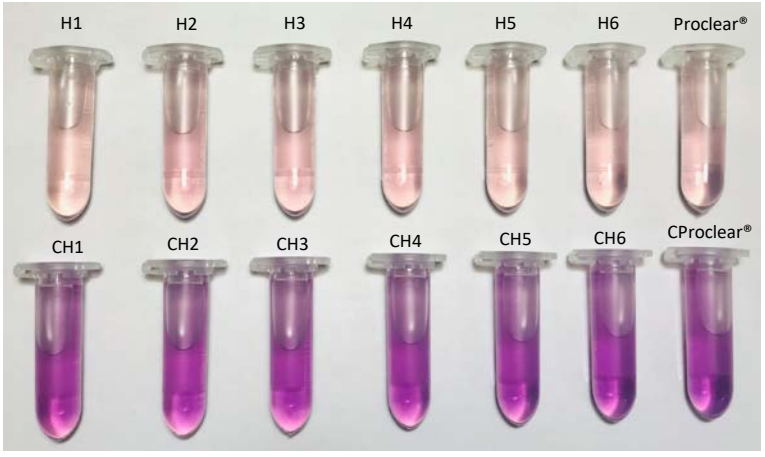


Figure 4.22. Antioxidant activity of resveratrol released from HEMA-hydrogels (up) and their respective controls (down).

USC
UNIVERSIDADE DE SANTIAGO DE COMPOSTELA

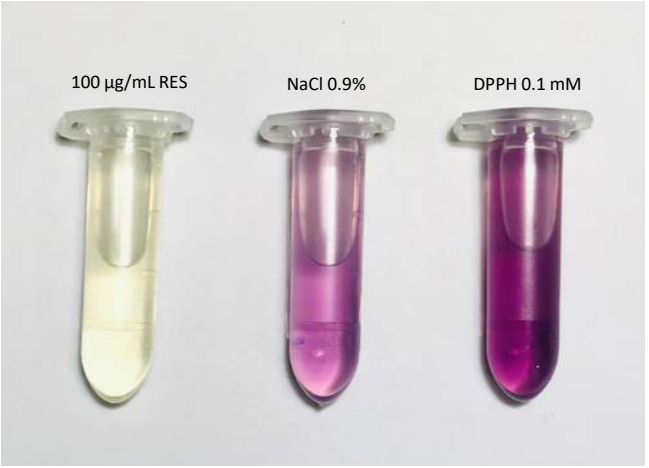


Figure 4.23. Antioxidant activity of a 100 µg/mL resveratrol solution in ethanol:water 10:90 *v/v* medium, a NaCl 0.9% solution, and a DPPH 0.1 mM solution.

4.4 CONCLUSIONS

The use of MPC as a comonomer of HEMA- and silicone-based hydrogels and their loading with resveratrol has been studied here for first time to obtain hydrogels with antioxidant and antibiofilm properties. MPC increased the water uptake and decreased the amount of protein adsorbed while preserving the mechanical properties of the hydrogels. Only silicone hydrogels prepared with the highest proportions of MPC investigated (80 and 101 mM) evidenced a decrease in light transmission. All hydrogels were able to uptake relevant amounts of resveratrol. The higher affinity of silicone hydrogels for resveratrol, probably due to hydrophobic interactions, notably increased the amount loaded but also caused the release to occur more slowly. As a consequence, the amounts of resveratrol accumulated in the cornea and sclera were lower when delivered from the silicone hydrogels. Regarding the antibiofilm activity, resveratrol

USC UNIVERSIDADE DE SANTIAGO DE COMPOSTELA

decreased biofilm formation by *P. aeruginosa*, but no protective effect was recorded for MPC against the two strains investigated. Nevertheless, the fact that the hydrogels prepared with MPC showed preferential sorption of lysozyme with respect to albumin may contribute to the antibacterial effects in vivo, which should be evaluated in future studies. The inconclusive antibiofilm performance of the hydrogels on *S. aureus* suggests that the loading should be increased in order to achieve an inhibitory concentration. Importantly, HEMA- and silicone-based hydrogels preserved the antioxidant activity of resveratrol and showed a protective effect against photodegradation. Overall, hydrogels containing MPC and loaded with resveratrol are demonstrated to be suitable candidates for the preparation of CLs with antibiofilm and antioxidant performance.

4.5 REFERENCES

Abengózar-Vela, A., Schaumburg, C. S., Stern, M. E., Calonge, M., Enríquez-de-Salamanca, A., & González-García, M. J. (2019). Topical quercetin and resveratrol protect the ocular surface in experimental dry eye disease. *Ocular Immunology and Inflammation*, *27*(6), 1023-1032.

Abu-Amero, K. K., Kondkar, A. A., & Chalam, K. V. (2016). Resveratrol and ophthalmic diseases. *Nutrients*, *8*(4), 200.

Alambiaga-Caravaca, A. M., Calatayud-Pascual, M. A., Rodilla, V., Concheiro, A., López-Castellano, A., & Alvarez-Lorenzo, C. (2020). Micelles of progesterone for topical eye administration: Interspecies and intertissues differences in ex vivo ocular permeability. *Pharmaceutics*, *12*(8), 702.

Al-Shohani, A., Awwad, S., Khaw, P. T., & Brocchini, S. (2017). The preparation of HEMA-MPC films for ocular drug delivery. *British Journal of Pharmacy*, *2*(1), 31-41.

USC UNIVERSIDADE DE SANTIAGO DE COMPOSTELA

Alvarez-Rivera, F., Concheiro, A., & Alvarez-Lorenzo, C. (2018). Epalrestat-loaded silicone hydrogels as contact lenses to address diabetic-eye complications. *European Journal of Pharmaceutics and Biopharmaceutics*, *122*, 126-136.

Alvarez-Rivera, F., Fernández-Villanueva, D., Concheiro, A., & Alvarez-Lorenzo, C. (2016). α-Lipoic acid in Soluplus® polymeric nanomicelles for ocular treatment of diabetes-associated corneal diseases. *Journal of Pharmaceutical Sciences*, *105*(9), 2855-2863.

Alvarez-Rivera, F., Serro, A. P., Silva, D., Concheiro, A., & Alvarez-Lorenzo, C. (2019). Hydrogels for diabetic eyes: Naltrexone loading, release profiles and cornea penetration. *Materials Science and Engineering: C*, *105*, 110092.

Alvarez-Lorenzo, C., Yanez, F., Barreiro-Iglesias, R., & Concheiro, A. (2006). Imprinted soft contact lenses as norfloxacin delivery systems. *Journal of Controlled Release*, *113*(3), 236-244.

Augustine, N., Goel, A. K., Sivakumar, K. C., Kumar, R. A., & Thomas, S. (2014). Resveratrol–a potential inhibitor of biofilm formation in *Vibrio cholerae*. *Phytomedicine*, *21*(3), 286-289.

Arshad, M., Carnt, N., Tan, J., Ekkeshis, I., & Stapleton, F. (2019). Water exposure and the risk of contact lens–related disease. *Cornea*, *38*(6), 791-797.

Bhatt, P., Fnu, G., Bhatia, D., Shahid, A., & Sutariya, V. (2020). Nanodelivery of resveratrol-loaded PLGA nanoparticles for age-related macular degeneration. *AAPS PharmSciTech*, *21*(8), 1-9.

Bispo, P. J., Haas, W., & Gilmore, M. S. (2015). Biofilms in infections of the eye. *Pathogens*, *4*(1), 111-136.

Bostanghadiri, N., Pormohammad, A., Chirani, A. S., Pouriran, R., Erfanimanesh, S., & Hashemi, A. (2017). Comprehensive review on the

USC
UNIVERSIDADE DE SANTIAGO DE COMPOSTELA

antimicrobial potency of the plant polyphenol Resveratrol. *Biomedicine & Pharmacotherapy*, *95*, 1588-1595.

Bruinsma, G. M., Van der Mei, H. C., & Busscher, H. J. (2001). Bacterial adhesion to surface hydrophilic and hydrophobic contact lenses. *Biomaterials*, *22*(24), 3217-3224.

Carapeto, A. P., Serro, A. P., Nunes, B. M. F., Martins, M. C. L., Todorovic, S., Duarte, M. T., ... & Saramago, B. (2010). Characterization of two DLC coatings for joint prosthesis: The role of albumin on the tribological behavior. *Surface and Coatings Technology*, *204*(21-22), 3451-3458.

Chan, C. M., Huang, C. H., Li, H. J., Hsiao, C. Y., Su, C. C., Lee, P. L., & Hung, C. F. (2015). Protective effects of resveratrol against UVA-induced damage in ARPE19 cells. *International Journal of Molecular Sciences*, *16*(3), 5789-5802.

Chang, W. H., Liu, P. Y., Lu, C. J., Lin, D. E., Lin, M. H., Jiang, Y. T., & Hsu, Y. H. H. (2020). Reduction of physical strength and enhancement of anti-protein and anti-lipid adsorption abilities of contact lenses by adding 2-methacryloyloxyethyl phosphorylcholine. *Macromolecular Research*, *28*(12), 1064-1073.

Chen, Y., Meng, J., Li, H., Wei, H., Bi, F., Liu, S., ... & Liu, W. (2019). Resveratrol exhibits an effect on attenuating retina inflammatory condition and damage of diabetic retinopathy via PON1. *Experimental Eye Research*, *181*, 356-366.

Chien, H. W., & Kuo, C. J. (2019). Preparation, material properties and antimicrobial efficacy of silicone hydrogel by modulating silicone and hydrophilic monomer. *Journal of Biomaterials Science, Polymer Edition*.

Cho, H. S., Lee, J. H., Cho, M. H., & Lee, J. (2015). Red wines and flavonoids diminish *Staphylococcus aureus* virulence with anti-biofilm and anti-hemolytic activities. *Biofouling*, *31*(1), 1-11.

USC UNIVERSIDADE DE SANTIAGO DE COMPOSTELA

Diaz-Gomez, L., Concheiro, A., & Alvarez-Lorenzo, C. (2018). Functionalization of titanium implants with phase-transited lysozyme for gentle immobilization of antimicrobial lysozyme. *Applied Surface Science*, *452*, 32-42.

Dinte, E., Vostinaru, O., Samoila, O., Sevastre, B., & Bodoki, E. (2020). Ophthalmic nanosystems with antioxidants for the prevention and treatment of eye diseases. *Coatings*, *10*(1), 36.

dos Santos, J. F. R., Alvarez-Lorenzo, C., Silva, M., Balsa, L., Couceiro, J., Torres-Labandeira, J. J., & Concheiro, A. (2009). Soft contact lenses functionalized with pendant cyclodextrins for controlled drug delivery. *Biomaterials*, *30*(7), 1348-1355.

Dutta, D., & Willcox, M. D. (2014). Antimicrobial contact lenses and lens cases: a review. *Eye & Contact Lens*, *40*(5), 312-324.

El-Ganiny, A. M., Shaker, G. H., Aboelazm, A. A., & El-Dash, H. A. (2017). Prevention of bacterial biofilm formation on soft contact lenses using natural compounds. *Journal of Ophthalmic Inflammation and Infection*, *7*(1), 1-7.

Filipe, H. P., Bozukova, D., Pimenta, A., Vieira, A. P., Oliveira, A. S., Galante, R., ... & Serro, A. P. (2019). Moxifloxacin-loaded acrylic intraocular lenses: In vitro and in vivo performance. *Journal of Cataract & Refractive Surgery*, *45*(12), 1808-1817.

Fleiszig, S. M., Kroken, A. R., Nieto, V., Grosser, M. R., Wan, S. J., Metruccio, M. M., & Evans, D. J. (2020). Contact lens-related corneal infection: Intrinsic resistance and its compromise. *Progress in Retinal and Eye Research*, *76*, 100804.

Fujii, K., Matsumoto, H. N., Koyama, Y., Iwasaki, Y., Ishihara, K., & Takakuda, K. (2008). Prevention of biofilm formation with a coating of 2-methacryloyloxyethyl phosphorylcholine polymer. *Journal of Veterinary Medical Science*, *70*(2), 167-173.

USC
UNIVERSIDADE DE SANTIAGO DE COMPOSTELA

Fulga, F., & Nicolau, D. V. (2006). Biomolecular layers: Quantification of mass and thickness. *Wiley Encyclopedia of Biomedical Engineering*.

Garrett, Q., Garrett, R. W., & Milthorpe, B. K. (1999). Lysozyme sorption in hydrogel contact lenses. *Investigative Ophthalmology & Visual Science*, *40*(5), 897-903.

Gispert, M. P., Serro, A. P., Colaço, R., & Saramago, B. (2008). Bovine serum albumin adsorption onto 316L stainless steel and alumina: a comparative study using depletion, protein radiolabeling, quartz crystal microbalance and atomic force microscopy. *Surface and Interface Analysis: An International Journal Devoted to the Development and Application of Techniques for the Analysis of Surfaces, Interfaces and Thin Films*, *40*(12), 1529-1537.

Goda, T., & Ishihara, K. (2006). Soft contact lens biomaterials from bioinspired phospholipid polymers. *Expert Review of Medical Devices*, *3*(2), 167-174.

Goutham, G., Manikandan, R., Beulaja, M., Thiagarajan, R., Arulvasu, C., Arumugam, M., ... & Nabavi, S. M. (2017). A focus on resveratrol and ocular problems, especially cataract: From chemistry to medical uses and clinical relevance. *Biomedicine & Pharmacotherapy*, *86*, 232-241.

Gülçin, İ. (2010). Antioxidant properties of resveratrol: A structure–activity insight. *Innovative Food Science & Emerging Technologies*, *11*(1), 210-218.

Henriques, M., Sousa, C., Lira, M., Elisabete, M., Oliveira, R., Oliveira, R., & Azeredo, J. (2005). Adhesion of *Pseudomonas aeruginosa* and *Staphylococcus epidermidis* to silicone–hydrogel contact lenses. *Optometry and vision science*, *82*(6), 446-450.

Horst, C. R., Brodland, B., Jones, L. W., & Brodland, G. W. (2012). Measuring the modulus of silicone hydrogel contact lenses. *Optometry and Vision Science*, *89*(10), 1468-1476.

USC UNIVERSIDADE DE SANTIAGO DE COMPOSTELA

Huang, X. D., Yao, K., Zhang, H., Huang, X. J., & Xu, Z. K. (2007). Surface modification of silicone intraocular lens by 2-methacryloyloxyethyl phosphoryl-choline binding to reduce *Staphylococcus epidermidis* adherence. *Clinical & Experimental Ophthalmology*, *35*(5), 462-467.

Huang, X. D., Yao, K., Zhang, Z., Zhang, Y., & Wang, Y. (2010). Uveal and capsular biocompatibility of an intraocular lens with a hydrophilic anterior surface and a hydrophobic posterior surface. *Journal of Cataract & Refractive Surgery*, *36*(2), 290-298.

Jin, J., Han, Y., Zhang, C., Liu, J., Jiang, W., Yin, J., & Liang, H. (2015). Effect of grafted PEG chain conformation on albumin and lysozyme adsorption: A combined study using QCM-D and DPI. *Colloids and Surfaces B: Biointerfaces*, *136*, 838-844.

Khan, S. A., & Lee, C. S. (2020). Recent progress and strategies to develop antimicrobial contact lenses and lens cases for different types of microbial keratitis. *Acta Biomaterialia*.

Lançon, A., Frazzi, R., & Latruffe, N. (2016). Anti-oxidant, anti-inflammatory and anti-angiogenic properties of resveratrol in ocular diseases. *Molecules*, *21*(3), 304.

Lee, K., Lee, J. H., Ryu, S. Y., Cho, M. H., & Lee, J. (2014). Stilbenes reduce Staphylococcus aureus hemolysis, biofilm formation, and virulence. *Foodborne Pathogens and Disease*, *11*(9), 710-717.

Li, L., & Xin, Z. (2011). Surface-hydrophilic and protein-resistant tris (trimethylsiloxy)-3-methacryloxypropylsilane-containing polymer by the introduction of phosphorylcholine groups. *Colloids and Surfaces A: Physicochemical and Engineering Aspects*, *384*(1-3), 713-719.

Lin, M. C., & Svitova, T. F. (2010). Contact lenses wettability in vitro: effect of surface-active ingredients. *Optometry and vision science: official publication of the American Academy of Optometry*, *87*(6), 440.

USC
UNIVERSIDADE DE SANTIAGO DE COMPOSTELA

Liu, Y. (2011) Polymerizable Contact Lens Formulations and Contact Lenses Obtained Therefrom. U.S. Patent No. 8,011,784

Losso, J. N., Truax, R. E., & Richard, G. (2010). Trans-resveratrol inhibits hyperglycemia-induced inflammation and connexin downregulation in retinal pigment epithelial cells. *Journal of Agricultural and Food Chemistry*, *58*(14), 8246-8252.

Luensmann, D., & Jones, L. (2012). Protein deposition on contact lenses: the past, the present, and the future. *Contact Lens and Anterior Eye*, *35*(2), 53-64.

Mah, T. F. C., & O'Toole, G. A. (2001). Mechanisms of biofilm resistance to antimicrobial agents. *Trends in Microbiology*, *9*(1), 34-39.

Mayer, C., Muras, A., Romero, M., López, M., Tomás, M., & Otero, A. (2018). Multiple quorum quenching enzymes are active in the nosocomial pathogen *Acinetobacter baumannii* ATCC17978. *Frontiers in Cellular and Infection Microbiology*, *8*, 310.

Moon, J. K., & Shibamoto, T. (2009). Antioxidant assays for plant and food components. *Journal of Agricultural and Food Chemistry*, *57*(5), 1655-1666.

Muras, A., & Otero, A. (2020). Breaking bad: Understanding how bacterial communication regulates biofilm-related oral diseases. *Trends in Quorum Sensing and Quorum Quenching*, 175-185.

Natesan, S., Pandian, S., Ponnusamy, C., Palanichamy, R., Muthusamy, S., & Kandasamy, R. (2017). Co-encapsulated resveratrol and quercetin in chitosan and peg modified chitosan nanoparticles: For efficient intra ocular pressure reduction. *International Journal of Biological Macromolecules*, *104*, 1837-1845.

National Institute of Environmental Health Sciences. (2010). *ICCVAM Test Method Evaluation Report: Current Validation Status of In Vitro Test Methods Proposed for Identifying Eye Injury Hazard Potential of Chemicals*

USC UNIVERSIDADE DE SANTIAGO DE COMPOSTELA

and Products (Vol. 7553). Appendix B3, *National Institute of Enviromental Health Sciences*: Durham, NC, USA. Publication No. 10.

Nicolson, P. C., & Vogt, J. (2001). Soft contact lens polymers: an evolution. *Biomaterials*, *22*(24), 3273-3283.

Nøhr-Meldgaard, K., Ovsepian, A., Ingmer, H., & Vestergaard, M. (2018). Resveratrol enhances the efficacy of aminoglycosides against *Staphylococcus aureus*. *International Journal of Antimicrobial Agents*, *52*(3), 390-396.

Paradiso, P., Galante, R., Santos, L., Alves de Matos, A. P., Colaço, R., Serro, A. P., & Saramago, B. (2014). Comparison of two hydrogel formulations for drug release in ophthalmic lenses. *Journal of Biomedical Materials Research Part B: Applied Biomaterials*, *102*(6), 1170-1180.

Paulo, L., Ferreira, S., Gallardo, E., Queiroz, J. A., & Domingues, F. (2010). Antimicrobial activity and effects of resveratrol on human pathogenic bacteria. *World Journal of Microbiology and Biotechnology*, *26*(8), 1533-1538.

Pimenta, A. F. R., Ascenso, J., Fernandes, J. C. S., Colaço, R., Serro, A. P., & Saramago, B. (2016). Controlled drug release from hydrogels for contact lenses: Drug partitioning and diffusion. *International Journal of Pharmaceutics*, *515*(1-2), 467-475.

Qin, N., Tan, X., Jiao, Y., Liu, L., Zhao, W., Yang, S., & Jia, A. (2014). RNA-Seq-based transcriptome analysis of methicillin-resistant *Staphylococcus aureus* biofilm inhibition by ursolic acid and resveratrol. *Scientific reports*, *4*(1), 1-9.

Richter, K., Van den Driessche, F., & Coenye, T. (2017). Innovative approaches to treat *Staphylococcus aureus* biofilm-related infections. *Essays in biochemistry*, *61*(1), 61-70.

USC
UNIVERSIDADE DE SANTIAGO DE COMPOSTELA

Robertson, D. M. (2013). The effects of silicone hydrogel lens wear on the corneal epithelium and risk for microbial keratitis. *Eye & Contact Lens*, *39*(1), 67.

Sanchez, I., Carmona, F. J., Gonzalez-Puertas, S., Valiente, A., & Martin, R. (2020). Intrasession repeatability of the contact angle measured using the captive bubble method and agreement assessed between different analysis software programs. *Eye & Contact Lens*, *46*(6), 385-390.

Sekar, P., Dixon, P. J., & Chauhan, A. (2019). Pigmented contact lenses for managing ocular disorders. *International Journal of Pharmaceutics*, *555*, 184-197.

Shimamura, Y., Hirai, C., Sugiyama, Y., Shibata, M., Ozaki, J., Murata, M., ... & Masuda, S. (2017). Inhibitory effects of food additives derived from polyphenols on staphylococcal enterotoxin A production and biofilm formation by *Staphylococcus aureus*. *Bioscience, Biotechnology, and Biochemistry*, *81*(12), 2346-2352.

Shimizu, T., Goda, T., Minoura, N., Takai, M., & Ishihara, K. (2010). Super-hydrophilic silicone hydrogels with interpenetrating poly (2-methacryloyloxyethyl phosphorylcholine) networks. *Biomaterials*, *31*(12), 3274-3280.

Silva, D., de Sousa, H. C., Gil, M. H., Santos, L. F., Amaral, R. A., Saraiva, J. A., ... & Saramago, B. (2021). Imprinted hydrogels with LbL coating for dual drug release from soft contact lenses materials. *Materials Science and Engineering: C*, *120*, 111687.

Silva, D., de Sousa, H. C., Gil, M. H., Santos, L. F., Moutinho, G. M., Serro, A. P., & Saramago, B. (2018). Antibacterial layer-by-layer coatings to control drug release from soft contact lenses material. *International journal of Pharmaceutics*, *553*(1-2), 186-200.

Silva, C. G., Monteiro, J., Marques, R. R., Silva, A. M., Martínez, C., Canle, M., & Faria, J. L. (2013). Photochemical and photocatalytic degradation of

USC UNIVERSIDADE DE SANTIAGO DE COMPOSTELA

trans-resveratrol. *Photochemical & Photobiological Sciences*, *12*(4), 638-644.

Silva, D., Pinto, L. F., Bozukova, D., Santos, L. F., Serro, A. P., & Saramago, B. (2016). Chitosan/alginate based multilayers to control drug release from ophthalmic lens. *Colloids and Surfaces B: Biointerfaces*, *147*, 81-89.

Stepanenko, A. A., & Dmitrenko, V. V. (2015). Pitfalls of the MTT assay: Direct and off-target effects of inhibitors can result in over/underestimation of cell viability. *Gene*, *574*(2), 193-203.

Subramanian, M., Goswami, M., Chakraborty, S., & Jawali, N. (2014). Resveratrol induced inhibition of Escherichia coli proceeds via membrane oxidation and independent of diffusible reactive oxygen species generation. *Redox Biology*, *2*, 865-872.

Tan, X., Zhan, J., Zhu, Y., Cao, J., Wang, L., Liu, S., ... & Ren, L. (2017). Improvement of uveal and capsular biocompatibility of hydrophobic acrylic intraocular lens by surface grafting with 2-methacryloyloxyethyl phosphorylcholine-methacrylic acid copolymer. *Scientific Reports*, *7*(1), 1-13.

Teichroeb, J. H., Forrest, J. A., Jones, L. W., Chan, J., & Dalton, K. (2008). Quartz crystal microbalance study of protein adsorption kinetics on poly (2-hydroxyethyl methacrylate). *Journal of Colloid and Interface Science*, *325*(1), 157-164.

Tieppo, A., Boggs, A. C., Pourjavad, P., & Byrne, M. E. (2014). Analysis of release kinetics of ocular therapeutics from drug releasing contact lenses: best methods and practices to advance the field. *Contact Lens and Anterior Eye*, *37*(4), 305-313.

Tran, N. P. D., & Yang, M. C. (2019). Synthesis and characterization of silicone contact lenses based on TRIS-DMA-NVP-HEMA hydrogels. *Polymers*, *11*(6), 944.

USC
UNIVERSIDADE DE SANTIAGO DE COMPOSTELA

Vales, T. P., Jee, J. P., Lee, W. Y., Cho, S., Lee, G. M., Kim, H. J., & Kim, J. S. (2020). Development of poly (2-methacryloyloxyethyl phosphorylcholine)-functionalized hydrogels for reducing protein and bacterial adsorption. *Materials*, *13*(4), 943.

Van Meerloo, J., Kaspers, G. J., & Cloos, J. (2011). Cell sensitivity assays: the MTT assay. *Cancer Cell Culture* , 237-245

Varela-Garcia, A., Concheiro, A., & Alvarez-Lorenzo, C. (2020). Cytosine-functionalized bioinspired hydrogels for ocular delivery of antioxidant transferulic acid. *Biomaterials Science*, *8*(4), 1171-1180.

Vasavi, H. S., Sudeep, H. V., Lingaraju, H. B., & Prasad, K. S. (2017). Bioavailability-enhanced Resveramax™ modulates quorum sensing and inhibits biofilm formation in *Pseudomonas aeruginosa* PAO1. *Microbial pathogenesis*, *104*, 64-71.

Vivero-Lopez, M., Xu, X., Muras, A., Otero, A., Concheiro, A., Gaisford, S., ... & Goyanes, A. (2021). Anti-biofilm multi drug-loaded 3d printed hearing aids. *Materials Science and Engineering: C*, *119*, 111606.

Wang, J., & Li, X. (2011). Enhancing protein resistance of hydrogels based on poly (2-hydroxyethyl methacrylate) and poly (2-methacryloyloxyethyl phosphorylcholine) with interpenetrating network structure. *Journal of Applied Polymer Science*, *121*(6), 3347-3352.

Wang, J. J., & Liu, F. (2011). Photoinduced graft polymerization of 2-methacryloyloxyethyl phosphorylcholine on silicone hydrogels for reducing protein adsorption. *Journal of Materials Science: Materials in Medicine*, *22*(12), 2651-2657.

Wang, S., Wang, Z., Yang, S., Yin, T., Zhang, Y., Qin, Y., ... & Sun, X. (2017). Tissue distribution of trans-resveratrol and its metabolites after oral administration in human eyes. *Journal of Ophthalmology*, *2017*.

Wang, B., Ye, Z., Tang, Y., Han, Y., Lin, Q., Liu, H., ... & Nan, K. (2017). Fabrication of nonfouling, bactericidal, and bacteria corpse release

USC UNIVERSIDADE DE SANTIAGO DE COMPOSTELA

multifunctional surface through surface-initiated RAFT polymerization. *International Journal of Nanomedicine*, *12*, 111.

Wiley, L., Bridge, D. R., Wiley, L. A., Odom, J. V., Elliott, T., & Olson, J. C. (2012). Bacterial biofilm diversity in contact lens-related disease: emerging role of *Achromobacter*, *Stenotrophomonas*, and *Delftia*. *Investigative ophthalmology & visual science*, *53*(7), 3896-3905.

Willcox, M. D. P., Harmis, N., Cowell, B. A., Williams, T., & Holden, B. A. (2001). Bacterial interactions with contact lenses; effects of lens material, lens wear and microbial physiology. *Biomaterials*, *22*(24), 3235-3247.

Xu, L., Ma, P., Yuan, B., Chen, Q., Lin, S., Chen, X., ... & Shen, J. (2014). Anti-biofouling contact lenses bearing surface-immobilized layers of zwitterionic polymer by one-step modification. *RSC Advances*, *4*(29), 15030-15035.

Yang, J & Mattison, K. P(2003). Protein characterization using dynamic and static light scattering. *China Particuology*, *1*, 219–222

Zhang, N., Zhang, K., Melo, M. A. S., Chen, C., Fouad, A. F., Bai, Y., & Xu, H. H. (2016). Novel protein-repellent and biofilm-repellent orthodontic cement containing 2-methacryloyloxyethyl phosphorylcholine. *Journal of Biomedical Materials Research Part B: Applied Biomaterials*, *104*(5), 949-959.

Zegans, M. E., Shanks, R. M., & O'toole, G. A. (2005). Bacterial biofilms and ocular infections. *The Ocular Surface*, *3*(2), 73-80.

Zhou, J. W., Chen, T. T., Tan, X. J., Sheng, J. Y., & Jia, A. Q. (2018). Can the quorum sensing inhibitor resveratrol function as an aminoglycoside antibiotic accelerant against *Pseudomonas aeruginosa*?. *International Journal of Antimicrobial Agents*, *52*(1), 35-41.

Zupančič, Š., Lavrič, Z., & Kristl, J. (2015). Stability and solubility of trans-resveratrol are strongly influenced by pH and temperature. *European Journal of Pharmaceutics and Biopharmaceutics*, *93*, 196-204.

USC
UNIVERSIDADE DE SANTIAGO DE COMPOSTELA

Chapter 5

USC
UNIVERSIDADE
DE SANTIAGO
DE COMPOSTELA

USC
UNIVERSIDADE
DE SANTIAGO
DE COMPOSTELA

5. RESVERATROL-LOADED CONTACT LENSES: *IN VITRO* RELEASE AND *IN VIVO* PERFORMANCE

5.1 INTRODUCTION

Nowadays, more than 140 million people wear contact lenses (CLs) worldwide and the number of wearers is expected to increase further in the future considering the improvements that are constantly being made in the design of CL materials and the new therapeutical applications of CLs like drug release systems [Pucker and Tichenor, 2020; Toffoletto et al., 2020; DiPasquale et al., 2021; Tahhan et al., 2021]. Despite these improvements to prepare CLs that are more and more comfortable and offer better visual acuity, the incidence of microbial-related ocular diseases has not decreased [Dutta et al., 2014]. The tendency of CLs to form bacterial biofilms on their surface may cause severe ocular infections like microbial keratitis which can lead to vision impairment and even blindness [Fleiszig et al., 2020]. CL wearing continues to be the principal risk factor for the development of microbial keratitis [Xiao et al., 2018; Khan and Lee, 2020]. Moreover, the presence of the CL on the ocular surface can damage the corneal epithelium and interfere with tearing and blinking facilitating the development of microbial keratitis [Robertson, 2013; Bispo et al., 2015; Fleiszig et al., 2020]. Therefore, there is an urgent

USC UNIVERSIDADE DE SANTIAGO DE COMPOSTELA

need of developing new CLs with antibiofilm performances to decrease the incidence of ocular infections associated to their use [Khan and Lee, 2020].

Recently, in our research group two strategies to endow CLs with antibiofilm features have been evaluated, as described in **Chapter 4**. (i) The incorporation of antibiofouling monomer 2-methacryloyloxyethyl phosphorylcholine (MPC) **(Figure 5.1)** to silicone and pHEMA-based hydrogels did not only endow the CLs with antibiofilm properties [Vivero-Lopez et al., 2021], but it also increased the wettability of the CLs, which may make them more comfortable to the wearers, and attenuated the adhesion of proteins on the surface of the hydrogels [Huang et al., 2007; Xu et al., 2014]. MPC was incorporated in the monomers mixture in the concentration range of 0 to 101 mM (**Chapter 4**). And (ii) the loading of the natural antioxidant compound resveratrol (trans-3,5,4'-trihydroxystilbene) **(Figure 5.1)** with good ocular tolerance and known antibacterial activity against the Gram-negative *Pseudomonas aeruginosa* and the Gram-positive *Staphylococcus aureus* [Qin et al., 2014; Zhou et al., 2018], responsible of most of the bacterial biofilms implicated in microbial keratitis [Dutta and Willcox, 2014; El-Ganiny et al., 2017; Fleiszig et al., 2020]. Moreover, associated to its antioxidant activity, resveratrol may help to prevent a variety of oxidative-stress related eye diseases and aid in the healing of corneal epithelial cells [Tsai et al., 2015].

Compared to silicone hydrogels, HEMA-based hydrogels loaded lower amounts of resveratrol but could release the total dose loaded avoiding irreversible binding found for silicone hydrogels. Resveratrol was shown to preserve its antioxidant features once delivered from the hydrogels and accumulated into corneal and scleral tissues in *ex vivo* experiments in porcine tissues (**Chapter 4**) [Vivero-Lopez et at.,

USC UNIVERSIDADE DE SANTIAGO DE COMPOSTELA

2021]. Nevertheless, the antibiofilm and antioxidant performances were not fully satisfactory probably because the MPC content was limited to 101 mM because of lack of miscibility with silicone macromers.

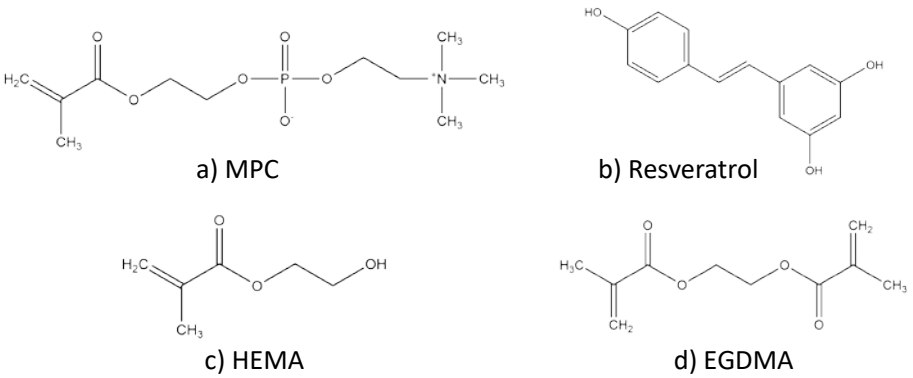


Figure 5.1. Chemical structure of a) 2-methacryloyloxyethyl phosphorylcholine (MPC), b) *trans*-resveratrol, c) 2-hydroxyethylmethacrylate (HEMA), and d) ethylene glycol dimethacrylate (EGDMA).

This part of the Thesis is based on the hypothesis that increasing the MPC content could improve the amount of resveratrol loaded and released from the CLs, optimizing the antibiofilm and antioxidant properties of the material and allowing the treatment and prevention of eye infections and ocular pathologies associated with oxidative stress. The optimized CLs could provide a sustained controlled release of resveratrol on the cornea avoiding its premature clearance and facilitating its access to posterior tissues of the eye like aqueous and vitreous humors. Thus, the aim of this part of the Thesis was to improve the antibiofilm capacity of the CLs by increasing the content

USC UNIVERSIDADE DE SANTIAGO DE COMPOSTELA

in MPC and to investigate their capability to release therapeutically relevant amounts of resveratrol to the eye tissues.

To carry out the work, HEMA-based hydrogels were synthesized with higher proportions of MPC than in **Chapter 4**. The loading and release profiles of resveratrol were evaluated before and after the sterilization of the CLs by steam heat. Searching for biorelevant release medium, the effect of adding proteins commonly present in tear fluid on the release profiles was investigated. Then, after successful preliminary studies of biocompatibility, an *in vivo* test in New Zealand white rabbits was carried out in collaboration with the team of Prof. Gonzalo Carracedo at Ocupharm and University Complutense of Madrid to determine the safety and ocular tolerance of the developed CLs and the resveratrol accumulation in eye tissues. The experiments fulfilled 3R's principles and had the corresponding permission of the Ethics Committee, Finally, correlations between the release profiles of resveratrol *in vitro* and *in vivo* were investigated, and levels of resveratrol in different eye tissues were analyzed from the perspective of potential antioxidant and antimicrobial properties. To the best of our knowledge, this is the first time that resveratrol-loaded CLs are evaluated *in vivo* and that *in vitro-in vivo* correlations are attempted.

5.2 MATERIALS AND METHODS

5.2.1 Materials

2-Hydroxyethyl methacrylate (HEMA) was from Merck KGaA (Darmstadt, Germany); 2-methacryloyloxyethyl phosphorylcholine (MPC), ethylene glycol dimethacrylate (EGDMA), 2,2'-azobis(2-methylpropionitrile) (AIBN) and albumin from bovine serum were

USC UNIVERSIDADE DE SANTIAGO DE COMPOSTELA

from Sigma-Aldrich (St. Luois, MO, USA). Lysozyme from egg white was from Fluka Analytical (Germany). Resveratrol was from ChemCruz, Santa Cruz Biotechnology Inc. (Dallas, TX, USA). Sodium chloride (NaCl) was from Labkem (Barcelona, Spain). Sodium bicarbonate ($NaHCO_3$) was from Probus S.A. (Barcelona, Spain). Calcium chloride dihydrate ($CaCl_2 \cdot 2H_2O$) was from Merck KGaA (Darmstadt, Germany). Potassium chloride (KCl) was from Scharlab S.L. (Barcelona, Spain). Ethanol absolute pure was from PanReac AppliChem ITW Reagents (Barcelona, Spain). Methanol 99.9% for LC-MS grade was from Fisher Scientific (Loughborough, UK). Acetonitrile for HPLC LC-MS grade was from VWR Chemicals (Fontenary-Sous-Bois, France). Ultrapure water (resistivity > 18.2 MΩ·cm) was obtained by reverse osmosis (MilliQ®, Millipore Ibérica, Madrid, Spain). Simulated lachrymal fluid (SLF) pH 7.4 was prepared as follows: 6.78 g/L NaCl, 2.18 g/L $NaHCO_3$, 1.38 g/L KCl and 0.084 g/L $CaCl_2 2H_2O$ [Alvarez-Rivera et al., 2019]. Phosphate buffer pH 7.4 was prepared with 8.30 g of NaCl, 0.406 g of NaH_2PO_4 and 2.376 g of Na_2HPO_4 for 1 L (UNE-EN ISO 18369-3:2018). Schirmer test strips were from Contactcare Ophthalmics and Diagnostics (Gujarat, India).

5.2.2 Contact lenses preparation

CLs were synthesized by adding 3 mL of HEMA into a vial containing 337.5 mg of MPC at room temperature under magnetic stirring (150 rpm) for 1 h. EGDMA (12.10 µL) and AIBN (32.85 mg) were added later as crosslinker and initiator, respectively. The system was kept under magnetic stirring at 150 rpm for 30 min more to ensure the complete dissolution of the AIBN. Then, 60 µL of this monomers solution were placed in curved polypropylene molds (n =

USC UNIVERSIDADE DE SANTIAGO DE COMPOSTELA

20) and the polymerization was carried out at 50 °C for 12 h and 70 °C for other 24 h. After polymerization, the CLs were hydrated in MilliQ® water (1 L) to be later demolded and alternatively washed under magnetic stirring (130 rpm) in 500 mL of MilliQ® water and NaCl 0.9%, at least three times per day. Complete removal of unreacted monomers was monitored by measuring the absorbance of aliquots of the washing medium (UV-Vis spectrophotometer Agilent 8453, Waldbronn, Germany). The dimensions of the CLs obtained in the hydrated state in phosphate buffer pH 7.4 (100.6 ± 1.7 % water content) were 14.1 ± 0.1 mm diameter, 8.8 ± 0.1 mm curvature, and 0.1 ± 0.0 mm thickness. Finally, the CLs were washed in 1 L of MilliQ® water to remove the phosphate buffer pH 7.4 and dried at 40 °C for 2 h and 70°C for 2 h to be used in further experiments.

5.2.3 Resveratrol loading and release tests

5.2.3.1 Loading of resveratrol in non-sterilized and sterilized CLs

The loading of resveratrol in non-sterilized CLs was carried out by soaking dried CLs (37 °C, 24 h, 17 mg weight) in 15 mL Falcon® tubes with 7 mL of a 100 µg/mL resveratrol in ethanol:water 10:90 v/v solution, as previously described (**Chapter 4**) [Vivero-Lopez et al., 2021]. The Falcon® tubes were kept protected from light, to avoid resveratrol degradation, at 36 °C and 180 rpm for 24 h in an incubating shaker (Incubator 1000, Heidolph, Germany). The absorbance of the loading medium was measured every 2 h for the first 8 h and then at 24 h at 305 nm (UV-Vis spectrophotometer Agilent 8534, Waldbronn, Germany) after leveling the aliquots (250 µL for the first 8 h and 500 µL after) to 5 mL with ethanol:water 10:90 v/v. The amount of resveratrol loaded was assessed from the

USC UNIVERSIDADE DE SANTIAGO DE COMPOSTELA

difference between the initial and final amount of resveratrol in the loading solution using a validated calibration curve of resveratrol in the same medium and considering the amount of resveratrol lost in the monitoring.

Then, the loading of resveratrol in sterilized CLs was carried out. Dried CLs (37 °C, 24 h, 24 mg weight) were sterilized in 15 mL Falcon® tubes in an autoclave at 121 °C and 1 atm for 20 min (Raypa Steam Sterilizer, Terrassa, Spain). Immediately after, 7 mL of resveratrol in ethanol:water 10:90 v/v solution (100 µg/mL) previously filtered (0.22 µm, polyethersulfone syringe filter, Filter-Lab®, Barcelona, Spain) were added to the tubes containing the sterilized CLs under sterile conditions in a biological safety cabinet. The loading was carried out as explained above at 36 °C and 180 rpm for 24 - 48 h without intermediate measurements. These experiments were carried out at least in triplicate.

5.2.3.2 *In vitro* release of resveratrol from loaded CLs

The release from both, sterilized and non-sterilized CLs was performed in the same way. After the loading, the CLs were rinsed with NaCl 0.9% and placed into 15 mL Falcon® tubes with 6 mL of NaCl 0.9%. The release was carried out protected from light at 36 °C and 180 rpm for 24 h in an incubating shaker (Incubator 1000, Unimax 1010). The absorbance of the release medium was measured at 305 nm (UV-Vis spectrophotometer Agilent 8534, Waldbronn, Germany) by taking aliquots of 3 mL at times 5, 15 and 30 min that were immediately returned to the Falcon® tubes after the measurement. After that, aliquots of 1 mL were taken at times 1, 2, 3, 4, 5, 6, 7, 8, 9, 10 and 24 h, which were replaced with the same volume of NaCl 0.9% fresh solution, except at 8 h that 6 mL more of NaCl 0.9% fresh solution were added increasing the release medium

USC UNIVERSIDADE DE SANTIAGO DE COMPOSTELA

in all tubes to 12 mL to avoid the saturation of the medium and false plateaus. The amount of resveratrol released from the CLs was quantified using a validated calibration curve of resveratrol in NaCl 0.9% and considering the amounts removed and the corresponding dilution of the samples.

Release experiments in the presence of lysozyme or bovine serum albumin (BSA) were also carried out by immersing the resveratrol-loaded sterilized CLs in 6 mL of NaCl 0.9% with or without 2.68 mg/mL of BSA and lysozyme [Marques et al., 2011]. The release experiment was carried out following the protocol described above but removing (200 µL) of the release medium at each time and replacing with the same volume of fresh medium (NaCl 0.9% or NaCl 0.9% plus lysozyme or BSA). The amount of resveratrol released was quantified, previous dilution of the samples in ethanol:water 50:50 v/v, using a JASCO (Tokyo, Japan) HPLC (AS-4140 autosampler, PU-4180 pump, LC-NetII/ADC interface box, CO-4060 Column oven, MD-4010 photodiode array detector), fitted with a C18 column (Waters Symmetry C18, 5 µm, 4.6 x 250 mm) and operated with ChromNAV software (JASCO, Tokyo, Japan). In the case of the protein-containing medium, denaturation was carried out as explained below in 5.2.4.2. The analysis was carried out by isocratic elution using a phase mobile of methanol:water 50:50 v/v at a flow rate of 1 mL/min, 35 °C and with 8 min of run time. The injection volume was 50 µL and the UV detector was set at 305 nm. Retention time was 4.6 min. Validation of the method was performed using a calibration curve of resveratrol in ethanol:water 50:50 v/v in the 0.05 – 6 µg/mL range. All release experiments were performed at least in triplicate.

USC
UNIVERSIDADE DE SANTIAGO DE COMPOSTELA

5.2.4 *In vivo* experiments: resveratrol released and accumulated in the ocular tissues

All *in vivo* experiments were carried out following the Association for Research in Vision and Ophthalmology (ARVO) Statement for the Use of Animals in Ophthalmic and Vision Research and the European Directive 2010/63/EU. Moreover, the Committee for Animal Experimentation of the University Complutense of Madrid approved the protocols carried out [Registration number: O00023280e2100023620]. The study was supported by Grupo de Referencia Competitiva (2020 GRC I+D FARMA; ED431C 2020/17). The founder had no role in the study.

Male New Zealand white rabbits (4.11 ± 0.53 Kg) included in the experiments were stabled in individual cages with total access to food and water at 18 °C and 30% relative humidity inside a light-controlled room with 12 h light-dark cycles. Rabbits with low weight, illness or corneal disruptions were discarded.

The rabbits (n = 10) were divided into two groups: one group to be treated with CLs (CLs group, n = 6), and one group to be treated with eye drops (eye drops group, n = 4). In the eye drops group, after 8 h of experiment the rabbits were euthanized. CLs group was divided into two other subgroups, one with rabbits (n = 3) that wore the CLs for 8 h and were euthanized after this period, and the other one with rabbits (n = 3) that wore the CLs for 10 h and were euthanized after 24 h (**Figure 5.2**).

To minimize the effects of subjective bias, the experiments were carried out in three days and the rabbits where randomly assigned to each assay day. The first day, two rabbits of 8h wear CLs, and one rabbit of eye drop groups were assayed. The second day, one rabbit of 8h wear CLs and three rabbits of the eye drop groups were assayed.

USC UNIVERSIDADE DE SANTIAGO DE COMPOSTELA

The third day, the three rabbits of 10 h wear CLs group were assayed. All experiments started at 7:30 – 8:30 a.m. No animal or data was discarded. No adverse events were detected.

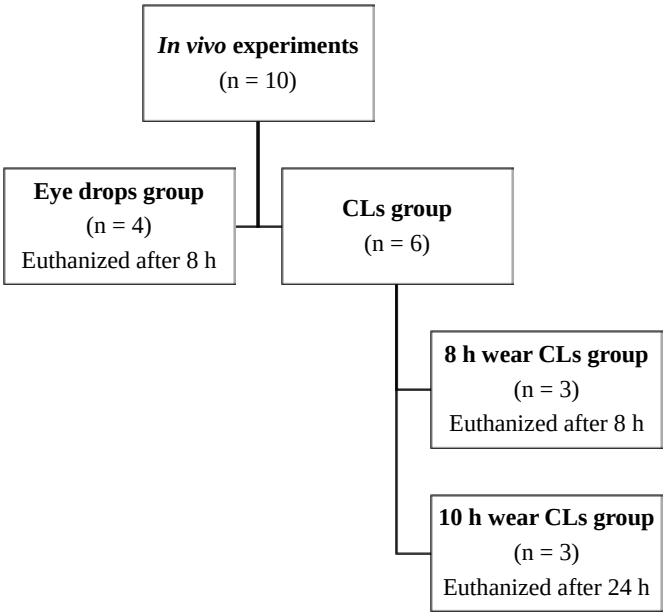


Figure 5.2. Distribution of the animals for *in vivo* experiments.

5.2.4.1 *In vivo* release

In the CLs group, dried CLs were sterilized in 15 mL Falcon® tubes by steam heat following the protocol described above. After sterilization, CLs were stored at room temperature until being loaded. The loading was carried out for 48 (8 h wear CLs group) or 72 h (10 h wear CLs group) following the protocol described in section 5.2.3.1. Then, the CLs were removed from the loading solution, rinsed with sterile saline solution (Avizor sterile saline unidose 5 mL) and placed

USC UNIVERSIDADE DE SANTIAGO DE COMPOSTELA

on the right eye cornea below the nictitating membrane without local anesthesia. The rabbits were maintained in rabbit restrainers with continuously monitoring to not remove the CLs placed on the ocular surface. Moreover, the eyes of the rabbits were closed every few minutes to ensure the hydration of the CLs.

In the eye drops group, a single drop (50 µL) of a 4 mg/mL resveratrol-loaded 10 mM Pluronic® F127 dispersion (named as P10R) was gently instilled in the lower conjunctival sac of the right eye using a micropipette. The amount of resveratrol loaded in the dispersion was fix considering the amount of resveratrol loaded by the CLs. The preparation of the P10R dispersion was carried out as described in the **Chapter 6** of this Thesis.

For both groups, the ocular surface of the rabbits was carefully observed with a VX75 slit lamp (Luneau Technology, Chartres, France) before the beginning of the experiment and at the end. Samples of tear fluid were collected before and after administration (t = 5 min, 15 min, 30 min, and every hour for 8 to 10 h) using Schirmer test strips which were placed in the tarsal conjunctiva of the inferior lid for 10 s with closed eyes to avoid the reflex secretion associated with blinking [Whittaker and Williams, 2015]. The volume collected was recorded looking at the millimeters of wetted strip. Left eyes of all rabbits acted as controls without treatment.

5.2.4.2 Quantification of resveratrol in the tear fluid

The Schirmer test strips were cut into small pieces and placed protected from light into 1.5 mL Eppendorf® tubes to which 200 µL of ethanol:water 50:50 v/v solution were added. The tubes were vortexed for 1 min and left in the fridge at 4 °C for approximately 15 h. Then, the samples were vortexed again for 2 min and the strips removed from the tubes. Protein denaturation was performed by heating the

USC UNIVERSIDADE DE SANTIAGO DE COMPOSTELA

tubes with the ethanol:water 50:50 v/v solution at 98 °C for 2 min. The tubes were then placed in an ice bath for 10 min and centrifuged at 13,000 rpm for 10 min at 25 °C. Finally, the supernatants were collected and stored at -80 °C until HPLC analysis, as described in section 5.2.3.3.

In vitro – in vivo correlations (IVIVC) were investigated using Levy plot analysis, representing the percentage of resveratrol released *in vitro* at a certain time (X-axis) *vs.* the percentage of resveratrol released in the lachrymal fluid at the same time (Y-axis) calculated using the following equation [Xu et al., 2019]:

$$In\ vivo\ drug\ release\ (\%) = \left(\frac{AUC_{0-t}}{AUC_{0-last}}\right) \times 100$$

5.2.4.3 Quantification of resveratrol in the ocular tissues

After the experiments, all rabbits were euthanized by intravenous injection of 0.75 mL/Kg of propofol and 0.5 mL/Kg of pentobarbital sodium (Exagon 400 mg/mL). Then, the aqueous humor of both eyes was directly extracted from the anterior chamber with an insulin needle in 1.5 mL Eppendorf® tubes. The eyes were enucleated and immediately stored in 50 mL Falcon® tubes at -80 °C until being dissected. The dissection was carried out separating cornea, crystalline lens, vitreous humor, retina and sclera in 1.5 mL Eppendorf® tubes. Ethanol:water 50:50 v/v was added to cornea (500 µL), crystalline lens (500 µL), sclera (800 µL) and retina (200 µL). All Eppendorf® tubes were kept in the fridge protected from light at 4 °C for 12 h and then the protein denaturation process was carried out as described above. The supernatants stored at -80 °C until UPLC analysis. Before UPLC analysis all samples were diluted 1.5 times with acetronitrile and mixed using an Automated Liquid Handling System, Caliper

USC UNIVERSIDADE DE SANTIAGO DE COMPOSTELA

Zephyr, 3 cycles of 50 µL at 78 µL/s. The plate was then centrifuged at 3700 rpm at 4ºC for 30 min. The quantification of resveratrol in the different tissues was carried out using a Waters Acquity UPLC H-Class coupled with a Xevo TQD MS System fitted with an HypersilGOLD C18 column (1.9 µm 2.1 x 50 mm, Thermo-Fischer) with a column temperature of 35 °C. The analysis was done by gradient elution using water + 0.1% formic acid as solvent A, and acetonitrile + 0.1% formic acid as solvent B, as follows: 0–0.1min 5% B, 0.1-1.0 min 5–100% B, 1.0–2.0 min 100% B, 2.0-2.1 min 100-95% B, and 2.1–2.5 min 5% B, and at a flow rate of 0.6 mL/min. Electrospray ionization (ESI) was run in positive mode with a source temperature of 150 °C and a desolvation temperature of 500 °C. Capillary voltage was set to 3 kV and the cone voltage was set to 45 V. Desolvation gas flow was 900 L/h and cone gas flow was set to 50 L/h. The compound of interest was monitored using multiple reaction monitoring (MRM)/ES+ mode Precursor and product ion transition for analyte resveratrol 229.045 > 106.993 was monitored. The injection volume was 4 µL and the retention time was 1.18 min.

5.2.4.4 Quantification of the antioxidant activity of resveratrol remaining in CLs after the *in vivo* wearing

The assay was developed as previously described in **Chapter 4** with slight modifications. After the *in vivo* experiment the CLs were stored in closed vials at room temperature and protected from light for a few days to be later immersed in 3 mL of ethanol:water 50:50 v/v solution to extract the remnant amount of resveratrol inside the lenses at 36 °C and 180 rpm for 4 h (Incubator 1000, Heidolph, Germany). To carry out the test, a 0.026 mM DPPH solution (50 mL) in ethanol was freshly prepared and stored protected from light. Then, an aliquot of the extraction medium (500 µL) was mixed with the same volume of DPPH solution and vortexed for 5 s. The absorbance was measured

USC UNIVERSIDADE DE SANTIAGO DE COMPOSTELA

at 517 nm (UV-Vis spectrophotometer Agilent 8534, Germany) after 30 min of incubation in darkness. The antioxidant activity of the ethanol:water 50:50 v/v solution without resveratrol was also measured and act as control. The test was carried out in triplicate for 8 h wear CLs, 10 h wear CLs and controls. The DPPH scavenging capacity was expressed as µg/mL of DPPH in the reaction medium calculated from a previously developed and validated calibration curve of DPPH in ethanol (2.56 – 20.5 µg/mL) and as DPPH scavenging effect in percentage through the following equation where A_c and A_s are the absorbance at 517 nm of the controls and extraction medium respectively.

$$DPPH\ scavenging\ effect\ (\%) = \left(1 - \frac{A_s}{A_c}\right) \times 100$$

5.2.5 Statistical analysis

Differences between formulations on resveratrol levels in tear fluid and eye tissues were analyzed using ANOVA and multiple range test with software Statgraphics Centurion 18, v. 18.1.13 (StatPoint Technologies Inc., Warrenton VA, USA).

5.3. RESULTS AND DISCUSSION

5.3.1. Contact lenses preparation and resveratrol loading

CLs were synthesized using an MPC content of 381 mM, which was 3.8 times higher than the proportion tested in **Chapter 4** and the proportion used to prepare commercially available Proclear® 1 day CLs [Liu, 2011]. It is expected that the increased content in MPC, compared to the 101 mM tested in **Chapter 4**, may improve the

USC UNIVERSIDADE DE SANTIAGO DE COMPOSTELA

loading and release of resveratrol and the antibiofilm properties of HEMA-based hydrogels. Moreover, MPC presents ideal characteristics to improve the comfort of the CLs due to its capacity to enhance the wettability and biocompatibility of the material, to protect corneal cells from damage, and to decrease protein adsorption and microorganisms adherence [Goda and Ishihara, 2006; Goda et al., 2015; Ishihara, 2019; Olivieri et al., 2021]. In the present part of this Thesis, unlike most of previously published works, the incorporation of MPC was carried out by adding it as a comonomer during the synthesis and not as a surface component of post-synthesis-modified materials [Vales et al., 2020; Ishihara et al., 2021; Shi et al., 2021]. The chosen MPC proportion easily dissolved in the HEMA solution under magnetic stirring at 150 rpm for 1 h. MPC proportions above 400 mM required long time to be dissolved and thus were discarded. The amounts of AIBN and EGDMA were also increased in comparison with previously synthesized hydrogels containing MPC to ensure the complete polymerization of the thinner CLs.

Resveratrol loading was carried out for both, sterilized and non-sterilized CLs by soaking in 7 mL of a 100 μg/mL resveratrol in ethanol:water 10:90 v/v solution with the aim to elucidate whether the sterilization process could affect the total amount of resveratrol loaded. The loading and sterilization of the CLs could not be carried out as a single step due to thermal degradation of resveratrol [Zupancic et al., 2015; da Silva et al., 2017]. The loading was carried out for at least 24 h, but equilibrium was attained in less than 6 h **(Figure 5.3)**. No differences in the total amount of resveratrol loaded were registered between non-sterilized (10.73 ± 0.96 mg/g) and sterilized CLs for 24 h (10.56 ± 0.20 mg/g) or 48 h (11.45 ± 0.78) loading. In addition, intermediate sampling with the consequent loss of minor amounts of resveratrol from the loading medium did not

USC UNIVERSIDADE DE SANTIAGO DE COMPOSTELA

significantly affect the total amount loaded. The amount of resveratrol loaded was higher than for previously developed silicone or HEMA-based hydrogels (reported in **Chapter 4**) which could be due to the increase in lens wettability produced by MPC (100.6 ± 1.7 % water content) and also to an increase in the affinity of the network for resveratrol ($K_{N/W}$ = 111.8 ± 1.8) [Wang et al., 2011; Shimizu et al., 2010].

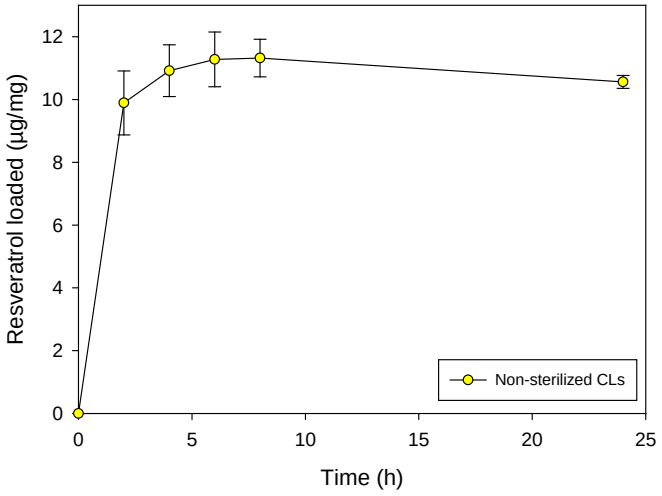


Figure 5.3. Resveratrol loading profile of non-sterilized CLs at 36 °C and 180 rpm for 24 h.

5.3.2 Release of resveratrol from loaded CLs

The release of resveratrol was tested using both sterilized and non-sterilized CLs and with/without the presence of proteins in the release medium (6 mL). The volume of the release medium was incremented to 12 mL after 8 h to avoid saturation and artifact plateaus considering the solubility of resveratrol in NaCl 0.9% (27.4 ±

USC UNIVERSIDADE DE SANTIAGO DE COMPOSTELA

1.4 µg/mL). Although all CLs loaded similar amounts of resveratrol, the total amount of resveratrol released at 24 h was higher for non-sterilized (9.20 ± 0.31 µg/mg) than for sterilized CLs (7.31 ± 0.59 µg/mg) **(Figure 5.4)**. More sustained release of resveratrol was provided by sterilized CLs. In any case, the CLs sustained the *in vitro* release for 1 day **(Figure 5.4)** and the amount of resveratrol released at 24 h was higher than for previously developed silicone (2.89 ± 0.58 µg/mg; 5.90 ± 0.63 %) or HEMA-based (4.40 ± 0.18 µg/mg; 53.06 ± 4.77 %) hydrogels with a 101 mM content in MPC (**Chapter 4**). Overall, considering that resveratrol levels of 2.28 µg/mL protect retinal epithelial cells from UVA-induced oxidative damage (cell cultures) [Chan et al., 2015] and from hyperglycemia-induced inflammation and gap junction intercellular communication degradation [Losso et al., 2010], the amount of resveratrol released would be enough for therapeutic effects.

USC
UNIVERSIDADE DE SANTIAGO DE COMPOSTELA

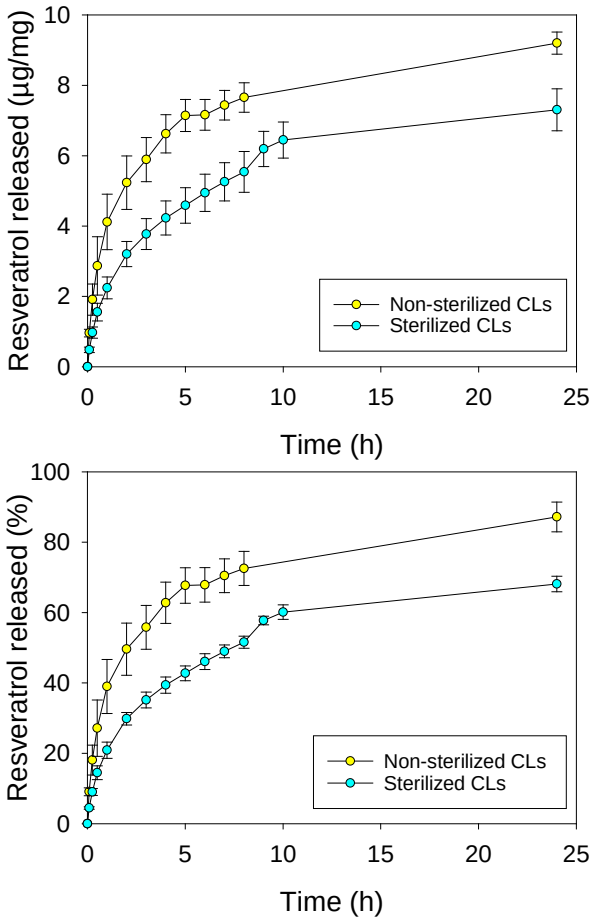


Figure 5.4. Resveratrol release profiles in NaCl 0.9% medium at 36 °C and 180 rpm for 24 h.

A release study in the presence of BSA and lysozyme, two of the major proteins present in the tear fluid, was also carried out for sterilized CLs. The concentration of each protein was fixed to 2.68 mg/mL [Marques et al., 2011]. There were no differences in the release patterns recorded in NaCl 0.9% without proteins (6.44 ± 0.57 µg/mg) and in the presence of lysozyme (6.74 ± 0.75 µg/mg) **(Figure 5.5)**. Differently, the amount of resveratrol released decreased in the

USC UNIVERSIDADE DE SANTIAGO DE COMPOSTELA

presence of BSA; 0.47 ± 0.16 µg/mg at 24 h **(Figure 5.5)**. This correlates with a previously published work, where the amount of moxifloxacin released from Proclear® 1 day CLs also decreased in artificial tear fluid which included albumin in its composition [Lorentz et al., 2011; Phan et al., 2016].

USC UNIVERSIDADE DE SANTIAGO DE COMPOSTELA

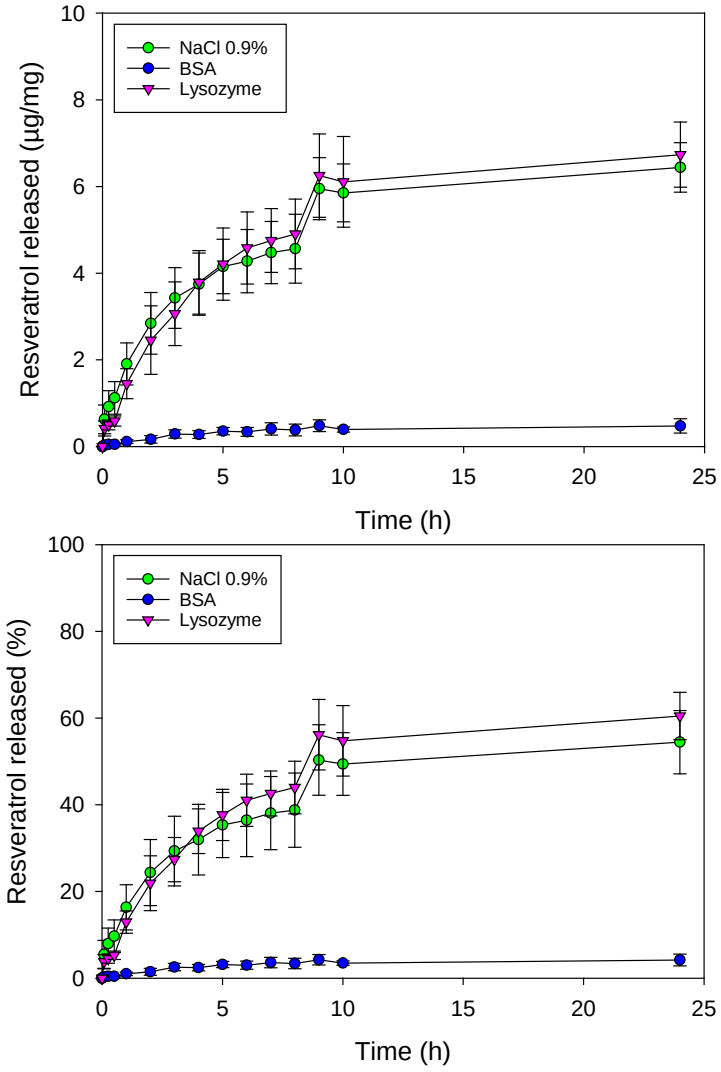


Figure 5.5. Resveratrol release profiles from sterilized CLs in NaCl 0.9% without and with incorporation of lysozyme and bovine serum albumin (BSA). (n=4; mean values and standard deviations).

USC
UNIVERSIDADE DE SANTIAGO DE COMPOSTELA

5.3.3 *In vivo* experiments: resveratrol released and accumulated in the ocular tissues

An *in vivo* experiment using 10 male white New Zealand rabbits was performed to evaluate the capability of the developed CLs to release relevant therapeutical amounts of resveratrol in the tear fluid and the capacity of resveratrol to pass through and accumulate into the different ocular tissues. New Zealand rabbit eyes have been extensively used in ophthalmology research due to their similarity with human eyes [Vézina, 2012; Zernii et al., 2016]. As control, an eye drop formulation was prepared encapsulating resveratrol in Pluronic® micelles (P10R), as explained in detail in **Chapter 6**. Resveratrol solubility in water was too low for being able to supply in one drop the same dose as the amount loaded in the CLs. Thus, solubilization in micelles was needed. It should be noted that this micelle formulation control may facilitate itself drug penetration [Mandal et al., 2017; Grimaudo et al., 2019, Durgun et al., 2020]. Therefore, it should be noted that the CLs were challenged against a formulation that may provide improved outcomes compared to drug solutions in water.

The slit-lamp images of the ocular surface of the rabbits collected, for both groups, before the beginning of the experiment and at the end demonstrated that all formulations were well tolerated. No signs of ocular irritation or damage were observed in the CLs group or eye drops group of rabbits.

USC UNIVERSIDADE DE SANTIAGO DE COMPOSTELA

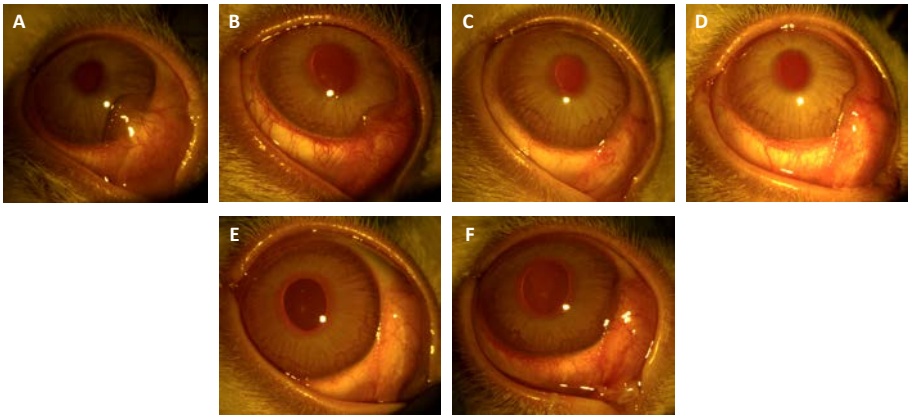


Figure 5.6. Slit-lamp images of rabbit's eyes without treatment before (A, C, E) and after 8 h-wear of the CLs (B), 10 h-wear of the CLs (D) and 8 h the instillation of a single eye drop (4 mg/mL) (F).

The *in vivo* release profiles of resveratrol in tear fluid are shown in **Figure 5.7**. The highest concentration of resveratrol in the rabbit tear fluid was obtained 5 min post-administration of a single drop of P10R. After this point, in the eye drops group, the concentration of resveratrol in the tear fluid was decreasing up to 4 h, where the concentration of resveratrol (8.66 ± 10.40 µg/mL) remained almost constant until the end of the experiment. This correlated well with a previously *in vivo* study where the pharmacological effect of Pluronic® micelles loaded with metipranolol was studied [Lin and Chan, 2013]. All loaded CLs led to lower concentrations of resveratrol at the peak, but the release was sustained over a period of 8 h; the highest concentration was 375.0 ± 207.3 µg/mL at 0.5 h.

USC
UNIVERSIDADE DE SANTIAGO DE COMPOSTELA

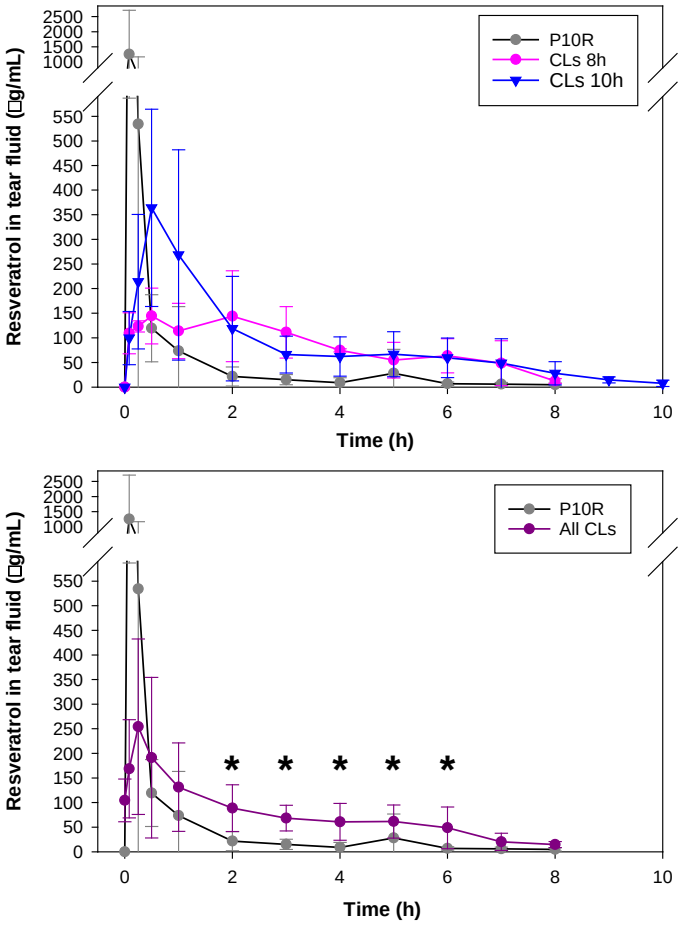


Figure 5.7. *In vivo* tear fluid levels of resveratrol recorded after instillation of one drop of resveratrol-loaded Pluronic® F127 dispersion (50 µL, 4 mg/mL, n = 4) and during wearing of CLs for 8 h (n=3) and 10 h (n=3). In the upper plot the profiles recorded for each CL group are shown in separate. In the plot below, the resveratrol levels recorded for all CLs (n = 6 for 8 h) are shown together (mean values and standard deviations). * Statistical differences ($p < 0.05$) between eye drop group and CL groups.

USC
UNIVERSIDADE DE SANTIAGO DE COMPOSTELA

Statistical analysis of resveratrol levels in tear fluid was carried out by comparing the data recorded after instillation of the eye drop and the data recorded during CLs wearing for 8 h (for all rabbits that wore CLs). ANOVA and multiple range test (Statgraphics Centurion 18, Warrenton VA, USA) revealed that resveratrol-loaded CLs provided notably higher resveratrol levels, compared to the micelle dispersion, at time points 120, 180, 240, 300 and 360 min.

Biodistribution of resveratrol in the anterior and posterior ocular segments was also evaluated (**Figure 5.8**). Resveratrol was detected after all treatments in cornea, aqueous humor, lens, vitreous humor, sclera and retina after 8 h treatment with micelle eye drops and CLs wearing and after 14 h discontinuation of wearing CLs for 10 h.

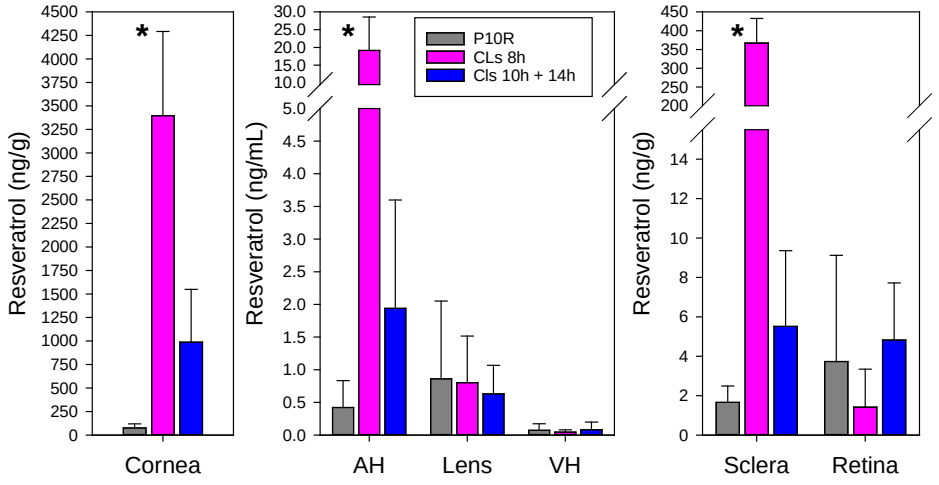


Figure 5.8. Levels of resveratrol in rabbit eye tissues recorded 8 h after instillation of one drop of resveratrol-loaded Pluronic® F127 dispersion (50 µL, 4 mg/mL, n = 4) and after wearing of resveratrol-loaded CLs for 8 h (n = 3), and levels recorded 14 h after discontinuation of resveratrol-loaded CLs that were worn for 10 h (n = 3). The bars represent mean values and standard deviations. * Statistical differences found for CLs worn for 8 h compared to micelle dispersion and CLs worn for 10 h with a clearance period of 14 h ($p < 0.05$).

USC
UNIVERSIDADE DE SANTIAGO DE COMPOSTELA

Wearing of resveratrol-loaded CLs (approx. 200 µg dose) for 8 h provided significantly larger values, compared to the two other treatment groups (in spite the dose was the same), in cornea, sclera, and aqueous humor (ANOVA, p <0.05; multiple range test). This treatment group led to resveratrol levels that ranked in the order cornea (3396 ng/g; s.d. 896) > sclera (367 ng/g; s.d. 65) > aqueous humor (19.2 ng/mL; s.d. 9.4) > retina (1.42 ng/g; s.d. 1.92) > lens (0.80 ng/g; s.d. 0.71) > vitreous humor (0.045 ng/mL; s.d. 0.035). Interestingly after wearing of resveratrol-loaded CLs for 10 h and a subsequent clearance period of 14 h, significant levels of resveratrol were still detected in cornea (987 ng/g; s.d. 561), sclera (5.52 ng/g; s.d. 3.84), retina (4.82 ng/g; 2.90) and aqueous humor (1.94 ng/mL; s.d. 1.66). Thus, compared to the eye drops, the administration of the same dose of resveratrol in CLs allowed for more efficient ocular delivery both regarding sustained supply of resveratrol to the eye surface and access of resveratrol to anterior and posterior segment tissues.

The number of papers reporting on drug levels in tissues after CL wearing (rabbits) is still limited. Ofloxacin levels in ocular tissues were recorded after 1-hour wearing HEMA-based corneal CLs loaded with 282 µg ofloxacin and ranked cornea (~ 60 µg/g) > aqueous humor (~ 10 µg/mL) > sclera (~ 2 µg/g) [Shikamura et al., 2016]. CLs loaded with timolol (277 µg) that were worn for 5 h led to higher levels in cornea (~ 15 µg/g) followed by aqueous humor (~ 6 µg/g) and sclera (~ 3 µg/g) [Maulvi et al., 2019]. Thus, although the values recorded for resveratrol were lower, the tissue concentrations ranked in an order similar to the previous reports. The lower values recorded for resveratrol may be linked to the sampling time of 8 h, in which the CL is almost exhausted and clearance mechanisms may predominate.

USC
UNIVERSIDADE DE SANTIAGO DE COMPOSTELA

5.3.4Antioxidant activity of resveratrol in worn CL

An antioxidant DPPH assay was performed to evaluate the capacity of the CLs to preserve the antioxidant activity of the resveratrol remaining in the polymeric network after the *in vivo* experiment. This, in turn, could demonstrate the capacity of the CLs to protect resveratrol from light degradation under the conditions in which the *in vivo* test was performed. The extraction of the CLs was not carried out immediately after the test so that the presence of antioxidant activity in the extraction medium is a good indicator of the antioxidant activity of resveratrol released during the *in vivo* test. The antioxidant activity of freshly prepared ethanol:water 50:50 v/v solution (extraction medium) was also evaluated to discard artifacts. The antioxidant activity was expressed as µg/mL of DPPH in the medium and as percentage as previously described [Gülçin et al., 2010; Vivero-Lopez et al., 2021].

The concentration of DPPH radicals in the resveratrol extractiom medium was lower than for the controls **(Table 5.1)**. This means that the designed CLs effectively protected resveratrol from its degradation and the resveratrol remnant preserved its antioxidant activity. The high standard deviation observed for 10 h wear CLs together with the negative antioxidant scavenging effect was due to that two replicates were nearly exhausted and the concentration of resveratrol in the extraction medium was too low, 0.19 ± 0.06 µg/mL. The amount of resveratrol in the extraction medium for the other lenses (worn for 8 h and 10 h) was 0.76 ± 0.29 µg/mL. In any case, a change of the color from purple to yellow with the consequent decrease in absorbance at 517 nm was observed due to the DPPH radical scavenging activity of resveratrol **(Figure 5.9)**.

USC
UNIVERSIDADE DE SANTIAGO DE COMPOSTELA

Table 5.1. DPPH levels (µg/mL) and scavenging effect (%) for all CLs and ethanol:water 50:50 v/v solution. All data are mean ± standard deviations (n = 3).

CLs	DPPH (µg/mL)	DPPH scavenging effect (%)
CL 8h wear	3.50 ± 0.59	27.23 ± 11.46
CL 10h wear	6.79 ± 3.64	-36.65 ± 70.83
Controls	4.90 ± 0.05	

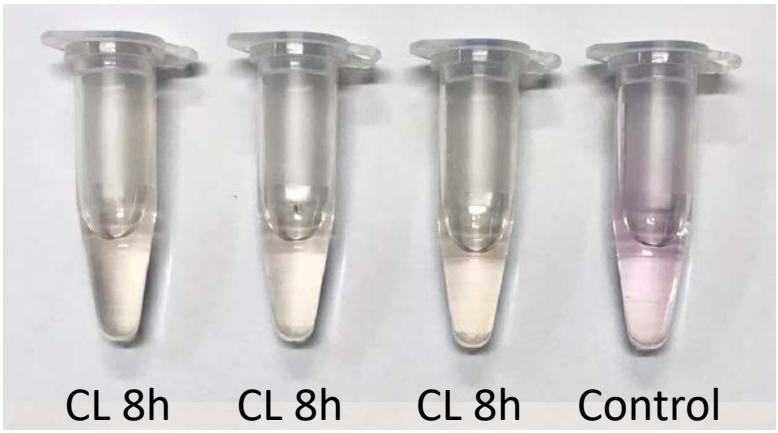


Figure 5.9. Antioxidant activity of resveratrol extracted from CLs after for 8 wearing compared to the control (ethanol:water 50:50 v/v) without resveratrol.

5.3.5 *In vivo – in vitro* correlations (IVIVC)

Mimicking *in vitro* the conditions in which drug release occurs from a CL in the ocular surface has largely remained elusive due to the many factors that may exert an influence: tear fluid dynamic, tears volume and composition, blinking,… Capability to predict *in vivo* behavior and quality assessment during production could strongly benefit from *in vitro* release tests that may provide biorelevant information. So far the few attempts to correlate *in vivo* and *in vitro* release from CLs pointed out that *in vitro* tests carried out with a small

USC UNIVERSIDADE DE SANTIAGO DE COMPOSTELA

volume may be more predictive [Maulvi et al., 2017; Zhu et al., 2018]. In the case of resveratrol, a minimum volume of 6 mL NaCl 0.9% was chosen due to its low aqueous solubility in order to prevent a rapid saturation of the release medium that could create artifacts in the release profile (as explained in section 5.3.3).

In vivo release profiles were constructed from the area under the curve of concentrations of resveratrol in tears versus time [Xu et al., 2019] and then compared to the *in vitro* release profiles recorded in the absence of proteins (**Figure 5.10A)**. In the first 30 min of the release, the process was faster *in vitro* than *in vivo*, probably because of the much more volume available *in vitro* (compared to the few microliters available on eye surface) which create a more intense concentration gradient. Differently, after one hour wearing the release *in vivo* becomes faster than *in vitro*, which may due to components in the tears that favor the release and also to the continuous renovation of the tear layer.

USC
UNIVERSIDADE DE SANTIAGO DE COMPOSTELA

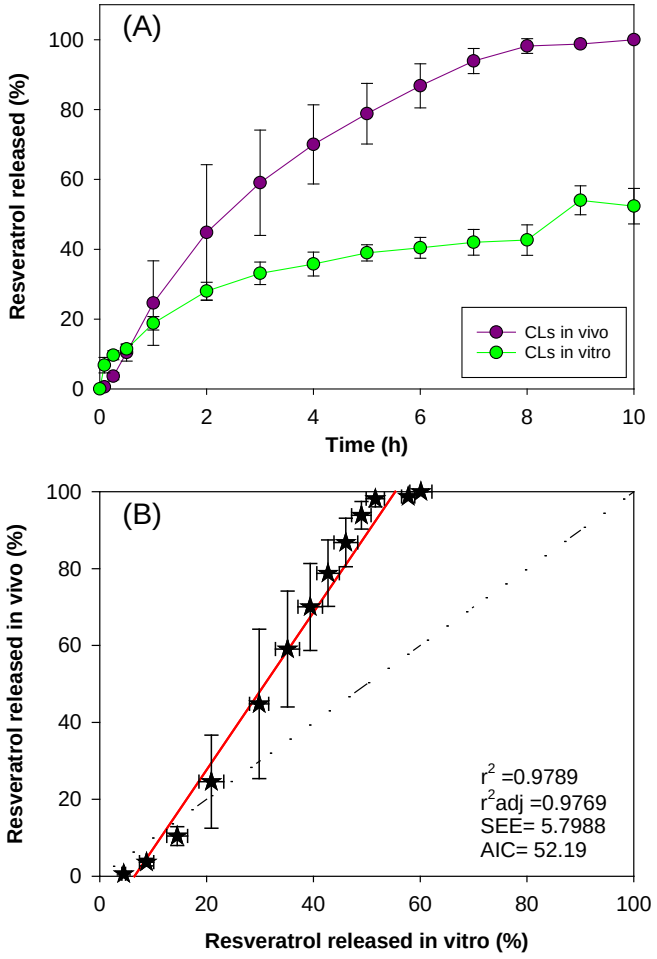


Figure 5.10. (A) *In vivo* resveratrol release profiles calculated from the levels in tear fluid provided by all CLs (n = 6 for time ≤8 h; n= 3 for time >8 h) and *in vitro* release profiles from sterilized CLs in NaCl 0.9% (n = 4); and (B) Levy plot to estimate IVIVC. SEE: Standard Error of Estimate; AIC: Akaike Information Criterion. Slope 1 is shown as reference with a dotted line.

The Levy plot showed a positive deviation with respect to slope 1; the experimental slope was 2.048. This means that after the initial 30

USC UNIVERSIDADE DE SANTIAGO DE COMPOSTELA

min, the *in vivo* release rate was almost double that recorded *in vitro*. Similar patterns for the IVIVC have previously been reported for betaxolol hydrochloride when formulated in a film-embedded CL [Zhu et al., 2018] and for timolol and latanoprost formulated in CL containing the drug encapsulated in micelles [Xu et al., 2019]. Nevertheless, the goodness of the fitting found for resveratrol was significantly better than for previously reported drug-loaded CLs.

5.4 CONCLUSIONS

In this part of the Thesis the synthesis of CLs with higher amounts of MPC was successfully carried out. The amount of MPC was increased 3.8 times in relation to the amount present in HEMA-based hydrogels previously developed and in Proclear® 1 day CLs. This increase in MPC content notably enhanced the loading of resveratrol by the CLs both before and after sterilization, compared to the results reported in **Chapter 4**. Sterilized CLs provided more sustained release of resveratrol. The presence of lysozyme in the *in vitro* release medium did not modify the kinetics. Differently, albumin slowed down the release. *In vivo* tests in a rabbit model evidenced that the developed CLs, as well as the P10R micelles, were well tolerated and no irritant effects or damage were observed on slit-lamp images after 8-10 h wearing. Moreover, differently from the resveratrol peak in tear fluid recorded in the first 5 minutes after instillation of micelle dispersion followed by a fast exponential decrease, CLs wearing sustained resveratrol release over a period of 8 h. CLs provided higher resveratrol concentrations than eye drops in the 2-6 h time interval after application. Relevantly, wearing of CLs for 8 h facilitated resveratrol penetration in eye tissues, and for a same dose the levels of resveratrol in cornea, sclera and aqueous humor were remarkably

USC UNIVERSIDADE DE SANTIAGO DE COMPOSTELA

higher after CL wearing for 8 h compared to eye drop instillation. All treatment groups (eye drop and CL) allowed resveratrol also reaching lens, vitreous humor and retina, although the low values recorded may be related to the late time point of the analysis (8 h or 24 h after starting the treatment) and predominance of clearance with respect to penetration. The antioxidant activity of resveratrol extracted from CLs used in the *in vivo* experiment demonstrated that the CLs protected resveratrol from photodegradation and preserved its antioxidant properties. Finally, construction of Levy plot searching for IVIVC evidenced that after an initial lag time *in vivo* release occurred faster than *in vitro* under the tested conditions. A strong correlation was found between the resveratrol percentages released *in vivo* and *in vitro*. Nevertheless, identification of *in vitro* conditions that may resemble better the *in vivo* behavior is still a challenge. In sum, CLs prepared with high proportion in MPC are pointed out as suitable platforms for the sustained release of resveratrol aimed to address ocular diseases that affect the anterior and posterior segment of the eye and that require antimicrobial and antioxidant management.

5.5 REFERENCES

Alvarez-Rivera, F., Serro, A. P., Silva, D., Concheiro, A., Alvarez-Lorenzo, C. (2019). Hydrogels for diabetic eyes: Naltrexone loading, release profiles and cornea penetration. *Materials Science and Engineering: C*, *105*, 110092.

Bispo, P. J., Haas, W., Gilmore, M. S. (2015). Biofilms in infections of the eye. *Pathogens*, *4*(1), 111-136.

Chan, C. M., Huang, C. H., Li, H. J., Hsiao, C. Y., Su, C. C., Lee, P. L., & Hung, C. F. (2015). Protective effects of resveratrol against UVA-induced

USC UNIVERSIDADE DE SANTIAGO DE COMPOSTELA

damage in ARPE19 cells. *International Journal of Molecular Sciences, 16*(3), 5789-5802.

da Silva, R. D. C., Teixeira, J. A., Nunes, W. D. G., Zangaro, G. A. C., Pivatto, M., Caires, F. J., & Ionashiro, M. (2017). Resveratrol: a thermoanalytical study. *Food Chemistry, 237*, 561-565.

DiPasquale, S.A., Uricoli, B., DiCerbo, M.C., Brown, T.L., & Byrne, M.E. (2021). Controlled release of multiple therapeutics from silicone hydrogel contact lenses for post-cataract/post-refractive surgery and uveitis treatment. *Translational Vision Science & Technology, 10*, 5.

Durgun, M.E., Güngör, S., & Özsoy, Y. (2020). Micelles: Promising ocular drug carriers for anterior and posterior segment diseases. *Journal of Ocular Pharmacology and Therapeutics, 36*, 323-341.

Dutta, D., & Willcox, M. D. (2014). Antimicrobial contact lenses and lens cases: a review. *Eye & Contact Lens, 40*(5), 312-324.

El-Ganiny, A. M., Shaker, G. H., Aboelazm, A. A., & El-Dash, H. A. (2017). Prevention of bacterial biofilm formation on soft contact lenses using natural compounds. *Journal of Ophthalmic Inflammation and Infection, 7*(1), 1-7.

Fleiszig, S. M., Kroken, A. R., Nieto, V., Grosser, M. R., Wan, S. J., Metruccio, M. M., Evans, D. J. (2020). Contact lens-related corneal infection: Intrinsic resistance and its compromise. *Progress in Retinal and Eye Research, 76*, 100804.

Goda, T., Ishihara, K. (2006). Soft contact lens biomaterials from bioinspired phospholipid polymers. *Expert Review of Medical Devices, 3*(2), 167-174.

Goda, T., Ishihara, K., & Miyahara, Y. (2015). Critical update on 2-methacryloyloxyethyl phosphorylcholine (MPC) polymer science. *Journal of Applied Polymer Science, 132* (16), 41766.

USC
UNIVERSIDADE DE SANTIAGO DE COMPOSTELA

Grimaudo, M. A., Pescina, S., Padula, C., Santi, P., Concheiro, A., Alvarez-Lorenzo, C., & Nicoli, S. (2019). Topical application of polymeric nanomicelles in ophthalmology: A review on research efforts for the noninvasive delivery of ocular therapeutics. *Expert Opinion on Drug Delivery*, *16*(4), 397-413.

Gülçin, İ. (2010). Antioxidant properties of resveratrol: A structure–activity insight. *Innovative Food Science & Emerging Technologies*, *11*(1), 210-218.

Huang, X. D., Yao, K., Zhang, H., Huang, X. J., & Xu, Z. K. (2007). Surface modification of silicone intraocular lens by 2-methacryloyloxyethyl phosphoryl-choline binding to reduce *Staphylococcus epidermidis* adherence. *Clinical & Experimental Ophthalmology*, *35*(5), 462-467.

Ishihara, K. (2019). Revolutionary advances in 2-methacryloyloxyethyl phosphorylcholine polymers as biomaterials. *Journal of Biomedical Materials Research Part A*, *107*(5), 933-943.

Ishihara, K., Fukazawa, K., Sharma, V., Liang, S., Shows, A., Dunbar, D. C., ... & Wu, J. Y. (2021). Antifouling silicone hydrogel contact lenses with a bioinspired 2-methacryloyloxyethyl phosphorylcholine polymer surface. *ACS Omega*, *6*(10), 7058-7067.

Khan, S. A., Lee, C. S. (2020). Recent progress and strategies to develop antimicrobial contact lenses and lens cases for different types of microbial keratitis. *Acta Biomaterialia*, 113, 101-108.

Lin, H. R., & Chang, P. C. (2013). Novel pluronic-chitosan micelle as an ocular delivery system. *Journal of Biomedical Materials Research Part B: Applied Biomaterials*, *101*(5), 689-699.

Liu, Y. (2011). Polymerizable contact lens formulations and contact lenses obtained therefrom. *U.S. Patent No. 8,011,784*. U.S. Patent and Trademark Office, Washington, DC.

USC UNIVERSIDADE DE SANTIAGO DE COMPOSTELA

Lorentz, H., Heynen, M., Kay, L. M., Dominici, C. Y., Khan, W., Ng, W. W., & Jones, L. (2011). Contact lens physical properties and lipid deposition in a novel characterized artificial tear solution. *Molecular Vision*, *17*, 3392.

Losso, J. N., Truax, R. E., & Richard, G. (2010). Trans-resveratrol inhibits hyperglycemia-induced inflammation and connexin downregulation in retinal pigment epithelial cells. *Journal of Agricultural and Food Chemistry*, *58*(14), 8246-8252.

Mandal, A., Bisht, R., Rupenthal, I.D., Mitra, A.S. (2017). Polymeric micelles for ocular drug delivery: From structural frameworks to recent preclinical studies. *Journal of Controlled Release, 248*, 96-116.

Marques, M. R., Loebenberg, R., & Almukainzi, M. (2011). Simulated biological fluids with possible application in dissolution testing. *Dissolution Technology*, *18*(3), 15-28.

Maulvi, F.A., Desai, A.R., Choksi, H.H., Patil, R.J., Ranch, K.M., Vyas, B.A., & Shah, D.O. (2017). Effect of surfactant chain length on drug release kinetics from microemulsion-laden contact lenses. International Journal of Pharmaceutics, *524*, 193-204.

Maulvi, F. A., Patil, R. J., Desai, A. R., Shukla, M. R., Vaidya, R. J., Ranch, K. M., ... & Shah, D. O. (2019). Effect of gold nanoparticles on timolol uptake and its release kinetics from contact lenses: *in vitro* and *in vivo* evaluation. *Acta Biomaterialia*, *86*, 350-362.

Olivieri, M., Cristaldi, M., Pezzino, S., Spampinato, G., Corsaro, R., Anfuso, C. D., ... & Rusciano, D. (2021). Poly 2-methacryloyloxyethyl phosphorylcholine protects corneal cells and contact lenses from desiccation damage. *Optometry and Vision Science*, *98*(2), 159-169.

Phan, C. M., Bajgrowicz-Cieslak, M., Subbaraman, L. N., & Jones, L. (2016). Release of moxifloxacin from contact lenses using an in vitro eye model: impact of artificial tear fluid composition and mechanical rubbing. *Translational vision science & technology*, *5*(6), 3-3.

USC UNIVERSIDADE DE SANTIAGO DE COMPOSTELA

Pucker, A. D., & Tichenor, A. A. (2020). A review of contact lens dropout. *Clinical Optometry*, *12*, 85.

Qin, N., Tan, X., Jiao, Y., Liu, L., Zhao, W., Yang, S., & Jia, A. (2014). RNA-Seq-based transcriptome analysis of methicillin-resistant *Staphylococcus aureus* biofilm inhibition by ursolic acid and resveratrol. *Scientific Reports*, *4*(1), 1-9.

Robertson, D. M. (2013). The effects of silicone hydrogel lens wear on the corneal epithelium and risk for microbial keratitis. *Eye & Contact Lens*, *39*(1), 67.

Shi, X., Cantu-Crouch, D., Sharma, V., Pruitt, J., Yao, G., Fukazawa, K., ... & Ishihara, K. (2021). Surface characterization of a silicone hydrogel contact lens having bioinspired 2-methacryloyloxyethyl phosphorylcholine polymer layer in hydrated state. *Colloids and Surfaces B: Biointerfaces*, *199*, 111539.

Shikamura, Y., Yamazaki, Y., Matsunaga, T., Sato, T., Ohtori, A., & Tojo, K. (2016). Hydrogel ring for topical drug delivery to the ocular posterior segment. *Current eye research*, *41*(5), 653-661.

Shimizu, T., Goda, T., Minoura, N., Takai, M., & Ishihara, K. (2010). Super-hydrophilic silicone hydrogels with interpenetrating poly (2-methacryloyloxyethyl phosphorylcholine) networks. *Biomaterials*, *31*(12), 3274-3280.

Tahhan, N., Naduvilath, T. J., Woods, C., & Papas, E. (2021). Review of 20 years of soft contact lens wearer ocular physiology data. *Contact Lens and Anterior Eye*, *45*, 101525.

Toffoletto, N., Saramago, B., & Serro, A.P. (2020). Therapeutic ophthalmic lenses: A review. *Pharmaceutics*, *13*, 36.

Tsai, T.Y., Chen, T.C., Wang, I.J., Yeh, C.Y., Su, M.J., Chen, R.H., Tsai, T.H., Hu, F.R. (2015). The effect of resveratrol on protecting corneal

USC UNIVERSIDADE DE SANTIAGO DE COMPOSTELA

epithelial cells from cytotoxicity caused by moxifloxacin and benzalkonium chloride. *Investigative Ophthalmology & Visual Science*, *56*, 1575-1584.

Vales, T. P., Jee, J. P., Lee, W. Y., Cho, S., Lee, G. M., Kim, H. J., & Kim, J. S. (2020). Development of poly (2-methacryloyloxyethyl phosphorylcholine)-functionalized hydrogels for reducing protein and bacterial adsorption. *Materials*, *13*(4), 943.

Vézina, M. (2012). Comparative ocular anatomy in commonly used laboratory animals. In *Assessing ocular toxicology in laboratory animals* (Weirm A.B., Collins, M., Eds.). Humana Press, Totowa, NJ., pp. 1-21.

Vivero-Lopez, M., Muras, A., Silva, D., Serro, A. P., Otero, A., Concheiro, A., & Alvarez-Lorenzo, C. (2021). Resveratrol-loaded hydrogel contact lenses with antioxidant and antibiofilm performance. *Pharmaceutics*, *13*(4), 532.

Wang, J., & Li, X. (2011). Interpenetrating polymer network hydrogels based on silicone and poly (2-methacryloyloxyethyl phosphorylcholine). *Polymers for Advanced Technologies*, *22*(12), 2091-2095.

Whittaker, A. L., & Williams, D. L. (2015). Evaluation of lacrimation characteristics in clinically normal New Zealand white rabbits by using the Schirmer tear test I. *Journal of the American Association for Laboratory Animal Science*, *54*(6), 783-787.

Wiley, L., Bridge, D. R., Wiley, L. A., Odom, J. V., Elliott, T., Olson, J. C. (2012). Bacterial biofilm diversity in contact lens-related disease: emerging role of *Achromobacter*, *Stenotrophomonas*, and *Delftia*. *Investigative Ophthalmology & Visual Science*, *53*(7), 3896-3905.

Xiao, A., Dhand, C., Leung, C. M., Beuerman, R. W., Ramakrishna, S., Lakshminarayanan, R. (2018). Strategies to design antimicrobial contact lenses and contact lens cases. *Journal of Materials Chemistry B*, *6*(15), 2171-2186.

USC
UNIVERSIDADE DE SANTIAGO DE COMPOSTELA

Xu, L., Ma, P., Yuan, B., Chen, Q., Lin, S., Chen, X., ... & Shen, J. (2014). Anti-biofouling contact lenses bearing surface-immobilized layers of zwitterionic polymer by one-step modification. *RSC Advances*, *4*(29), 15030-15035.

Xu, J., Ge, Y., Bu, R., Zhang, A., Feng, S., Wang, J., Gou, J., Yin, T., He, H., Zhang, Y., & Tang, X. (2019). Co-delivery of latanoprost and timolol from micelles-laden contact lenses for the treatment of glaucoma, *Journal of Controlled Release, 305*, 18–28.

Zernii, E.Y., Baksheeva, V.E., Iomdina, E.N., Averina, O.A., Permyakov, S.E., Philippov, P.P., ... & Senin, I.I. (2016). Rabbit models of ocular diseases: new relevance for classical approaches. *CNS & Neurological Disorders-Drug Targets*, *15*(3), 267-291.

Zhou, J. W., Chen, T. T., Tan, X. J., Sheng, J. Y., & Jia, A. Q. (2018). Can the quorum sensing inhibitor resveratrol function as an aminoglycoside antibiotic accelerant against *Pseudomonas aeruginosa*?. *International Journal of Antimicrobial Agents*, *52*(1), 35-41.

Zhu, Q., Cheng, H., Huo, Y., & Mao, S. (2018). Sustained ophthalmic delivery of highly soluble drug using pH-triggered inner layer-embedded contact lens. *International Journal of Pharmaceutics*, *544*(1), 100-111.

Zupančič, Š., Lavrič, Z., & Kristl, J. (2015). Stability and solubility of trans-resveratrol are strongly influenced by pH and temperature. *European Journal of Pharmaceutics and Biopharmaceutics*, *93*, 196-204.

USC
UNIVERSIDADE DE SANTIAGO DE COMPOSTELA

USC
UNIVERSIDADE
DE SANTIAGO
DE COMPOSTELA

USC
UNIVERSIDADE
DE SANTIAGO
DE COMPOSTELA

USC
UNIVERSIDADE
DE SANTIAGO
DE COMPOSTELA

Chapter 6

USC
UNIVERSIDADE
DE SANTIAGO
DE COMPOSTELA

USC
UNIVERSIDADE
DE SANTIAGO
DE COMPOSTELA

6. PLURONIC®/CASEIN MIXED MICELLES FOR OPHTHALMIC DELIVERY OF RESVERATROL

6.1 INTRODUCTION

The eye is susceptible to oxidative damage and inflammation due to its high metabolic activity and intense exposure to radiations, atmospheric oxygen and pollutants [Pinazo-Durán et al., 2014; Ung et al., 2017; Behl et al., 2016; Dammak et al., 2021]. The most susceptible structures are the lens and, especially, the retina because of its high proportion of lipids, high exposure to visible light and high oxygen consumption needed to provide the elevated amount of energy demanded [Pinazo-Durán et al., 2014; Ung et al., 2017; Behl et al., 2016; Calderon et al., 2017].

Oxidative stress is caused by reactive oxygen species (ROS) such as superoxide anion (O_2^{-*}), hydroxyl radical (OH^*), hydrogen peroxide (H_2O_2) and singlet oxygen ($^1O_2$) [Pinazo-Durán et al., 2014; Behl et al., 2016; Nita and Grzybowski, 2016; Ung et al., 2017; Dogru et al., 2018; Pinazo-Durán et al., 2018]. These ROS are produced mainly by the mitochondrial respiratory chain, but also in numerous enzymatic and oxidation reactions due to a partial reduction of molecular oxygen [Behl et al., 2016; Dogru et al., 2018; Ung et al., 2017; Nita and Grzybowski, 2016]. The exposition to ROS causes cell injures through oxidative damage of DNA, oxidative modification of proteins and

USC UNIVERSIDADE DE SANTIAGO DE COMPOSTELA

lipid peroxidation of membranes. When a decrease in antioxidant defenses (both enzymatic and non-enzymatic) occurs, the imbalance between antioxidants and pro-oxidants triggers the generation of proinflammatory cytokines, and proteolytic enzymes and activates pro-angiogenic routes [Chrysostomou et al., 2013; Cejka and Čejková, 2015; Behl et al., 2016; Calderon et al., 2017; Nita and Grzybowski, 2016; Ung et al., 2017; Dogru et al., 2018; Pinazo-Durán et al., 2018]. Oxidative stress and inflammation are both related and become exacerbated in elderly people due to malfunction of antioxidant defense mechanisms [Pinazo-Durán et al., 2014; Nita and Grzybowski, 2016; Kimura et al., 2017].

Oxidative stress and inflammation play, therefore, a key role in the initiation and progression of many different age-related ocular diseases like surface disorders (keratoconus and corneal ectasia), age-related macular degeneration (AMD), diabetic retinopathy (DR), cataract, glaucoma and uveitis, which can lead to progressive loss of vision and blindness without proper treatment [Cejka and Čejková, 2015; Behl et al., 2016; Nita and Grzybowski, 2016; Calderon et al., 2017; Datta et al., 2017; Kimura et al., 2017; Ung et al., 2017; Dogru et al., 2018; Pinazo-Durán et al., 2018]. In fact, DR is the leading cause of blindness in working adults and elderly people worldwide with projections of 191 million people affected by 2030. In early stages, DR occurs without neovascularization but is characterized by the formation of microaneurysms and small dilation of retinal blood vessels (non-proliferative diabetic retinopathy). Then, due to high glucose levels, the retinal capillary basement membrane starts to narrow, the retinal vascular permeability increases, and tissue ischemia and release of various vasoactive substances occur leading to neovascularization. New blood vessels appear on the surface of the retina with the consequent vitreous hemorrhage and retinal

USC UNIVERSIDADE DE SANTIAGO DE COMPOSTELA

detachment (proliferative diabetic retinopathy). In addition, in the pathogenesis of DR retinal neurodegeneration, death of retinal ganglion cells and modification of retinal glial cells also takes place [Kang and Yang, 2020]. Oxidative stress plays a key role in the pathogenesis of this disease leading to mitochondrial damage, cellular apoptosis, inflammation, lipid peroxidation and structural and functional alterations in the retina. Oxidative stress contributes to and results from the metabolic abnormalities induced by hyperglycemia (increased flux of polyol and hexosamine pathways, hyperactivation of protein kinase C isoforms and accumulation of advanced glycation end products). Hyperglycemia also causes epigenetic modifications that repress the antioxidant defense system leading to an imbalance between the scavenging and production of ROS. Moreover, today it is well known the importance of the inflammatory process in the pathogenesis of this devastating disease and its complications [Rodríguez et al., 2019; Semeraro et al., 2019].

Considering all the above mentioned, a therapeutic strategy which targets oxidative stress is required to prevent oxidative stress-related ocular diseases or slow down their progression [Pinazo-Durán et al., 2014; Kimura et al., 2017]. Indeed, the effectiveness of different antioxidants (vitamins, carotenoids, flavonoids, polyphenols, lutein, zeaxanthin and omega-3 fatty acids, among others) against some age-related ocular diseases including DR has already been demonstrated in animal models and humans [Chrysostomou et al., 2013; Kimura et al., 2017; Pinazo-Durán et al., 2018; Kang and Yang, 2020].

Resveratrol (trans-3,5,4'-trihydroxystilbene) **(Figure 6.1)** is a natural polyphenolic compound with antioxidant, radical scavenging, antiproliferative, antiangiogenic, anti-inflammatory, anti-apoptotic and vasodilator properties which may be useful for eye health [Gülçin, 2010; Bola et al., 2014; Ghadiri et al., 2015; Lançon et al., 2016; Liu

USC UNIVERSIDADE DE SANTIAGO DE COMPOSTELA

et al., 2017; Chen et al., 2019]. In the specific case of DR, resveratrol acts through multiple molecular mechanisms [Ahmad and Hoda, 2020; Kang and Yang, 2020] and different *in vitro* and *in vivo* (most of them using oral administration) studies have demonstrated its beneficial effects [Kim et al., 2012; Toro et al., 2019; Huang et al., 2020; Delmas et al., 2021]. Despite its excellent potential, the clinical efficacy of resveratrol is compromised by its poor aqueous solubility (30 μg/mL), instability when exposed to light, and low oral bioavailability (< 1%) [Amri et al., 2012; Summerlin et al., 2015; Liu et al., 2017; Peñalva et al., 2018; Olvera-Montano et al., 2019].

In the last few decades, polymeric micelles have become one of the most promising delivery systems of hydrophobic drugs for the treatment of anterior and posterior ocular diseases thanks to their mucoadhesive nature and small size, which increases the contact with the ocular surface and allows better tissue penetration across cornea and sclera [Mandal et al., 2017; Grimaudo et al., 2019; Durgun et al., 2020]. Combination of high encapsulation efficiency, drug protection and enhanced permeability facilitates the achievement of greater ocular bioavailability without interference with vision (clear solution). Resveratrol-loaded nanoparticles (1 mg/mL) and micelles (0.5 mg/mL) have been shown safe in preclinical ocular tests [Natesan et al., 2017; Pandian et al., 2017; Li et al., 2020].

Bovine milk protein micelles are attracting increasing attention as drug nanocarriers since they combine widely available natural sources, capability to transport poorly soluble molecules (natural transporters of calcium phosphate) and activity as radical scavengers [Kimpel and Schmitt, 2015; Rehan et al., 2019]. Casein **(Figure 6.1)** represents a family of phosphoproteins which constitutes approximately 80% of all bovine milk proteins [Phadungath, 2005; Kelly et al., 2009; Rehan et al., 2019]. Casein is not heat sensitive, but

USC UNIVERSIDADE DE SANTIAGO DE COMPOSTELA

at temperature above 120 °C it gradually becomes insoluble. Differently, it is sensitive to pH and precipitate at its isoelectric point of 4.6 [Phadungath, 2005; Kelly et al., 2009]. It is made up of αs1-casein, αs2-casein, β-casein, and κ-casein [Phadungath, 2005; Kelly et al., 2009; Glab and Boratyński, 2017; Rehan et al., 2019]. The αs- and β-caseins are highly phosphorylated and precipitate with excess Ca^{2+} ions. Differently, κ-caseins are stable in the presence of calcium ions and protect other caseins from precipitation, which makes casein micelles more stable. In fact, in milk about 80-95% of the casein is forming part of spherical micelles (50-500 nm; 10^6-10^9 Da) made of a 94% of protein and a 6% of colloidal calcium phosphate [Phadungath, 2005; Rehan et al., 2019] although the exact conformation is still unknown.

So far, casein micelles-based systems have been tested for the delivery of metformin [Raj et al., 2015], quercetin [Peñalva et al., 2018], celecoxib [Tuorvsky et al., 2015; Bachar et al., 2012], doxorubicin [Gandhi et al., 2019], ibuprofen [Turovsky et al., 2015] and mitoxantrone [Shapira et al., 2010]. The studies regarding interaction with resveratrol are still limited [Bourassa et al., 2013] and mainly focused on its oral administration searching for antitumoral action [El-Far et al., 2018; Peñalva et al., 2018]. To the best of our knowledge, encapsulation of resveratrol or other compounds in casein micelles for ocular delivery has not been investigated yet. It has been shown that β-casein may form mixed micelles with Pluronic® F127 copolymer (Lutrol F127; **Figure 6.1),** which may be useful to shield the ionic charges of the protein and to confer stealth properties [Portnaya et al., 2011]. Pluronics or poloxamers are amphiphilic linear polymers of poly(ethylene oxide)-poly(propylene oxide)-poly(ethylene oxide) (PEO-PPO-PEO) widely tested for ocular formulations and some drug products in the market contain

USC UNIVERSIDADE DE SANTIAGO DE COMPOSTELA

poloxamers as main excipients (EMA, 2021). Advantages of mixed micelles are related to lower critical micelle concentration (CMC) and enhanced stability against both physical and chemical agents [Ribeiro et al., 2012; Del Regno et al., 2021].

This part of the Thesis relies on the hypothesis of that Pluronic® F127/casein mixed micelles may lead to nanocarriers with enhanced capability to encapsulate resveratrol, to preserve its antioxidant features and to facilitate its penetration through the ocular structures. Thus, the aim of this work was to prepare and characterize for the first time Pluronic® F127/casein mixed micelles and to evaluate their features as resveratrol nanocarriers suitable for ocular treatments. Considering the low aqueous solubility of resveratrol together with its instability against both physical and chemical agents and the ability of both Pluronic® F127 and casein to solubilize poorly soluble compounds, the preparation of single and mixed micelles was carried out. Micelles were prepared from mixtures of Pluronic® F127 and casein at various ratios **(Table 6.1)** and characterized regarding size, zeta potential and pH. The capacity of all developed formulations to solubilize resveratrol was also evaluated together with their stability against both physical and chemical agents. The most promising dispersions were evaluated in terms of *ex-vivo* porcine corneal and scleral permeability of resveratrol, antioxidant capacity, rheological behavior and ability to inhibit bacterial growth. Finally, a toxicity study using the zebrafish model was carried out to elucidate the biocompatibility of the most promising developed formulations.

USC
UNIVERSIDADE DE SANTIAGO DE COMPOSTELA

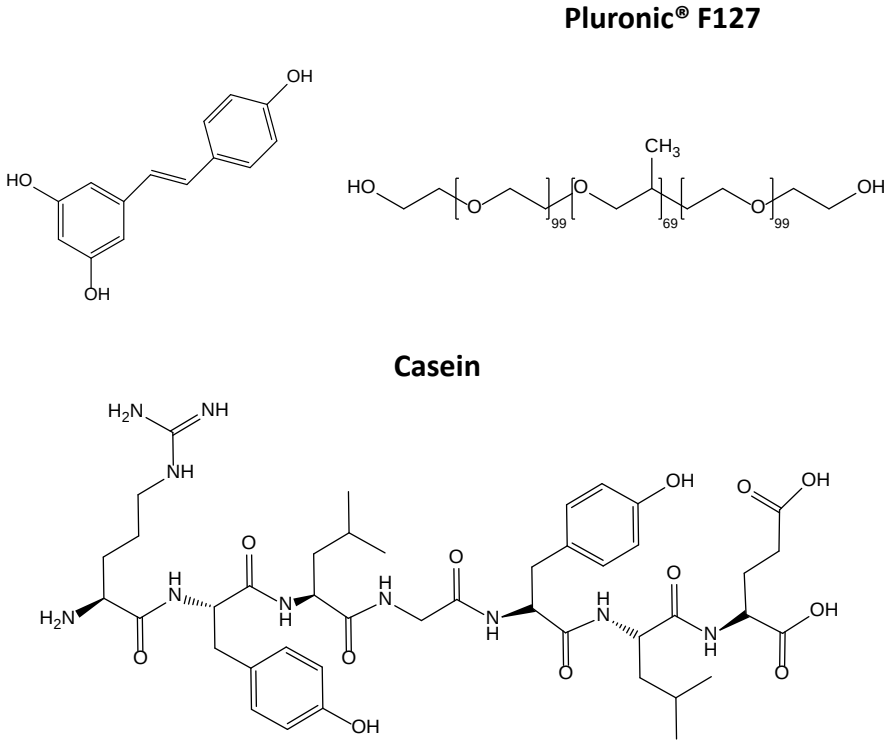


Figure 6.1. Chemical structure of trans-resveratrol, Pluronic® F127 and casein.

6.2 MATERIALS AND METHODS

6.2.1 Materials

Casein from bovine milk purified power (C-5890), phosphate buffer saline 10x concentrate and 2,2-diphenyl-1-picrylhydrazyl (DPPH) were purchased from Sigma-Aldrich (St. Louis, MO, USA). Kolliphor® P 407 (Lutrol F 127) was from BASF ChemTrade GmbH (Burgbernheim, Germany). Resveratrol was from ChemCruz Santa Cruz Biotechnology Inc. (Dallas, TX, USA). Propylene glycol was from Ginama (Valencia, Spain). Disodium hydrogen phosphate

USC UNIVERSIDADE DE SANTIAGO DE COMPOSTELA

anhydrous (Na_2HPO_4) was from Acofarma (Barcelona, Spain). Potassium di-hydrogen phosphate (KH_2PO_4) was from PanReac Química S.L.U. (Barcelona, Spain). Potassium chloride (KCl) and Luria Bertani (LB) broth were from Scharlab S.L. (Barcelona, Spain). Sodium dihydrogen phosphate anhydrous (NaH_2PO_4) and sodium chloride (NaCl) were from Labkem (Barcelona, Spain). Sodium bicarbonate ($NaHCO_3$) was from Probus S.A. (Barcelona, Spain). Calcium chloride dihydrate ($CaCl_2 \cdot 2H_2O$) was from Merck KGaA (Darmstadt, Germany). Ethanol absolute 99.9% and sodium hydroxide (NaOH) were from VWR Chemicals (Fontenary-Sous-Bois, France). Tryptic soy broth (TSB) was from Oxoid S.A. (Madrid, Spain). Ultrapure water (resistivity >18.2 MΩ·cm) was obtained by reverse osmosis (MilliQ®, Millipore Ibérica, Madrid, Spain). Phosphate-buffered saline (PBS) pH 6.5 medium was prepared with 8 g of NaCl, 0.3 g of KCl, 0.73 g of Na_2HPO_4 and 0.2 g of KH_2PO_4 for 1 L. Simulated lachrymal fluid (SLF) pH 7.5 was prepared with 6.78 g/L NaCl, 2.18 g/L $NaHCO_3$, 1.38 g/L KCl and 0.084 g/L $CaCl_2 \cdot 2H_2O$ with pH 7.5 [Alvarez-Rivera et al., 2019]. TSB-1 medium was prepared with 6 g of TSB and 1 g of NaCl for 200 mL. LB medium was prepared with 5 g of LB for 200 mL.

6.2.2 Single and mixed micelles preparation

Casein solution (4 mg/mL; 200 mL) was prepared by adding slowly (to avoid denaturalization) the corresponding amount of casein to phosphate buffer pH 7 (3.05 mM NaH_2PO_4 and 5.65 mM Na_2HPO_4) at 29 °C and kept at 200 rpm for 24 h [Portnaya et al., 2011]. Pluronic® F127 dispersions (25.2, 16.8, 12.6, 8.4 and 4.2 % p/p; 50 mL) were prepared in duplicate by adding the corresponding amount of copolymer to the corresponding amount of phosphate

USC UNIVERSIDADE DE SANTIAGO DE COMPOSTELA

buffer pH 7 under intense stirring. The dispersions were kept under magnetic stirring at 300 rpm for 5 h in an ice bath and stored at 4 °C until the next day to ensure the complete dispersion of the copolymer [Schmolka, 1972]. The next day, after 1 h under magnetic stirring in an ice bath at 300 rpm, 16.67 mL of phosphate buffer pH 7 or casein (4 mg/mL) solution were added to the Pluronic® dispersions to obtain finally 66.67 mL of formulations with the composition indicated in **Table 6.1**. All systems were magnetically stirred at 300 rpm for 7-8 h in an ice bath to facilitate the mixing and to avoid the gelling of the systems with higher content in Pluronic®. All dispersions were kept in the fridge until use.

Table 6.1. Composition of Pluronic® F127 (P), Pluronic® F127/casein (PC) and casein (C) formulations prepared in phosphate buffer pH 7.

Formulation	Pluronic (%)	Pluronic (mM)	Casein (mg/mL)
P2.5	3.15	2.5	-
P5	6.3	5	-
P7.5	9.45	7.5	-
P10	12.6	10	-
P15	18.9	15	-
PC2.5	3.15	2.5	1
PC5	6.3	5	1
PC7.5	9.45	7.5	1
PC10	12.6	10	1
PC15	18.9	15	1
C	-	-	1

6.2.3 Micelle size, Z-potential and pH

Particle size, size distribution, PDI and Z-potential of non-loaded and resveratrol-loaded micelle dispersions were measured in a Zetasizer® Pro-Blue (Malvern Instruments, UK). The measurements

USC UNIVERSIDADE DE SANTIAGO DE COMPOSTELA

were carried out in triplicate and duplicate for loaded and non-loaded dispersions respectively, at 10 °C to avoid the gelling of the dispersions with higher content in Pluronic® F127. Folded capillary cuvettes (DTS1070) were used for the measurements. The pH was measured with a GLP22 pH meter (Crison Instruments, Spain) at room temperature at least in duplicate.

6.2.4 Solubility study

Aliquots (10 mL) of each micelle dispersion were poured in 50 mL Falcon® tubes to which resveratrol was added in excess (approximately 100 mg). Solubility of resveratrol in phosphate buffer pH 7 was also tested. All systems were maintained under magnetic stirring (300 rpm) in an ice bath for 3 days and then centrifuged (Eppendorf® 5804R, Germany) at 5 °C and 4000 rpm for 30 min. Absorbance of the supernatants was measured at 305 nm (UV-Vis spectrophotometer Agilent 8453, Germany) previous dilution of aliquots (100 µL) of each dispersion in ethanol:water 50:50 v/v (100-2000x depending on the dispersion). Resveratrol concentration was calculated from the absorbance using a previously developed and validated calibration curve of resveratrol in ethanol:water 50:50 v/v (0.25-10 µg/mL).

Resveratrol solubility data were used to estimate the molar solubilization capacity (χ; Eq. 6.1), the micelle-water partition coefficient (P; Eq. 6.2), the molar micelle-water partition coefficient (PM; Eq. 6.3) for a copolymer concentration of 1 M, the standard-free Gibbs energy of solubilization (ΔG_S; Eq. 6.4), and the proportion of drug molecules encapsulated in the micelles (Eq. 6.5) as follows [Rangel-Yagui et al., 2005]:

USC UNIVERSIDADE DE SANTIAGO DE COMPOSTELA

$$\chi = \frac{S_{tot} - S_w}{C_{copol} - CMC} \quad \text{(Eq. 6.1)}$$

$$P = \frac{S_{tot} - S_w}{S_w} \quad \text{(Eq. 6.2)}$$

$$PM = \frac{\chi \cdot (1 - CMC)}{S_w} \quad \text{(Eq. 6.3)}$$

$$\Delta Gs = -RTln(PM) \quad \text{(Eq. 6.4)}$$

$$m_f = \frac{S_{tot} - S_w}{S_{tot}} \quad \text{(Eq. 6.5)}$$

In these equations, S_{tot} represents the total solubility of resveratrol in the micellar solution, S_w the solubility of resveratrol in phosphate buffer pH 7, C_{copol} is the copolymer concentration in each micellar solution, and R is the universal constant of gases.

6.2.5 Stability of loaded and not loaded micelles

All micellar systems were stored at 4 °C, protected from light to avoid resveratrol degradation, and monitored over 30 days regarding pH, size, polydispersion index and Z-potential. The amount of resveratrol within the micelles was also monitored from the absorbance at 305 nm (UV–Vis spectrophotometer Agilent 8534, Germany) previous dilutions of aliquots (100 µL) of each dispersion in ethanol:water 50:50 v/v and using a validated calibration curve of resveratrol in the same medium (0.25-10 µg/mL). Stability against dilution was evaluated by pouring aliquots of resveratrol-loaded micelle dispersions (30 µL) into quartz cells at 35 °C already containing 2970 µL of SLF (total volume 3000 µL). The 100-fold diluted dispersion was gently shaken, and the absorbance measured at 305 nm every 30 s for 30 min (UV-Vis spectrophotometer Agilent

USC UNIVERSIDADE DE SANTIAGO DE COMPOSTELA

8453, Germany). All experiments were carried out at least in duplicate.

6.2.6 Rheological behavior

The evolution of storage (G') and loss (G'') moduli for P5-P15 and PC5-PC15 dispersions (2 mL), with and without resveratrol was evaluated in a Rheolyst AR-1000N (TA Instruments, UK) rheometer fitted with a Peltier plate and a 60 mm in diameter cone (2.1 °) as a function of temperature (10-45 °C). The oscillation stress was fixed at 0.1 Pa and the angular frequency at 5 rad/s.

6.2.7 HET-CAM test and zebrafish embryo toxicity test

Ocular irritation potential of micelles with and without resveratrol was tested using the Hen's Egg Test on the Chorioallantoic Membrane (HET-CAM) as previously described [Alvarez-Rivera et al., 2016]. After 8 days of incubation of the fertilized hens' eggs (50-60 g, Coren, Spain) in a climatic chamber (Ineltec CC SR 0150, Barcelona, Spain) at 37 °C and 60% relative humidity, a circular cut of approximately 1 cm in diameter was made on the eggshell to remove the inner membrane and expose the chorioallantoic membrane (CAM). Then, aliquots (200 µL) of each formulation were directly poured on the CAM. 0.9% NaCl and 0.1 N NaOH solutions were used as negative and positive controls, respectively. CAM vessels were monitored for 5 min and the time at which hemorrhage, vascular lysis or coagulation occurred was recorded to calculate the irritation score (IS) as previously reported [ICCVAM, 2010]. According to he IS values obtained, formulations were classified as non-irritant ($IS < 1$), mildly irritant ($1 \leq IS < 5$), moderately irritant ($5 \leq IS < 10$), or severely

USC UNIVERSIDADE DE SANTIAGO DE COMPOSTELA

irritant (IS > 10). The assay was carried out in duplicate and independently for each formulation.

A fish embryo toxicity test (FET) was performed to elucidate the effect of P5 and PC5 formulations either blank or loaded (0.4 mg/mL) with resveratrol on the development of zebrafish embryos following the Organization for Economic Co-operation and Development (OCDE) normative [OECD, 2006]. Fertilized fish eggs before 5 h post-fecundation (hpf) were placed into 96-well cell culture plates, 20 embryos per well, before adding 10 µL of the corresponding formulation (well total volume = 200 µL). Sterilized reversed osmosis water was added to 4 wells of the cell culture plate to be used as negative controls. In addition, one 96-well cell culture plate more was used as negative control in its totality for each formulation. 3,4-dichloroaniline was used as positive control. The experiment was carried out in triplicate for 96 h being monitored each 24 h and the four lethal effects indicated in FET (coagulation of the embryo, absence of somite formation, absence of separation of the tail from the yolk and absence of heartbeat) were registered. To be a valid test, the mortality of fish embyos in the negative control after 96 h must not exceed 10% and the mortality in the positive control (3,4-dichloroaniline) must be at least 30%. The number of embryos used in the test was of approximately 60 (20 per replicate).

6.2.8 Antioxidant properties

The antioxidant activity of resveratrol in phosphate buffer pH 7 and in all micelle formulations was determined in triplicate by using a modified DPPH assay [Gülçin, 2010; Vivero-Lopez et al., 2021]. Micelles without resveratrol were used as controls. An aliquot of each dispersion (0.1 mL) was mixed with 4.5 mL of ethanol and 0.4 mL of

USC UNIVERSIDADE DE SANTIAGO DE COMPOSTELA

a freshly prepared 0.4 mM DPPH solution in ethanol and vortexed for 5 s. After 30 min of incubation in the dark, the absorbance was measured at 517 nm (UV-Vis spectrophotometer Agilent 8534, Germany). The free radical scavenging activity was expressed in two different ways: a) as µg/mL of DPPH in the reaction medium by interpolation into a validated calibration curve performed with DPPH in ethanol (5.91-31.55 µg/mL), and b) as percentage using the following equation (Eq. 6.6) where Ac is the absorbance at 517 nm of the control and As is the absorbance of the test compound [Vivero-Lopez et al., 2021].

$$DPPH\ scavenging\ activiy\ (\%) = \left(1 - \frac{A_S}{A_C}\right) \times 100 \qquad \text{(Eq. 6.6)}$$

6.2.9 Ability to inhibit bacterial growth

P5, P10, P15 and PC5, PC10, PC15 non-loaded and resveratrol-loaded micelles as well as resveratrol solutions in ethanol:water 50:50 v/v medium were tested regarding their capability to inhibit *Pseudomonas aeruginosa* and *Staphylococcus aureus* growth. The effect of the dilution of the culture medium with ethanol and PBS was also studied to elucidate the inhibitory bacterial growth due exclusively to resveratrol and to the formulations. All experiments were carried out at least in sextuplicate. As control, bacterial growth with no resveratrol or dispersions in the culture medium was monitored.

6.2.9.1 Bacterial strains and growth conditions

P. aeruginosa PAO1 (Lausanne sub-line, donated by M. Cámara, Univ. of Nottingham, Nottingham, UK) and *S. aureus* ATCC25923 (ATCC, Manassas, VA, USA) bacteria were routinely

USC UNIVERSIDADE DE SANTIAGO DE COMPOSTELA

grown (37 °C) in Luria-Bertani Broth (LB) and 1% Tryptic Soy Broth (TSB-1), respectively as previously described [Vivero-Lopez et al., 2021a; Vivero-Lopez et al., 2021b].

6.2.9.2 Pre-inocula and inocula preparation

Pre-inocula and inocula preparation was carried out according to previous described protocols with slight modifications [Vivero-Lopez et al., 2021a; Vivero-Lopez et al., 2021b]. A colony of 24 h plate of the corresponding bacterial pathogen was inoculated in sterile Erlenmeyer flasks containing culture medium (10 mL) at 37 °C for 12 h (*P. aeruginosa*) or 24 h (*S. aureus*) at 100 rpm. Then, the optical density of the pre-inocula (1 mL) was measured at 600 nm (UV–Vis spectrophotometer Thermo Scientific Helios Omega) after their previous centrifugation at 13000 rpm for 3 min and following resuspension in 1 mL of fresh medium. The optical density was adjusted to 0.05 (*S. aureus*) or 0.01 (*P. aeruginosa*) by dilution with the corresponding culture medium in sterile Falcon® tubes of 50 mL. The inocula were gently homogenized and divided among 96-well cell culture plates. All procedures were performed in a biological safety cabinet under sterile conditions.

6.2.9.3 Plates preparation and incubation

Firstly, the capacity of different concentrations of resveratrol (10, 50, 100, 200 and 300 µg/mL) in ethanol:water 50:50 v/v to inhibit the growing of *P. aeruginosa* and *S. aureus* bacteria was evaluated. To do this, more concentrated (3000, 2000, 500 and 100 µg/mL) resveratrol in ethanol:water 50:50 v/v solutions were prepared and later diluted by adding the corresponding amount (10 or 20 µg/mL) of each solution previously filtered (Biofil® Syringe Filter, 0.22 µm PES membrane) to a 96-well plate containing 180 µL of the inoculum plus 10 µL of ethanol:water 50:50 v/v solution or 190 µL of inoculum per

USC UNIVERSIDADE DE SANTIAGO DE COMPOSTELA

well to achieve the desired concentrations previously described. In all cases, the concentrated solutions of resveratrol were diluted 10-fold and the concentration of ethanol remained at 5%. Wells with bacteria inoculum (200 µL), bacteria inoculum (180 µL) plus ethanol:water 50:50 v/v (20 µL), and medium without bacteria (200 µL) were also prepared (n=6). The capacity of all single and mixed dispersions previously referred to inhibit the growing of both bacteria was also evaluated by adding 20 µL of each one to each well of a 96-well plate containing 180 µL of the corresponding inoculum bacteria. Then, plates were incubated for 24 h at 37 °C without stirring and optical densities of all wells were measured at predetermined times (0, 2, 4, 6, 8 and 24 h) at 595 nm in a plate reader (FLUOstar optima, BMG LabTech, Ortenberg, Germany). Before each measurement, bacteria were resuspended to homogenize the suspension and avoid aggregates that could interfere with the measurement.

6.2.10 *Ex vivo* corneal and scleral permeability tests

Resveratrol corneal and scleral permeability tests were carried out, at least in triplicate, following a previously described protocol [Varela-Garcia et al., 2020] for P10R and PC10R formulations. Fresh porcine eyes from a local slaughterhouse were transported immersed in PBS in an ice bath. Then, isolated scleras and corneas were washed with PBS and fitted into vertical diffusion Franz cells filled with a mixture of propylene glycol (PEG): water 40:60 v/v medium. The receptor medium (6 mL) was kept at 37 °C and under gentle magnetic stirring (400 rpm). After equilibration (30 min), the medium of the donor chambers (PEG:water 40:60 v/v) was removed and replaced by the formulations (1 mL). The area available for permeation was 0.785 cm^2. The donor chambers were covered with parafilm to prevent

USC UNIVERSIDADE DE SANTIAGO DE COMPOSTELA

evaporation and protected from light to avoid resveratrol degradation. After 30 min and then each hour for 6 h, 1 mL of sample was taken from the receptor chamber and replaced with the same volume of PEG:water 40:60 v/v, taking care of removing any bubble from the diffusion cells.

A JASCO (Tokyo, Japan) HPLC (AS-4140 autosampler, PU-4180 pump, LC-NetII/ADC interface box, CO-4060 column oven, MD-4010 photodiode array detector), fitted with a C18 column (Waters Symmetry C18, 5 µm, 4.6 × 250 mm) and operated with ChromNAV software (ver. 2.2.8.5, JASCO, Tokyo, Japan) was used to quantify the amount of resveratrol permeated. The analysis was done by isocratic elution with a mobile phase of water:methanol (50:50 v/v) at 1 mL/min and 35 °C using a run time of 8 min (retention time was 4.6 min). The injection volume was 50 µL and the UV detector was set at 305 nm. Resveratrol content in the samples was calculated from a validated calibration curve in methanol:water 50:50 v/v [Vivero-Lopez et al., 2021a].

Aliquots of the donor chambers were collected after 6 h of assay to quantify the amount of resveratrol remnant. The corneas and scleras were visually inspected to verify that none of them had cracks or modifications and then placed in Falcon® tubes with 3 mL of ethanol: water (50:50 v/v) at 37 °C. After 24 h, they were sonicated for 99 min at 37 °C, centrifuged (1000 rpm, 5 min, 25 °C), and the supernatant was filtered (PTFE hydrophilic, Scharlau® Syringe Filter, 0.22 µm 13 mm), centrifuged again (14,000 rpm, 20 min, 25 °C), and filtered again to be analyzed by HPLC as described above.

USC
UNIVERSIDADE DE SANTIAGO DE COMPOSTELA

6.2.11 Statistical analysis

Differences between formulations on bacteria growth were analyzed using ANOVA and multiple range test with software Statgraphics Centurion 18, v. 18.1.13 (StatPoint Technologies Inc., Warrenton VA, USA).

6.3 RESULTS AND DISCUSSION

6.3.1. Micelles preparation

Pluronic® F127 and casein easily dispersed in phosphate buffer pH 7 at the chosen concentrations **(Table 6.1)**. The highest Pluronic® F127 concentration was 15 mM to avoid a gelling transition at room temperature. Pluronic® F127 dispersions at high concentrations may be beneficial for increasing the permanence of the formulation in the ocular surface, but at the same time may hinder the solubilization process if the viscosity is too high during the processing [Taveira et al., 2018]. The CMC for Pluronic® F127 has been reported to be 0.39 mM at 25 °C in phosphate buffers from surface tension measurements [Rodríguez-Perez et al., 2006]. Thus, for all dispersions, the Pluronic® F127 concentration ranging from 2.5 to 15 mM was above the CMC value. The CMC for casein has been reported to be 1.0 mg/mL and specifically 0.3-0.7 mg/mL for β-casein depending on the pH, temperature and ionic strength [Glab and Boratynski, 2017]. The CMC at 29 °C in phosphate buffer was found to be 1.368 mg/mL (0.057 mM) using isothermal titration calorimetry (ITC) [Portnaya et al., 2010]. The commercial natural casein chosen for the present study was a mixture of α-s1 casein, α-s2 casein, β-casein, and κ-casein, and for comparative purpose the concentration was fixed at 1 mg/mL. In preliminary studies, we observed that dispersions prepared at higher

USC UNIVERSIDADE DE SANTIAGO DE COMPOSTELA

concentrations underwent phase separation in few days. Assuming a molecular weight of 24,000 Da for casein, a casein concentration of 1 mg/mL was equal to 0.0416 mM. This concentration was shown to be able to form mixed micelles when a minimum concentration of 0.076 mM Pluronic® F127 was added [Portnaya et al., 2010]. Thus, the CMC of the mixed micelles was estimated to be 0.1176 mM (slightly above the CMC of Pluronic® F127 solely, 0.096 mM, recorded by ITC). From that previous information, the formation of casein-Pluronic® F127 mixed micelles was assumed to occur under the conditions tested in the present study.

6.3.2 Micelle size, zeta potential and pH

Size, polydispersion index and Z-potential of single and mixed micelles before and after the loading with resveratrol are shown in **Tables 6.2** and **6.3**. The measurements were carried out at 10 °C to avoid gelling in the measuring cell of the systems with higher content in Pluronic®. The analysis of size by intensity distribution **(Figure 6.2)** showed multiple populations specially after the loading with resveratrol. In addition, the size of the micelles by intensity was larger because large particles scatter much more light than small particles and the scattering intensity is proportional to the sixth power of the particle diameter based on the Rayleigh's approximation. However, the analysis of size by number **(Figure 6.3)** showed unimodal size distribution and smaller sizes for single and mixed micelles before and after the loading with resveratrol. The size of PC mixed micelles without resveratrol increased with increasing Pluronic® content, but this trend was not observed after the loading with resveratrol and all loaded formulations had very close and smaller size values **(Tables 6.2** and **6.3)**. All single micelles before and after being loaded with

USC UNIVERSIDADE DE SANTIAGO DE COMPOSTELA

resveratrol showed almost the same size, which means that resveratrol loading did not affect the size. As expected, the Z-potential of Pluronic® F127 micelles was close to zero [Portnaya et al., 2010]. Differently, casein micelles had strongly negative surface since the pH of the medium was above the isoelectric point of the protein. Namely, casein molecules are formed by a short highly charged domain and a long hydrophobic segment, which favors their self-assembly [Phadungath, 2005]. Mixed micelles showed less negative values, with lower absolute values as the concentration in Pluronic® increased. The same trend was observed for mixed micelles of α-casein and PEG400 [Kessler et al., 2014]. This finding indicated that Pluronic® F127 successfully hided protein charges, probably by the shielding with the PEO chains [Portnaya et al., 2010].

Table 6.2. Size, polydispersion index (PDI), Z-potential and pH of single and mixed micelles in PBS pH 7 before being loaded with resveratrol (Mean values ± standard deviations).

Formulation	Size (nm)	PDI	Z-Pot (mV)	pH
P2.5	3.1 ± 0.2	0.6 ± 0.3	-3.4 ± 1.6	7.3 ± 0.1
P5	3.2 ± 0.4	0.6 ± 0.2	-1.3 ± 0.4	7.3 ± 0.1
P7.5	2.6 ± 0.0	0.6 ± 0.1	-4.2 ± 1.2	7.3 ± 0.1
P10	2.2 ± 0.2	1.5 ± 0.1	-1.0 ± 0.4	7.4 ± 0.0
P15	2.2 ± 0.2	0.7 ± 0.2	-1.1 ± 0.6	7.4 ± 0.1
PC2.5	11.9 ± 19.0	0.9 ± 0.2	-11.4 ± 1.4	7.0 ± 0.0
PC5	80.8 ± 128.3	0.7 ± 0.2	-7.1 ± 0.7	7.0 ± 0.1
PC7.5	206.6 ± 136.2	0.6 ± 0.0	-5.1 ± 0.8	7.1 ± 0.0
PC10	239.0 ± 84.1	0.7 ± 0.2	-4.4 ± 0.8	7.2 ± 0.0
PC15	639.3 ± 271.1	0.5 ± 0.1	-2.5 ± 0.6	7.3 ± 0.0
C	73.1 ± 31.1	0.5 ± 0.0	-6.1 ± 0.8	7.0 ± 0.0

USC UNIVERSIDADE DE SANTIAGO DE COMPOSTELA

Table 6.3. Size, polydispersion index (PDI), Z-potential and pH of single and mixed micelles in PBS pH 7 after being loaded with resveratrol (named with R) (Mean values ± standard deviations).

Formulation	Size (nm)	PDI	Z-Pot (mV)	pH
P2.5R	3.6 ± 0.3	0.3 ± 0.1	-1.5 ± 1.3	7.2 ± 0.0
P5R	3.1 ± 0.5	0.5 ± 0.1	-0.1 ± 0.1	7.2 ± 0.0
P7.5R	3.1 ± 0.1	0.5 ± 0.0	-0.9 ± 0.8	7.2 ± 0.0
P10R	2.7 ± 0.2	0.6 ± 0.2	0.0 ± 0.4	7.3 ± 0.0
P15R	2.1 ± 0.2	0.3 ± 0.1	-0.3 ± 0.2	7.3 ± 0.0
PC2.5R	10.9 ± 11.3	1.1 ± 0.1	-17.0 ± 0.7	7.1 ± 0.0
PC5R	32.7 ± 5.2	0.8 ± 0.0	-9.6 ± 1.3	7.1 ± 0.1
PC7.5R	2.6 ± 0.8	0.8 ± 0.1	-4.4 ± 0.6	7.1 ± 0.0
PC10R	2.4 ± 0.8	0.9 ± 0.0	-2.2 ± 0.5	7.1 ± 0.0
PC15R	2.4 ± 0.2	1.0 ± 0.6	-0.2 ± 0.2	7.2 ± 0.1
CR	23 ± 5	0.4 ± 0.0	-10.5 ± 2.3	7.0 ± 0.0

USC
UNIVERSIDADE DE SANTIAGO DE COMPOSTELA

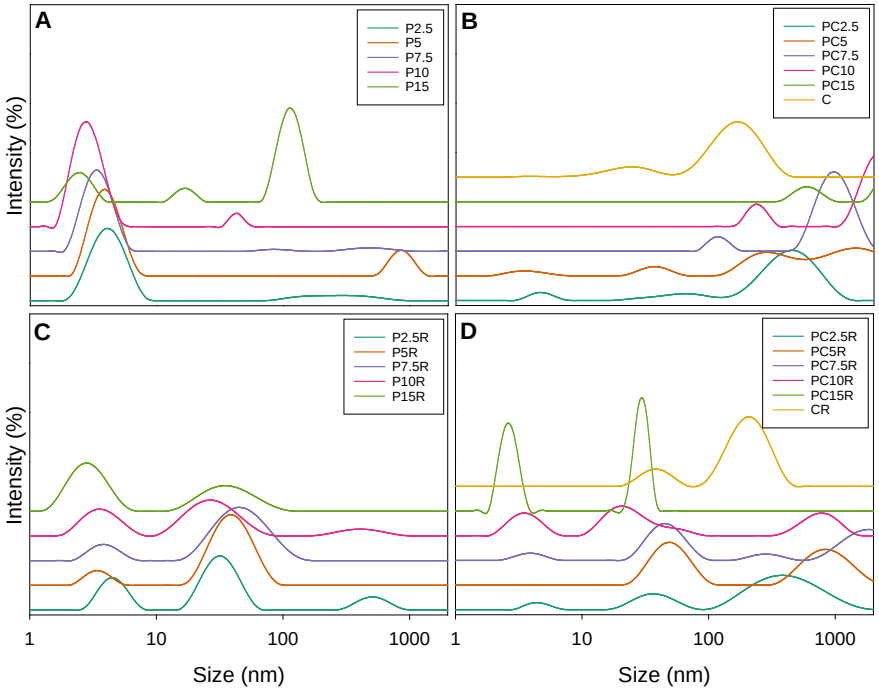


Figure 6.2. Size distribution by intensity (%) for single (A, C) and mixed (B, D) micelles before (A, B) and after (C, D) being loaded with resveratrol.

USC
UNIVERSIDADE DE SANTIAGO DE COMPOSTELA

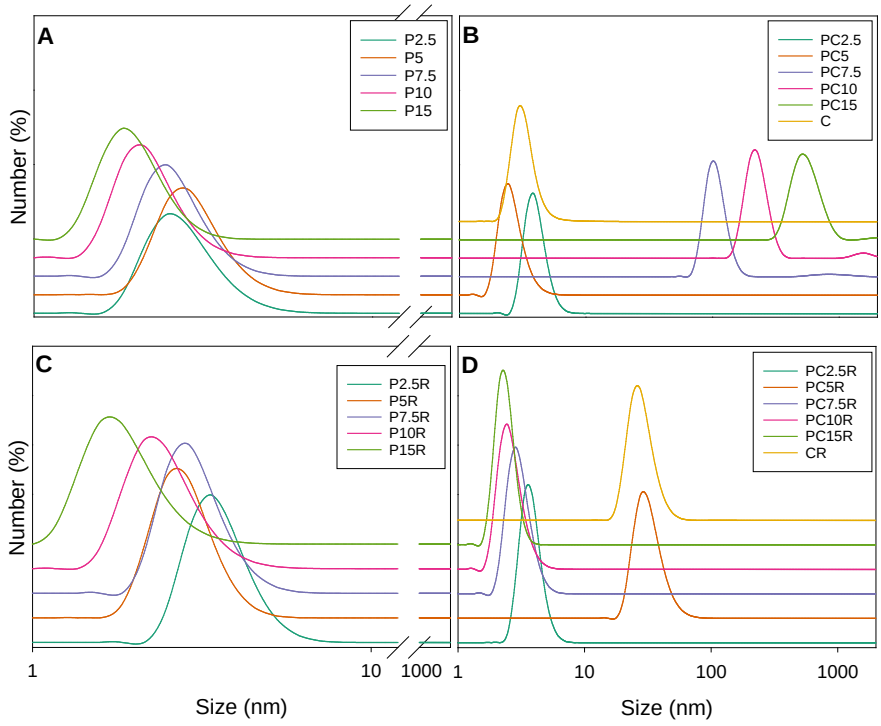


Figure 6.3 Size and distribution by number (%) for single (A, C) and mixed (B, D) micelles before (A, B) and after (C, D) being loaded with resveratrol.

The pH values registered for all dispersions **(Tables 6.2** and **6.3)**, loaded and not with resveratrol, were very similar among them and close to the pH of the phosphate buffer in which they were prepared showing no modification due to the Pluronic® F127, casein or resveratrol addition. Moreover, the pH values were close to physiological tear value (6.5-7.6) [Abelson et al., 1981; Coles and Jaros, 1984]. These pH values may ensure good ocular tolerance and also resveratrol stability [Robinson et al., 2015].

USC
UNIVERSIDADE DE SANTIAGO DE COMPOSTELA

6.3.3 Solubility study

No previous studies have been reported on the capability of Pluronic® F127 to solubilize resveratrol for ophthalmic applications, and none Pluronic® F127/casein mixed micelles have been previously developed to encapsulate resveratrol. Resveratrol has previously been loaded in nanoparticles, β-cyclodextrins and Soluplus micelles for topical ocular administration [Natesan et al., 2017; Pandian et al., 2017; Dong et al., 2019; Dinte et al., 2020; Li et al., 2020].

Solubility of resveratrol in phosphate buffer pH 7 was 16.31 ± 1.55 µg/mL (~ 0.07 mM), a value slightly lower than the values previously reported in the literature (21 µg/mL) [Cadena et al., 2013]. Both, single and mixed micelles increased the apparent solubility of resveratrol (**Table 6.4)**. Parameters used to quantify the efficiency of solubilization are shown in **Table 6.5**. Since Pluronic® F127 was the major species in the dispersion, for comparative purposes the estimation of χ, *PM*, and ΔG of the mixed micelles was made assuming a CMC value similar to that of single Pluronic® F127, i.e., 0.39 mM, which was slightly higher than that found by ITC (0.1176 mM) [Portnaya et al., 2010].

USC
UNIVERSIDADE DE SANTIAGO DE COMPOSTELA

Table 6.4. Resveratrol apparent solubility in single and mixed micelles Mean values ± standard deviations).

Formulation	Resveratrol solubility (mg/mL)	Resveratrol solubility (mM)
P2.5R	0.17 ± 0.02	0.72 ± 0.11
P5R	0.65 ± 0.29	2.85 ± 1.25
P7.5R	4.33 ± 0.77	19.0 ± 3.4
P10R	8.14 ± 0.41	35.7 ± 1.8
P15R	7.71 ± 0.52	33.8 ± 2.3
PC2.5R	0.23 ± 0.14	1.02 ± 0.60
PC5R	1.33 ± 0.06	5.85 ± 0.25
PC7.5R	4.39 ± 0.31	19.2 ± 1.4
PC10R	9.36 ± 0.07	41.0 ± 0.3
PC15R	8.14 ± 0.30	35.7 ± 1.3
CR	0.02 ± 0.00	0.08 ± 0.01

The highly negative free energy of solubilization indicated that solubilization of resveratrol in the micelles occurred spontaneously. Casein single micelles had low solubilization capability and most resveratrol remained free in solution. Differently, Pluronic® F127 single and mixed micelles notably enhanced the apparent solubility, and the increase was higher as Pluronic® F127 concentration raised, as previously reported for other Pluronic® F127 mixed micelles [Katekar et al., 2020]. This could be due to a stable interaction between the aromatic ring in resveratrol and the propylene oxide groups in Pluronic® F127 [Jadhav et al., 2016; Katekar et al., 2020]. However, the highest solubility was recorded for 10 mM Pluronic® F127 both as single micelles and as mixed micelles. Probably the increase in viscosity, even at low temperature, observed for 15 mM Pluronic® F127 was behind the obtained plateau [Taveira et al., 2018]. Both Pluronic® single and mixed micelles showed partition coefficient

USC UNIVERSIDADE DE SANTIAGO DE COMPOSTELA

values well above 1 indicating an efficient incorporation of resveratrol to the micelle cores, with increases in resveratrol apparent solubility of up to 500 times and 576 times, respectively. These values were in the range or even larger than those reported for Soluplus (3.3 to 10%) micelles that solubilized 1.67 to 4.44 mg resveratrol per mL [Li et al., 2020]. It should be noted that an ophthalmic formulation of resveratrol at concentration of 1 mg/mL (encapsulated in PEG-chitosan) have shown therapeutically relevant ocular effects, notably decreasing intraocular pressure [Pandian et al., 2017]. Therefore, this concentration threshold can be readily fulfilled even with 5 mM Pluronic® when formulated as mixed micelles **(Table 6.5)**.

Table 6.5. Solubilization parameters estimated using equations 6.1-6.5. Solubility of resveratrol in phosphate buffer pH 7 was 16.31 ± 1.55 µg/mL. χ, molar solubilization capacity; P, partition coefficient; PM, molar partition coefficient; mf, molar fraction of drug encapsulated inside the micelle Mean values ± standard deviations).

Formulation	x	P	PM	ΔG (KJ/mol)	mf
P2.5R	0.31 ± 0.05	9.1 ± 1.5	2.64 ± 0.44	-2384 ± 394	0.90 ± 0.01
P5R	0.60 ± 0.27	38.8 ± 17.5	5.14 ± 2.32	-3895 ± 1060	0.97 ± 0.01
P7.5R	2.66 ± 0.47	264.3 ± 46.9	22.7 ± 4.0	-7703 ± 449	1.00 ± 0.00
P10R	3.71 ± 0.19	498.2 ± 25.3	31.6 ± 1.6	-8551 ± 127	1.00 ± 0.00
P15R	2.31 ± 0.16	471.7 ± 32.1	19.7 ± 1.34	-7376 ± 172	1.00 ± 0.00
PC2.5R	0.45 ± 0.28	13.2 ± 8.4	3.88 ± 2.43	-3016 ± 1444	0.91 ± 0.04
PC5R	1.25 ± 0.05	80.8 ± 3.5	10.69 ± 0.46	-5866 ± 105	0.99 ± 0.00
PC7.5R	2.70 ± 0.19	268.2 ± 18.9	23.01 ± 1.62	-7762 ± 177	1.00 ± 0.00
PC10R	4.26 ± 0.03	572.8 ± 4.3	36.36 ± 0.27	-8899 ± 18	1.00 ± 0.00
PC15R	2.44 ± 0.09	497.9 ± 18.6	20.79 ± 0.79	-7513 ± 93	1.00 ± 0.00
CR	-0.02 ± 0.01	0.12 ± 0.08	-0.29 ± 0.19	-	0.10 ± 0.06

USC UNIVERSIDADE DE SANTIAGO DE COMPOSTELA

6.3.4 Stability of loaded and not loaded micelles

Pluronic® F127 single micelle dispersions kept their size constant over the 30 days of storage **(Figure 6.4)**. Differently, some differences in size were recorded for micellar systems composed of casein and Pluronic® F127, especially for non-loaded micelles **(Figure 6.4)**. Incorporation of resveratrol into the micelles increased their physical stability. The polydispersion index (PDI) showed values around 0.5-1 for all formulations **(Figure 6.5)**. The Z-potential followed an opposite trend for single and mixed micelles since the values decreased and increased, respectively **(Figure 6.6)**. The monitoring of all micellar systems showed pH values around 7 and constant for the 30 days **(Figure 6.7)**. The amount of resveratrol incorporated into the micelles remained constant over the whole 30-day period for all micellar systems **(Figure 6.8)**.

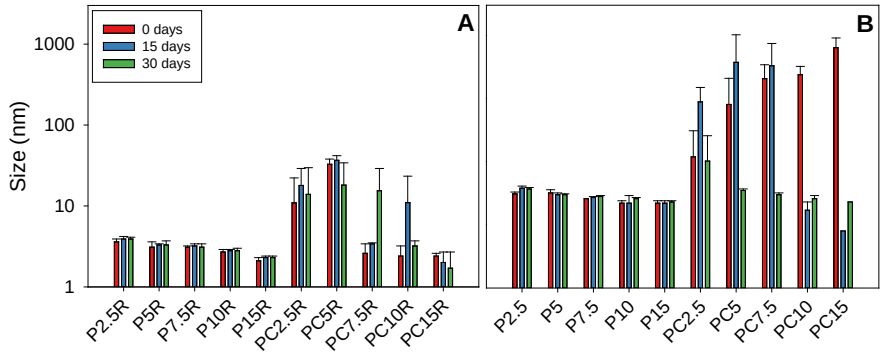


Figure 6.4. Size (nm) of all formulations loaded (A) and not (B) with resveratrol at 0, 15 and 30 days storage at 4 °C.

USC UNIVERSIDADE DE SANTIAGO DE COMPOSTELA

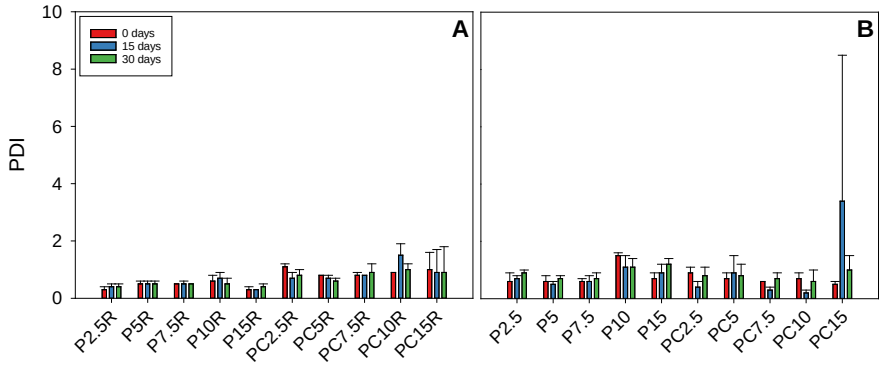


Figure 6.5.PDI of all formulations loaded (A) and not (B) with resveratrol at 0, 15 and 30 days storage at 4 °C.

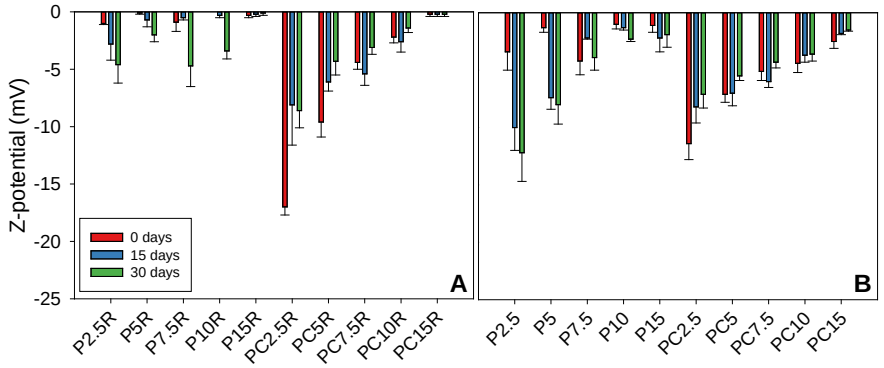


Figure 6.6.Z-potential of all formulations loaded (A) and not (B) with resveratrol at 0, 15 and 30 days storage at 4 °C.

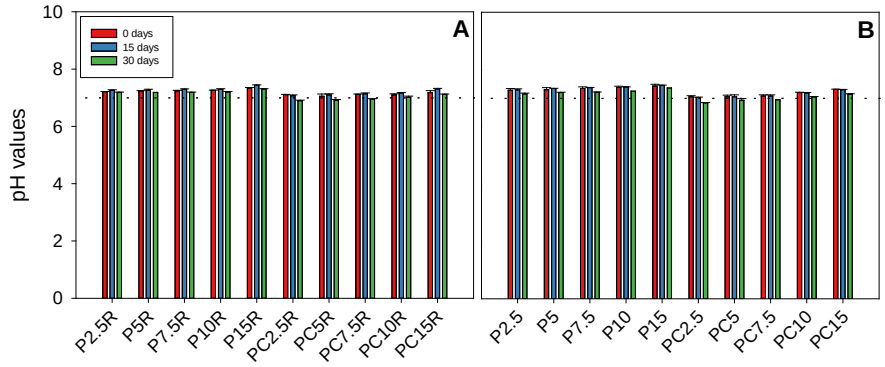


Figure 6.7. pH values of all formulations loaded (A) and not (B) with resveratrol at 0, 15 and 30 days storage at 4 °C.

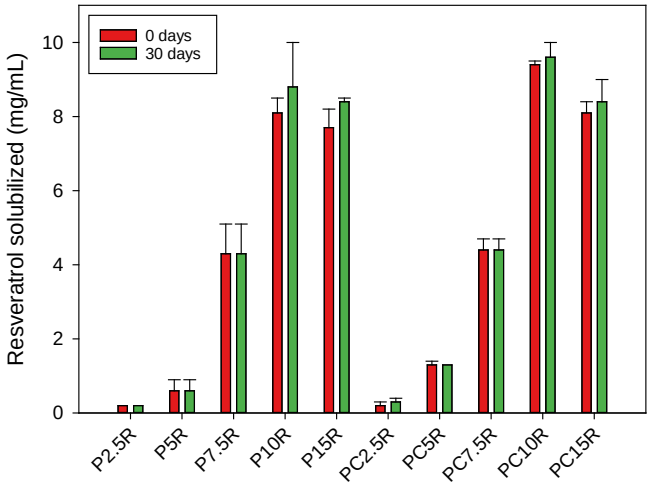


Figure 6.8. Resveratrol solubilized into single and mixed micelles at 0 and 30 days storage at 4 °C.

USC
UNIVERSIDADE DE SANTIAGO DE COMPOSTELA

Since ocular formulations undergo strong dilution once they enter in contact with the lachrymal fluid, the capability of all formulations to retain resveratrol once abruptly diluted was evaluated. The absorbance values remained higher for formulations that loaded higher amounts of resveratrol and the values were almost constant during 30 minutes after dilution **(Figure 6.9).**

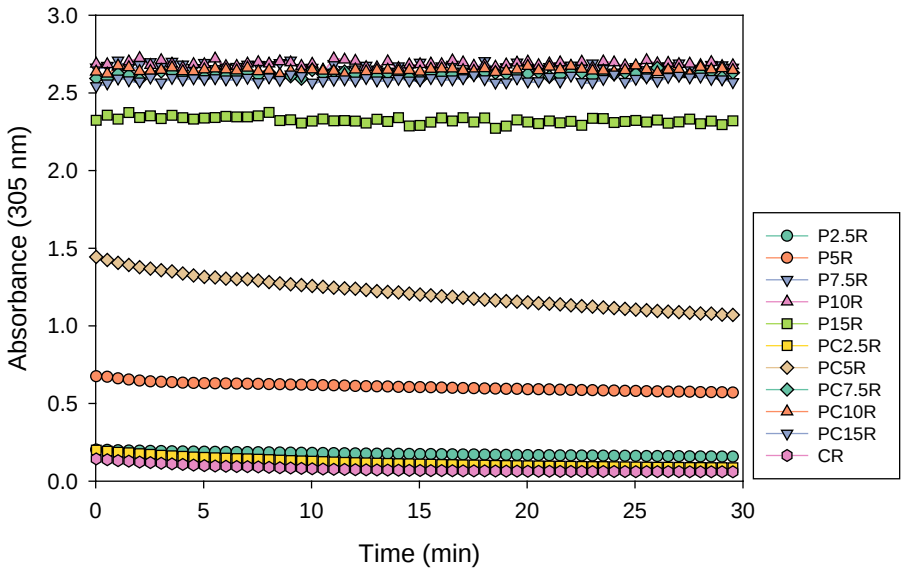


Figure 6.9. Evolution of the absorbance of resveratrol-loaded micelles after 100-fold dilution in simulated lachrymal fluid pH 7.5. Mean values and the error bars correspond to the SDs of at least 2 samples prepared separately.

6.3.5 Rheological behavior

Rheological properties of eyedrops should show a good balance between easy instillation and prolonged retention on the ocular surface. *In-situ* gelling polymers, such as Pluronic® F127, may be advantageous in this regard [Dumortier et al., 2006; Al Khabet et al.,

USC UNIVERSIDADE DE SANTIAGO DE COMPOSTELA

2016; Nagai et al., 2020]. The sol-gel transition of unloaded and loaded single and mixed dispersions with a 5, 10 and 15 mM content in Pluronic® F127 was evaluated as a function of temperature **(Figure 6.10)**. P and PC dispersions with 5 mM Pluronic® F127 showed negligible G' values in the 10-45 °C interval performing as a free-flowing liquid-like system in good agreement with previous reports [Shriky et al., 2020; Di Donato et al., 2020]. Differently, all other dispersions showed an increase in G' and G'' values as temperature raised. For non-loaded P10 and P15 dispersions **(Figure 6.10A and B)**, marked increase in G' and G'' occurred when the temperature reached 26.7 °C and 20.3 °C, respectively; the gel point (cross-over point of G' and G'') was 28.2 °C and 21 °C respectively. This correlates with previously studies that showed an increase in viscosity above 22 °C when Pluronic® F127 content exceeded 10% w/w, and similar gel points were recorded [Shriky et al., 2020]. The same trend was observed for the mixed micelles showing an increase in G' and G'' values above 26.4 °C and 19.9 °C and temperature gel points of 27.5 °C and 20.6 °C for PC10 and PC15, respectively. In addition, the loading of these dispersions with resveratrol **(Figure 6.10C and D)** led to a decrease in the gel point for single (23.9 °C and 15.2 °C) and mixed micelles (27.1 °C and 15.2 °C) with a content in Pluronic® F127 of 10 and 15 mM respectively. This means that the encapsulation of hydrophobic resveratrol favors dehydration and gel transition as was previously observed with other drug molecules like naproxen and indomethacin [Sharma and Bhatia, 2004]. No differences were observed between P and PC mixed dispersions suggesting no significant effects on the rheological behavior due to the incorporation of casein. Considering all the above mentioned, P and PC dispersions with a content in Pluronic® above 10 mM (either loaded or not loaded with resveratrol) showed the most adequate sol-

USC UNIVERSIDADE DE SANTIAGO DE COMPOSTELA

gel transition temperature, allowing their easy administration as a low viscosity liquid and rapidly transforming into gels at the temperature of the ocular surface (35 °C).

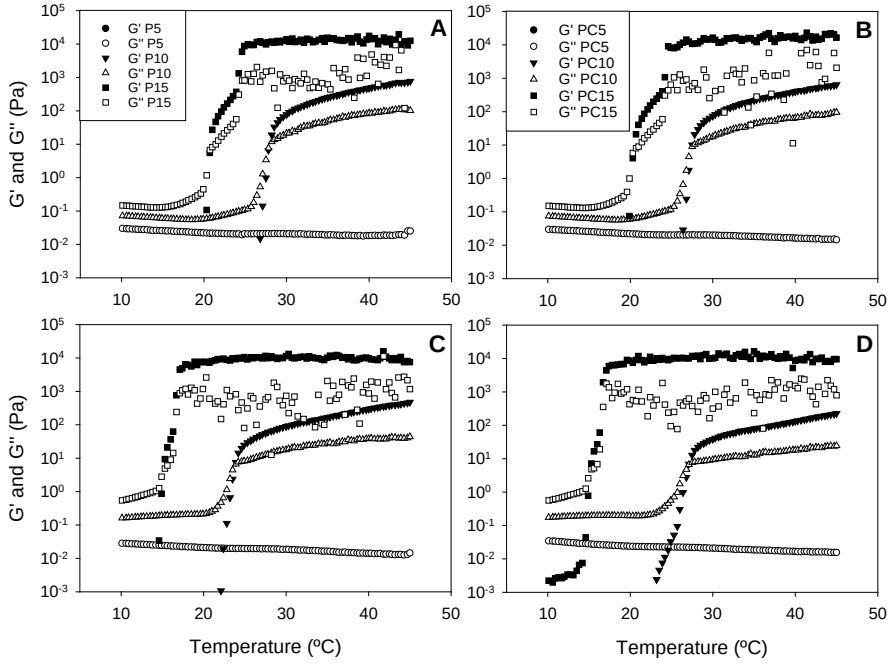


Figure 6.10. Rheological behavior of Pluronic® (A, C) and Pluronic®/casein (B, D) dispersions non-loaded (A, B) and loaded with resveratrol (C, D) in phosphate buffer pH 7 as a function of temperature.

6.3.6 HET-CAM test and zebra fish model

Resveratrol has shown ocular safety when instilled in a rabbit model (Draize test) encapsulated in Soluplus® micelles at concentration as high as 5 mg/mL. Chronic toxicity tests, carried out using human corneal epithelial cells (HCECs) cultures at lower concentrations, revealed cytocompatibility up to 0.5 mg of resveratrol

USC UNIVERSIDADE DE SANTIAGO DE COMPOSTELA

per mL [Li et al., 2020]. The search for alternatives to the Draize test have pointed out the Hen's Egg Test on the Chorioallantoic Membrane (HET-CAM) assay and the zebrafish embryo toxicity test (FET) as preferable methods that fulfil 3R´s principles. The HET-CAM assay and the FET test are not considered an animal procedure. The chick chorioallantoic membrane is not innervated, and the Institutional Animal Care and Use Committee (IACUC) and the USA National Institutes of Health established that a chick embryo does not experience pain until embryonal day (ED) 14 and is not considered as a living animal until ED17 [Ribatti, 2016; Kundeková et al., 2021]. According to the European Directive 2010/63/EU, the zebrafish embryos until the onset of independent feeding at 120 h post fertilization (hpf) are exempt from legal obligations regarding the protection of animals used for scientific purposes [European Union, 2010].

The HET-CAM assay allows evaluating, in a fast and sensitive way, the potential ocular irritancy of the formulations by monitoring changes in the CAM of fertilized eggs, which serves as an analog of the conjunctiva [ICCVAM, 2010]. Thus, the potential acute ocular irritation of the prepared formulations was monitored for 5 min in terms of hemorrhage, vascular lysis and coagulation [Alvarez-Rivera et al., 2018]. None of these events was observed for the resveratrol-loaded micelles neither for the non-loaded counterparts (**Figure 6.11**). The irritation score (IS) for the negative control and the tested formulations was 0.00. Differently, the IS registered for the positive control (NaOH 0.1 M) was 19.59. These findings mean that the micelle components (Pluronic® F127 and casein) at the concentrations tested as well as the exposition to remarkably high doses of resveratrol did not trigger ocular irritation.

USC
UNIVERSIDADE DE SANTIAGO DE COMPOSTELA

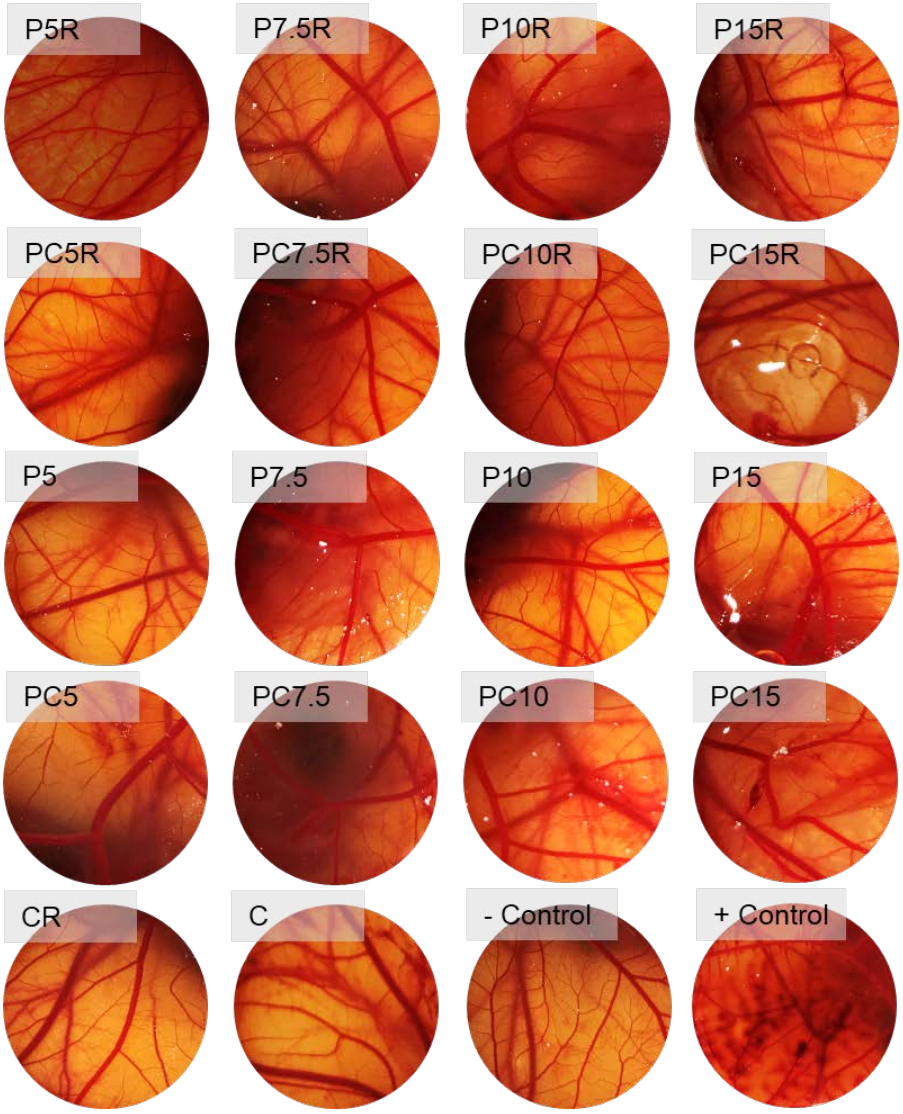


Figure 6.11. Images of the HET-CAM test. Codes as in Table 6.1 (R indicates formulations loaded with resveratrol). Negative control (0.9% NaCl) and positive control (0.1 N NaOH).

USC
UNIVERSIDADE DE SANTIAGO DE COMPOSTELA

The fish embryo toxicity test using zebrafish embryos is being pointed out as suitable for predicting both biocompatibility and ecotoxicity of nanomaterials and pharmaceutical excipients used to develop drug nanocarriers [Hering et al., 2020]. Moreover, many human diseases, including relevant ocular pathologies, can be reproduced in zebrafish embryos, which allows screening new treatments in terms of safety and efficacy in a much faster and cheaper way than using mammalian models and avoiding ethics concerns [Zhang et al., 2018; Lee and Yang, 2021]. Although the fish embryo toxicity tests carried out with polymeric micelles are still limited, a previous report revealed a LC50 of 5.21% for Pluronic® F127 at 72 hpf [Hering et al., 2020]. Therefore, single and mixed micelles prepared with 5 mM (6.3%) Pluronic® F127, both blank and loaded with resveratrol (0.4 mg/mL), were suitably diluted in the growing medium up to a final concentration of 0.02 mg resveratrol per mL. It should be noted that, when intended for ophthalmic purposes, few minutes after ocular instillation, the concentration on the eye surface of the formulation components (both drug and excipients) rapidly declines. Thus, the zebrafish embryo toxicity tests were carried out in the range of concentrations expected to be achieved in the anterior segment tissues if the drug would get access to them [Lee and Yang, 2021].

The percentages of mortality recorded for single micelle dispersions prepared with 5 mM Pluronic® F127 were 5% and 1.6% for blank and resveratrol-loaded formulations, respectively. Mixed micelles showed higher toxicity; the mortality for PC5 was 10% and for PC5R was 20%. Casein dispersion loaded and not with resveratrol caused 20% and 12.5% mortality, respectively. The percentage of mortality registered for the negative control was 2.5%. Overall, these values indicated that resveratrol-loaded single micelles are

USC UNIVERSIDADE DE SANTIAGO DE COMPOSTELA

biocompatible, while the presence of casein may induce some deleterious effects on long-term viability.

6.3.7 Antioxidant properties

The DPPH assay was carried out to elucidate the feasibility of the developed single and mixed micelles to load and release resveratrol without compromising its antioxidant activity. The possible antioxidant capacity of the phosphate buffer pH 7 in which all formulations were prepared and of blank micelles was also evaluated to confirm that there were no leaching substances that could cause artifacts during the test. The DPPH scavenging capacity was expressed as µg/mL in the reaction medium and as percentage as previously described [Vivero-Lopez et al., 2021a]. The changes in color of the tested formulations after the DPPH assay clearly evidenced the strong antioxidant activity of resveratrol encapsulated in the micelles, which turned the medium yellow, compared to the purple color of non-antioxidant non-loaded micelles **(Figures 6.12 and 6.13)**.

USC
UNIVERSIDADE DE SANTIAGO DE COMPOSTELA

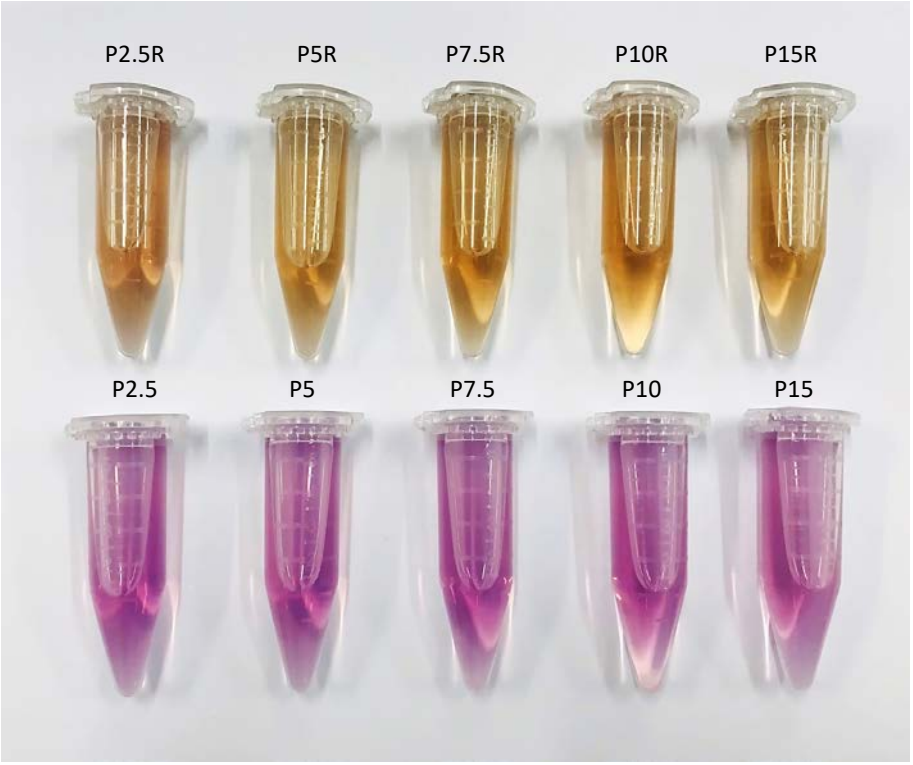


Figure 6.12. Antioxidant activity of resveratrol released from Pluronic® F127 single micelles (up) compared to the non-loaedd counterparts (down).

USC
UNIVERSIDADE DE SANTIAGO DE COMPOSTELA

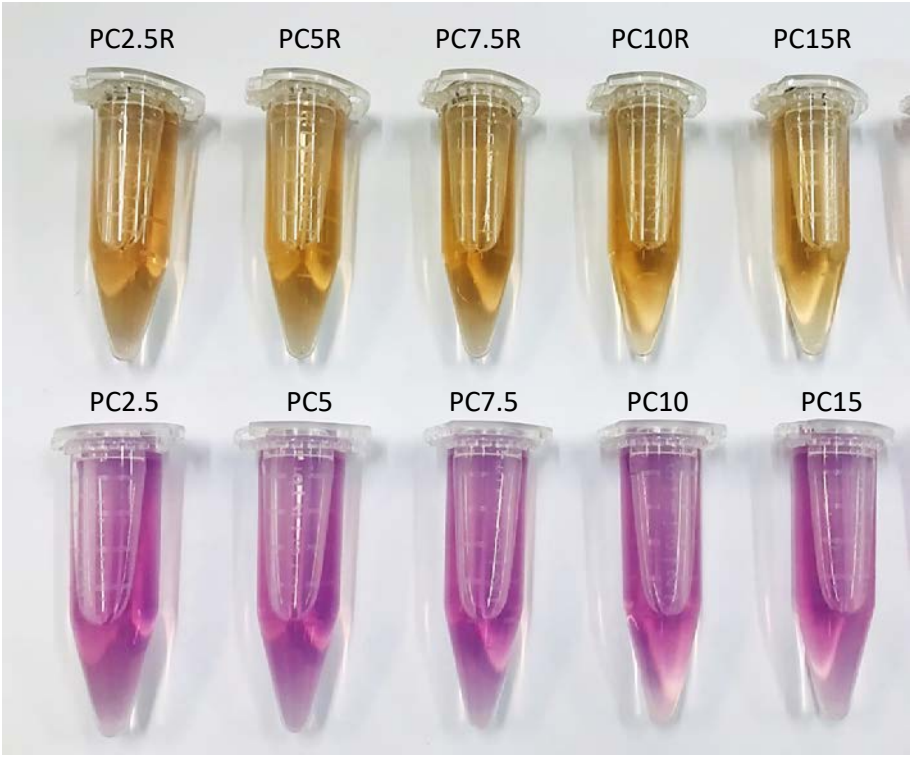


Figure 6.13. Antioxidant activity of resveratrol released from Pluronic® F127/casein mixed micelles (up) compared to the non-loaded counterparts (down).

According to the results **(Table 6.6)**, the scavenging effect registered was higher as the content in Pluronic® F127 increased in the micelles, especially for Pluronic® F127/casein mixed micelles, which was in good agreement with the higher content in resveratrol **(Table 6.5)**. The antioxidant capacity of the phosphate buffer pH 7 was significantly lower than that of the micelles. No statistically differences were registered between the phosphate buffer pH 7 and the non-loaded micelles. These results confirmed that the resveratrol can be incorporated and released from all formulations while preserving its antioxidant capacity. Indeed, even for the resveratrol encapsulated

USC UNIVERSIDADE DE SANTIAGO DE COMPOSTELA

in the single and mixed micelles prepared with 5 mM Pluronic® F127 (P5 and PC5) the antioxidant effect was remarkably high.

Table 6.6. DPPH levels (μg/mL) and DPPH scavenging effect (%). All data are mean ± SDs (n = 3).

Formulation	DPPH (μg/mL)	DPPH Scavenging Effect (%)
P2.5R	10.1 ± 0.3	20.3 ± 2.2
P5R	9.6 ± 0.1	27.7 ± 1.1
P7.5R	9.7 ± 0.0	27.5 ± 0.3
P10R	9.9 ± 0.2	26.6 ± 1.6
P15R	8.9 ± 0.6	34.6 ± 4.6
PC2.5R	9.7 ± 0.8	28.0 ± 5.9
PC5R	8.4 ± 0.1	38.0 ± 0.9
PC7.5R	8.8 ± 0.1	35.0 ± 1.1
PC10R	8.4 ± 0.7	38.9 ± 5.3
PC15R	7.2 ± 0.5	44.3 ± 4.4
PBS	12.7 ± 0.3	4.8 ± 2.0

6.3.8 Ability to inhibit bacterial growth

The contamination of multidose eyedrops is one of the main causes of ocular infections worldwide, which could be avoided [Nentwich et al., 2007]. Many of these infections are caused by *S. aureus* or *P. aeruginosa*, two of the main causal bacteria of microbial keratitis, a severe ophthalmic infection that can progress to blindness [Bispo et al., 2015; Teuchner et al., 2015; Tsegaw et al., 2017; Kyei et al., 2019]. The addition of preservatives in eye drops composition may prevent the development of severe ocular infections [da Costa et al., 2020], but at the same time may cause allergic of inflammatory reactions in long term use [Baudouin et al., 2010]. The development

USC UNIVERSIDADE DE SANTIAGO DE COMPOSTELA

of topical ophthalmic formulations with capacity to inhibit bacterial growth may avoid the use of preservatives and, in turn, the incidence of associated adverse effects.

The capacity of all formulations to inhibit bacterial growth was challenged against *S. aureus* and *P. aeruginosa*. First, resveratrol itself was tested at various concentrations (10-300 µg/mL) in ethanol:water 50:50 v/v. Higher concentrations of resveratrol in ethanol:water 50:50 v/v were not studied due to poor aqueous solubility of the compound and to avoid a high concentration of ethanol in the medium. In all cases, the concentration of ethanol remained at 5% in the bacterial growth medium. Thus, the growth of bacteria inoculum in the presence of 5% ethanol was also investigated.

Medium containing 5% ethanol slowed down the growth of both bacteria **(Figure 6.14A and B)** but did not affect the optical density obtained at 24 h that was similar for both bacteria (0.90 ± 0.09 for *S. aureus*, and 0.94 ± 0.45 for *P. aeruginosa*). A resveratrol concentration of 10 µg/mL did not affect and even increased the growth of *S. aureus* compared to the presence of ethanol in the medium. The growth of *S. aureus* was slowed down when the resveratrol concentration was equal to or higher than 50 µg/mL **(Figure 6.14A)**. Strong inhibitory concentrations were found for 200 and 300 µg resveratrol per mL. In the case of *P. aeruginosa*, a decrease in its growth was observed after 8 h of incubation **(Figure 6.14B)**. The optical density registered at 24 h decreased with the increase in resveratrol concentration.

USC
UNIVERSIDADE DE SANTIAGO DE COMPOSTELA

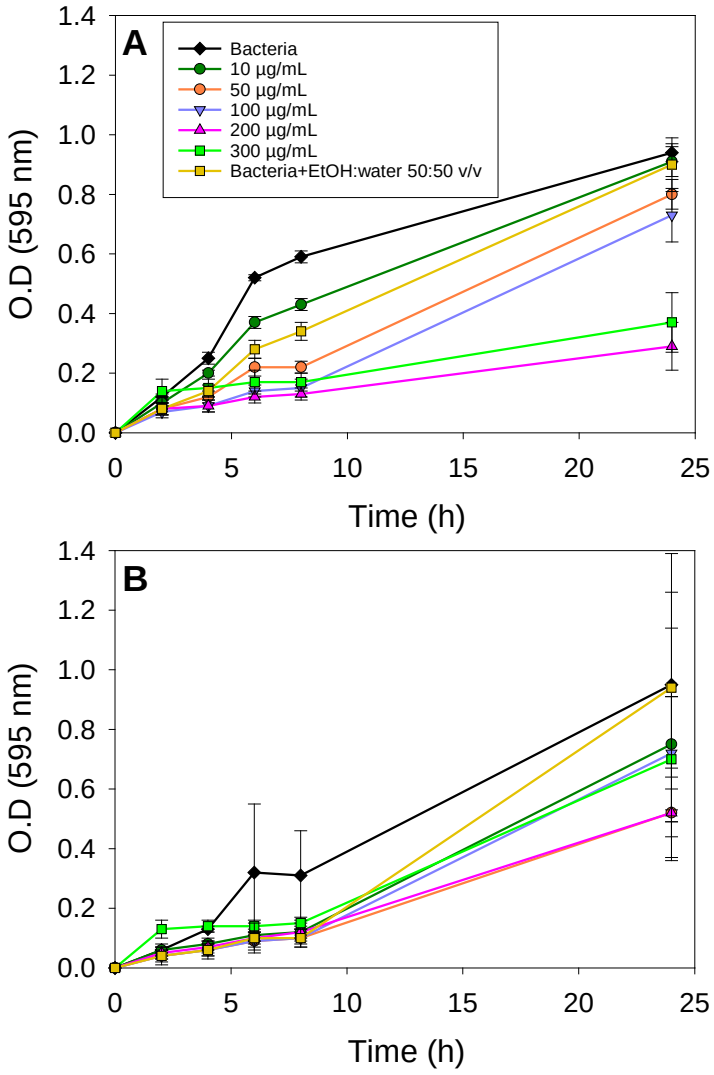


Figure 6.14. Growth of *Staphylococcus aureus* (A) and *Pseudomonas aeruginosa* (B) in media containing different concentrations of resveratrol.

Then, the capacity of single and mixed micelles, loaded and not with resveratrol, to inhibit the growth of both bacteria was studied.

USC UNIVERSIDADE DE SANTIAGO DE COMPOSTELA

Bacteria inoculum diluted with PBS was used as control for comparative purposes. In the case of *S. aureus*, a decrease in its growth was observed for resveratrol-loaded single micelles prepared with 10 mM (P10R) and 15 mM (P15R) Pluronic® **(Figure 6.15A**; codes 2 and 3 in **Table 6.7)**, something expected considering the higher amount of resveratrol encapsulated by these formulations. Also, blank micelles prepared with these same concentrations caused a statistically significant decrease in the growth of the bacteria at 6 and 8 h (codes 5 and 6 in **Table 6.7)**. For mixed micelles, once again P10R and P15R led to statistically significant decreases in bacteria growth at 4, 6 and 8 h **(Figure 6.15B).** The decrease was also significant for P15R at 24 h, and for blank micelles at 6 and 8 h (**Table 6.7**).

Table 6.7. Statistical analysis (ANOVA and multiple range test) of the optical density values recorded for *S. aureus* growth in the presence of P5R (1), P10R (2), P15R (3), P5 (4), P10 (5), P15 (6), and the bacteria inoculum diluted with PBS (7, control) (n = 6). Data in Figure 6.15A and B. In the multiple range test column, the values are ranked in increasing order. The code (7) of the bacteria growing in the absence of the formulations is highlighted in red.

Formulation	Time (h)	$F_{6,35}$	*p*	Multiple range test
Single micelle	4	63.15	0.000	2 3 6 5 4 7 1
	6	17.10	0.000	2 3 5 6 4 1 7
	8	28.15	0.000	5 3 6 2 4 1 7
	24	12.88	0.000	3 2 5 6 7 1 4
Mixed micelle	4	83.47	0.000	2 3 5 7 6 4 1
	6	26.93	0.000	5 6 3 2 4 7 1
	8	37.49	0.000	6 5 3 2 4 1 7
	24	2.82	0.024	3 2 5 7 6 4 1

USC UNIVERSIDADE DE SANTIAGO DE COMPOSTELA

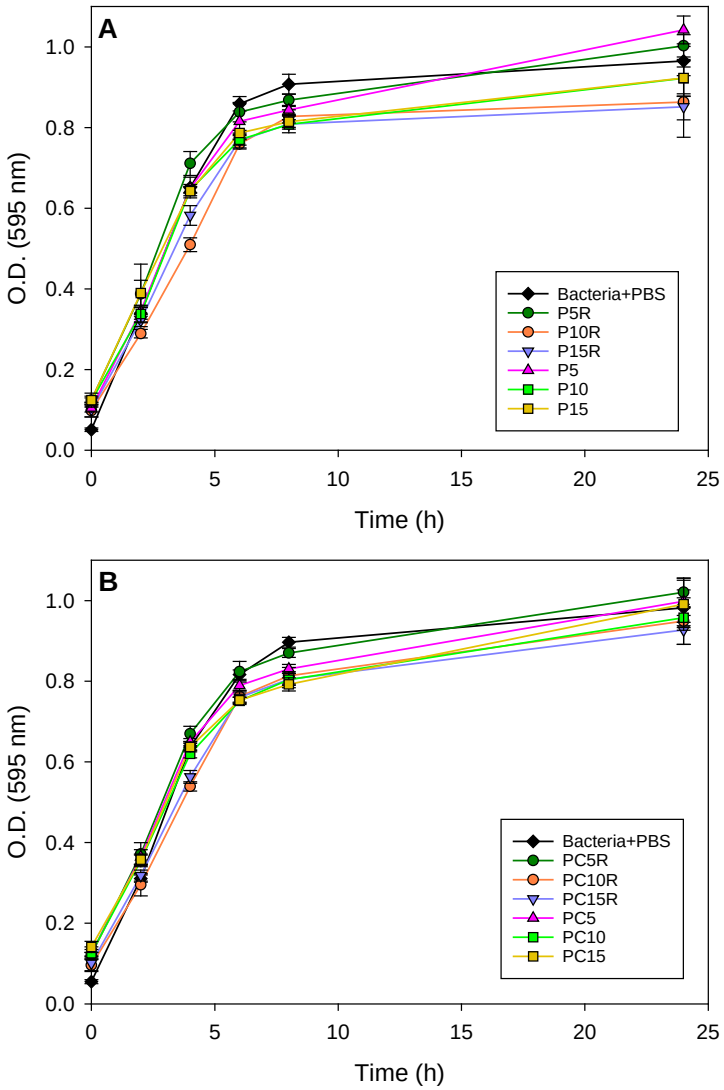


Figure 6.15. Bacterial growth of *Staphylococcus aureus* in the presence of different single (A) and mixed micelles (B).

USC
UNIVERSIDADE DE SANTIAGO DE COMPOSTELA

The growth of *P. aeruginosa* is shown in **Figures 6.16A and B**.

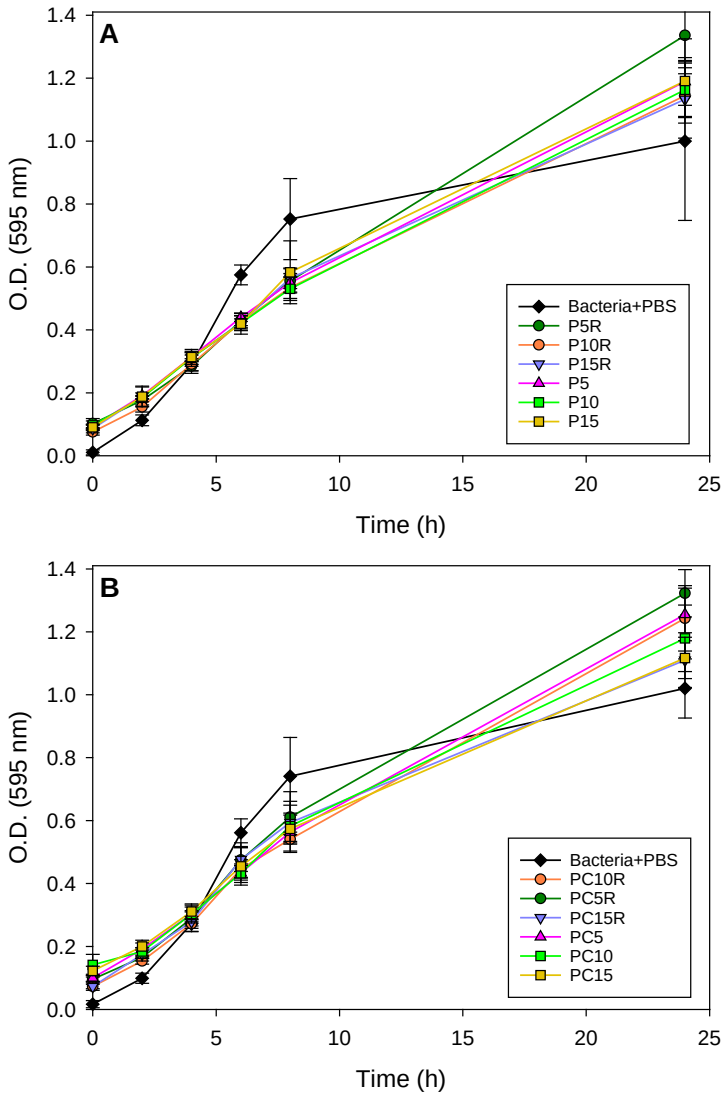


Figure 6.16. Bacterial growth of *Pseudomonas aeruginosa* in the presence of different single (A) and mixed micelles (B).

USC
UNIVERSIDADE DE SANTIAGO DE COMPOSTELA

The initial turbidity in *P. aeruginosa* growing media may be the contribution of both the formulations and the biofilm. Both blank and resveratrol-loaded single micelles reduced the growth at 6 h and 8 h, while mixed micelles only caused a decrease at 8 h (**Table 6.8**). No differences were shown between resveratrol-loaded and non-loaded micelles, which suggests that the decrease in the growth may be related to a direct effect of Pluronic® F127. This finding is in good agreement with a recent report on the effect of Pluronic® F127 dispersions (0.79 mM) on *Pseudomonas* spp. and *Klebsiella* spp. biofilms, showing an strong inhibitory activity [Eid et al., 2020]. The reasons are still to be elucidated.

Table 6.8. Statistical analysis (ANOVA and multiple range test) of the optical density values recorded for *P. aeruginosa* growth in the presence of P5R (1), P10R (2), P15R (3), P5 (4), P10 (5), P15 (6), and the bacteria inoculum diluted with PBS (7, control) (n = 6). Data in Figure 6.15A and B. In the multiple range test column, the values are ranked in increasing order. The code (7) of the bacteria growing in the absence of the formulations is highlighted in red.

Formulation	Time (h)	$F_{6,35}$	*p*	Multiple range test
Single micelle	4	2.35	0.052	No significant differences
	6	34.43	0.000	6 5 3 2 1 4 7
	8	7.74	0.000	5 2 4 1 3 6 7
	24	3.31	0.011	7 3 2 5 4 6 1
Mixed micelle	4	2.53	0.038	2 7 3 1 4 5 6
	6	0.85	0.658	No significant differences
	8	5.07	0.001	2 4 6 5 3 1 7
	24	8.13	0.000	7 3 6 5 2 4 1

USC UNIVERSIDADE DE SANTIAGO DE COMPOSTELA

6.3.9 Ex vivo corneal and scleral permeability tests

Polymeric micelles constitute an excellent system to improve the solubility and tissue permeability of hydrophobic compounds like resveratrol [Grimaudo et al., 2019; Mandal et al., 2017; Durgun et al., 2020]. The capacity of resveratrol released from P10R and PC10R formulations to permeate through porcine cornea and sclera together with its capacity to remain in these tissues was evaluated performing an *ex vivo* permeability test. The test was carried out using porcine tissues given its close similarity to the human eye [Alambiaga-Caravaca et al., 2020]. In cornea **(Figure 6.17)**, no quantifiable amounts of resveratrol were recorded in the donor chamber before 4 h of experiment. However, resveratrol showed an increased permeability through sclera **(Figure 6.18)** detecting quantifiable amounts from the first hour of experiment. No differences were recorded for the permeability through cornea between single and mixed micelles. Differently, single micelles loaded with resveratrol led to an increase in scleral permeability **(Figure 6.18).** Both single and mixed micelles have improved notably the permeability of resveratrol through both tissues compared to previously developed HEMA- and silicone-based hydrogels loaded with resveratrol and the resveratrol concentrated solution (70 µg/mL), which did not provide measurable amounts of resveratrol to the receptor chamber (as shown in **Chapter 4**). This correlates well with other works where the capacity of micellar systems composed of Soluplus® to increase the permeability of different drugs as acyclovir or α-lipoic acid was demonstrated [Alvarez-Rivera et al., 2016; Varela-Garcia et al., 2018].

USC
UNIVERSIDADE DE SANTIAGO DE COMPOSTELA

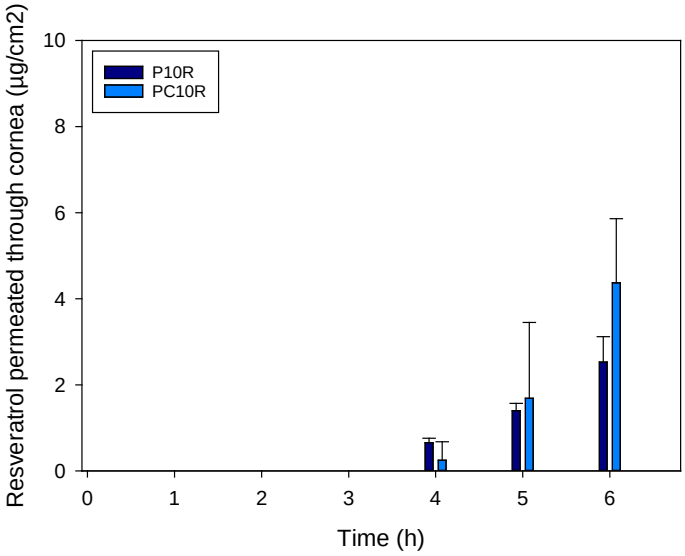


Figure 6.17. Amounts of resveratrol permeated trough cornea when released from P10R and PC10R micelles. (n = 3; mean values and standard deviations).

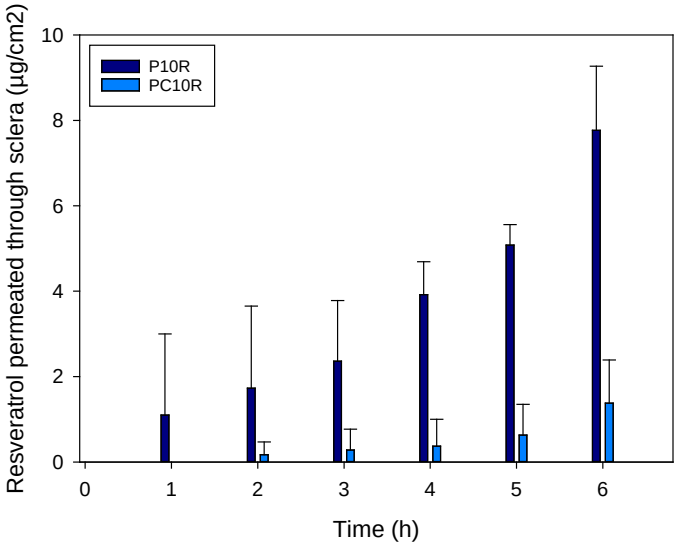


Figure 6.18. Amounts of resveratrol permeated trough sclera when released from P10R and PC10R micelles. (n = 3; mean values and standard deviations).

USC
UNIVERSIDADE DE SANTIAGO DE COMPOSTELA

The accumulation of resveratrol was higher in sclera for single (475.91 ± 219.99 µg/cm^2) and mixed (467.59 ± 20.51 µg/cm^2) micelles than in cornea for single (83.59 ± 19.45 µg/cm^2) and mixed (62.58 ± 6.85 µg/cm^2) micelles but no statistical differences were observed between both dispersions for each tissue **(Figure 6.19).** n summary, resveratrol passed more easily and accumulated more in the sclera than in the cornea, which was expected taking into account the greater permeability of this tissue and non-dependence on the hydrophilicity of the compound [Gaudana et al., 2010].

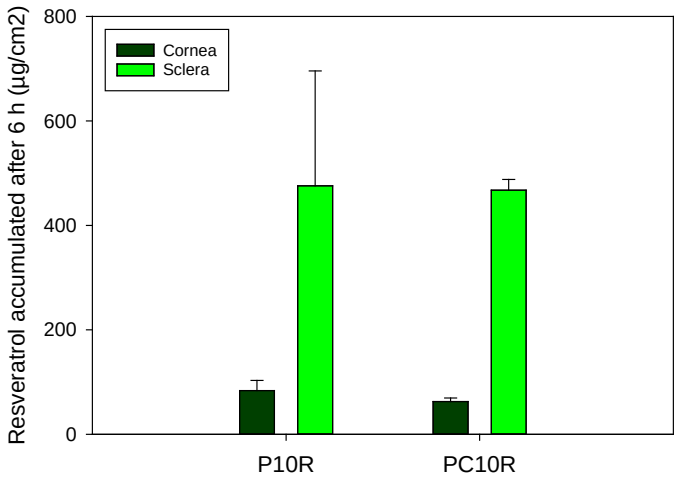


Figure 6.19. Amounts of resveratrol accumulated in cornea and sclera when released from P10R and PC10R micelles after 6 h of experiment. (n = 3; mean values and standard deviations).

The amount of resveratrol remnant in the donor chamber was also calculated for all dispersions and tissues (**Figure 6.20)**. The amount of resveratrol in the donor chamber after 6 h of experiment was higher for cornea than sclera tissue for both formulations but no big

USC UNIVERSIDADE DE SANTIAGO DE COMPOSTELA

differences were observed considering the higher amount of resveratrol permeated and accumulated through and into sclera.

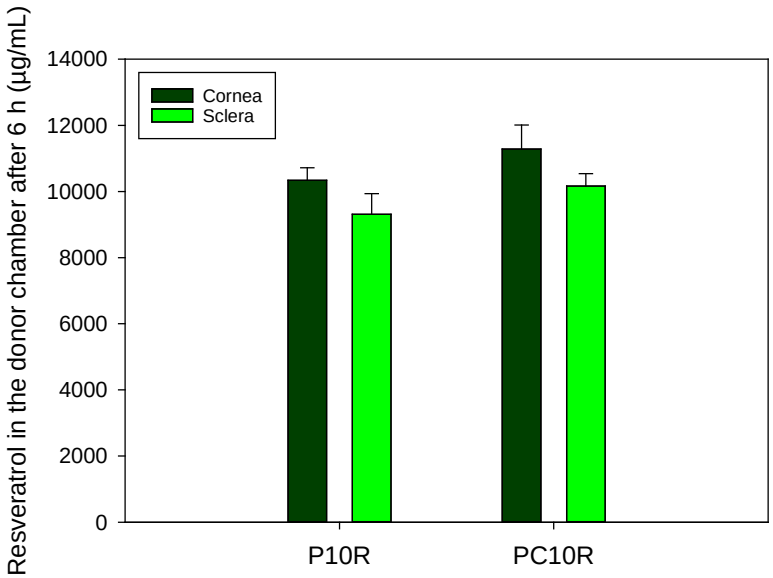


Figure 6.20. Concentration of resveratrol remanent in the donor chamber after 6 h of experiment. (n=3; mean values and standard deviations).

The permeability coefficient (P_{app}) and steady state flux (J) of resveratrol in both corneal and scleral tissues are shown in **Table 6.9**. The permeability coefficients obtained were lower than those previously reported for other drugs like α-lipoic acid, valaciclovir or transferulic acid, but the steady state flux values were in good agreement with the values reported for valaciclovir in Soluplus® micelles [Alvarez-Rivera et al., 2016; Varela-Garcia et al., 2018; Varela-Garcia et al., 2020].

USC UNIVERSIDADE DE SANTIAGO DE COMPOSTELA

Table 6.7. Steady state flux (J) and permeability coefficient of resveratrol released from P10R and PC10R dispersions for cornea and sclera tissues. (mean value ± standard deviations).

Formulation	Cornea		Sclera	
	J ($\mu g/cm^2h^{-1}$)	P_{app} (cm/s)	J ($\mu g/cm^2h^{-1}$)	P_{app} (cm/s)
P10R	0.43 ± 0.08	$1.14 \times 10^{-8} \pm 1.98 \times 10^{-9}$	1.26 ± 0.38	$3.78 \times 10^{-8} \pm 1.15 \times 10^{-8}$
PC10R	0.65 ± 0.25	$1.62 \times 10^{-8} \pm 7.38 \times 10^{-9}$	0.21 ± 0.18	$5.75 \times 10^{-9} \pm 4.70 \times 10^{-9}$

6.4. CONCLUSIONS

In this part of the Thesis the development of single and mixed micelles composed of Pluronic® F127 and Pluronic® F127/casein was successfully carried out. The size of PC mixed micelles without resveratrol increased with increasing Pluronic® content, and the loading of resveratrol did not affect the size for single micelles. As expected, the Z-potential of single micelles was close to zero but negative for casein micelles due to the pH of the medium. Good ocular tolerance and non-toxicity of most promising developed formulations was confirmed through the HET-CAM and FET tests. Also, the micelles showed excellent stability during storage and after strong dilution. Pluronic® 10 mM micelle dispersions are pointed out as the most adequate formulations since they combine remarkably high capability to solubilize resveratrol and to preserve its antioxidant properties, biofilm inhibition capability, gelling in an adequate temperature window, and favored resveratrol permeability through corneal and scleral tissues.

USC UNIVERSIDADE DE SANTIAGO DE COMPOSTELA

6.5 REFERENCES

Abelson, M. B., Udell, I. J., & Weston, J. H. (1981). Normal human tear pH by direct measurement. *Archives of Ophthalmology*, *99*(2), 301-301.

Ahmad, I., & Hoda, M. (2020). Attenuation of diabetic retinopathy and neuropathy by resveratrol: Review on its molecular mechanisms of action. *Life Sciences*, 245, 117350.

Alambiaga-Caravaca, A. M., Calatayud-Pascual, M. A., Rodilla, V., Concheiro, A., López-Castellano, A., & Alvarez-Lorenzo, C. (2020). Micelles of progesterone for topical eye administration: Interspecies and intertissues differences in ex vivo ocular permeability. *Pharmaceutics*, *12*(8), 702.

Al Khateb, K., Ozhmukhametova, E. K., Mussin, M. N., Seilkhanov, S. K., Rakhypbekov, T. K., Lau, W. M., & Khutoryanskiy, V. V. (2016). In situ gelling systems based on Pluronic F127/Pluronic F68 formulations for ocular drug delivery. *International Journal of Pharmaceutics*, *502*(1-2), 70-79.

Alvarez-Rivera, F., Fernández-Villanueva, D., Concheiro, A., & Alvarez-Lorenzo, C. (2016). α-Lipoic acid in Soluplus® polymeric nanomicelles for ocular treatment of diabetes-associated corneal diseases. *Journal of Pharmaceutical Sciences*, *105*(9), 2855-2863.

Alvarez-Rivera, F.; Concheiro, A.; Alvarez-Lorenzo, C (2018). Epalrestat-loaded silicone hydrogels as contact lenses to address diabetic-eye complications. *European Journal of Pharmaceutics and Biopharmaceutics, 122*, 126–136.

Alvarez-Rivera, F., Serro, A. P., Silva, D., Concheiro, A., & Alvarez-Lorenzo, C. (2019). Hydrogels for diabetic eyes: Naltrexone loading, release profiles and cornea penetration. *Materials Science and Engineering: C*, *105*, 110092.

USC
UNIVERSIDADE DE SANTIAGO DE COMPOSTELA

Amri, A., Chaumeil, J. C., Sfar, S., & Charrueau, C. (2012). Administration of resveratrol: what formulation solutions to bioavailability limitations?. *Journal of Controlled Release*, *158*(2), 182-193.

Bachar, M., Mandelbaum, A., Portnaya, I., Perlstein, H., Even-Chen, S., Barenholz, Y., & Danino, D. (2012). Development and characterization of a novel drug nanocarrier for oral delivery, based on self-assembled β-casein micelles. *Journal of Controlled Release*, *160*(2), 164-171.

Baudouin, C., Labbé, A., Liang, H., Pauly, A., & Brignole-Baudouin, F. (2010). Preservatives in eyedrops: the good, the bad and the ugly. *Progress in Retinal and Eye Research*, *29*(4), 312-334.

Behl, T., Kaur, I., & Kotwani, A. (2016). Implication of oxidative stress in progression of diabetic retinopathy. *Survey of Ophthalmology*, *61*(2), 187-196.

Bispo, P. J., Haas, W., & Gilmore, M. S. (2015). Biofilms in infections of the eye. *Pathogens*, *4*(1), 111-136.

Bola, C., Bartlett, H., & Eperjesi, F. (2014). Resveratrol and the eye: activity and molecular mechanisms. *Graefe's Archive for Clinical and Experimental Ophthalmology*, *252*(5), 699-713.

Bourassa, P., Bariyanga, J., & Tajmir-Riahi, H. A. (2013). Binding sites of resveratrol, genistein, and curcumin with milk α-and β-caseins. *The Journal of Physical Chemistry B*, *117*(5), 1287-1295.

Cabrera, F. J., Wang, D. C., Reddy, K., Acharya, G., & Shin, C. S. (2019). Challenges and opportunities for drug delivery to the posterior of the eye. *Drug Discovery Today*, *24*(8), 1679-1684.

Cadena, P. G., Pereira, M. A., Cordeiro, R. B., Cavalcanti, I. M., Neto, B. B., Maria do Carmo, C. B., ... & Santos-Magalhães, N. S. (2013). Nanoencapsulation of quercetin and resveratrol into elastic liposomes. *Biochimica et Biophysica Acta (BBA)-Biomembranes*, *1828*(2), 309-316.

USC
UNIVERSIDADE DE SANTIAGO DE COMPOSTELA

Calderon, G. D., Juarez, O. H., Hernandez, G. E., Punzo, S. M., & De la Cruz, Z. D. (2017). Oxidative stress and diabetic retinopathy: development and treatment. *Eye*, *31*(8), 1122-1130.

Cejka, C., & Cejkova, J. (2015). Oxidative stress to the cornea, changes in corneal optical properties, and advances in treatment of corneal oxidative injuries. *Oxidative medicine and cellular longevity*, *2015*, 591530.

Chen, Y., Meng, J., Li, H., Wei, H., Bi, F., Liu, S., ... & Liu, W. (2019). Resveratrol exhibits an effect on attenuating retina inflammatory condition and damage of diabetic retinopathy via PON1. *Experimental Eye Research*, *181*, 356-366.

Chrysostomou, V., Rezania, F., Trounce, I. A., & Crowston, J. G. (2013). Oxidative stress and mitochondrial dysfunction in glaucoma. *Current Opinion in Pharmacology*, *13*(1), 12-15.

Coles, W. H., & Jaros, P. A. (1984). Dynamics of ocular surface pH. *British Journal of Ophthalmology*, *68*(8), 549-552.

da Costa, A. X., Yu, M. C. Z., de Freitas, D., Cristovam, P. C., LaMonica, L. C., Dos Santos, V. R., & Gomes, J. A. P. (2020). Microbial cross-contamination in multidose eyedrops: The impact of instillation angle and bottle geometry. *Translational Vision Science & Technology*, *9*(7), 7-7.

Dammak, A.; Huete-Toral, F.; Carpena-Torres, C.; Martin, A.; Pastrana, C.; Carracedo G. (2021). From oxidative stress to inflammation in the posterior ocular diseases: diagnosis and treatment. *Pharmaceutics*, 13, 1376.

Datta, S., Cano, M., Ebrahimi, K., Wang, L., & Handa, J. T. (2017). The impact of oxidative stress and inflammation on RPE degeneration in non-neovascular AMD. *Progress in Retinal and Eye Research*, *60*, 201-218.

Del Regno, A., Warren, P. B., Bray, D. J., & Anderson, R. L. (2021). Critical micelle concentrations in surfactant mixtures and blends by simulation. *Journal of Physical Chemistry B*, *125*, 5983-5990.

USC UNIVERSIDADE DE SANTIAGO DE COMPOSTELA

Delmas, D., Cornebise, C., Courtaut, F., Xiao, J., & Aires, V. (2021). New highlights of resveratrol: A review of properties against ocular diseases. *International Journal of Molecular Sciences*, 22(3), 1295.

Di Donato, C., Iacovino, R., Isernia, C., Malgieri, G., Varela-Garcia, A., Concheiro, A., & Alvarez-Lorenzo, C. (2020). Polypseudorotaxanes of Pluronic® F127 with combinations of α-and β-cyclodextrins for topical formulation of acyclovir. *Nanomaterials*, *10*(4), 613.

Dinte, E., Vostinaru, O., Samoila, O., Sevastre, B., & Bodoki, E. (2020). Ophthalmic nanosystems with antioxidants for the prevention and treatment of eye diseases. *Coatings*, *10*(1), 36.

Dogru, M., Kojima, T., Simsek, C., & Tsubota, K. (2018). Potential role of oxidative stress in ocular surface inflammation and dry eye disease. *Investigative Ophthalmology & Visual Science*, *59*(14), DES163-DES168.

Dong, Y., Wan, G., Yan, P., Qian, C., Li, F., & Peng, G. (2019). Fabrication of resveratrol coated gold nanoparticles and investigation of their effect on diabetic retinopathy in streptozotocin induced diabetic rats. *Journal of Photochemistry and Photobiology B: Biology*, *195*, 51-57.

Dumortier, G., Grossiord, J. L., Agnely, F., & Chaumeil, J. C. (2006). A review of poloxamer 407 pharmaceutical and pharmacological characteristics. *Pharmaceutical Research*, *23*(12), 2709-2728.

Durgun, M.E., Güngör, S., & Özsoy, Y. (2020). Micelles: Promising ocular drug carriers for anterior and posterior segment diseases. *Journal of Ocular Pharmacology and Therapeutics*, *36*, 323-341.

Edsman, K., Carlfors, J., & Petersson, R. (1998). Rheological evaluation of poloxamer as an in situ gel for ophthalmic use. *European Journal of Pharmaceutical Sciences*, *6*(2), 105-112.

USC
UNIVERSIDADE DE SANTIAGO DE COMPOSTELA

Eid, D., Sayed, O.M., Hozayen, W.G., & Azmy, A.F. (2020). Battling biofilm forming nosocomial pathogens using chitosan and Pluronic F127. *Journal of Pure and Applied Microbiology*, 14(3), 1893-1903.

El-Far, S. W., Helmy, M. W., Khattab, S. N., Bekhit, A. A., Hussein, A. A., & Elzoghby, A. O. (2018). Phytosomal bilayer-enveloped casein micelles for codelivery of monascus yellow pigments and resveratrol to breast cancer. *Nanomedicine*, *13*(5), 481-499.

EMA.https://www.ema.europa.eu/en/search/search?search_api_views_fulltext=poloxamer+AND+ocular; accessed January 2022.

European Union (2010). Directive 2010/63/EU of the European Parliament and of the Council of 22 September 2010 on the protection of animals used for scientific purposes. https://eur-lex.europa.eu/legal-content/EN/TXT/HTML/?uri=CELEX:32010L0063&from=EN; accessed January 2022.

Gandhi, S., & Roy, I. (2019). Doxorubicin-loaded casein nanoparticles for drug delivery: Preparation, characterization and in vitro evaluation. *International Journal of Biological Macromolecules*, *121*, 6-12.

Gaudana, R., Ananthula, H. K., Parenky, A., & Mitra, A. K. (2010). Ocular drug delivery. *The AAPS journal*, *12*(3), 348-360.

Ghadiri Soufi, F., Arbabi-Aval, E., Rezaei Kanavi, M., & Ahmadieh, H. (2015). Anti-inflammatory properties of resveratrol in the retinas of type 2 diabetic rats. *Clinical and Experimental Pharmacology and Physiology*, *42*(1), 63-68.

Glab, T. K., & Boratyński, J. (2017). Potential of casein as a carrier for biologically active agents. *Topics in Current Chemistry*, *375*(4), 1-20.

Grimaudo, M. A., Pescina, S., Padula, C., Santi, P., Concheiro, A., Alvarez-Lorenzo, C., & Nicoli, S. (2019). Topical application of polymeric nanomicelles in ophthalmology: A review on research efforts for the

USC UNIVERSIDADE DE SANTIAGO DE COMPOSTELA

noninvasive delivery of ocular therapeutics. *Expert Opinion on Drug Delivery*, *16*(4), 397-413.

Grimaudo, M. A., Amato, G., Carbone, C., Diaz-Rodriguez, P., Musumeci, T., Concheiro, A., ... & Puglisi, G. (2020). Micelle-nanogel platform for ferulic acid ocular delivery. *International Journal of Pharmaceutics*, *576*, 118986.

Gülçin, İ. (2010). Antioxidant properties of resveratrol: A structure–activity insight. *Innovative Food Science & Emerging Technologies*, *11*(1), 210-218.

Hering, I., Eilebrecht, E., Parnham, M.J., Günday-Türeli, N., Türeli, A.E., Weiler, M., Schäfers, C., Fenske, M., Wacker, M.G. (2020). Evaluation of potential environmental toxicity of polymeric nanomaterials and surfactants. *Environmental Toxicology and Pharmacology*, *76*, 103353.

Huang, D. D., Shi, G., Jiang, Y., Yao, C., & Zhu, C. (2020). A review on the potential of Resveratrol in prevention and therapy of diabetes and diabetic complications. *Biomedicine & Pharmacotherapy*, *125*, 109767.

ICCVAM. *ICCVAM Test Method Evaluation Report: Current Validation Status of In Vitro Test Methods Proposed for Identifying Eye Injury Hazard Potential of Chemicals and Products*; NIH Publication No. 10-7553; Research Triangle Park, National Institute of Environmental Health Sciences: Durham, NC, USA, 2010; p. 1324.

Jadhav, P., Bothiraja, C., & Pawar, A. (2016). Resveratrol-piperine loaded mixed micelles: formulation, characterization, bioavailability, safety and in vitro anticancer activity. *RSC Advances*, *6*(114), 112795-112805.

Kang, Q., & Yang, C. (2020). Oxidative stress and diabetic retinopathy: Molecular mechanisms, pathogenetic role and therapeutic implications. *Redox Biology*, *37*, 101799.

Katekar, R., Thombre, G., Riyazuddin, M., Husain, A., Rani, H., Praveena, K. S., & Gayen, J. R. (2020). Pharmacokinetics and brain targeting of trans-resveratrol loaded mixed micelles in rats following intravenous

USC UNIVERSIDADE DE SANTIAGO DE COMPOSTELA

administration. *Pharmaceutical Development and Technology*, *25*(3), 300-307.

Kelly, P., Woonton, B. W., & Smithers, G. W. (2009). Improving the sensory quality, shelf-life and functionality of milk. In *Functional and speciality beverage technology* (Paquin, P., Ed.). Woodhead Publishing, pp. 170-231.

Kessler, A., Menéndez-Aguirre, O., Hinrichs, J., Stubenrauch, C., & Weiss, J. (2014). αs-Casein—PE6400 mixtures: Surface properties, miscibility and self-assembly. *Colloids and Surfaces B: Biointerfaces*, *118*, 49-56.

Kim, Y. H., Kim, Y. S., Roh, G. S., Choi, W. S., & Cho, G. J. (2012). Resveratrol blocks diabetes-induced early vascular lesions and vascular endothelial growth factor induction in mouse retinas. *Acta Ophthalmologica*, *90*(1), e31-e37.

Kim, H. M., & Woo, S. J. (2021). Ocular drug delivery to the retina: current innovations and future perspectives. *Pharmaceutics*, *13*, 108.

Kimpel, F., & Schmitt, J. J. (2015). Milk proteins as nanocarrier systems for hydrophobic nutraceuticals. *Journal of Food Science*, *80*(11), R2361-R2366.

Kimura, A., Namekata, K., Guo, X., Noro, T., Harada, C., & Harada, T. (2017). Targeting oxidative stress for treatment of glaucoma and optic neuritis. *Oxidative Medicine and Cellular Longevity*, *2017*, 2817252.

Kundeková, B.; Mácajová, M.; Meta, M.; Cavarga, I.; Bilcík, B. (2021). Chorioallantoic membrane models of various avian species: differences and applications. *Biology*, *10*, 301.

Kyei, S., France, D., & Asiedu, K. (2019). Microbial contamination of multiple-use bottles of fluorescein ophthalmic solution. *Clinical and Experimental Optometry*, *102*(1), 30-34.

Lançon, A., Frazzi, R., & Latruffe, N. (2016). Anti-oxidant, anti-inflammatory and anti-angiogenic properties of resveratrol in ocular diseases. *Molecules*, *21*(3), 304.

USC UNIVERSIDADE DE SANTIAGO DE COMPOSTELA

Lee, Y., Yang, J. (2021). Development of a zebrafish screening model for diabetic retinopathy induced by hyperglycemia: Reproducibility verification in animal model. *Biomedicine & Pharmacotherapy* 135, 111201.

Li, M., Zhang, L., Li, R., & Yan, M. (2020). New resveratrol micelle formulation for ocular delivery: characterization and in vitro/in vivo evaluation. *Drug Development and Industrial Pharmacy*, *46*(12), 1960-1970.

Liu, Y., Lin, L., Song, J., Zhao, Y., Chao, Z., & Li, H. (2017). Preparation, characterization and anticancer activities of resveratrol loaded redox-sensitive F127-SS-TOC micelles. *RSC Advances*, *7*(74), 47091-47098.

Lorenzo-Veiga, B., Sigurdsson, H. H., Loftsson, T., & Alvarez-Lorenzo, C. (2019). Cyclodextrin–amphiphilic copolymer supramolecular assemblies for the ocular delivery of natamycin. *Nanomaterials*, *9*(5), 745.

Mah, T. F. C., & O'Toole, G. A. (2001). Mechanisms of biofilm resistance to antimicrobial agents. *Trends in microbiology*, *9*(1), 34-39.

Mandal, A., Bisht, R., Rupenthal, I.D., Mitra, A.S. (2017). Polymeric micelles for ocular drug delivery: From structural frameworks to recent preclinical studies. *Journal of Controlled Release*, 248, 96-116.

Moon, J. K., & Shibamoto, T. (2009). Antioxidant assays for plant and food components. *Journal of Agricultural and Food Chemistry*, *57*(5), 1655-1666.

Nagai, N., Isaka, T., Deguchi, S., Minami, M., Yamaguchi, M., Otake, H., ... & Nakazawa, Y. (2020). In situ gelling systems using pluronic F127 enhance corneal permeability of indomethacin nanocrystals. *International Journal of Molecular Sciences*, *21*(19), 7083.

Natesan, S., Pandian, S., Ponnusamy, C., Palanichamy, R., Muthusamy, S., & Kandasamy, R. (2017). Co-encapsulated resveratrol and quercetin in chitosan and PEG modified chitosan nanoparticles: For efficient intra ocular pressure reduction. *International Journal of Biological Macromolecules*, *104*, 1837-1845.

USC
UNIVERSIDADE DE SANTIAGO DE COMPOSTELA

Nentwich, M. M., Kollmann, K. H. M., Meshack, J., Ilako, D. R., & Schaller, U. C. (2007). Microbial contamination of multi-use ophthalmic solutions in Kenya. *British Journal of Pphthalmology*, *91*(10), 1265-1268.

Nita, M., & Grzybowski, A. (2016). The role of the reactive oxygen species and oxidative stress in the pathomechanism of the age-related ocular diseases and other pathologies of the anterior and posterior eye segments in adults. *Oxidative medicine and cellular longevity*, *2016*, *3164734*.

OECD (2006). Fish embryo toxicity (FET) test. OECD guideline for testing of Chemicals. https://www.oecd-ilibrary.org/docserver/9789264203709-en.pdf?expires=1642188277&id=id&accname=guest&checksum=C2E677D38844874F436140FE5D30A0C4; accessed January 2022.

Olvera-Montano, C., Castellanos-Gonzalez, J. A., Navarro-Partida, J., Cardona-Munoz, E. G., Lopez-Contreras, A. K., Roman-Pintos, L. M., ... & Rodriguez-Carrizalez, A. D. (2019). Oxidative stress as the main target in diabetic retinopathy pathophysiology. *Journal of Diabetes Research*, *2019*, 8562408.

Pandian, S., Jeevanesan, V., Ponnusamy, C., & Natesan, S. (2017). RES-loaded pegylated CS NPs for efficient ocular delivery. *IET nanobiotechnology*, *11*(1), 32-39.

Peñalva, R., Morales, J., González-Navarro, C. J., Larrañeta, E., Quincoces, G., Peñuelas, I., & Irache, J. M. (2018). Increased oral bioavailability of resveratrol by its encapsulation in casein nanoparticles. *International Journal of Molecular Sciences*, *19*(9), 2816.

Phadungath, C. (2005). Casein micelle structure: a concise review. *Songklanakarin Journal of Science and Technology*, *27*(1), 201-212.

Pinazo-Durán, M. D., Gallego-Pinazo, R., García-Medina, J. J., Zanón-Moreno, V., Nucci, C., Dolz-Marco, R., ... & Díaz-Llópis, M. (2014). Oxidative stress and its downstream signaling in aging eyes. *Clinical interventions in aging*, *9*, 637.

USC UNIVERSIDADE DE SANTIAGO DE COMPOSTELA

Pinazo-Duran, M. D., Shoaie-Nia, K., Zanon-Moreno, V., Sanz-Gonzalez, S. M., del Castillo, J. B., & Garcia-Medina, J. J. (2018). Strategies to reduce oxidative stress in glaucoma patients. *Current Neuropharmacology*, *16*(7), 903-918.

Portnaya, I., Khalfin, R., Kesselman, E., Ramon, O., Cogan, U., & Danino, D. (2011). Mixed micellization between natural and synthetic block copolymers: β-casein and Lutrol F-127. *Physical Chemistry Chemical Physics*, *13*(8), 3153-3160.

Rangel-Yagui, C. O., Pessoa Jr, A., & Tavares, L. C. (2005). Micellar solubilization of drugs. *Journal of Pharmacy and Pharmaceutical Sciences*, *8*(2), 147-163.

Rehan, F., Ahemad, N., & Gupta, M. (2019). Casein nanomicelle as an emerging biomaterial–A comprehensive review. *Colloids and Surfaces B: Biointerfaces*, *179*, 280-292.

Rey-Rico, A., Silva, M., Couceiro, J., Concheiro, A., & Alvarez-Lorenzo, C. (2011). Osteogenic efficiency of in situ gelling poloxamine systems with and without bone morphogenetic protein-2. *European Cells and Materials*, *21*(4), 317-340.

Ribatti, D. (2016). The Chick Embryo Chorioallantoic Membrane (CAM). A multifaceted experimental model. *Mechanisms of Development*, *141*, 70–77.

Ribeiro, A., Sosnik, A., Chiappetta, D. A., Veiga, F., Concheiro, A., & Alvarez-Lorenzo, C. (2012). Single and mixed poloxamine micelles as nanocarriers for solubilization and sustained release of ethoxzolamide for topical glaucoma therapy. *Journal of the Royal Society Interface*, *9*(74), 2059-2069.

Robinson, K., Mock, C., & Liang, D. (2015). Pre-formulation studies of resveratrol. *Drug Development and Industrial Pharmacy*, *41*(9), 1464-1469.

Rodríguez, M. L., Pérez, S., Mena-Mollá, S., Desco, M. C., & Ortega, A. L. (2019). Oxidative stress and microvascular alterations in diabetic

USC UNIVERSIDADE DE SANTIAGO DE COMPOSTELA

retinopathy: Future Therapies. *Oxidative Medicine and Cellular Longevity, 2019*, 4940825.

Rodriguez-Perez, A. I., Rodriguez-Tenreiro, C., Alvarez-Lorenzo, C., Concheiro, A., & Torres-Labandeira, J. J. (2006). Drug solubilization and delivery from cyclodextrin-pluronic aggregates. *Journal of Nanoscience and Nanotechnology*, *6*(9-10), 3179-3186.

Schmolka, I. R. (1972). Artificial skin I. Preparation and properties of pluronic F-127 gels for treatment of burns. *Journal of biomedical materials research*, *6*(6), 571-582.

Semeraro, F., Morescalchi, F., Cancarini, A., Russo, A., Rezzola, S., & Costagliola, C. (2019). Diabetic retinopathy, a vascular and inflammatory disease: therapeutic implications. *Diabetes & Metabolism*, 45(6), 517-527.

Shapira, A., Markman, G., Assaraf, Y. G., & Livney, Y. D. (2010). β-casein–based nanovehicles for oral delivery of chemotherapeutic drugs: drug-protein interactions and mitoxantrone loading capacity. *Nanomedicine: Nanotechnology, Biology and Medicine*, *6*(4), 547-555.

Sharma, P. K., & Bhatia, S. R. (2004). Effect of anti-inflammatories on Pluronic® F127: micellar assembly, gelation and partitioning. *International Journal of Pharmaceutics*, *278*(2), 361-377.

Shell, J. W. (1982). Pharmacokinetics of topically applied ophthalmic drugs. *Survey of ophthalmology*, *26*(4), 207-218.

Shoham, A., Hadziahmetovic, M., Dunaief, J. L., Mydlarski, M. B., & Schipper, H. M. (2008). Oxidative stress in diseases of the human cornea. *Free Radical Biology and Medicine*, *45*(8), 1047-1055.

Shriky, B., Kelly, A., Isreb, M., Babenko, M., Mahmoudi, N., Rogers, S., ... & Gough, T. (2020). Pluronic F127 thermosensitive injectable smart hydrogels for controlled drug delivery system development. *Journal of Colloid and Interface Science*, *565*, 119-130.

USC UNIVERSIDADE DE SANTIAGO DE COMPOSTELA

Summerlin, N., Soo, E., Thakur, S., Qu, Z., Jambhrunkar, S., & Popat, A. (2015). Resveratrol nanoformulations: challenges and opportunities. *International Journal of Pharmaceutics*, *479*(2), 282-290.

Taveira, S. F., Varela-Garcia, A., dos Santos Souza, B., Marreto, R. N., Martin-Pastor, M., Concheiro, A., & Alvarez-Lorenzo, C. (2018). Cyclodextrin-based poly (pseudo) rotaxanes for transdermal delivery of carvedilol. *Carbohydrate Polymers*, *200*, 278-288.

Teuchner, B., Wagner, J., Bechrakis, N. E., Orth-Höller, D., & Nagl, M. (2015). Microbial contamination of glaucoma eyedrops used by patients compared with ocular medications used in the hospital. *Medicine*, *94*(8), e583.

Toro, M. D., Nowomiejska, K., Avitabile, T., Rejdak, R., Tripodi, S., Porta, A., ... & Fiedorowicz, M. (2019). Effect of resveratrol on in vitro and in vivo models of diabetic retinophathy: a systematic review. *International Journal of Molecular Sciences*, *20(14)*, 3503.

Tsegaw, A., Tsegaw, A., & Tefera Abula, Y. A. (2017). Bacterial contamination of multi-dose eye drops at ophthalmology department, University of Gondar, Northwest Ethiopia. *Middle East African Journal of Ophthalmology*, *24*(2), 81.

Turovsky, T., Khalfin, R., Kababya, S., Schmidt, A., Barenholz, Y., & Danino, D. (2015). Celecoxib encapsulation in β-casein micelles: structure, interactions, and conformation. *Langmuir*, *31*(26), 7183-7192.

Turovsky, T., Portnaya, I., Kesselman, E., Ionita-Abutbul, I., Dan, N., & Danino, D. (2015). Effect of temperature and loading on the structure of β-casein/ibuprofen assemblies. *Journal of Colloid and Interface Science*, *449*, 514-521.

Ung, L., Pattamatta, U., Carnt, N., Wilkinson-Berka, J. L., Liew, G., & White, A. J. (2017). Oxidative stress and reactive oxygen species: a review of their role in ocular disease. *Clinical Science*, *131*(24), 2865-2883.

USC
UNIVERSIDADE DE SANTIAGO DE COMPOSTELA

Varela-Garcia, A.; Concheiro, A.; Alvarez-Lorenzo, C. (2020). Cytosine-functionalized bioinspired hydrogels for ocular delivery of antioxidant transferulic acid. *Biomater. Sci.*, *8*, 1171–1180.

Varela-Garcia, A., Concheiro, A., & Alvarez-Lorenzo, C. (2018). Soluplus micelles for acyclovir ocular delivery: Formulation and cornea and sclera permeability. *International Journal of Pharmaceutics*, *552*(1-2), 39-47.

Vivero-Lopez, M., Muras, A., Silva, D., Serro, A. P., Otero, A., Concheiro, A., & Alvarez-Lorenzo, C. (2021a). Resveratrol-Loaded Hydrogel Contact Lenses with Antioxidant and Antibiofilm Performance. *Pharmaceutics*, *13*(4), 532.

Vivero-Lopez, M., Xu, X., Muras, A., Otero, A., Concheiro, A., Gaisford, S., ... & Goyanes, A. (2021b). Anti-biofilm multi drug-loaded 3d printed hearing aids. *Materials Science and Engineering: C*, *119*, 111606.

Wang, L., Zhou, M. B., & Zhang, H. (2021). The Emerging Role of Topical Ocular Drugs to Target the Posterior Eye. *Ophthalmology and Therapy*, *10*, 465-494.

Zhang, L., Maddison, L.A., Chen, W. (2018). Zebrafish as a model for obesity and diabetes. *Frontiers in Cell and Developmental Biology*, *6*, 91.

USC
UNIVERSIDADE DE SANTIAGO DE COMPOSTELA

USC
UNIVERSIDADE
DE SANTIAGO
DE COMPOSTELA

USC
UNIVERSIDADE
DE SANTIAGO
DE COMPOSTELA

USC
UNIVERSIDADE
DE SANTIAGO
DE COMPOSTELA

Conclusions

USC
UNIVERSIDADE
DE SANTIAGO
DE COMPOSTELA

USC
UNIVERSIDADE
DE SANTIAGO
DE COMPOSTELA

7. CONCLUSIONS

According to the aims of this Thesis, the development of hearing aids and contact lenses was carried out, and the possibility of loading them with substances suitable for inhibiting biofilm formation or addressing already stablished infections was evaluated. Different approaches were explored, and the obtained systems were characterized in detail.

The research was carried out in four steps, and the following conclusions can be drawn.

1. The incorporation of a mixture of ciprofloxacin and fluocinolone acetonide into DLP 3D printed hearing aids to prevent or treat biofilm-related infections was successfully carried out for the first time. The drug-loaded hearing aids were prepared using two different commercial resins and included different drug loadings. All drug-loaded hearing aids showed hydrophilic surface, excellent hemocompatibility, and mechanical properties similar to those of the homologues without drug. The devices sustained the release of both drugs for more than 7 days, accomplishing the therapeutic levels required for the treatment of acute otitis. In addition, the developed hearing aids successfully inhibited the biofilm formation of *S. aureus* and *P. aeruginosa* on the surface and also decreased the growing of

USC UNIVERSIDADE DE SANTIAGO DE COMPOSTELA

both bacteria in the surrounding medium. These findings highlight the capacity of the 3D printing technologies to produce drug-loaded medical devices with antibiofilm properties, which can be extended from hearing aids to other related medical devices.

2. The synthesis of pHEMA- and silicone-based hydrogels adding MPC as a comonomer and subsequent loading with resveratrol was carried out here for first time to obtain hydrogels with antioxidant and antibiofilm properties. MPC increased the swelling and decreased the adsorption of proteins on the hydrogels, without changes in the mechanical properties. All hydrogels were able to uptake relevant amounts of resveratrol. The higher affinity of silicone hydrogels for resveratrol, probably due to hydrophobic interactions, notably increased the amount loaded but also caused the release to occur more slowly. Consequently, the amounts of resveratrol accumulated in the cornea and sclera were higher when delivered from the pHEMA hydrogels. Regarding the antibiofilm activity, resveratrol decreased *P. aeruginosa* biofilm formation, but no protective effect was observed for MPC against the two strains investigated. However, the preferential sorption of lysozyme by hydrogels containing MPC may contribute to the antibacterial effects *in vivo*. It should be noted that all developed hydrogels protected resveratrol against photodegradation maintaining its antioxidant activity. Overall, hydrogels containing MPC moieties and loaded with resveratrol may be suitable candidates for the preparation of CLs with antibiofilm and antioxidant properties.

3. An increase in the proportion of MPC added to HEMA hydrogels, up to 381 mM, allowed obtaining CLs with enhanced ability to load resveratrol. Steam-heat sterilization of the CLs did not

USC UNIVERSIDADE DE SANTIAGO DE COMPOSTELA

affect the loading of resveratrol but led to a more sustained release. The presence of lysozyme in the *in vitro* release medium did not modify the kinetics. Differently, albumin slowed down the release. *In vivo* tests in a rabbit model demonstrated the safety of the developed CLs as well as their capability of providing sustained release of resveratrol over a period of 8 h, with higher concentrations in tear fluid than those provided by eye drops in the 2-6 h time interval after application. Relevantly, wearing of CLs for 8 h facilitated resveratrol penetration in ocular tissues providing higher concentrations of resveratrol in cornea, sclera and aqueous humor than the eye drop instillation. Also, these CLs protected resveratrol from photodegradation during wearing under daylight and preserved its antioxidant activity. Finally, the Levy plot evidenced a strong correlation between the percentages of resveratrol released *in vivo* and *in vitro* and that, after an initial lag time, the release occurred faster *in vivo* than *in vitro*. Nevertheless, identification of *in vitro* conditions that may resemble better the *in vivo* behavior is still a challenge. In sum, CLs prepared with high proportion in MPC are pointed out as suitable platforms for the sustained release of resveratrol aimed to address ocular diseases that affect the anterior and posterior segment of the eye and that require antimicrobial and antioxidant management.

4. Pluronic® F127 single micelles and Pluronic® F127/casein mixed micelles increased more than 500 times the apparent solubility of resveratrol in aqueous medium and showed excellent stability both during storage and when exposed to a strong dilution mimicking an *in vivo* administration. Single and mixed micelles prepared with Pluronic® F127 at 10 mM are pointed out as the most suitable ones, since they undergo sol-gel transitions in an adequate temperature window to enable easy instillation and prolonged permanence time on

USC UNIVERSIDADE DE SANTIAGO DE COMPOSTELA

the application site, successfully pass preclinical safety assays, allow resveratrol for fully developing the antioxidant activity, exhibit remarkable antibiofilm properties both with and without resveratrol, and favored resveratrol permeability through corneal and scleral tissues.

Taken together, the results achieved in this Doctoral Thesis open new doors for the formulation of resveratrol and development of drug-device combination products that bring together enhanced patient comfort, ability to prevent the formation of bacterial films, and capability of sustaining the release of drugs that may reinforce the antimicrobial features and even help in the management of various ear and eye pathologies.

USC
UNIVERSIDADE DE SANTIAGO DE COMPOSTELA

Annexes

USC
UNIVERSIDADE
DE SANTIAGO
DE COMPOSTELA

USC
UNIVERSIDADE
DE SANTIAGO
DE COMPOSTELA

ANNEXES

CHECKLIST FOR THESIS THAT INCLUDE EXPERIMENTAL ANIMALS. **EXPERIMENTAL ANIMALS ARRIVE**

Yes/No/NA		page
	Title	
Yes	Provide as accurate and concise a description of the content of the article as possible.	219
	Abstract	
Yes	Provide an accurate summary of the background, research objectives, including details of the species or strain of animal used, key methods, principal findings and conclusions of the study.	11-13
	Background	
Yes	Provide an accurate summary of the background, research objectives, including details of the species or strain of animal used, key methods, principal findings and conclusions of the study.	219-249
Yes	Explain how and why the animal species and model being used can address the scientific objectives and, where appropriate, the study's relevance to human biology.	239-243
	Objectives	
Yes	Clearly describe the primary and any secondary objectives of the study, or specific hypotheses being tested.	221-222
	Methods	
	Ethical statement	
Yes	Indicate the nature of the ethical review permissions, relevant licenses, and national or institutional guidelines for the care and use of animals, that cover the research.	227
	Study design	
Yes	Number of experimental and control groups	227-228
Yes	Steps taken to minimize the effects of subjective bias when allocating animals to treatment (e.g. randomization procedure) and when assessing results (e.g. if done, describe who was blinded and when).	227

USC UNIVERSIDADE DE SANTIAGO DE COMPOSTELA

Yes	The experimental unit (e.g. a single animal, group or cage of animals). A time-line diagram or flow chart can be useful to illustrate how complex study designs were carried out.	227-228
	Experimental procedures	
Yes	How (e.g. drug formulation and dose, site and route of administration, anesthesia and analgesia used [including monitoring], surgical procedure, method of euthanasia). Provide details of any specialist equipment used, including supplier(s).	227-230
Yes	When (e.g. time of day).	228
Yes	Where (e.g. home cage, laboratory, water maze).	227-228
Yes	Why (e.g. rationale for choice of specific anesthetic, route of administration, drug dose used).	227-229
	Experimental animals	
Yes	Provide details of the animals used, including species, strain, sex, developmental stage (e.g. mean or median age plus age range) and weight (e.g. mean or median weight plus weight range).	227
Yes	Provide further relevant information such as the source of animals, international strain nomenclature, genetic modification status (e.g. knock-out or transgenic), genotype, health/immune status, drug or test naïve, previous procedures, etc.	227
	Housing and husbandry	
Yes	Housing (type of facility e.g. specific pathogen free [SPF]; type of cage or housing; bedding material; number of cage companions; tank shape and material etc. for fish).	227-228
Yes	Husbandry conditions (e.g. breeding program, light/dark cycle, temperature, quality of water etc for fish, type of food, access to food and water, environmental enrichment).	227
Yes	Welfare-related assessments and interventions that were carried out prior to, during, or after the experiment.	228-229
	Sample size	
Yes	Specify the total number of animals used in each experiment, and the number of animals in each experimental group.	227-228
Yes	Explain how the number of animals was arrived at. Provide details of any sample size calculation used.	227-228

USC UNIVERSIDADE DE SANTIAGO DE COMPOSTELA

Yes	Indicate the number of independent replications of each experiment, if relevant.	227-228
	Allocating animals to experimental groups	
Yes	Indicate the number of independent replications of each experiment, if relevant.	227-228
Yes	Describe the order in which the animals in the different experimental groups were treated and assessed.	227-228
	Experimental outcomes	
Yes	Clearly define the primary and secondary experimental outcomes assessed (e.g. cell death, molecular markers, behavioral changes).	228-231
	Statistical methods	
Yes	Provide details of the statistical methods used for each analysis.	232
Yes	Specify the unit of analysis for each dataset (e.g. single animal, group of animals, single neuron).	232, 241, 242, 243
Yes	Describe any methods used to assess whether the data met the assumptions of the statistical approach.	232, 241, 242, 243
	Results and discussion	
	Basal data	
Yes	For each experimental group, report relevant characteristics and health status of animals (e.g. weight, microbiological status, and drug or test naïve) prior to treatment or testing (this information can often be tabulated).	227, 229
	Numbers analyzed	
Yes	Report the number of animals in each group included in each analysis. Report absolute numbers (e.g. 10/20, not 50%).	227-228
Yes	If any animals or data were not included in the analysis, explain why.	228
	Outcomes and estimation	
Yes	Report the results for each analysis carried out, with a measure of precision (e.g. standard error or confidence interval).	240-243
	Adverse events	
Yes	Give details of all important adverse events in each experimental group.	220, 240

USC UNIVERSIDADE DE SANTIAGO DE COMPOSTELA

Yes	Describe any modifications to the experimental protocols made to reduce adverse events.	227-228
	Interpretation/scientific implications	
Yes	Interpret the results, taking into account the study objectives and hypotheses, current theory and other relevant studies in the literature.	239-243
Yes	Comment on the study limitations including any potential sources of bias, any limitations of the animal model, and the imprecision associated with the results.	227
NA	Describe any implications of your experimental methods or findings for the replacement, refinement or reduction (the 3Rs) of the use of animals in research.	
	Generalizability/translation	
Yes	Comment on whether, and how, the findings of this study are likely to translate to other species or systems, including any relevance to human biology.	239-243
	Funding	
Yes	List all funding sources (including grant number) and the role of the funder(s) in the study.	227

Based on The ARRIVE guidelines: Animal Research: Reporting of In Vivo Experiments.

PhD Student signature

DECLARACIÓNS, CONFLITO DE INTERESES E RELACIÓN DE PUBLICACIÓNS QUE ACHEGAN CONTIDOS

CONFLITO DE INTERESE

A doutoranda declara non ter ningún conflito de interese en relación coa Tese de Doutoramento.

RELACIÓN DE PUBLICACIÓNS QUE ACHEGAN CONTIDOS

1.- Autores (p.o. de firma): C. Alvarez-Lorenzo, S. Anguiano-Igea, A. Varela-Garcia, M. Vivero-Lopez, A. Concheiro.

Título: Bioinspired hydrogels for drug-eluting contact lenses.

Revista: *Acta Biomaterialia* 84, 49-62, 2019.

Factor de impacto: 7.242; Q1 (D1) en Engineering, Biomedical; Q1 (D1) Materials Science, Biomaterials.

Contribución da doutoranda: Pesquisa bibliográfica e participación na redacción do texto da revisión.

2- Autores (p.o. de firma): M. Vivero-Lopez, X. Xu, A. Muras, A. Otero, A. Concheiro, S. Gaisford, C. Alvarez-Lorenzo, A. Goyanes.

Título: Anti-biofilm multi drug-loaded 3D printed hearing aids

Revista: *Materials Science & Engineering C* 119, 111606, 2021.

Factor de impacto: 7.328; Q1 en Materials Science, Biomaterials (en 2020).

Contribución da doutoranda: Pesquisa bibliográfica, colaboración no deseño dos experimentos, realización da experimentación relacionada coa cesión dos fármacos e a actividade antibiofilm, análise dos resultados, redacción do borrador do traballo e participación na preparación do texto definitivo.

USC UNIVERSIDADE DE SANTIAGO DE COMPOSTELA

3.- Autores (p.o. de firma): M. Vivero-Lopez, A. Muras, D. Silva, A. P. Serro, A. Otero, A. Concheiro, C. Alvarez-Lorenzo.

Título: Resveratrol-loaded hydrogel contact lenses with antioxidant and antibiofilm performances.

Revista: *Pharmaceutics* 13, 532, 2021.

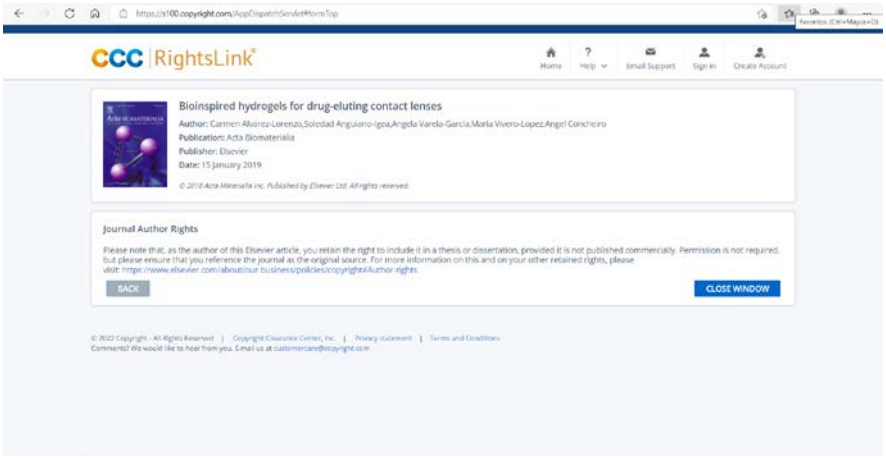
Factor de impacto: 6.321; Q1 en Pharmacology&Pharmacy (en 2020).

Contribución da doutoranda: Pesquisa bibliográfica, colaboración no deseño dos experimentos, realización de máis do 90% da experimentación, análise dos resultados, redacción do borrador do traballo e participación na preparación do texto definitivo.

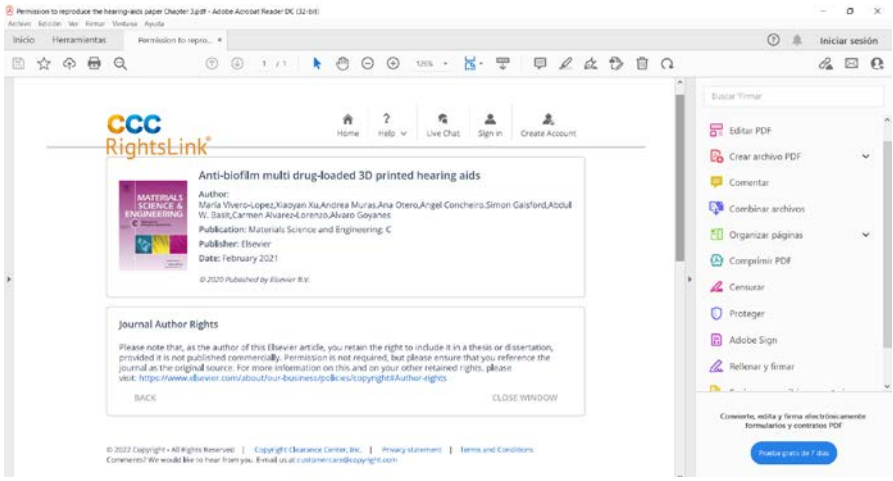
USC
UNIVERSIDADE DE SANTIAGO DE COMPOSTELA

PERMISOS DE REPRODUCIÓN DE FIGURAS E TEXTO DE TRABALLOS PUBLICADOS POLA DOUTORANDA

-1. INTRODUCIÓN



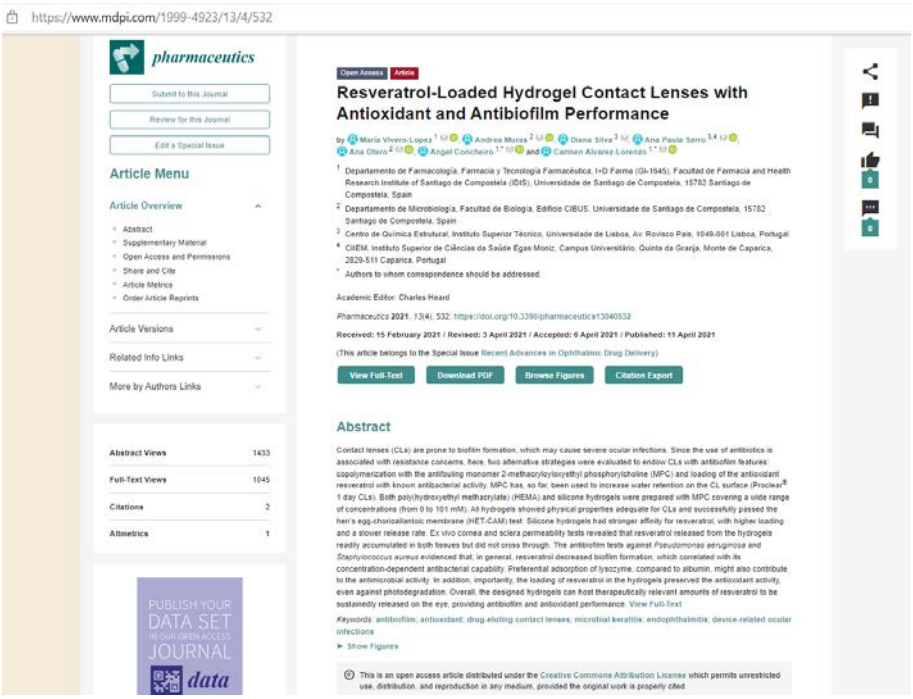
-3. ANTI-BIOFILM MULTIDRUG-LOADED 3D PRINTED HEARING AIDS



-4. RESVERATROL-LOADED HYDROGEL CONTACT LENSES WITH ANTIOXIDANT AND ANTIBIOFILM PERFORMANCE

Traballo publicado en Open Access.

This is an open access article distributed under the **Creative Commons Attribution License** which permits unrestricted use, distribution, and reproduction in any medium, provided the original work is properly cited.



https://www.mdpi.com/1999-4923/13/4/532

pharmaceutics

Submit to this Journal

Review for this Journal

Edit a Special Issue

Article Menu

Article Overview

- Abstract
- Supplementary Material
- Open Access and Permissions
- Share and Cite
- Article Metrics
- Order Article Reprints

Article Versions

Related Info Links

More by Authors Links

Abstract Views	1433
Full-Text Views	1045
Citations	2
Altmetrics	1

PUBLISH YOUR DATA SET IN OUR OPEN ACCESS JOURNAL data

Open Access Article

Resveratrol-Loaded Hydrogel Contact Lenses with Antioxidant and Antibiofilm Performance

by María Vivero-Lopez [1], Andrea Muras [2], Diana Silva [3], Ana Paula Serro [3,4], Ana Otero [2], Angel Concheiro [1,*] and Carmen Alvarez-Lorenzo [1,*]

[1] Departamento de Farmacología, Farmacia y Tecnología Farmacéutica, I+D Farma (GI-1945), Facultad de Farmacia and Health Research Institute of Santiago de Compostela (IDIS), Universidade de Santiago de Compostela, 15782 Santiago de Compostela, Spain

[2] Departamento de Microbiología, Facultad de Biología, Edificio CIBUS, Universidade de Santiago de Compostela, 15782 Santiago de Compostela, Spain

[3] Centro de Química Estrutural, Instituto Superior Técnico, Universidade de Lisboa, Av. Rovisco Pais, 1049-001 Lisboa, Portugal

[4] CitEM, Instituto Superior de Ciências da Saúde Egas Moniz, Campus Universitário, Quinta da Granja, Monte de Caparica, 2829-511 Caparica, Portugal

* Authors to whom correspondence should be addressed.

Academic Editor: Charles Heard

Pharmaceutics **2021**, *13*(4), 532; https://doi.org/10.3390/pharmaceutics13040532

Received: 15 February 2021 / **Revised:** 3 April 2021 / **Accepted:** 6 April 2021 / **Published:** 11 April 2021

(This article belongs to the Special Issue Recent Advances in Ophthalmic Drug Delivery)

View Full-Text | Download PDF | Browse Figures | Citation Export

Abstract

Contact lenses (CLs) are prone to biofilm formation, which may cause severe ocular infections. Since the use of antibiotics is associated with resistance concerns, here, two alternative strategies were evaluated to endow CLs with antibiofilm features: copolymerization with the antifouling monomer 2-methacryloyloxyethyl phosphorylcholine (MPC) and loading of the antioxidant resveratrol with known antibacterial activity. MPC has, so far, been used to increase water retention on the CL surface (Proclear® 1 day CLs). Both poly(hydroxyethyl methacrylate) (HEMA) and silicone hydrogels were prepared with MPC covering a wide range of concentrations (from 0 to 101 mM). All hydrogels showed physical properties adequate for CLs and successfully passed the hen's egg-chorioallantoic membrane (HET-CAM) test. Silicone hydrogels had stronger affinity for resveratrol, with higher loading and a slower release rate. Ex vivo cornea and sclera permeability tests revealed that resveratrol released from the hydrogels readily accumulated in both tissues but did not cross through. The antibiofilm tests against *Pseudomonas aeruginosa* and *Staphylococcus aureus* evidenced that, in general, resveratrol decreased biofilm formation, which correlated with its concentration-dependent antibacterial capability. Preferential adsorption of lysozyme, compared to albumin, might also contribute to the antimicrobial activity. In addition, importantly, the loading of resveratrol in the hydrogels preserved the antioxidant activity, even against photodegradation. Overall, the designed hydrogels can host therapeutically relevant amounts of resveratrol to be sustainedly released on the eye, providing antibiofilm and antioxidant performance. View Full-Text

Keywords: antibiofilm; antioxidant; drug-eluting contact lenses; microbial keratitis; endophthalmitis; device-related ocular infections

► Show Figures

This is an open access article distributed under the Creative Commons Attribution License which permits unrestricted use, distribution, and reproduction in any medium, provided the original work is properly cited

This PhD Thesis deals with the prophylaxis and treatment of infections associated to medical devices. Anti-biofilm multidrug-loaded 3D printed hearing aids were prepared to treat ear infections. Resveratrol-loaded hydrogel contact lenses were designed to decrease the incidence of ocular infections and manage oxidative stress-related diseases. Their optimization was carried out together with the evaluation of the in vivo release profile and the penetration into different ocular tissues of resveratrol. Polymeric micelles for ophthalmic administration were prepared to reinforce the therapeutic results previously achieved. This Thesis opens new doors for the formulation of resveratrol and development of drug-device combination products improving patient comfort, preventing biofilm formation and sustaining the release.